KfK 4774
EUR 13151 EN
September 1990

Nuclear Fusion Project Annual Report of the Association KfK/EURATOM

October 1989 – September 1990

Projekt Kernfusion

Kernforschungszentrum Karlsruhe

KfK 4774
EUR 13151 EN
September 1990

Nuclear Fusion Project Annual Report of the Association KfK/EURATOM

October 1989 - September 1990

compiled by

G. Kast

Kernforschungszentrum Karlsruhe

Kernforschungszentrum Karlsruhe GmbH
Postfach 3640, 7500 Karlsruhe 1

ISSN 0303-4003

Preface

KfK's fusion project and its contribution as a laboratory associated to the European Fusion Programme had its origin in 1983 when the European Fusion Technology Programme was initiated: At the same time the Next European Torus (NET) study group was founded. The NET project had the objective to demonstrate a stable plasma burn and to demonstrate technologies relevant and needed for a fusion power reactor. With its background from nuclear technology projects, particle accelerator development, superconductivity research, and expertise in material science, KfK was able to add additional resources to the European effort. On a national basis the contribution of KfK complemented the work on plasma physics of IPP Garching and on plasma wall interaction of KFA Jülich, the two other German laboratories associated to the European Fusion Programme.

The expertise for the complex technology tasks was distributed over many departments of KfK which made necessary an organization as a project with a small management group coordinating the work inside KfK and establishing and maintaining the links to outside partners and institutions. The general guidelines for the work are derived from the European Community Programme, the KfK part of the work is discussed and agreed with the European Commission, which in turn gets advice from the Fusion Technology Steering Committee. Within KfK, the fusion project draws on about 20 % of the scientific and technical potential of the organization in balance with several non fusion activities. While competing with these other programmes on the resources, the nuclear fusion project capitalizes on expertise being gained in neighbouring work fields such as nuclear safety for light water reactors, fast breeder activities and materials development. A variety of special services support the project: Data processing, assistance in operation of larger experiments, central workshops, irradiation- and hot cell facilities are centralized institutions of KfK whose contributions are a support for the project.

Our fusion technology work refers to critical issues in the NET programme and to tasks addressing fusion power reactors. For NET, the development of tritium processing components and loops, superconducting magnets and remote operation within the plasma chamber are highlights of the KfK program. Breeding blanket development, investigations into radiation and high heat load resistant structural materials and safety studies are topics of the long term programme. Gyrotrons as power sources to heat the reactor plasma are a special item which originated from earlier particle accelerator work.

These various activities are described in the present annual report which compiles actual scientific results and serves to provide the interested reader with some information on the participating research staff and with references for more insight into the work reported.

J.E. Vetter

Contents

Report on the Technology Programme for NET

NET-Technology Tasks Related to Plasma Facing Components

Introduction:

Due to its strong involvement in the Long Term Fusion Materals Development Programme KfK holds only a moderate share in the NET-Plasma Facing Components development and testing.

Apart from participation in solving the thermal fatigue issue for the NET-structural steel both under experimental and theoretical aspects the other tasks at KfK have mainly to do with the investigation of the heat load capacities of protective materials and their possible degradation by neutrons. Besides that, two facilities are or will be available for testing First Wall or Divertor assemblies under heat loads typical of normal operation conditions for a sufficient number of cycles.

Considerable progress has been achieved in most of the tasks addressed. The thermal cycling tests on austenitic steel tubes have been completed and the results have been compared to isothermal uniaxial conditions. An apparatus to perform multiaxial conditions is under construction. The calculation model for elastoplastic behaviour has been set up (PSM 3.9).

To investigate the possible influence of coatings for enhanced thermal, radiative contact such coatings have been characterized both microstructurally and optically. Preliminary thermal cycling tests have shown excellent adherence of the ceramic layer and no influence on fatigue of the parent metal. Tube samples with improved emissivity coatings are not available yet for thermal cycling (PSM 8.1/2).

The data base on SiC as a backup candidate for First Wall protection has been further increased. In particular cyclic heat load tests have been performed with small tiles. The outcome was a considerable reduction of the critical heat flux density as compared to single tests. Furthermore the post-irradiation mechanical tests have shown a drastic decrease in strength. It can therefore be concluded that the conditions under which SiC-materials could be used for First Wall Protection are very limited. Further investigations will be devoted to carbon-fibre reinforced carbon materials in close collaboration with KFA (PPM 1.4).

A special kind of „protective" material are ceramic insulators needed as windows for radiofrequency power admittance to the plasma. The data base for different, mostly oxidic, candidates has been completed, and the influence of neutron irradiation on strength and heat conductivity has been largely investigated. Again there is a remarkable deterioration of properties, at least up to temperatures which could just be tolerated for operation (PPM 4.1).

All measurements have now concentrated on the low temperature regime where much better thermal and dielectric data are anticipated, but where much concern exists that even low doses could jeopardize the advantages. An important improvement in the sensitivity of the Fabry-Perot method for dielectric loss measurement has been attained, and the cryogenic system has been put into routine operation. Thus it was possible to verify the favorable low loss properties of sapphire down to 150 K. The influence of low dose irradiation at temperatures slightly above ambience („cryogenic" irradiations are not easily achievable) showed a considerable increase of tan δ which has to be avoided by a properly shielded position of windows (PPM 4.2).

Work has started both on window design and lifetime prediction for the component, although contract awarding is still pending. In order to include cyclic stress effects in the model, fatigue measurements have been carried out for Al_2O_3 ceramic showing a distinct decrease in lifetime.

Preparations for thermomechanical testing of First Wall mock-ups have made good progress. Graphite resistance heater tests have demonstrated sufficient lifetime at temperatures up to 2200°C which are necessary to provide NET-relevant surface heat loads for the test assemblies. The vacuum vessel to house the experiments has been installed. A broad program has been started how to equip the test pieces with thermocouples and strain gauges without unduly disturbing the temperature and strain fields, and to provide the tools for a calculation of the thermomechanical behaviour of the specimens. At the same time such calculations are useful to adjust the testing conditions such that measurable effects will be attained in practicable testing times (PDT 1.4).

The test program on the thermomechanical behaviour of candidate divertor materials using a modified plasma spray facility is well under way. Most of the carbon based materials specimens have survived the target number of 1000 cycles with 15 MW/m^2 peak heat flux. The next test campain will be with refractory metals before bonded samples can te tested which are due for delivery in 1991 (PDT 2.1).

PSM 3 Pre- and Post-Irradiation Low Cycle Fatigue of Reference 316 L Steel and Welds

Subtask 3.9: Determination of Thermal Cycling in Cylindrical Geometry Simulating Loading of the Internal Surface of FW Cooling Tube

The cyclic thermal loading of the first wall in a fusion reactor causes cyclic multiaxial stress states. These cyclic stresses may initiate cracks and failure of the structure. To understand crack initiation and propagation caused by these multiaxial thermocyclic loads and to investigate, whether this damage is different from uniaxial isothermal loading, experiments have to be performed under multiaxial cyclic thermal and isothermal conditions. The most exposed region in the FW is the inner side of the cooling tube where the highest tensile amplitudes arise. However, there are high amplitudes at higher temperatures at the FW surface, too. Therefore, it is useful to investigate the crack initiation on the inner and outer surface of tubes loaded in a similar manner.

1) Thermal fatigue of the reference steel 1.4436

Thermal fatigue experiments on tubes of steel 1.4436 have been finished. The measured cycles to failure of specimens under uniaxial isothermal loads were compared to the failure of specimens under thermal fatigue with the same effective strain after the first loading (cf. last semi annual report). Further calculations with inelastic material models have shown that there may be an influence of reversed loading on the effective strain. That would influence the comparison. Experiments to verify the calculations are planned.

2) Thermal and isothermal fatigue of AISI 316 LSPH under multiaxial stress states

Thermal fatigue tests on steel 1.4436 showed shorter lifetimes than uniaxial isothermal tests. In further investigations thermal fatigue tests will be performed on AISI 316 LSPH. The influence of multiaxial stresses will be investigated separately.
For comparison LCF specimen for uniaxial tests were fabricated from plates of AISI 316 LSPH. First fatigue tests under isothermal conditions have been finished.

To perform isothermal tests under similar multiaxial conditions as in thermocyclic tests an experimental set up is in development to test tubes under tensile loads and internal/external pressure. The first cyclic tests on tubes without external pressure and constant internal pressure made of a reference steel have been finished. Fig. 1 shows the experimental set up. Applying the same axial strain range, the time to failure is much smaller if internal pressure is present (compare Fig. 2).

Since no tubes made of steel 316 LSPH are available, fabrication of tubes from raw material was ordered. The raw material has been produced. The production of the tubes will start soon.

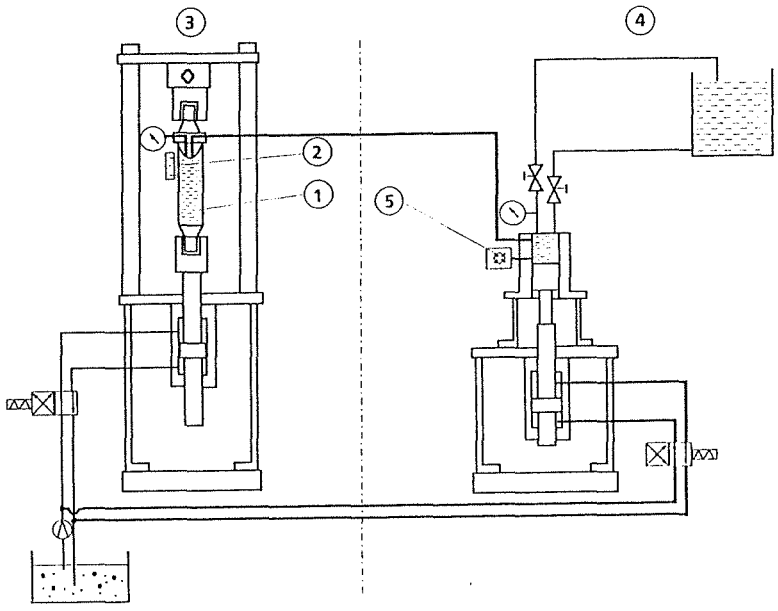

Fig. 1: Schematic sketch of the experimental set up for biaxial fatigue tests
1. Specimen is a tube with internal pressure
2. Extensiometer for axial elongation
3. Machine for tension tests
4. Machine to produce the internal pressure
5. Pressure transducer

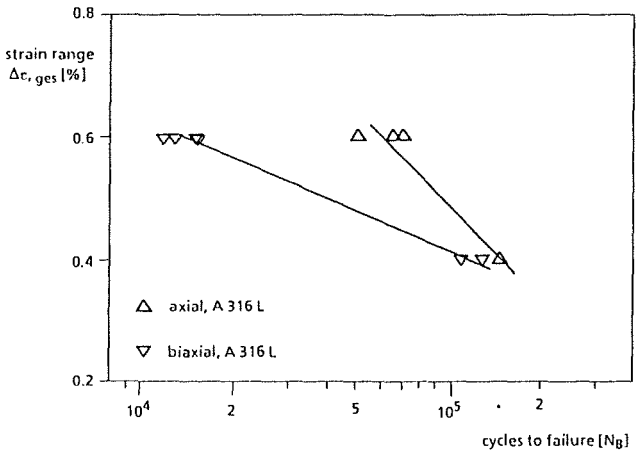

Fig. 2: Cycles to failure of tube-specimens under isothermal uniaxial fatigue as a function of the cyclic range of the axial strain

Staff:

E. Diegele
W. Hartlieb
B. Schinke
G. Schweinfurther

PSM 8 Coatings and Surface Effects on 316 L

Subtask 8.1: Development of Surface Coatings to Maximize Emissivity

The objective of this investigation is to develop and examine oxide coatings for the first wall of a fusion device with radiatively cooled protective tiles. The purpose of the coatings is to act as efficient absorber of the thermal energy radiated by the tiles. Therefore its major properties are high emissivity, sufficient adhesion and thermal stability.

Al_2O_3-TiO_2 coatings of different compositions had been fabricated by subcontractors using atmospheric plasma spraying (APS) and low pressure plasma spraying (LPPS). The APS coatings had a thickness of 100 - 150 µm and a NiCrAlY intermediate layer, The LPPS coatings(~ 20 µm) had no intermediate layers. Emissivity measurements carried out by subcontractors in the temperature ranges 100 - 250 °C and 450 - 900 °C have shown values of 0.86 and ~ 0.8 - 0.9, respectively, for the degree of total emission ε_n. The characterization of the coatings up to now included also phase identification by X-ray diffraction, microstructure by ceramography and SEM, and adhesion in scratch tests.

Regarding the results obtained so far for the most important properties, emissivity and adhesion, both types of coatings (APS and LPPS) seem to meet the demands of a heat absorber.

However, since the spectral emissivity is high also at longer wavelength ≥ 4µm, the heat transfer would be maintained also during the dwell phase of the pulsed operation. This could result in an undesired cooling of the tiles to temperature ≤ 700 K.

Staff:

K. Biemüller
H. Janzer
A. Skokan

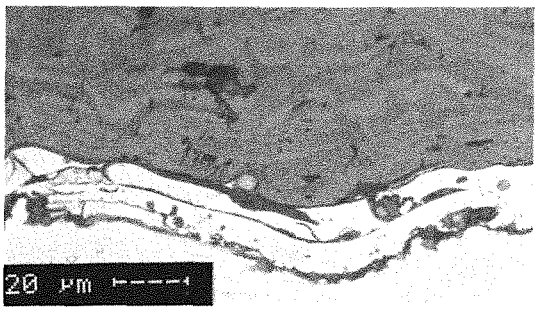

Fig. 1: Al_2O_3 - 13% TiO_2 APS coating with NiCrAlY intermediate layer on 316 L

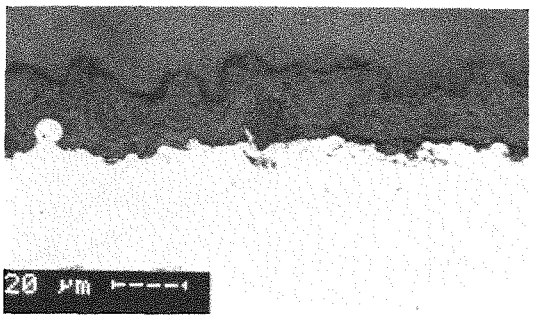

Fig. 2: Al_2O_3 - 13 % TiO_2 LPPS coating on 316 L

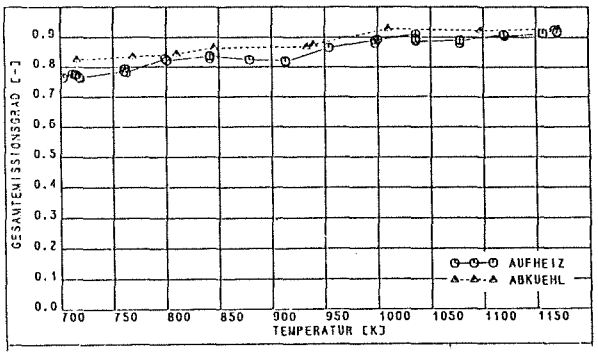

Fig. 3: Total emissivity of Al_2O_3 - 13 % TiO_2 LPPS coating

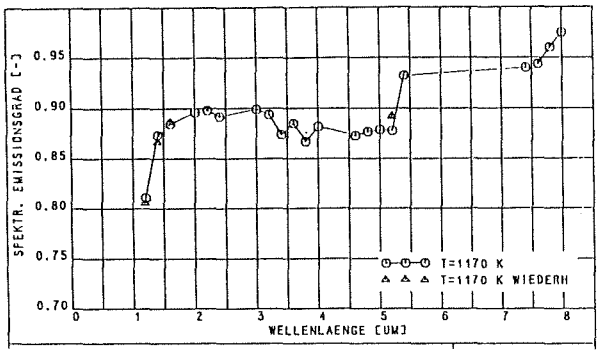

Fig. 4: Spectral emissivity of Al_2O_3 - 13 % TiO_2 LPPS coating

Subtask 8.2: Thermal Cycling Tests of Samples with High Emissivity Coatings

The objective of this investigation is both to study the adherence and integrity of the coatings and to investigate a possible influence of surface modifications on crack initiation in the base material.

Thermal cycle fatigue tests have been performed with tubes made of austenitic steel, preferably AISI 316 LSPH, with outer surface coatings. An equipment for thermal fatigue testing has been developed which, however, needs tubular specimens with a diameter of 60 mm, a wall thickness of 3.5 mm and a heated length of 150 mm.

With such kind of specimens first tests were done by Neumann [1]. Investigating the adhesive strength of a ceramic layer he found:

- No macroscopic damage of the layer was found before the end of the experiment.
- Cracks started from the inner side of the tube which was not coated.
- No cracks were found in the layer, even if the steel was heated up.

Further tests in the same way will be done in future with other kinds of coatings. Up to now, more tubes made of the reference steel 1.4436 have been fabricated and delivered to subcontractors to manufacture the coatings (316 material was not available in the required sizes). The cyclic tests with these specimens will be done in autumn '90.

The experimental set-up is the same as in PSM 3.9. A description is given there.

Reference:

[1] J. Neumann, unpublished report of KfK.

Staff:

B. Schinke

PPM 1 Material Characterization and Neutron Irradiation Effects in Graphites, CFCs and Ceramic Composites

Subtask 1.4: Thermal, Physical and Mechanical Properties of Si-SiC and HIP-SiC

SiC qualities of industrial manufacturers are to be tested concerning the durability of tiles protecting the first wall against plasma instabilities and disruptions. KfK work has concentrated on determining the critical heat load under quasi-stationary conditions, including the consideration of property changes measured after neutron irradiation.

The laboratory experiment concerned was correlated with a former KfK proposal for wall protection. Small tiles are used with a front plate of 25 mm x 25 mm x 14 mm (thickness) and a tail specially shaped to be attached and cooled between two cooling tubes each. A 50 kW acetylene/oxygen burner was used to uniformly heat the whole front face of a single tile which is laterally insulated. The heat flux density is varied with the distance from the burner plate.

Test results are presented in Fig.1, relating to about 10 samples per SiC type. The three SiC types tested were
1) S-SiC with 1.9 % boron content and 6 % porosity (KF),
2) S-SiC with 0.4 % boron and 7.5 % porosity (KH),
3) HIP-SiC (KE).
The broken lines represent results of single heating tests which were already reported in the preceding semi-annual report. In order to guarantee, that the tile specimens classified as non-failed were not severely damaged by undetected internal or reclosed cracks, the single tests have been supplemented by cyclic tests. These consisted in a 50-fold repetition of the single test run, with a 2.5 min heating + 2.5 min cooling period each. If failures occurred, fragmentation was mostly observed after about 20 heating cycles.

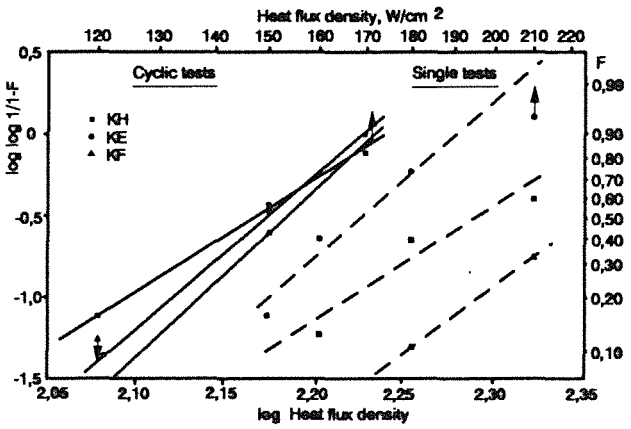

Fig 1 : Failure probability F of SiC tiles dependent on the heat flux density at the front face

Fig. 1 shows that the critical heat flux density was considerably reduced under cycling conditions, to about 150 W/cm^2 at 50 % failure probability for tile fragmentation. Simultaneously, the results of different materials moved closer together. It seemed that 50 cycles already reached beyond a domain of fast, complex crack growth. The Weibull plot allows an extrapolation to technically relevant, low failure probability. At F = 10^{-3} an attainable heat flux density of 70 - 80 W/cm^2 results from cycling tests for the KF and KE specimens. This appears still sufficient for a provisional proof of qualification with regard to normal operating conditions of first wall protection tiles.

Concerning the investigation of irradiation effects, bending tests were conducted to determine the ultimate bending strength (UBS) on about 70 HIP-SiC and CVD-SiC samples from the neutron irradiation experiment CERAM-D217-1 (HFR-Petten, 1000 - 1200 °C, 1.2 - 1.6x10^{26} n/m^2, 15 - 20 dpa). The results show a reduction of the mean UBS to 50 - 60 % of the initial value of about 500 MPa. Thus no decisive advantage was recognizable compared with literature data for S-SiC, the less so since the Weibull modulus decreased from 9 - 10 to < 5. But one has to mention that these results are somewhat questionable, because there were indications of considerable oxidation of sample surfaces in the irradiation capsule with inert gas circulation. We have therefore to wait for other irradiation results, especially from PHENIX-MAT 6 (Phenix-Marcoule, about 500 °C, 20 - 40 dpa).

In order to prepare for planned investigations on carbon fibre-reinforced carbon materials (CFC), bending tests were conducted to determine UBS of three different fine-grained nuclear grades of monolithic graphite. Weibull plots of the results are shown in Fig. 2. The mean UBS values are in excellent agreement with the producers' data sheet. The Weibull modulus shows a technically interesting dependence on the UBS level.

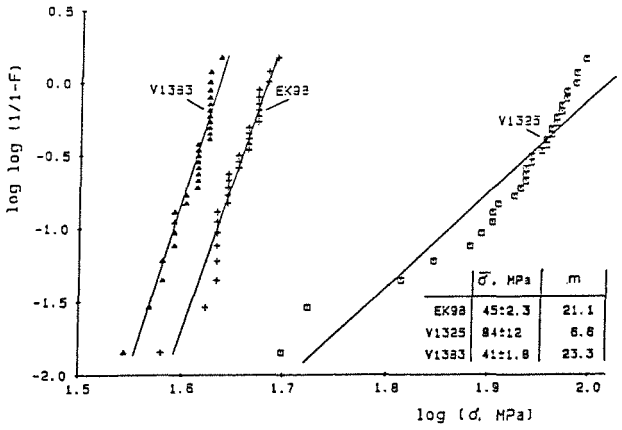

Fig 2.: Weibull plot of the UBS distribution of three different graphite grades

Staff:
M. Blumhofer
W. Dienst
G. Gausmann
H. Zimmermann

PPM 4 Material Characterization and Irradiation Effects in Ceramic Insulators

Subtasks 4.1 and 4.2:

Thermo-mechanical and Dielectric Properties above RT and at Cryogenic Temperatures

Ceramic insulator materials (like Al_2O_3, $MgAl_2O_4$, AlN) are to be selected with regard to their resistance to thermal crack formation by dielectric loss in RF-windows. These windows shall be applied to separate wave guides for ECR heating from the plasma vacuum. KfK work has concentrated on the extension of the data base for dielectric properties, especially at 145 GHz, including further improvement in the measuring accuracy and, particularly, measurements at cryogenic temperatures. The irradiation-induced deterioration of all relevant properties, also of thermal conductivity and mechanical strength, is investigated in several neutron irradiation experiments.

The post-irradiation examination of the experiment CERAM-D217-1 (HFR-Petten, 390 °C, 1.4×10^{26} n/m², E > 0.1 MeV) was started with bending tests on samples of three Al_2O_3 types and of HIP-AlN. The mean ultimate bending strength and the Weibull modulus of the different samples sets, both unirradiated and irradiated is given in Table.

Table : Strength change under neutron irradiation CERAM-D217-1 (d = mean grain size).

Material	UBS, MPa		Weibull modulus	
	unirr.	irrad.	unirr.	irrad.
AL23, 99.5 % Al_2O_3 d = 8 µm	208	128	8.4	4.6
BIO, 99.9 % Al_2O_3 d = 0.9 µm	322	174	9.8	6.2
Al_2O_3 single crystal rod axis 20 - 30° from c	372	179	8.1	8.4
AlN, HIP	284	155	12.2	14.1

The strength reduction is rather similar for all the sample materials, to 50 - 60 % of the initial values, surprisingly also for single crystal Al_2O_3. But it could be of considerable technical interest that the Weibull modulus of this material remained unchanged, likewise that of HIP-AlN. As the number of irradiated samples was small (about 6 each), conclusions have to be based also on the results of the subsequent irradiation experiment PHENIX-MAT 6 (Phenix-Marcoule, about 500 °C, 35 - 40 dpa).

Fig. 1 shows the combination of BIO-Al_2O_3 results from

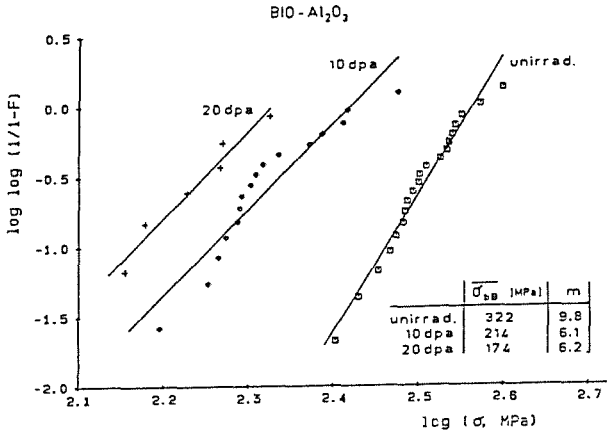

Fig. 1: Change of UBS distribution of BIO-Al_2O_3 at 550 °C/10dpa and 390 °C/20 dpa

CERAM-D217-1 ("20dpa") and the preceding experiment Coccinelle 01 in Osiris-Saclay ("10 dpa"). It appears that the main step in strength deterioration has already taken place at 10 dpa.

The thermal shock resistance of BIO-Al_2O_3 from Coccinelle 01 and of AL23 from CERAM-D217-1 was examined in metal-melt immersion tests on 13 mm diam. pellets heated from room temperature. For BIO-Al_2O_3 50 % failure probability was found at ΔT = 520 K for unirradiated pellets and at ΔT < 400 K for irradiated pellets, while the corresponding AL23 results were ΔT = 387 K and 383 K. So the low-strength materials AL23 (see Table) exhibited a comparatively large resistance to crack growth after irradiation.

The data base for the thermal conductivity of nonirradiated $MgAl_2O_4$ and AlN was completed with samples prepared at KfK. A comparison is given referring to the expression $\lambda = 1/(a + bT)$:

	a (cm·K/W)	b (cm/W)
AlN		
KfK	0.69	1.82×10^{-3}
Shapal	0.182	1.85×10^{-3}
$MgAl_2O_4$		
KfK	2.43	13.2×10^{-3} (R.T. < T < 1371 K)
Single Crystal	4.90	5.0×10^{-3} (R.T. < T < 600 K)

While for AlN both materials differ only in their defect concentration (see quantity "a"), $MgAl_2O_4$ of KfK behaves quite different from the single crystal material. Because of the homogeneity range of the phase $MgAl_2O_4$, the chemical

composition may be different in the spinel types, which has to be investigated.

New results of the thermal conductivity of irradiated AlN (Fig. 2) and $MgAl_2O_4$ (Fig. 3) could be obtained. For AlN the result is similar to that of Al_2O_3. With increasing irradiation defect concentration, the $\lambda \sim T^{-1}$ relationship changes into a root law as expected in theory. A quite different behaviour is found for the $MgAl_2O_4$ single crystal. Above about 500 K its thermal conductivity does not fit the 1/T relationship, due to internal radiation. On the other hand, the irradiated material does not follow a root law for the thermal conductivity but corresponds to $\lambda \sim T^{-1}$ above 1000 K. This indicates that the optical properties of the irradiated single crystal are changed under irradiation.

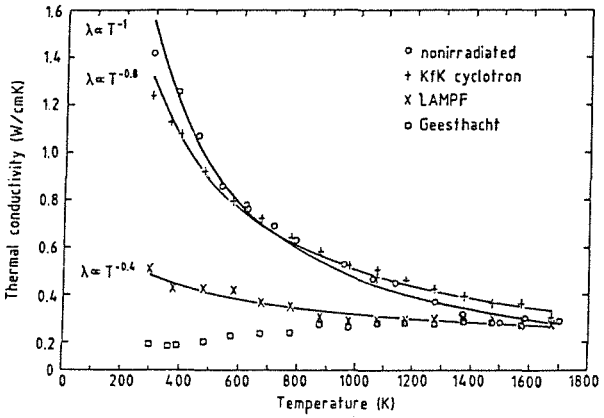

Fig. 2: Thermal conductivity of AlN

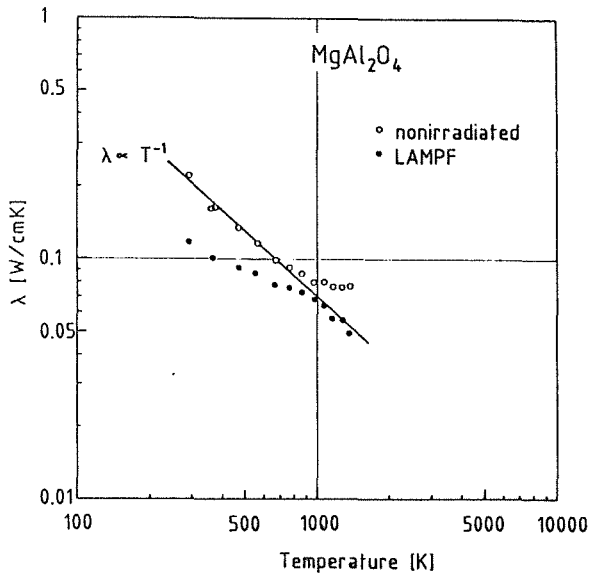

Fig. 3: Thermal conductivity of $MgAl_2O_4$ single crystal

A differential scanning calorimeter for specific heat measurement at cryogenic temperatures has been mounted and is ready for service.

The measurements of dielectric loss could be improved with optimized Fabry-Pérot resonator set-ups suited for determining the dielectric loss tangent down to $\tan \delta = 10^{-5}$. For sapphire, it was possible to demonstrate that the observed loss values are in accordance with extrapolations based on the parameters of the fundamental lattice absorption in the infrared domain (Fig. 4). Predominance of lattice absorption is a criterion for a highly developed low loss dielectric and is characterized by a linear relationship between tan δ and frequency.

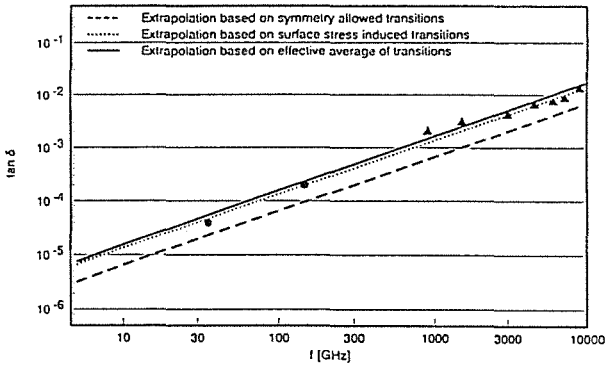

Fig. 4: Dielectric loss data of sapphire (ordinary ray) at mm-wavelengths (•) related to absorption bands in the infrared domain (Δ)

A specimen set of different sapphire and polycrystalline Al_2O_3 grades as well as both mono- and polycrystalline $MgAl_2O_4$ was examined after a fast neutron irradiation at GKSS Geesthacht (3.5×10^{19} f n/cm², 50 - 100 °C). Dielectric loss tangent in sapphire (E ⊥ c) increased from 0.3×10^{-4} to 5.7×10^{-4} at 35 GHz and from 1.9×10^{-4} to 8×10^{-4} at 145 GHz, and in polycrystalline AL23 from 0.8×10^{-4} to 8.0×10^{-4} at 35 GHz and from 3×10^{-4} to 8×10^{-4} at 145 GHz. For VITOX alumina, tan δ was raised from 5×10^{-4} to 7.4×10^{-4} at 35 GHz. Volume swelling in the different alumina grades always amounted to 0.3 %.

The cryogenic system for a Fabry-Pérot resonator operated at 143 - 146 GHz was put into routine service. Measurements were performed on different grades of sapphire which showed a T^2 dependence of tan δ at least for the temperature range of 150 - 330 K. No difference between the various available grades was detected. The sapphire irradiated at GKSS still displayed the above-mentioned T^2 dependence, even though the level of absorption was higher by a factor of 3 - 4. The loss behaviour at cryogenic temperatures of various polycrystalline alumina materials gave evidence of a more complex dependence. While the AL23 grade did not change its dielectric loss significantly with temperature, a translucent alumina grade from NGK Insulators (Japan) gave a marked drop in tan δ similar to sapphire.

Staff:

M. Blumhofer
W. Dienst
G. Gausmann
G. Haase
R. Heidinger
M. Rohde
B. Schulz
H. Zimmerman

HF-windows

In the last years the failure behaviour of HF-windows was investigated with respect to spontaneous failure caused by exceeding the strength and by delayed failure due to subcritical crack growth. Since the HF-sources operate in a non-steady mode also fatigue has to be taken into consideration for lifetime predictions. Cyclic fatigue of ceramics containing natural cracks can be caused by the subcritical crack growth determined in static tests. In addition, "real" fatigue damage may occur. This cyclic effect can be proved by comparing cyclic lifetimes from experiments with predictions from static tests assuming only subcritical crack growth.

An example of cyclic fatigue is illustrated in Fig. 5 for a

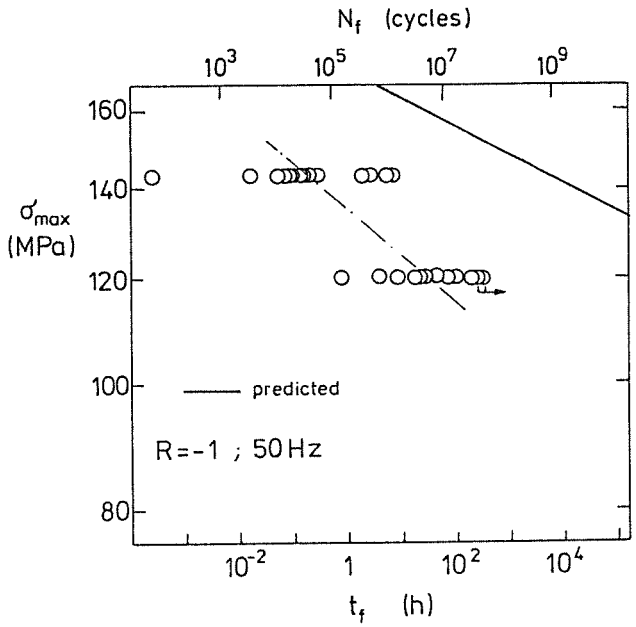

Fig. 5: Cyclic lifetimes for specimens with natural cracks compared with predictions based on static tests at room temperature; points marked with arrow are survivors.

99.6%Al_2O_3-ceramic. Fig. 5 shows the prediction from the static tests as solid line and the measurements as open circles. The predicted and measured lifetimes are significantly different. It has to be concluded from these results that the cyclic fatigue effect is very strong. In future this cyclic behaviour has to be measured for all candidate materials.

Staff:

T. Fett
D. Munz

PDT 1 Thermomechanical Tests of First Wall Mock-ups

Subtask 1.4: Demonstration of Thermomechanical Performance of FW Mock-ups

A test program FIWATKA is planned at KfK for testing first wall (FW) sections in order to:

1. provide an experimental basis to improve confidence in the prediction of thermal fatigue life by:
   a) validation of computational methods for
      - thermo-mechanical analysis
      - crack initiation by cyclic plastic deformations
      - fatigue crack propagation in complicated geometries.
   b) life time determination including
      - observation during life
      - study of faliure modes for prototype FW sections under representative thermomechanical conditions.
2. compare integral behaviour of different FW concepts including protection.

The test specimens will be tested under mechanical boundary conditions and thermal loads as close as possible to those of NET.

The specimen will be positioned in a vacuum chamber; it will be actively cooled with water and will be heated by thermal radiation in a cyclic manner.

A resistance heater made of a graphite plate at temperatures up to 2200 °C in vacuum will serve as a heat source. It will radiate heat for a few minutes onto the surfaces of two specimens placed on both sides of the heater plate in a distance of two or three centimeters. The heater power will be turned down periodically for one or two minutes with the result that the temperature profile and the corresponding stress and strain profiles in the specimen change also periodically and cause thermal fatigue. To achieve this the heater plate must stand fast temperature changes of about 1000 K within less than 30 seconds for a sufficient number of cycles.

Heater pretests, some results of which were summarized in the last semiannual report, have shown that several grapite grades exhibit sufficient life time to be used as heater plates under the conditions mentioned above. Their lifetime seems to be limited by the formation of a thin carbon layer on the surface of the heater; the layer is disconnected from the heater plate electrically and in terms of heat conduction and acts as a radiation shield which increases the heater temperature and makes it become nonuniform. The mechanisms of the layer deposition is not yet unterstood; it might have to do with redeposition of sublimated carbon. It can be tolerated since it developes only at very high temperatures and/or long service times.

The vacuum vessel to house the experiment is schematically shown in Fig. 1 and was delivered and installed recently together with the coolant circuitry. Instrumentation and control for the test rig will be added with the goal to make the apparatus ready to receive the first specimen by the end of the year.

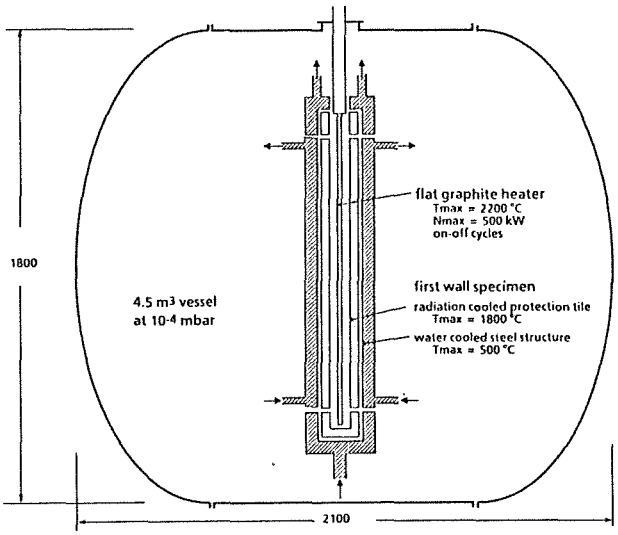

Fig. 1: Schematic of first wall thermal fatigue test facility FIWATKA

The first specimen will be instrumented with thermocouples and strain gauges. Both measurement techniques may cause local disturbances of the original temperature field, as was found by using FEM-calculations (compare last seminannual report). More information is expected from an experiment. A set-up was developed to heat a steel-plate from one side and cool it from the other side. The plate was instrumented with different kinds of thermocouples set up in different ways. First results of the measurements are expected soon.

The prediction of the thermo-mechanical behaviour of the First Wall mock-up depends on the inelastic behaviour of the material. Therefore, further calculations with more advanced viscoplastic material models are necessary. The parameters of these models are not known in the temperature range that is relevant to application in fusion technology. Therefore, cyclic tests with complex load histories were performed on steel 316 LSPH up to 400 °C. The numerical adjustment of the parameters is under way.

Furthermore a study to predict the life time of the test specimens was performed.

The calculations have been carried out using the FE-code ABAQUS and include

- two load cases, that model reactor conditions and FIWATKA testing conditions, respectively, with varying "burn-off" time

- analysis of temperature cycles of graphite heater, graphite tile and steel wall

- analyses of the global deformation behaviour of the test segment

- investigations of stress and strain fields of the steel part at significant points during the loading period for elastic and inelastic material behaviour, as well as their time variation, i.e. rearrangements of stresses and plastic strains in time at exposed locations of the test segment.

From elastic analysis as well as from inelastic analyses a good conformity has been found in the stress states between both loading conditions considered. At locations of high stresses the agreement is very good, at locations of weak stress the conformity is fair.

Considering plastic strains, the difference between fusion and testing conditions is more distinct than in the stress fields. At the location of maximum strain, the cyclic plastic strain range under FIWATKA testing conditions will be 0.5 %. From fatigue curves at 450 °C the number of cycles to crack initiation could be assessed as 10 000 to 20 000, or, with other words, up to half a year of testing to get failure of the test segment is expected if no axaggeration measures are taken to enhance the damage process.

Staff:

E. Diegele
E. Eggert
G. Hofmann
H. Kreuzinger
B. Schinke
G. Schweinfurther

PDT 2 Tests of Divertor Samples and Mock-ups

Sub-Task 2.1: Pretests of Bulk Materials and Bonded Divertor Samples

A testing program on the thermomechanical behavior of candidate divertor and high heat flux component materials is under way using a modified plasma spray facility (PSA) as a heat source. The device enables to expose material samples of about 20 cm2 size to heat fluxes typical for divertor operation, i.e., up to 15 MW/m2, for selected pulse lengths, thereby creating stress and temperature cycles relevant to divertor components. The first phase of the current program involves screening tests with samples out of 45 different materials. The second phase will employ bonded samples of the same size, i.e., typically 0.4 cm carbon fiber composite brazed to a 0.4 cm thick refractory metal substrate.

The test device has been briefly described in the last semiannual report. The data acquisition is reported in [1]. Here a short explanation of the sample arrangement will be given before summarizing the intermediate results.

Fig. 1 is an explosive view of one of the six sample holders attached to the manifold at the vertical drive shaft. The circular sample of 5 cm diameter and 0.8 cm thickness is clamped between the holder and the threaded ring using flexible graphite gaskets as complient layers at both sides of the sample flange. Hence the sample is nearly free to expand and bend giving definite mechanical boundary conditions. The copper sample holder is actively cooled but the sample itself is nearly adiabatically heated during the short heat pulse. Temperatures are monitored at the sample surface center by pyrometer and at the rear face center by thermocouples.

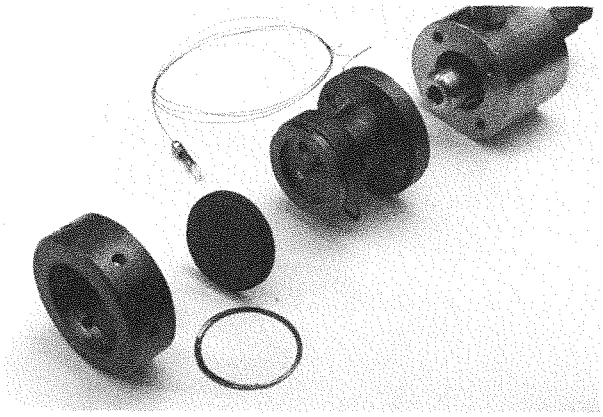

Fig. 1: Sample holder arrangement showing from the left: clamping ring, sample, copper holder with thermocouple, manifold (dummy)

So far 26 carbon based materials have been cycled applying the following test parameters: calibrated peak heat flux = 15 MW/m2, heating time = 2.3 s, cool-down time = 43 s, temperature at begin of pulse ≈ 100 °C, total number of pulses = 1000 unless early failure occurred. The materials tested can be grouped as follows:

- fine grained graphite:
  EK986, V1325h, V1383h, V1393h, V1325s, V1383s, V1393s from Ringsdorff (h = highly pure, s = super pure);
  FE98, FE219, FU9512 from Schunk;
  1116PT, 5890PT from Le Carbone-Lorraine

- Carbon fiber composites (with the good thermal conductivity parallel (II) and perpendicular (⊥) to heat flux:
  CF322⊥, CF322II, CFC Random from Schunk;
  A46⊥, A46II, A46II monolithic, A223G , A223GII, A05⊥,
  A05II, A05II monolithic, A05+SiCII from Le Carbone-Lorraine

- Ceramics:
  SiC30, CFC coated with SiC from Schunk

With regard to the thermal behavior the test results are summarized below:

Fig. 2 shows an example of a temperature history plot of a typical cycle. The six staggered curves at the bottom represent the rear face temperature of the six successively heated samples tested at a time, using the materials (from the left): 2 x A05 II, 2 x A05 II monolithic, 2 x(A05 + SiC II). The saw-tooth curve is the reading of the pyrometer which sees each sample during the heating phase only and drops out of range while the sample holder is rotated to the next position. The circles indicate the readings at the end of pulse. Maximum surface temperatures range from 1100 to 2400 °C. Maximum rear face temperatures range from 475 to 1000 °C, depending on the material.

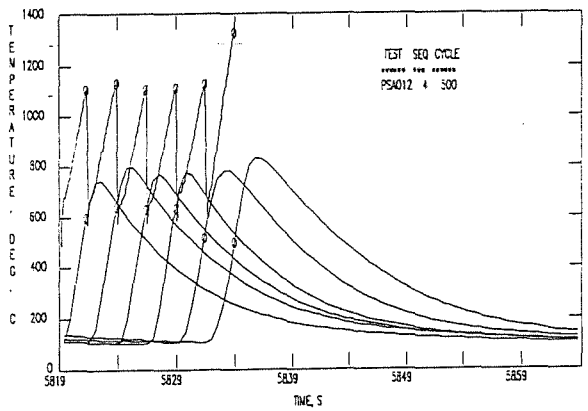

Fig. 2: Measured temperature history of a typical cycle in test PSA012

The temperature difference, ΔT, across the sample thickness at end of pulse is a measure for the thermal conductivity of the material. A first deduction of the temperature-average thermal conductivity ranges from 0.4 to 0.6 W/cm K for the fine grained graphites, 0.45 to 0.85 for the CFCII grades and to only 0.1 to 0.15 for the CFC$\perp$ grades. This corresponds to the scarce data provided by the suppliers.

The thermal behavior remains essentially stable throughout the 1000 cycles except for device related fluctuations in the temperature readings on the order of up to $\pm$ 8 % with typical standard deviations of 2 - 3 %. This means that the thermal conductivity is not altered by thermal cycling.

The weight loss due to thermal erosion is typically 20 - 60 mg per 1000 cycles corresponding to erosion depths after 1000 cycles of a few µm up to about 60 µm with large scatter. CFCs (in particular CFC II) seem to erode less than the fine grained graphites, perhaps as a result of lower peak surface temperatures.

With regard to the mechanical behavior of the samples the following intermediate results are obtained.

In general both the fine grained graphites and the CFCs survived the 1000 cycles without macroscopic mechanical damage with two restrictions:

Fine grained graphite is susceptible to circumferential fracture at the clamping flange. This is mainly attributed to imperfect fixation of the samples but shows the sensitivity of the brittle material to fracture. Five out of 38 samples failed in this way. Secondly, the CFCII samples are made up of a stack of plates bonded together. The bonding failed at 2 out of 11 samples of this kind.

The SiC30 samples failed by diametrical fracture within a few cycles. This catastrophic failure is in agreement with stress analyses, yielding thermal stresses far in excess of yield strength values found in the literature.

The SiC coating of the coated CFC samples failed within a few cycles. The 0.2 mm coating was flaked-off at the front face within the central region of about 3 cm diameter. This demonstrates the non-compliance of the ceramic coating on a CFC substrate.

The screening tests are accompanied by finite element stress analyses (as far as material data are available) [2] and post test examination which are in progress. They will be continued with further materials and the most promising ones in terms of thermal and mechanical behavior will undergo extended cycling before entering the second phase with bonded samples, which are due for delivery in early 1991.

Sub-Task 2.3: Electron Beam Facility (DIVA)

The NET Team decided to use th existing French electron beam facility as test bed for divertor mock-ups. Therefore work at DIVA was terminated after finishing the report on the pretests performed during the last period [3].

Staff:

G. Class
K. Kleefeldt
K.H. Lang
K. Schramm
E. Wolf

References:

[1] G. Class, unpublished report of KfK.

[2] C. Strobl, K. Kleefeldt, unpublished report of KfK.

[3] K. Kleefeldt, H. Lämmermann, unpublished report of KfK.

Superconducting Magnets

Introduction:

The confinement of plasmas in NET/ITER relies on a superconducting magnet system consisting of 16 D-shaped toroidal field coils, a central solenoid to drive the plasma current and a set of poloidal field coils for plasma stabilization. KfK is together with the NET team and other associated European laboratories involved in the development of these magnet systems. It develops technical conductors up to industrial production feasibility (MTC 1). Components of these conductors, subsize conductor assemblies and test coils are examined for their performances (MOC 1, MOC 2). Materials to be used in coil construction are qualified for their application under cycling load (see NET Study Contracts). Cryogenic loops and components are developed to establish stable forced flow conditions to cool the magnets. An important task consists of upgrading the existing large magnet test facility TOSKA to test prototype coils made out of different industrially manufactured conductors (MTF 2).

The safety of superconducting magnets is analyzed by code development and by experimental studies of effects, potentially initiating a sequence of events leading to an accident (MSA 1).

Transfer of data immediately referring to the NET design are reported as NET study contracts.

MTC 1 Industrial Manufacturing of a Few km of React-and-Wind Nb_3Sn Conductors and of TF Model Coils

Subtask 1.1

For studying both the fabrication procedure and the physical properties of react-and-wind conductors a reduced size NET conductor at the scale of 1 : 1.75 with $I_c < 10$ kA at 12 T has been industrially manufactured by Vacuumschmelze (VAC) and tested at KfK. This subscale conductor, shown in Fig. 1 can be divided into three major components: the core, the electrical stabilizer and the steel jacket.

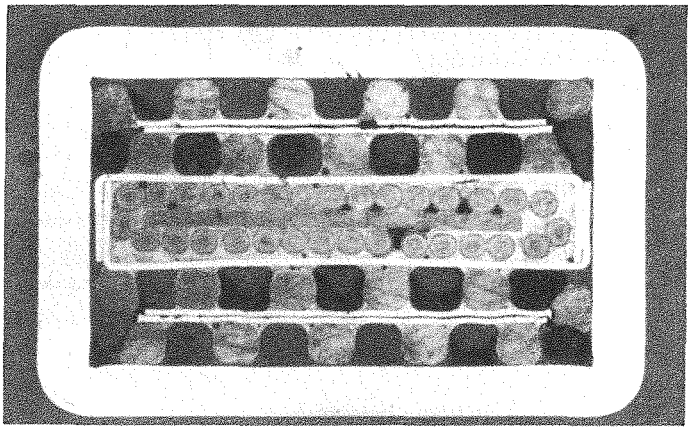

Fig. 1: The NET/KfK subsize conductor (scale 1:1.75) Overall dimensions: 11.4 x 17.6 mm²

The present report describes the effect of axial static and cyclic stresses on the conductor comprising the steel jacket. Due to the relatively short production length (~ 10 m), the steel jacket was not laser welded, but was drawn by Dour Metal on the assembly consisting of the already reacted Nb_3Sn core and the electrical stabilizer soldered to it. All measured samples showed no degradation on j_c after the introduction of the steel jacket: The critical current of the conductor at 12 T was 4.6 kA, i.e. the same as without the steel jacket.

The effect of static and mechanical stresses was measured in the FBI superconductor test facility in our laboratory allowing the testing of short (1.2 m length) straight samples at T = 4.2 K up to 12.5 T under applied forces up to 100 kN. The results are represented in Fig. 2. It is seen that the I_c vs. ε behavior does not vary essentially from that observed on the previous measurements without the steel jacket, the prestrain being now at $\varepsilon_m = 0.35$ %, thus confirming the expectations. This means that in contrast to the cable in conduit process, the steel jacket in the KfK/NET conductor does not lead to an additional prestrain, which would lead to a degradation of I_c. Fig. 2 shows the data on the assembly consisting of core and stabilizer and those on the full conductor comprising the steel jacket.

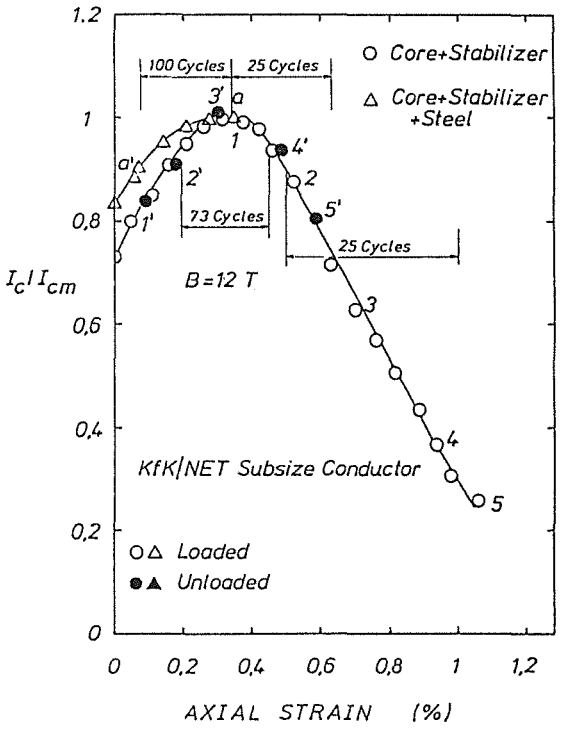

Fig. 2: Normalized critical current for the KfK/NET subsize conductor (the number of cycles is specified for each cyclic strain range)

For the latter case, I_c was measured under static load up to $\varepsilon_a = 0.35$ % (point a, Fig. 2) and without load at the residual strain of 0.06 % (point a'). Then the sample was 100 times cyclically strained between 0.07 and 0.35 % and I_c was tested again under both statically loaded ($\varepsilon_a = 0.35$ %) and unloaded conditions ($\varepsilon_a = 0.07$ %). In all cases no degradation of I_c was observed. At further straining the sample was unfortunately broken due to a failure of the apparatus, but the I_c vs. ε_a characteristics at $\varepsilon_a > \varepsilon_m$ of this sample should be similar to that of the conductor without steel. In any case, this strain region is less important for the practical application of such conductors, which have to be operated in the compressive regime.

Further test with considerably enhanced number of cycles are under preparation for the final NET subsize conductor. It can be anticipated that there will be no influence on I_c as long as the cycling strain remains below the irreversible strain limit. As a summary, the present tests show a very advantageos strain behaviour of I_c for the react and wind NET/KfK conductor.

Staff:

R. Flükiger, W. Goldacker, H. Kiesel, M. Klemm, A. Nyilas, H. Orschulko, H. Raber, W. Specking

MOC 1 Manufacturing and Testing of Short Length Full Size NbTi Conductor (Outer Coil)

Subtask 1.2

The aim of the task is the development, manufacturing and testing of NbTi conductors for the outer poloidal field coils of NET. The development steps are

- Development and testing of a subscale conductor in an overall verification test in a model coil.
- Manufacturing and testing of a PF coil in TORE SUPRA using previous developments and design principles (MOC 2).
- Manufacturing and testing of full size (40 kA) conductor for the outer PF coils of NET (MOC 1).

The first step is being performed at KfK. A superconducting poloidal model coil is under construction. The typical specifications for the operation of a poloidal field coil were taken from TORE SUPRA. The basic design principles of conductor and coil components are relevant for the TORE SUPRA and NET outer PF coils, respectively.

Both tasks MOC 1 and MOC 2 are joint efforts of KfK and CEA.

Conductor

The new set up of the laser beam welding line with a mirror systems for laser beam focusing was taken into operation. A length of 10 m was successfully welded and leak tested. The dynamic behaviour of the welding line was tested by a 30 m dummy length. Indispensible handling operations needed for the fabrication process were trained by the operators. An electronic circuit for switching off the laser beams by an unexpected stop of the feed was installed and tested. Consequently 4 x 150 m round cable were enclosed by simultaneous welding with two laser beams the two U shaped stainless steel profiles (Fig. 1). The leak test was performed using the carrier gas method. At the first attempt two lengths were tight (leak rate: $< 5 \times 10^{-7}$ mbarl/s). From the remaining two other lengths one length had one leak and the other length several. One leak was caused apparently by a disruption of the laser plasma the other ones were probably caused by outgasing by a misorientation of the perforation of the protection tube near the side of one weld seam. The leaks were successfully repaired by spot TIG-welding. Both length were found leak tight within the leak rate given above. The conductors were prepared for shipping and ready for winding the Polo model coil.

An alternative method of fabrication of a conductor jacket by extrusion and butt welding is in progress. After solving some welding problems of the butt weldment (orbital weldment and filling weldment of the corners) three extruded 3 m jacket pieces were welded to 9 m pieces. The 9 m pieces were welded to a 150 m long jacket on a drawing bench where the jacket got simultaneously the final calibration drawing. The butt weldments were x-ray inspected.

Construction of the Polo model coil

The contributions to the construction of the Polo model coil proceed (Fig. 2) with the testing of prototype components. The end termination of the conductor was tested at nitrogen temperatures and pressure cycles up to 2.5 MPa. The soldering quality of the subcables into the copper of the end termination will be checked after dismantling. An inductive

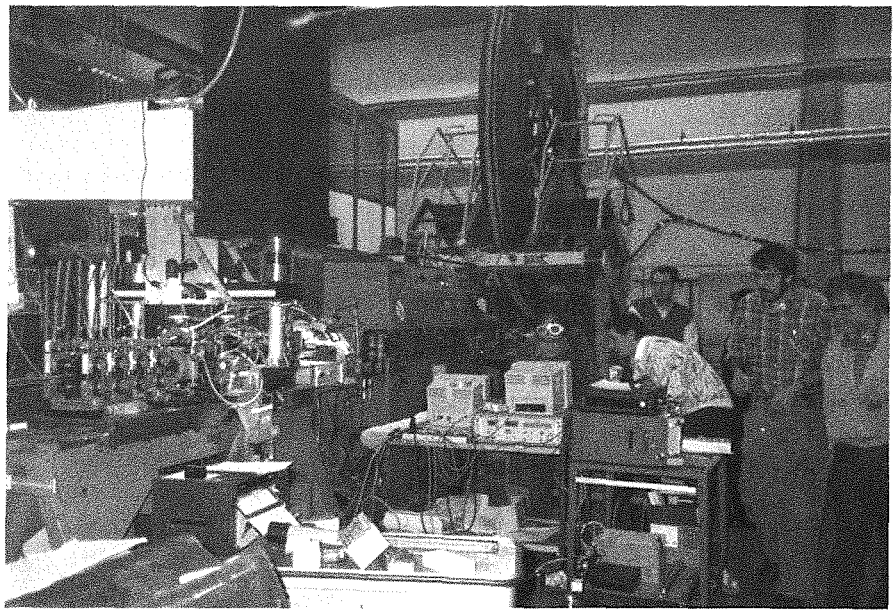

Fig. 1: Fabrication line of the Polo conductor (VAC Hanau, HIL Kleinostheim)

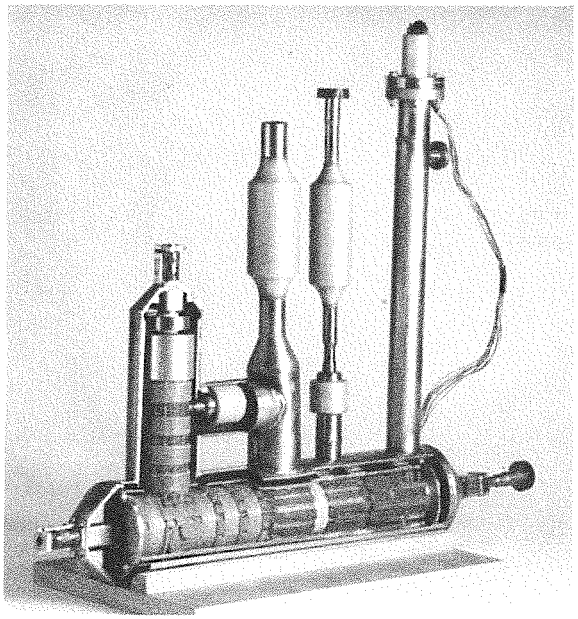

Fig. 2: Prototype of the midpoint connection dismanteled. Three Polo conductors are connected in it with each other (two conductor coming from a pancake, one conductor coming from a current lead). The prototype was manufactured by GEC-Alsthom, Belfort, France.

heater was successfully tested. The saddle coil on the conductor in the connection area drove the conductor normal at frequencies of 400 Hz and power of 4.3 kW peak within some seconds. The series tests of three radial high voltage breaks were successfully finished. After many trials a suitable insulation system and construction for the high voltage instrumentation cables was elaborated. The warm end termination of high voltage instrumentation cable is a vacuum feedthrough which is under construction. A prototype of the cold end connection of the instrumentation cable and its guiding potential surfaces is being under test.

Current leads

Three vapour cooled leads of 23 kA and 22 kV are needed for supplying the Polo model coil with current. The current leads have been designed and developed at KfK. The current leads are being under construction. For the completion of the optimization of current lead the utilization factor of the diameter of the cooling fins were determined (Fig. 3). It was found that the used diameter is an acceptable compromise between the warm end and cold end design (Fig. 4). The diameter of the holes in the cooling fins could be smaller.

All parts of the currents leads are being under construction in the workshops. Heat treatment and brazing experiments of the superconductors in the cold end of the copper busbar were performed. The electrical insulators for the current leads (operation voltage 22 kV) withstood their acceptance test in the factory and were delivered to KfK.

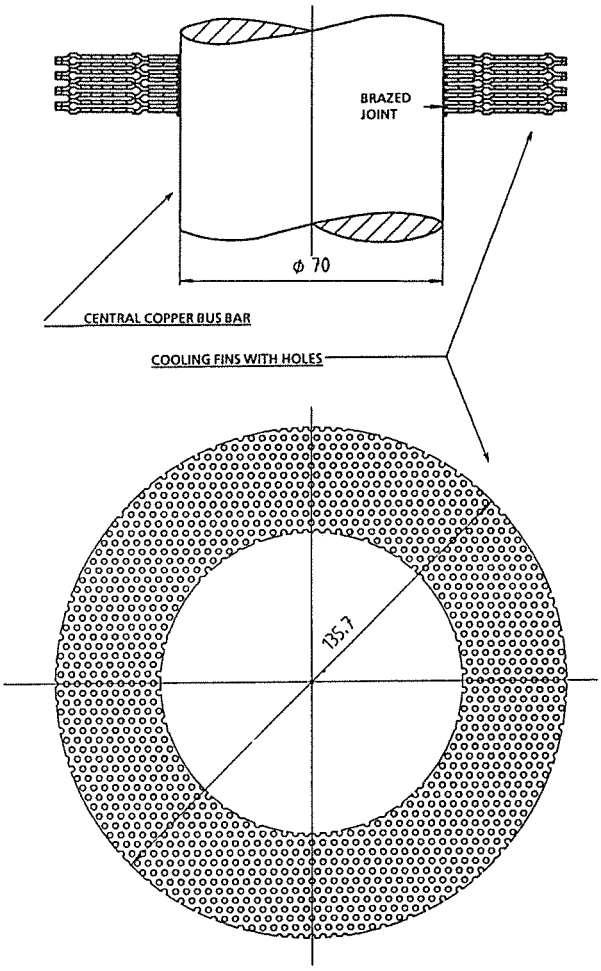

Fig. 3: The construction of the heat exchanger of the Polo current lead.

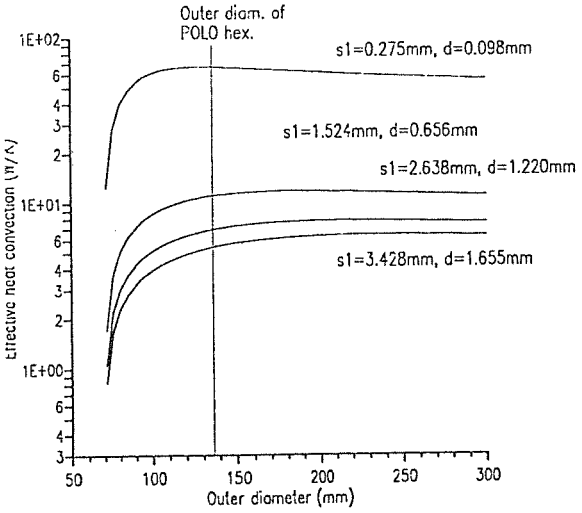

Fig. 4: The effective heat convection as a function of the diameter of the cooling fins. For heat transfer calculations the fin with holes is represented by a wire grid (d: wire diameter, s: wire distance) to use excisting tables for heat transfer coefficients.

Staff:

H. Bayer
I. Donner
P. Duelli
S. Förster
P. Gruber
T. Hardy
W. Heep
R. Heller
U. Jeske
D. Li (till Dec. 11, 1989)
G. Nöther
A. Nyilas
M. Oehmann (till Dec. 1989)
U. Padligur
W. Ratajczak (Jan. 1990)
C. Rieger
K. Rietzschel
L. Schappals
G. Schenk
C. Schmidt
K. Schweikert
E. Specht
H.-J. Spiegel
J. Seibert
F. Süß
M. Süßer
A. Ulbricht
D. Weigert
F. Wüchner
V. Zwecker

MOC 2 Design and Manufacture of One Outer Coil (NbTi) and Installation in TORE SUPRA

Subtasks 2.1 and 2.2

The aim of the task is the development and test of a superconducting poloidal field (PF) coil able to withstand the operating conditions of the outer PF coils of TORE SUPRA in order to validate the design principles for the outer NET PF coils. The TORE SUPRA PF coils will have the objectives to demonstrate the operations due to start up, control and disruptions as well as to confirm on a fairly large scale coil construction processes proposed for NET.

The activity is carried out by CEA. KfK contributes by its experience in the construction of the Polo Model coil and by component development and testing.

The main effort is concentrated on the industrial fabrication of the Polo conductor as described in MOC 1. The applicability of one of the technologies for conductor manufacturing is a key question for TORE SUPRA and NET conductors.

Two current leads designed for the EHS superconducting equilibrium field coil of TORE SUPRA were tested at KfK. The current leads were designed by the CEA Grenoble and optimized for a pulsed current cycle. The test results are being intensively analysed by the code "CURRENT LEAD". The two identical leads showed different losses which were explained by the specified quality of the used resistive copper. The used resistive copper (0.02 - 0.03 weight % content of phosphorus) had no standard specifications. A report on a detailed analysis of the test results is being prepared.

In a joint workshop CEA/KfK held in Karlsruhe the status of the work in the MOC/MIC tasks was discussed. In a technical meeting at April 27, 1990 in Cadarache the high voltage design principles for a current lead were presented by the example of the Polo current lead design. A design for the high voltage insulation of the TORE SUPRA current lead is in progress.

Staff:

H. Bayer
G. Friesinger
R. Heller
U. Jeske
M. Oehmann (till Dec, 1990)
C. Rieger
G. Schenk
C. Schmidt
K. Schweikert
A. Ulbricht

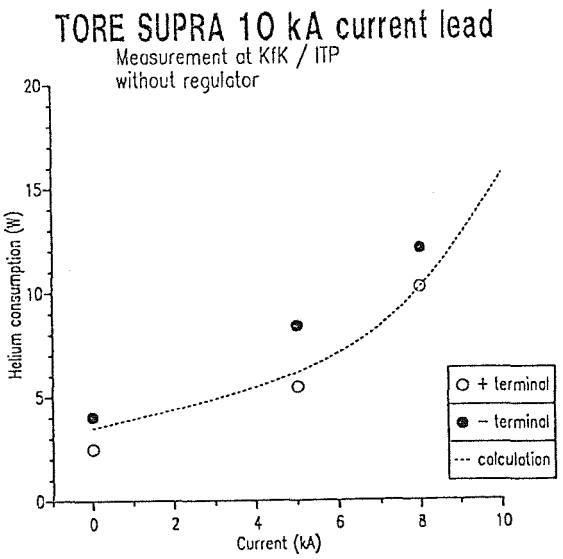

Fig. 1: Measured losses of the two tested current leads in comparison with calculations. The differences can be explained by the resistivity of the resistive copper which has no standard specification covering this special item.

MTF 2 Upgrade of the TOSKA-Facility for Model Coil Testing

Subtask 2.1

The aim of the task is the upgrading of the TOSKA facility for the operation of the EU-LCT coil at 1.8 K up to about 10 T and the testing of NET TF/PF model coils.

TF model coils prepared in task MTC shall be operated in this facility as close as possible to NET conditions in order to prove the development of the entire industrial manufacturing process of the conductors and the test coils.

The upgrading of TOSKA will take place in the following steps

- The EU-LCT coil shall be operated by forced flow superfluid helium at 1.8 K and tested up to the limits of the coil and/or conductor loading capability to prove the possibility of using this successfully tested conductor and coil design for NET-TF coils as a back up solution. The step included a reinforcement of the coil case.

- For first NET model coil tests this coil to give a sufficiently high background field to a neighbouring test coil (TWIN configuration).

- As soon as more model coils will be available a solenoid configuration shall be composed and tested.

The main activitities were the order of the new 2 kW refrigerator, the order of a 50 kA power supply, the start of the installation of the components of the 1.8 K circuit and the design of the reinforcement structure of the EU-LCT coil.

After an intensive period of preparations the new refrigerator was ordered in December 1989 including the building near the TOSKA facility. The He plant (4.4 K equivalent cooling power of 2 kW) is a flexible refrigerator and liquifier and will be capable for the operation of the facility TOSKA-Upgrade and other cryogenic experiments. The basic design refrigeration power will be 700 W at 3.3 K, 400 W at 4.4 K and 1000 at 80 K and 4 g/s liquifaction. Additional power during operation of experiments will be covered by liquid He from the 10000 Liter storage dewar. For the cooldown of large magnet systems the max. cooling power will be about 20 kW between 300 K and 100 K with liquid nitrogen precooling. The manufacturer Linde TVT München in cooperation with Sulzer Brothers, Switzerland, is working on the design of the He plant. The building is under construction. The new refrigerator will be ready for the operation in the middle of 1992.

The control cryostat for the 1.8 K circuit was installed. Later on heliums pumps and heat exchangers will be inserted in the control cryostat. The installation of the valve box and of the cryogenic pipes between control cryostat and the Linde refrigerator is almost finished.

A 50 kA, 30 V unipolar power supply was ordered. Options for upgrading to higher currents (~ 60 kA) and bipolar operation were provided if they are needed later on.

To estimate the necessary reinforcement of the LCT-coil for under increased forces at 1.8 K operation, stress calculations were performed.

The conversion of the NASTRAN Code finite element model of the EU-LCT coil in the ABAQUS code was finished checked and delivered by INTERATOM to KfK.

In test calculations the discrepancies in shear stresses of different finite element models (KfK, INTERATOM) and different element types were investigated. The increasing of shear stresses by the use of the higher order elements is not understood up to now. Equivalent stresses and principal stresses remain almost unchanged.

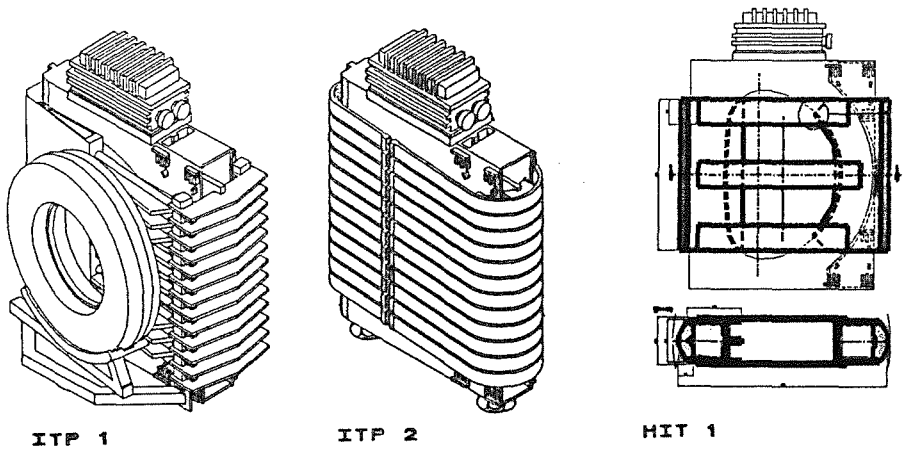

Fig. 1: Three proposals for the reinforcement of the Euratom LCT-coil

The calculations for the eddy currents in the nitrogen shield and vacuum vessel were specified.

In a course finite element model of the EU-LCT coil and its reinforcement structure three reinforcement structures were compared in order to make a preselection for the detailed design (Fig. 1). Comparing stresses in the EU-LCT coil and structure no differences were found to favour one of them. Other criteria like structure installation, lateral support of later model coils and cooling of the structure have to be considered.

Staff:

A. Grünhagen
R. Heller
W. Herz
K. Jentzsch
H. Kapulla
B. Kneifel
W. Maurer
L. Siewerdt
F. Spath
A. Ulbricht
G. Zahn

Subtask 2.2

The aim of the task MTF 2/2 is to develop the basic understanding and the technology for operating large superconducting coils with a forced flow of helium II. KfK activities are concentrated on a) the development of He II coolant loops operated with thermomechanical pumps and b) on an investigation of stability and transient behavior of coils operated with an internal flow of He II.

A thermomechanical pump (Fountain Effect Pump) for operation of the LCT coil with superfluid helium in TOSKA has been designed for the capability of extracting a thermal load of about 70 W from the coil. Fig. 2 shows the cross section of the device. The numeric code for the lay-out of heat exchangers for cooling of forced flow of HeI or He II to the temperature of a surrounding He II pool has been improved. As typical result, Fig. 3 shows the calculated efficiency which can be expected by use of Cu-tube heat exchangers operated at 2.7 K and 2.05 K inlet temperatures. The code HEATEX is now available for the layout of manifold configurations in He II cooling loops.

Staff:

F. Becker
A. Hofmann
B. Vogeley
K. Wagner

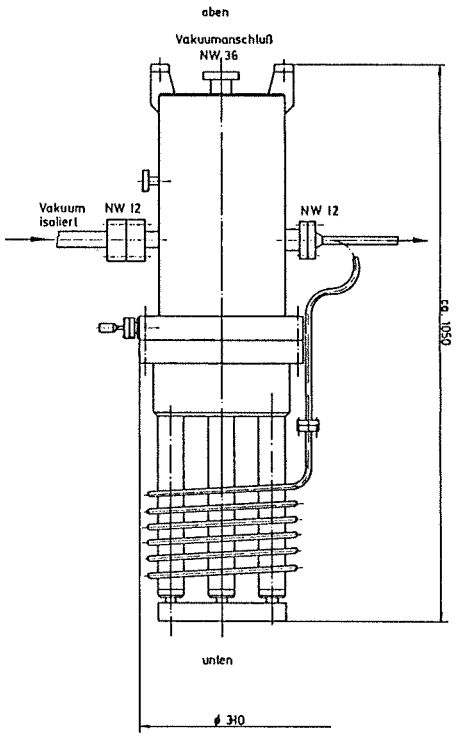

Fig. 2: Cross section of the high capacity thermo-mechanical pump

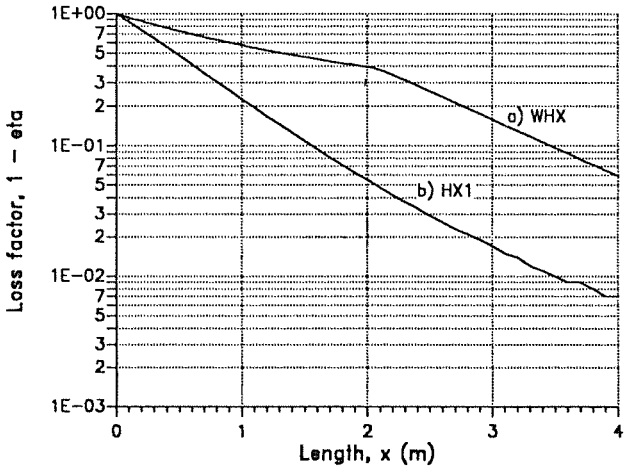

Fig. 3: Efficiency (loss factor) of "shell and tube" heat exchangers operated with forced flow of He II, as example for the applicability of the code HEATEX. WHX and HX1 are heat exchangers.

MSA 1 Safety Related Models and Experiments for the NET Magnets

Subtask 1.1: Code Development

The problem of an uncontrolled growing normal conducting zone investigated at KfK starts from the same sequence as the quench propagation problem investigated at NET. An information and code exchange is therefore performed between these developments to get an overall optimal result. However, some assumptions for a quench analysis are not applicable for an uncontrolled growing normal conducting zone. E.g. the current, the magnetic field and the strains in the winding pack become a function of time.

Since for circuit analysis and magnet field analysis tested codes are available, it was decided to develop the code system „MAGnet System" (MAGS) in order to avoid duplication of work. At KfK a lot of experience and source programs are available from the SSYST code system developement which was used as a starting point for MAGS. The code system separates strictly problem data from physical models. This allows a high flexibility and an easy exchange of updated modules. The modules prepared up to now are the following:

1) GRID

This module generates the geometrical data necessary for the 3D heat balance for the winding pack performed by module HEAT3 and for the thermohydraulic analysis for this winding pack performed by the module COOL. It uses information on the conductor cross section, the subdivision of the coil circumference, the number of windings and pancakes and location and orientation of the coil in the tokamak.

2) BOUND

This module updates all transient boundary conditions for the modules described later.

3) OHM

This module determines which part of the coil has quenched. For nodes that have quenched the heat generated due to ohmic heating is calculated.

4) COOL

This module calculates with a simple model the thermo-hydraulic of the Helium coolant channel. It uses mass flow and temperature inlet conditions and integrates the heat balance assuming a thermodynamic process of constant volume or of constant pressure. Heat transfer coefficients are calculated using Dittus Boelter correlation.

5) HEAT3

This module integrates the heat balance for the solid structures of the winding pack. A 3D anisotropic formulation is used. The winding pack considered can be either a 3D block (no COOL analysis possible) or a one in hand or two in hand wound winding pack. The material properties are prescribed in form of tables for possibly homogenized nodes respectivly meshes. Finite difference formulation is used.

Another version of HEAT3 is under development to provide a tool for more detailed investigations and checks of HEAT3 and to introduce more efficient integration techniques to reduce computing time. A steady state 3D and a transient 2D version of the code is available.

6) CONTROL

This module determines the time step size for the implicit integration.

7) MSCAP

This code calulates according to the resistance in the coil pack or possibly switched in dump resistors the coil current. This code was developed at EG&G Idaho [1].

8) EFFI

This code calculates the magnetic field for each node considered in the analysis. This code was developed in Lawrence Livermore National Laboratory [2].

With MAGS it is possible to model the two circuits of the TF coil system of ITER. It must be recoginzed however that this needs a lot of nodes so that for each circuit one coil should be modelled in detail only. First calculations indicate that even this probably will not be necessary. The quench propagation expands primarely within a pancake so that not all pancakes must be considered at once.

The typical procedure of MAGS for the integration of one step, in time, is the following sequence of module calls:

BOUND
OHM
COOL
HEAT3
CONTROL.

The module CONTROL checks whether the integration criteria are fulfilled or not. If they are fulfilled then the next step is taken. If not the step is repeated or even, the step size is reduced. The modules MSCAP and EFFI are called at a lower frequency because the change in current and field does not need so fine time steps as needed for the heat balance.

To get an idea how to homogenize the conductor for MAGS the adiabatic heatup of the conductor, presently proposed by NET/ITER, was investigated in a parametric study. For the conductor the nominal current of 42.1 kA is assumed. For the resistance only copper at 10 T is considered. The symmetric quadrant of conductor cross section was modelled using a one

node, a two by two node and a three by three node representation. For the one node model the following cases are calculated:

1) heatup of the cable space only
2) like 1) but capacity of cable steel jacket considered
3) like 2) but capacity of isolation considered.

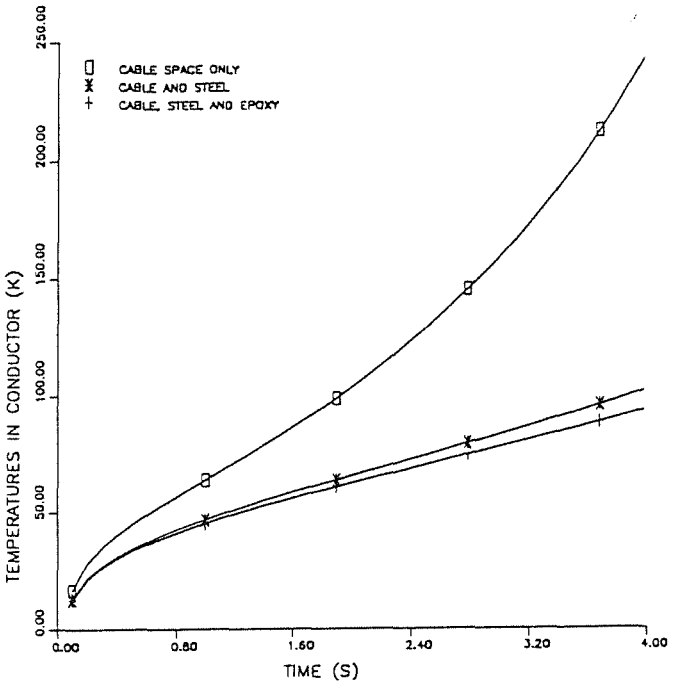

Fig. 1: Conductor temperature as a function of time, adiabatic model one node only

The results are given in Fig. 1. One can see that having only the heat capacity of the cable space the temperature rises beyond 200 K within 4 seconds. If the capacity of steel and epoxy is added the temperature rises up to 100 K roughly. In this difference, however, is included that for higher temperatures the resistance of copper and so the introduced power is higher.

In the two by two node model steel and epoxy are homogenized and represented as one material. Fig. 2 shows the results of this calculation. It can be seen that the rise in the cable space again is very steep and reaches more than 200 K.

In a three by three node model steel and isolation are represented as in reality. These results are given in Fig. 3. We find there now a medium temperature for the cable space of about 130 K after 4 seconds.

This study shows the importance of the steel jacket for the temperature history and power generated in the cable space. This is not only a question of the presence of the steel, it is also a question of a good bonding between the cable space and the jacket. For the calculations with the code system MAGS we can conclude that a homogenization as in the two by two nodes model cannot be used. I.e. to represent a cable cross

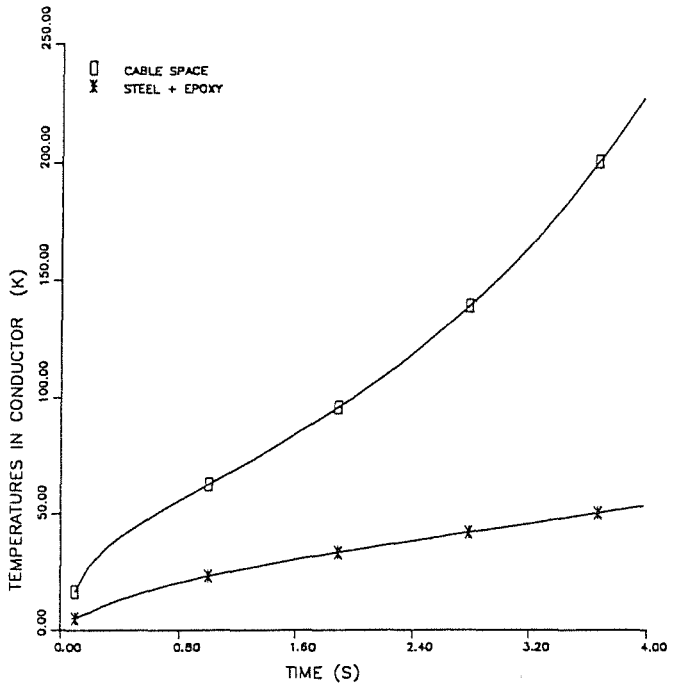

Fig. 2: Conductor temperature as a function of time, adiabatic model two by two nodes jacket and insulation homogenized

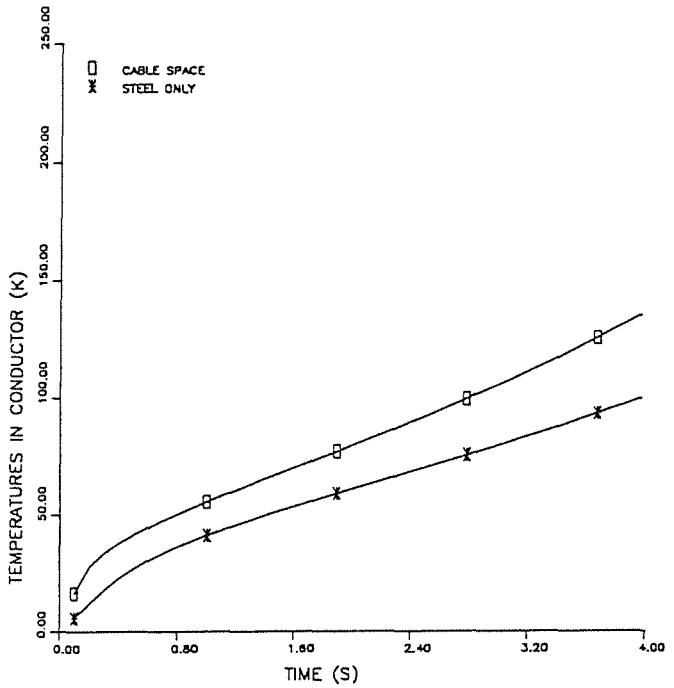

Fig. 3: Conductor temperature as a function of time, adiabatic model three by three nodes

section in MAGS for a cable cross section instead of three by three nodes four by four nodes are necessary.

Staff:

R. Meyder
Y. Hoang

References:

[1] H. Kraus, J. Jones: Hybrid Finite Difference / Finite Element Solution Method Development for Non-linear Superconducting Magnet and Electrical Circuit Breakdown Transient Analysis.
International Journal for Numerical Methods in Engineering Vol 23, p.1003-1022 (1986).

[2] S. Sackett: Calculation of Electromagnetic Fields and Forces in Coil Systems of Arbitrary Geometry.
Proc. 6. Symp.on Engineering Problems of Fusion Research, (San Diego, Ca 1975) IEEE No. 75CH1097-5-NPS, p 935-939.

Subtask 1.2: Experimental Investigations

The experimental investigations of arcs supplied by the magnet's energy have been finished successfully. In the last series of experiments the behaviour of arcs was investigated burning under spatial restrictions and exposed to a high magnetic field, i.e. under conditions like in a winding pack. For this purpose the arc chamber of massive copper was placed into or in front of the magnet PUMA, respectively. Moreover, the behaviour and the I-V-characteristics of arcs with a current up to 5000 A and arcs with a current density up to 30 A/mm^2 were studied.

The test arrangement made feasible the exposition of the arc to a perpendicular magnetic field of about 3 T. The high magnetic force pressed the arc against one of chamber's walls reducing dimensions and increasing cooling of the arc. Fig. 4

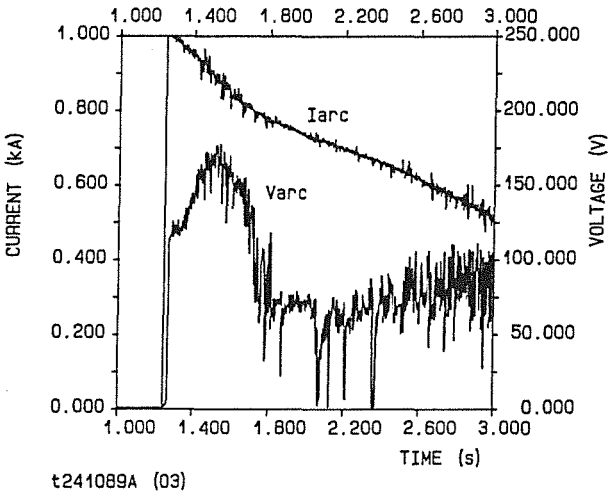

Fig. 4: Current and voltage transients for an arc exposed to a magnetic field of 1 T

shows the variation of arcing current and corresponding voltage with time. The arc's response to the action of the magnetic field was an increase of the burning voltage by about 30÷40 V, which can be seen regarding the higher initial voltage of 120 V. The rapid increase of the burning voltage to 170 V is caused by the intensive interactions of the arc with chamber's walls, among others. In addition, pinching of the arc by the magnetic field led to localized burning and destruction of the chamber in some preferred direction as can be seen in Fig. 5. This figure shows such a chamber after

Fig. 5: Arcing chamber after burning of an arc of 1000 A in the magnetic field of 1 T

burning of an arc of 1000 A exposed to a field of 1 T. The magnetic force acted on the arc in the direction perpendicular to the plane of the picture.

The results of the TESPE-S safety investigations are reproducible and explainable. Collected data make possible to transfer the results to other magnet systems like NET or ITER and to make a prediction of their behaviour in case of disturbances like shorts and arcs. A complete evaluation has to be done, though.

Staff:

P. Duelli
K.P. Jüngst
H. Kiesel
H. Kronhardt
G. Obermaier
M. Oehmann
J. Seibert
E. Süss

NET-Technology Tasks and Study Contracts Related to Vacuum and Fuel Cycle

Introduction:

Within the various elements of the Fuel Cycle development program KfK is dealing primarily with the plasma vacuum pumping and plasma exhaust processing issues. The Tritium Laboratory Karlsruhe (TLK) will be available not only for those experiments which need verification with NET-relevant amounts of tritium, but also for testing of prototype components and systems at a later stage of development.

One preferred option of vacuum pumping during burn and dwell phases, the cryocompound pumping method, is investigated in depth in a number of related subtasks beginning with the determination of suitable substrate-sorbate combinations and ending with helium pumping and endurance tests on medium-size panels under NET-simulated conditions. In addition provisions are being made to use the existing pumping chamber for a modified type of cryopumping with Argon spraying for helium trapping (TPV 2).

The number of brazed or cemented cryosorbent specimens surviving the stringent cycling between boiling He temperature (4K) and reactivation at 150 °C (the normal regeneration temperature is only ~ 90 K) has been surprisingly high (TPV 2.1).

Also the sorption capacity for helium as a measure for the tolerable operation period between two regenerations phases seems not to impose major restrictions. A first pumping panel has been put into operation for a number of cycles simulating 1 week of NET operation. Up to now 60 % of the target number have been reached without any deterioration in performance, and the pumping speed indicates a sticking coefficient near to the theoretical maximum (TPV 2.2).

A side problem in exhaust pumping is the appearance of dust mainly from plasma / wall interaction. In order to study the entrainment and deposition behaviour of solid particles during normal pumping and sudden venting an apparatus has been built up which now yields first results. In addition the consequences of dust propagation on valve tightness and suitable countermeasures, e.g. electrofiltering, shall be investigated (TPV 1.1).

The technical work on the NET-Vacuum System has been complemented by Study Contracts one of which has only recently been agreed. Monte Carlo calculations have been carried out on the transmission of the divertor ducts and the overall vacuum flow including cryopumps or turbomolecular pumps. These studies will be continued taking the directed molecular flow during burn time into account (394/89-8/FU-D/NET).

The new Study Contract will comprise elaboration of NET-Vacuum System prototype components and follow-up of industry study and development contracts related to these components.

A broad experimental and engineering program is devoted to plasma exhaust processing (TEP 1-3). A catalytic cracking process in conjunction with Pd/Ag permeators has been developed for an efficient recycling of tritium and deuterium from the plasma vessel. The concept has been supplemented with a water/gas shift reactor capable of coping with an increased humidity level during pump down phases.

After investigating the different steps of the process an engineering design for a NET-scale system has been carried out the results of which are documented in the final report (322/88-8/FU-D/NET), and a test loop simulating 1/8 of NET throughput has been installed for cold tests. An equivalent loop for tritium testing has been specified for operation in the TLK, and most of the components have been ordered meanwhile (TEP 2.2).

According to NET design concepts it may be preferable to insert cryosorption of impurities as a first step in the exhaust processing system. Systematic studies of adsorption capacities and cosorption effects have been started in a loop with a cryostat as the central component. Various analytical techniques are available for chemical and isotopical analyses (TEP 1.2).

The long-term performance of a Pd/Ag-permeator as a key component of tritium processing will be studied in the TLK in a separate loop. A specification and safety assessment of the permeator test has been elaborated, and almost all components have been ordered. Tests are onging on the available spiral vane forepumps (TEP 2.1).

An alternative option for impurity removal from the exhaust gas has been studied making use of hot metal getters. Different commercial getter alloys have been tested in the existing loop with various gas mixtures and mass flows, and concepts have been developed how to cope with methane which is always the most difficult species to decompose (TEP 2.3).

Because of the getter consumption problem this concept option will not be pursued, and experimental work, therefore, be terminated soon. Preparations are being made to use the existing loop for detritiation of large volumes with relatively low tritium contents as to be anticipated in secondary containment atmospheres (TEP 3.3).

ZrCo has been investigated for tritium storage in the hydride form at ambient temperatures. This alloy has some favourable features as compared to uranium and shall therefore, after completion of comprehensive cold tests, undergo aging and endurance tests in the TLK (TEP 3.1).

TPV 1 Development of Solid Particle Separators for Plasma Exhaust

Solid particles generated during plasma/wall interaction can be transported into the plasma exhaust pumping system where they can influence the operation of the vacuum components (valves, pumps). The objectives of the task are to investigate the transport of solid particles during normal operation and during accidents and to develop solid particle separators for installation in front of the plasma exhaust pumping system.

To investigate particle transport in steady-state gas flow such as in the burn or dwell mode, and to measure the ratio of resuspension and the transport properties under non-steady-state conditions, such as sudden venting or rupture of a coolant pipe, experiments will be performed in a horizontal tube of 100 mm inner diameter.

This test equipment is called SPARTA (Solid Particle Transport).

The test equipment is represented in Fig. 1. This is the arrangement of components, seen from left to right in direction of flow:

- Pneurop measuring dome for gas inlet, pressure measurement, and for flow homogenisation by means of reduction of the cross-sectional area.
- Inlet section made of stainless steel, 0.1 m dia., 3 m length, in order to obtain a developed flow in the test section.
- Dust dosage bin with pressure equalisation towards the pipe (bellows). It accommodates the dust dosage device for dosing graphite dust of 1 - 200 µm grain size with the solid particle flow being adjustable. The dust drops through a double diaphragm configuration in the T-piece into the test section made of glass, D = 0.108 m, 1 m length (capable of modification to 0.5 m length).
- The bottom is covered by a probe equipped with object holders on which the dust settles in direction of flow.
- The test section ends in the equalising tank of 99 l volume (capable of modification to 95 l) with a three-stage pumping set (1000 m^3/h, not represented in the figure) connected.
- The equalising tank consists in a sink into which the gas having passed the test section can flow in sudden venting experiments.

All components except for the primary Roots pump, are installed.

With the two-stage forepump the equipment has been set working for the time being and experiments have begun on dust transport in horizontal pipe flow at low atmospheric pressure.

By means of the dust dosing device a sufficient portion of nonagglomerated particles have been dosed into the test section and the distances covered by them have been evaluated.

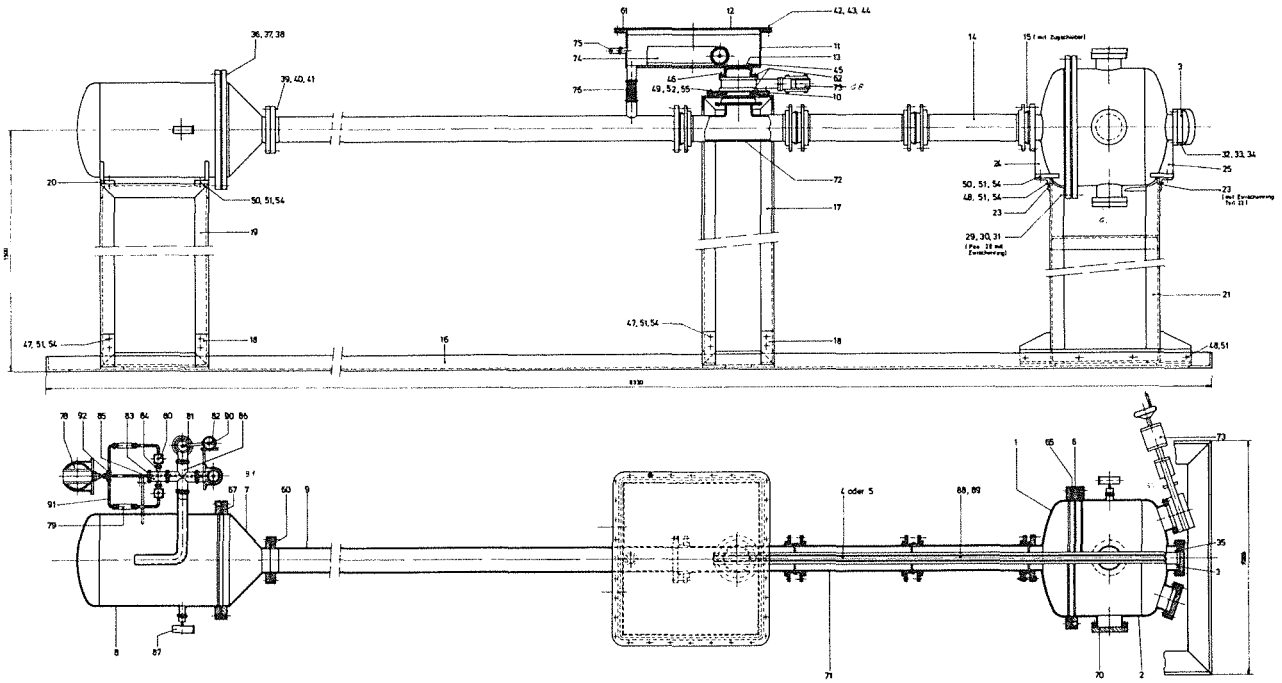

Fig 1: SPARTA Test equipment

The particles which settled on glass-made object holders provided on the probe have been evaluated under the microscope after dismounting of the probe.

The following provisional results have been obtained for the transport path of UF2 99.5 graphite dust, x = 1.8 µm (x = mean grain size according to the analysis of particles settled in the field of gravity, performed by the supplier):

Pressure P	0.1 mbar	7×10^{-2} mbar
Flow Q	0.5 mbar l/s	0.25 mbar l/s
Mean flow velocity v	0.54 m/s	0.39 m/s
Measured length of transport path	> 0.76 m	0.38 m

For comparison, the calculated length of transport path $L_{calc.}$ of an ideally spherical particle, x = 1.8 µm, is indicated in the following table for the same conditions:

Terminal setting velocity w_s	0.24 m/s	0.34 m/s
$L_{calc.} = (v/w_s) \cdot D$ with D = 0.108 m	0.24 m	0.12 m

The difference between the calculated and the measured transport path is under investigation.

The following influences are under consideration:

- Influence of the suspended dust particles (giant molecules) on the viscosity of the gas
- saltation
- grain shape effects
- electrostatic effects

In autumn 1989, KfK was requested by the NET team to perform the "Dust compatibility testing of Viton sealed ND 100 valves" in the SPARTA test equipment. In the course of testing the dual-seal gate valves, series 10, supplied by VAT, are to be subjected to 10 000 closing cycles in different orientations and under the impact of graphite dust loading; after 500 closing cycles the leak rate will have to be measured. For this a technical concept has been designed and a test programme developed.

Staff:

W. Höhn
M. Lieberknecht
D. Perinic

TPV 2 Optimization of Cryogenic Vacuum Pumping of Helium

This task is aimed at developing and optimizing cryogenic vacuum pumping of plasma exhaust containing helium. To develop cryosorption panels, a variety of eligible material combinations for helium cryosorption will be tested on a reduced scale. The best suited technical solutions will be optimized on a technical scale under simulated NET operating conditions. As a result of these investigations design data and requirements will be obtained with respect to the operation of the compound cryopumps to be used in the plasma exhaust pumping system of a fusion machine.

Status of work at the HELENE facility

As mentioned in previous reports, the HELENE [3] facility was built with a view to carry out cryosorption capacity measurements of the specimens (about 350 specimens) produced within the framework of this project. After the completion of the first test series in this facility, the original scope of testing had to be extended due to new requirements imposed by the NET team.

The original task of the HELENE facility consisted in the determination of those material combinations (sorbent-bonding material) which can be used for the finalizing tests in the TITAN [1] facility from the number of specimens which had survived the thermal cyclic loadings in the TARZAN [2] facility and on the basis of the resulting differences in the cryosorption capacities. Thus, only a limited number of specimens (D=400 mm) would have to be produced for the pumping speed measurements. With the adoption of a new concept for the torus pumping system of NET/ITER, in which pumping time of the cryopumps between the regeneration cycles had been reduced to t=80 min, pumping speed of the panels gained importance compared to sorption capacity. The experimental programme for the HELENE facility was modified such that these novel questions could be answered.

This means that in addition to the sorption capacities also the pumping speeds of the individual specimens had to be measured. These experiments were planned to be carried out taking into account the NET boundary conditions with respect to the flows to be expected, the gas composition and the operating temperature as well as the operating parameters specified for the HELENE facility, such as minimum consumption of refrigerant and minimization of the scheduled test periods in order to be able to investigate the large number of specimens within the shortest possible period of time. For further experiments at the TITAN test facility, the specimen matrix was to be reduced to a reasonable size with the criteria of selection of pumping speed and pumping capacity applied.

To meet the new requirements, the following details had to be taken into account:

- Attainment of the starting pressure of $p < 10^{-4}$ mbar;
- attainment of the corresponding starting temperature of $T_{LHe} = 4.2$ K;
- supply of the test gas (helium gas) under conditions similar to those in NET, i.e., within the range of $10^{-4} < Q$ [mbarl/s] $< 10^{-2}$;
- reduction of the scope of the test matrix such that a representative number of 50 specimens is included.

The starting pressure attained using the original test conduct was far below the required value of $p < 10^{-4}$ mbar and, hence, did not cause any problems in the course of this experiment. To meet the second new requirement imposed, the rig for analysis had to be modified.

It was the objective of this modification of the analytical rig to achieve an optimum thermal contact and, thus, to attain the T_{LHe} temperature required as early as at pressures of $p < 10^{-4}$ mbar. The design of the new rig for analysis was to take into account the aspects of manufacture, handling as well as of test engineering. In the course of the test series, several designs were examined for suitability. In all versions of immersion rigs variations of temperature transducer fixings were tested in addition to the holding units prepared in accordance with standard specifications for the planned temperature transducers. These variations included among others the extension and improved contacting of the temperature measurement line, the reduction of the measuring current of the temperature sensor with a view to minimizing the supply of thermal power and consequently falsification of the measurement as well as thermal contacting of the sensor itself by clamping or cementing into the respective holding unit. The improvements of the end temperatures were mainly achieved by the improved contacting or pressing of the specimen disks to the bottom plate of the immersion rig. The version shown in Fig. 1 was manufactured on the basis of the experience gained in the experiments using the different designs. The specimen is fixed in a specimen holder. Together with this holding unit the specimen can be screwed into the trapezoidal thread located at the bottom of the immersion tube using an assembly and clamping device. After the application of a torque the specimen can be pressed to the bottom plate. By partitioning of the trapezoidal thread and the insertion of a steel ring between the lower and the upper part of the copper made holder for the temperature sensors and the specimen disk and the clamping device and baffle, respectively, thermal decoupling was improved. As a result, the thermal power supplied could be better released to the liquid helium bath.

For the supply of the helium gas in the small amounts required, the dosage system which had been provided for the TITAN test facility had to be used. This dosage system allows dosage to be set in the range of $10^{-4} < Q$ [mbarl/s] < 16.6.

Parallel to these activities, the test matrix was reduced to a scope of about 50 specimens still to be investigated. Here, the

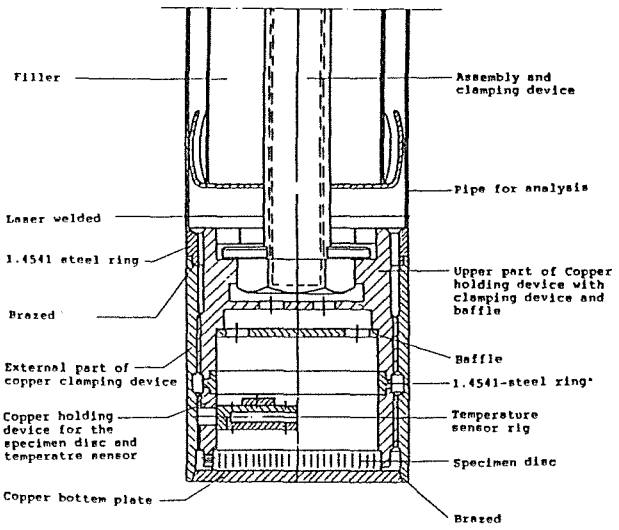

Fig. 1: Pipe for analysis with screwed in specimen holder (second version)

experience gained in the previous test series was taken into consideration.

In the course of the optimization tests at the HELENE facility, attempts were made to fulfil the experimental boundary conditions with respect to specimen contacting and test gas dosage. Due to the advantages offered with regard to process organisation, the pipe for analysis with the specimen holder screwed into it was chosen for further application. As a result of additional improvements of the design and the measurement technique, the requirements imposed by the NET team could be met.

On account of the good temperature following behaviour of the specimen temperature during cooling to the required liquid helium temperature T_{LHe}, dosage could be reduced to the NET-similar quantity of $10^{-4} < Q$ [mbarl/s] $< 10^{-2}$ as a further optimization with respect to test engineering. Contrary to the previous test conduct, the conduct now adopted can be divided into the following steps:

- Reactivation of the sorbent at $p < 10^{-3}$ mbar and $150 < T$ [°C] < 300;
- stepwise cooling of the immersion rig to T_{LN} and T_{LHe}, respectively;
- dosage of the test gas;
  - dosage of $Q \sim 10^{-4}$ mbarl/s with the duration of t = 90 min;
  - dosage of $Q \sim 10^{-2}$ mbarl/s with the duration of t = 60 min;
- heating of the immersion rig to T_{RT}.

On the basis of the experimental results, statements can be made on the pumping speed of the respective specimen in the pressure range of $p < 10^{-4}$ mbar. Furthermore, it is possible to draw comparisons between the sorption capacities as a function of the dosed volume of gas (m_{dos}) at high pressures.

After the completion of the first tests which had taken into account the new test parameters and test conduct, the HELENE facility was prepared for series operation with two rigs for analysis. Then, series operation was taken up with the investigations of the specimens included in the test matrix.

The results of the first test series are listed in Table 1. The pumping speed values have been calculated for the position in front of the double baffle which screens off the sorption specimen.

Table 1: Results of pumping speed and cryosorption capacity screening tests.

Specimen no.	427	566	504	680
Sorbent	Degusorb F30/470	Degusorb F12/470	m - sieve 5A Merck	Degusorb C-25
Bonding	Plasma sprayed copper	Thermo-guss	Thermo-guss	Fortafix
Start pressure [mbar]	6.6×10^{-5}	8.3×10^{-5}	1.1×10^{-5}	2×10^{-5}
End pressure [mbar] after 90 min	4×10^{-4}	3.5×10^{-3}	1.3×10^{-5}	7.2×10^{-5}
Pumping speed [l/s] after 90 min	1.30	0.2	3.63	4.54
Helium mass adsorbed [mbarl] [90 min]	2.80	3.2	2.51	2.26

Helium thoughput:	$4\text{-}5 \times 10^{-4}$ mbarl/s
Metering time:	90 min
Specimen temperature:	4.2 K
Substrate:	copper
Diameter specimens:	Ø 50 mm

The noted values refer to the projected surface of the sorption specimen.

Helium pipeline

At the moment, the HELENE and TITAN test facilities are operated with liquid helium (LHe) supplied from outside. For economical reasons, future LHe supply of the above facilities shall take place using the helium liquefier of the ITP (KfK Institute for Technical Physics). For this purpose, the helium gas has to be led back into the liquefier via a pipeline. This pipeline is planned to consist of three sections:

1. Connecting pipe between the TITAN and HELENE exhaust system and the junction point of the underground pipeline;

2. underground pipeline between the KfK buildings no. 602 and no. 406;

3. connecting pipe between the underground pipeline and the ITP gas storage tanks.

According to our cost analysis of internal LHe supply, amortisation of the LHe pipeline will have been achieved after a period of T = 1.5 a at the most.

After the completion of the conceptual phase and the preparation of a specification the application was filled for the construction of the underground pipeline (section 2). Eight companies were invited to submit a tender for the construction of the pipes described in the sections 1 and 3. Five companies actually have submitted tenders which are being examined at the moment.

Status of work at the TITAN facility

After the damage caused in transit had been repaired, the cryopump was connected to the test facility.On November 29, 1989 it was filled with liquid helium for the first time. Then operational tests were carried out.

Four cryopanels, 400 mm dia., have been manufactured with a view to recording the characteristic line of the pump. The material combinations have been taken from the HELENE screening tests. Table 2 is a survey of all panels fabricated.

Table 2: Adsorption panels for TITAN

Panel No.	1	2	3	4
Sorbent	PICA TA spec 6x35	Degusorb C25	Degusorb AS16/450	Degusorb C25
Sorbent mass [g]	237	107	221	38.1
Bonding type	activated braze Degussa 7200 Powder < 100 µm	activated braze Degussa 7200 Powder < 100 µm	activated braze Degussa 7200 Powder < 100 µm	Thermo-guß 2000 + Cu-Powder
Bonding mass [g]	124	184	143	204.3
Substrate	Copper	Copper	Copper	Copper

The surface achieved for panel no. 3 is dense and homogeneous with no solder residue entrapments in the surface-near pores. This panel had been selected for the first pumping tests. The behaviour with respect to temperature shocks was verified by immersion into LN and quick heating to 30°C. At the end of three cycles no peeling off or rupture of the adsorber coating has been observed.

Tests with different He-throughputs were performed in order to be able to assess the pumping speed. For this, the adsorber panel was heated to 150 °C before the test. The initial vacuum, measured with a Bayard-Alpert ionisation manometer, was 1.3 x 10^{-8} mbar. The He-throughputs with the related pressures and the resulting pumping speeds have been entered in Tab. 3.

A test comprising 84 cycles has started with the objective of studying the "poisoning behaviour" of the adsorber panel which had been polluted by impurities present in the NET/ITER exhaust. 84 cycles simulate permanent operation of one week duration of the pump under NET/ITER boundary conditions. For this, the facility is cooled down from LN-temperature to LHe-temperature within 30 minutes. Then a NET/ITER relevant gas mixture is metered in within 80 minutes. The throughput of 370 standard cm^3 simulates the NET/ITER exhaust rate, scaled with respect to the suction area of the TITAN pump in the Pneurop dome. After loading the LHe-tanks are heated to 90 K within about ten minutes. After another five minutes the recipient is evacuated. Then the pump is ready for the next cycle. The process gas used is a mixture consisting of 0.113 % Ar, 0.112 % CO_2, 0.225 % CO, 0.194 % N_2, 0.236 % O_2, 1.44 % CH_4, 5.02 % He; remainder H_2. Table 3 shows the range of pressures and the associated pumping speeds for the initial 30 tests cycles. No reduction of the pumping speed due to poisoning has been observed so far.

Table 3: Preliminary results of the pumping tests

Kind of gas	He	He	He	Mixture ++
Throughput [standard cm^3/min]	5	50	500	370
Pressure during dosage [mbar]	$2.4x10^{-5}$	$2.5x10^{-4}$	$2x10^{-3}$ ÷ $1x10^{-2}$	$1.1x10^{-3}$ ÷ $1.9x10^{-3}$
Pumping speed + [l s^{-1} cm^{-2}]	0.9	0.87	1.1 ÷ 0.22	1.46 ÷ 0.84
Loading capacity [mbarl]	0 ÷ 150	150 ÷ 1650	1650 ÷ 21650	0 ÷ 29600
Pressure before dosage at LN-temp. [mbar]	$1.3x10^{-8}$	not heated up before test	not heated up before test	$3.9x10^{-6}$ ÷ $1x10^{-4}$
Pressure before dosage at LHe-temp. [mbar]	$9.4x10^{-9}$	$1.7x10^{-8}$	$1.4x10^{-7}$	$4.8x10^{-6}$
Pressure after dosage at LHe-temp. [mbar]	$1.7x10^{-8}$	$1.4x10^{-7}$	$8.5x10^{-4}$	$1x10^{-4}$

\+ related to the suction area (700 mmØ)

++ composition see text

Staff:

H. Haas
J. Hanauer
W. Höhn
B. Kammerer
U. Kirchhof
H. Lukitsch
A. Mack
D. Perinic
R. Rinderspacher
D. Zimmerlin

---

1) TITAN = Versuchsanlage für Tieftemperatur-Adsorption (test facility for cryo-adsorption)
2) TARZAN = Temperatur-Zyklierungs-Anlage (thermal cycling facility)
3) HELENE = Helium-Kryosorptions-Experimente (helium cryosorption experiments)

TEP 2 Plasma Exhaust Processing Alternative Option

Subtask 2.1

Among the techniques proposed for the separation of hydrogen isotopes from impurities the use of a selective palladium/silver permeator is attractive because i) it involves proven technology, ii) the steady state tritium inventory during the separation is very low, iii) the purity of the permeated hydrogen isotopes is extremely high, and iv) no process specific waste is produced. In view of the above a process concept based on hydrogen permeation in combination with catalytic steps has been proposed for the reprocessing of the primary vacuum exhaust of the NET II fusion reactor during burn & dwell as well as for the recovery of tritium from waste gases produced during bake-out, glow discharge cleaning, carbonization, or pump down. A technical experiment for the integral demonstration of this process is in preparation. Paralell to this effort it is essential to show that a commercial permeator is capable of withstanding a long period of continuous operation in the presence of tritium as well as of the impurities characteristic to the fusion fuel cycle.

In the following an experiment to be implemented in the Tritium Laboratory Karlsruhe (TLK) is described, which was mainly designed to test the performance of a modified commercial palladium/silver permeator during continuous operation over a period of at least one year. In this experiment the conditions of a NET fuel processing system will be simulated with a hydrogen isotope/impurity mixture containing relevant amounts of tritium. The experiment will also provide information on the long-term performance with tritium of auxiliary equipment such as circulation pumps, pressure sensors, temperature sensors, valves and safety devices, as well as of in-line infrared process control analytics presently under development.

In the closed loop experiment, described herein by the acronym PETRA (Permeation Test Radiochemistry), gaseous hydrogen isotopes will be continously separated from an impurity mixture via a permeator. To accomplish continuous operation the bleed stream from the permeator is reunited with the impurity stream in a buffer vessel. Under these conditions a steady state concentration of hydrogen isotopes will establish in the permeation membranes and also, due to the decay of tritium, the transmutation product helium will build-up inside of the membranes. Because helium is only slightly soluble in the palladium/silver alloy, the formation of small bubbles of this gas in the metal alloy membrane can occur possibly causing loss of mechanical integrity and/or permeation capability. The performance of the permeator will be evaluated by periodic permeation tests and an examination of the dismantled permeator after completion of the experiment.

A storage bed containing ZrCo tritide will be used for the supply of tritium to the experiment. The gas will be released into the previously evacuated buffer vessel of the loop by heating the ZrCo tritide in the storage bed up to about 400 °C.

The ZrCo bed is also employed to stop the experiment at any given time. When this is required, the gas mixture (Q_2, He, CO, CO_2, CQ_4; Q = H, T) is circulated through the storage bed, which is kept at room temperature. Under these conditions gaseous hydrogen is removed quantitatively by the ZrCo alloy; the other impurities are transported unaltered through the bed. Tritiated methane, the only remaining tritium containing impurity, is then passed through a nickel catalyst bed heated up to 500 °C. At his temperature the hydrocarbon decomposes up to thermodynamic equilibrium into carbon and free hydrogen. If the reacted gas is again sent through the passed getter bed it will be once more depleted of elemental hydrogen. By circulation of the gas mixture for an appropiate period of time it is possible to trap all the hydrogen isotopes in the storage bed and bring the experiment into a safe condition.

For process surveillance two in-line infrared spectrophotometers will be employed. One infrared analyzer (MEKOS), capable of detecting CO, CO_2, and CH_4 will analyse the gas composition of the permeator bleed stream. In this way changes in the relative concentrations of the impurities caused by catalytic reactions and/or radiochemical reactions during the course of the experiment can be measured. The other IR analyzer (SPECTRAN), which is designed for the specific analysis of CO, is used to detect a loss of integrity of the permeation membrane. Experimentally it was shown that these infrared analyzers are highly sensitive and stable over a long period of time (see Fig. 1 and 2).

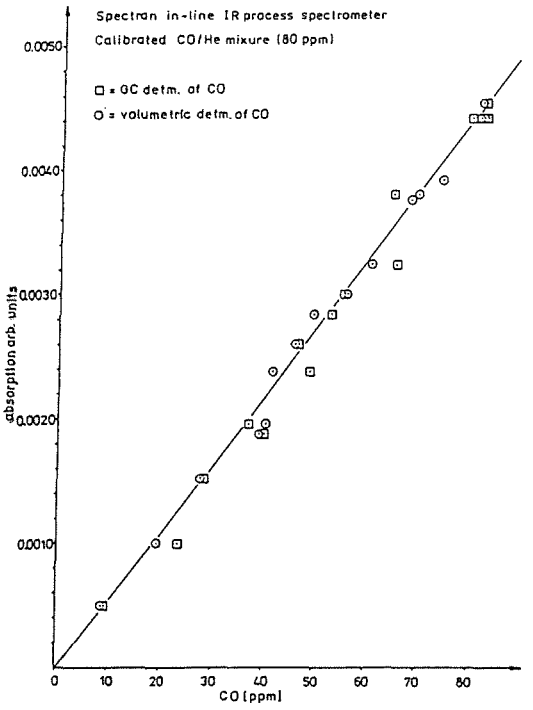

Fig. 1: Calibration with CO of the SPEKTRAN infrared analyzer

During the course of an experiment the performance of the permeator will be checked by two methods:

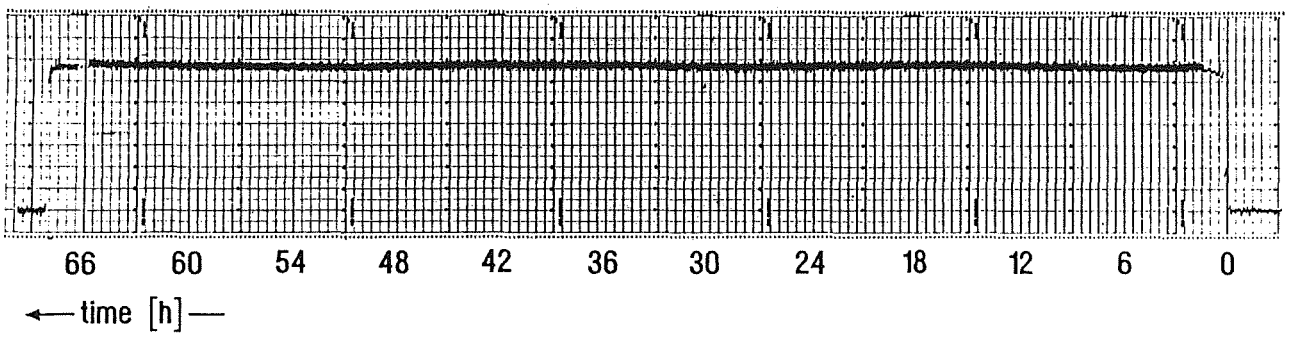

Fig. 2: Long-term stability of the SPEKTRAN infrared analyser

i) Periodic determination of the hydrogen permeation. While a sudden increase in permeation rate indicates a loss of mechanical integrity, a decrease in permeation efficiency suggests a progressice poisoning of the permeation surface.

ii) Continuous measurement of the CO partial pressure (lower ppm region) in the pure permeated gas throughout the experiment. A detection of CO will signalize leakage through the permeator.

Changes in the chemical composition of the gaseous mixture caused by catalytic reactions occuring on the permeator surface or by radiochemical reactions taking place within the loop will be detected by periodical gas chromatographical and mass spectrometrical analyses of small gas aliquots.

Before an experiment is started a careful calibration of all isolable volumes must be carried out employing standard procedures. The volumes are to be measured to 0.5 % accuracy. In addition, the catalyst must be activated. The catalyst activation is only carried out once before the introduction of tritium into the loop. To start an actual run, the tritium storage vessel containing an amount of tritium slightly exceeding that required for an experiment is connected to the loop. Thereafter the loop is evacuated to $< 10^{-8}$ mbar with the help of a turbomolecular pump. Next, the loop is isolated from the turbomolecular pump and the tritium storage bed opened to the loop. Finally, the bed is heated until a hydrogen isotope pressure of about 800 mbar is reached. After closing the valves to the storage vessel a PVT measurement and a determination of the tritium activity with the ionisation chambers is carried out. Complementary to this, a sample for gas analysis must be taken. By this procedure it is possible to determine the initial amount of tritium in the experiment with an accuracy of about 2 %.

A gaseous mixture consisting of helium (50 mol %), carbon monoxide (16.6 mol %), carbon dioxide (16.6 mol %), and methane (16.6 mol %) at a total pressure of about 1200 mbar, present in a vessel directly attached to the loop, is introduced by over-pressure into the loop. The gas mixture, consisting of H/T isotopes together with CH_4, CO, CO_2, and He, is then circulated through the catalyst vessel containing the smaller amount of nickel catalyst, to keep the hold-up as low as possible. The catalyst vessel is operated at a temperature of about 350 °C. At this temperature a tritium exchange between the H/T isotopes and CH_4 takes place (experiments with CH_4/D_2 mixtures have shown that equilibration is completed after about 120 minutes). After completion of the equilibration it is necessary to recover as much gas from the catalyst vessel as possible. This is done by evacuating the heated catalyst vessel (μ 500 °C) into the buffer vessel with a double stage metal bellows pump. The vacuum achievable in the catalyst vessel is estimated to < 100 mbar.

At this point the long-term experiment can be started. The gases are circulated through the loop with the help of a metal bellows pump (impurity gas stream) and pumped out from the secondary side of the permeator with a NORMETEX/metal bellows pump combination.

It is estimated that an experiment duration of more than 12 months is necessary for a conclusive evaluation of the performance of the permeator.

Assuming that the hydrogen solubility at 1 bar hydrogen and 300 °C is $< 2.5\ 10^{-4}$ mol H_2/g_{PdAg}, after one year of operation a decay helium build-up in the permeator membrane of the order of $< 4\ 10^{-5}\ g_{He}/g_{PdAg}$ can be estimated.

Presently, almost all components for the experiment have been purchased or are under construction. A detailed description of the experiment as well as a safety report are available. A first cold run is expected to start by the end of 1990.

Staff:

U. Berndt
S. Kuhnmünch
R.-D. Penzhorn

Subtask 2.2

The main hydrocarbon impurity expected from plasma/graphite wall interactions in a fusion reactor is methane. However, higher aliphatic as well as aromatic hydrocarbons have also been reported to be formed under conditions simulating the reactor plasma. Therefore, a

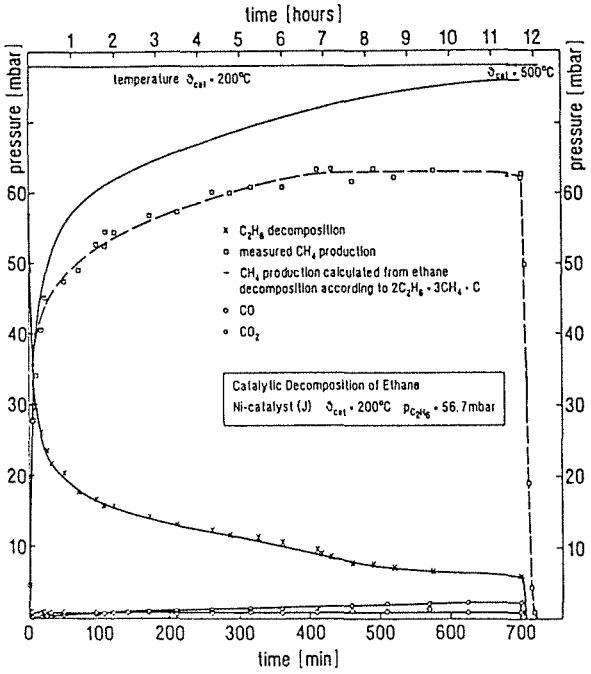

Fig. 3: Decomposition of Ethane on a Ni catalyst

systematic study on the catalytic decomposition of hydrocarbons other than methane was started, employing a loop that comprises a catalyst bed, three palladium silver permeators connected in series, a buffer vessel, a Metal Bellows pump, a UHV pumping system and conventional pressure and temperature instrumentation. Catalytic reactions were followed from pressure changes as well as via gas chromatographic analysis of the gas phase.

While the decomposition mechanism of methane on a nickel catalyst is now well understood and several rate measurements of this reaction are available, little is known on the catalytic decomposition of higher aliphatic hydrocarbons. Exeriments on the decomposition of ethane on a nickel catalyst at a temperature of 200 °C, without permeative hydrogen removal, showed that the decomposition follows the overall reaction

$$2\,C_2H_6 = C + 3\,CH_4, \qquad (1)$$

suggesting dissociative adsorption of the hydrocarbon as an intermediate step. A calculation of the methane production from the amount of decomposed ethane indicates that the experimentally observed methane is lower than expected (see Fig. 3). This is due either to an additional reaction path or to a partial decomposition at 200 °C of the methane formed in reaction (1), Since the partial pressure of molecular hydrogen accumulating in the system towards the end of the reaction was found to be approximately twice the pressure difference between the experimental and the calculated methane concentration, the second route appears to be the predominant reaction path. Because the carbon and hydrogen material balance between reactant and products agrees to within 1 %, the formation of significant amounts of unaccounted products, such as for instance polymers, can be excluded. Increasing the catalyst temperature to 500 °C and operating the permeator at 350 °C caused immediate and complete disappearance of the methane and of the remainig ethane. From thermodynamics the equilibrium constants for reaction (1) was calculated to be 1.81 x 10^9 and 5.51 x 10^{11} [bar] at 773 and 463 K, respectively. It follows, that the equilibrium concentration of ethane is extremely small at the temperatures employed and that therefore a quantitative decomposition of ethane in a single passage through the

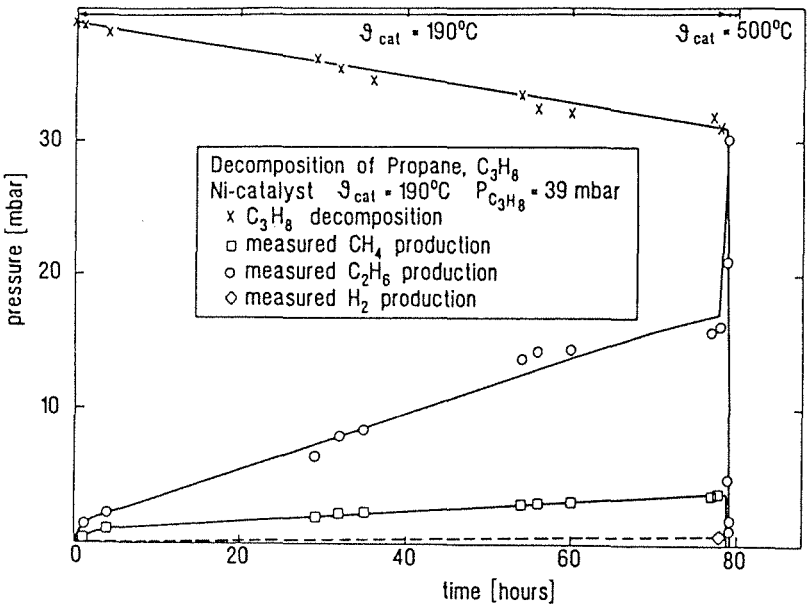

Fig. 4: Decomposition of Propane on a Ni catalyst

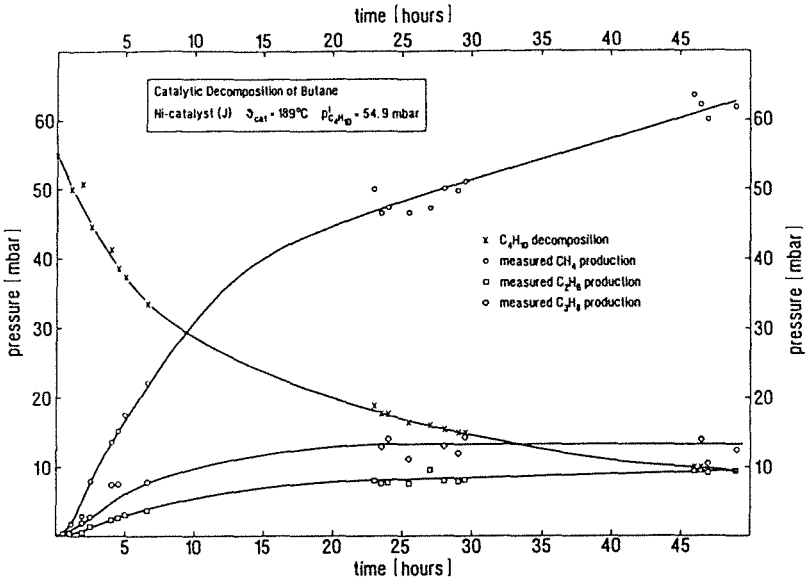

Fig. 5: Decomposition of Butane on a Ni catalyst

catalyst bed is possible. The recovery of hydrogen isotopes is therefore determined by the decomposition of methane, according to the reaction

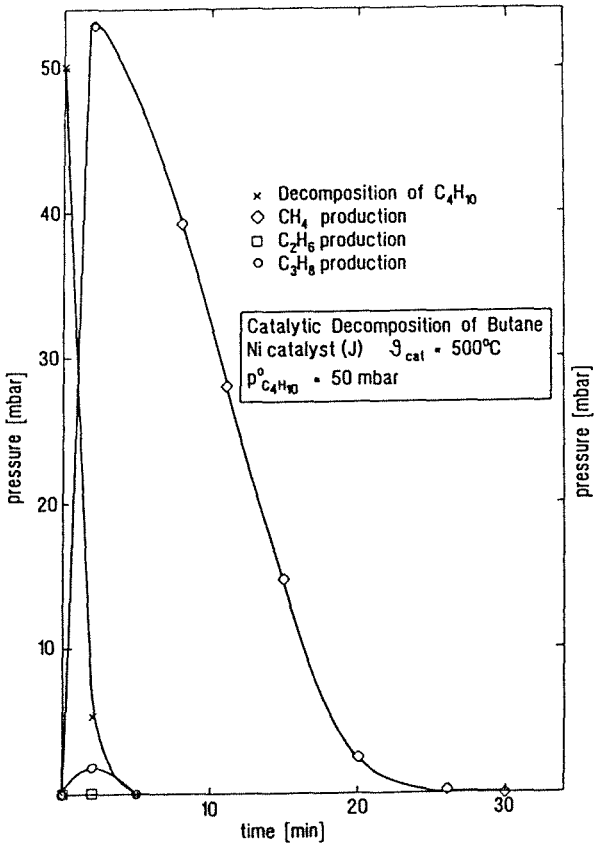

Fig. 6: Decomposition of Butane on a Ni catalyst

$$CH_4\,(g) = C\,(cr) + 2H_2\,(g). \qquad (2)$$

Propane degraded slowly on a nickel catalyst at 190 °C into methane, ethane and very little hydrogen. A carbon and hydrogen material balance between reactant and products agreed to better than 1.6 %. At 500 °C catalyst temperature and simultaneous permeative hydrogen removal the reaction proceeded to completion (conversion of all hydrocarbons into elemental carbon and molecular hydrogen) within a few minutes (see Fig. 4).

Butane cracked slowly into methane, ethane and propane when the gas was circulated over a nickel catalyst at 189 °C (see Fig. 5). When the temperature of the catalyst was raised to 500 °C and the hydrogen liberated was continuously removed by permeation through a palladium/silver membrane, butane rapidly disappeared cracking first into the intermediate products methane and propane. As the reaction progressed propane and methane decomposed into elemental carbon and hydrogen to concentrations below the gas chromatographic detection limit (see Fig. 6).

It is concluded from the results obtained that aliphatic hydrocarbons other than methane will be readily decomposed on a nickel catalyst at 500 °C.

Staff:

M. Glugla
S. Kuhnmünch
R.-D. Penzhorn
H. Schäfer

Subtask 2.3:

Introduction

An experimental program is carried out at the PEGASUS facility to investigate the applicability of commercial getter beds for gas purification in tritium technology. The aim is to remove gaseous impurities like N_2 or CO from a helium gas stream and to recover chemically bound hydrogen isotopes by decomposition of hydrocarbons, ammonia, and water.

In continuation of the CH_4 sorption tests with gas purifiers purchased from SAES and HWT, additional CH_4 tests were

carried out with a new HWT getter material to investigate the following items:

1. Comparison of two HWT getters;

2. Enhacement of cracking capability by continuous removal of the liberated hydrogen;

3. Dependence of sorption efficiency on gas flow rate;

4. Application of two getter beds at different temperatures to avoid undesirable co-sorption effects.

1. Comparison of two HWT Getters

The new HWT purifier (HTR-2) contained a Ti-V-Fe-Ni-Mn alloy (code No. 5850), which is characterized by a low storage capacity for hydrogen and a high decompostion pressure of its hydride. Owing to its content of 7 % Ni it was expected to have an improved cracking capability for CH_4 compared with the alloy tested before that did not contain any Ni (Code No. 5804, designation of the purifier: HTR-1). As shown in Fig. 7,

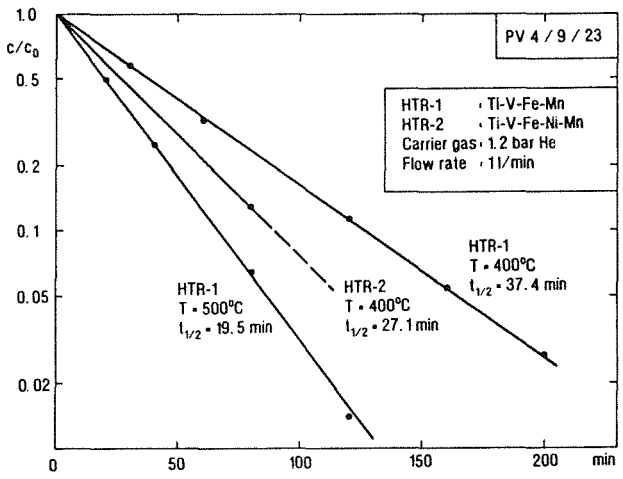

Fig. 7: Removal of CH_4 by two different HWT getters

the purification efficiency at 400°C was indeed considerably higher for the new getter material (the half period of the CH_4 removal was accordingly shorter). A further acceleration of the purification process can be achieved - of course - by increasing the temperature of the getter bed. A corresponding test at 500°C with getter bed HTR-2 will be performed in the near future.

A commercial HWT gas purifier contains 3 kg of getter material as well as an internal heater for a maximum temperature of 500°C. After installation in the test facility PEGASUS, the getter bed was activated by heating to 400°C and purging with a helium flow of 1 l/min for about 4 hours. During the sorption tests a gas volume of either 16.6 or 105 l He with an initial concentration of 0.1 - 1 % CH_4 was circulated through the purifier in a closed loop. Input and output concentrations (c_{in}, c_{out}) were measured by means of a gas chromatograph with a helium ionization detector.

2. Continuous Removal of the Released Hydrogen

The half period of 27.1 min measured in test PV-23 for the CH_4 removal at 400°C can be further decreased by additional provisions applied in test PV-22. Prior to this test the getter was dehydrided at 450°C to a hydrogen equilibrium pressure of 0.36 mb. During the test, the hydrogen resulting from the remaining equilibrium pressure as well as from the cracking of CH_4 was pumped off with a Pd/Ag diffusor (Leybold PA 150 with 290 cm^2 surface area). In this way, the reaction

$$CH_4 = C + 2\,H_2$$

was accelerated by continuously shifting the equilibrium to the right. The result is shown in Fig. 8. The half period of the

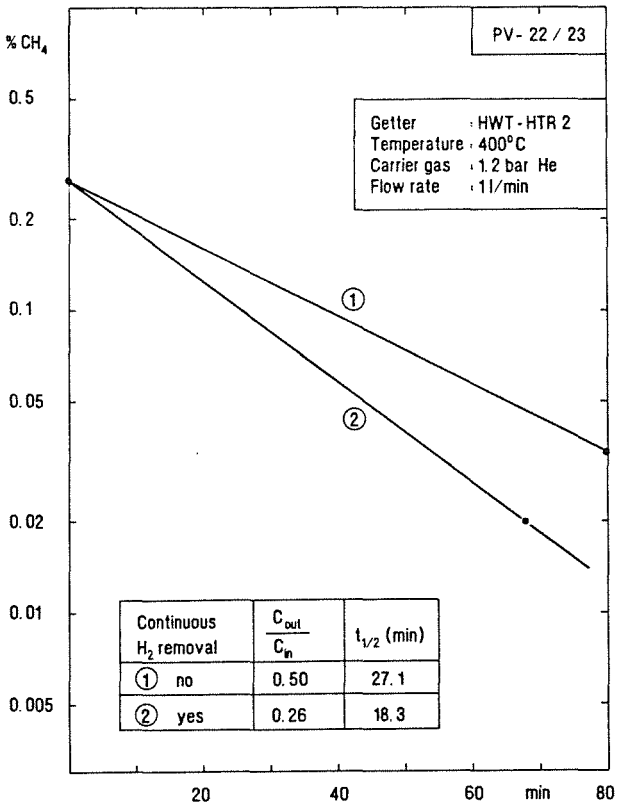

Fig. 8: Sorption of CH_4 with and without continuous removal of H_2

CH_4 removal was now 18.3 min, and the output/input ratio decreased by almost a factor of two.

For the application of this method it is essential that the dehydration of the getter is continued until its hydrogen equilibrium pressure is lower than the hydrogen pressure arising from the cracking of CH_4. That is because the liberated hydrogen must be directly sorbed by the getter (at least partially) - otherwise a shift of the thermodynamic equilibrium cannot be expected to occur. The diffusor is additionally used to remove as much hydrogen from the gas

phase as possible and to further reduce the equilibrium pressure of the getter.

3. Dependence of Sorption Efficiency on Gas Flow Rate

In the test series performed with the SAES purifiers it had been found that an increase of the gas flow rate (1 l/min instead of 0.5 l/min) leads to a faster decrease in the CH_4 concentration though the contact time between gas and getter becomes shorter during a single passage of the gas through the getter. Analogue tests were now carried out with the HWT getter HTR-2 applying flow rates of 1.0, 2.0, and 4.0 l/min.

The results show again a faster decrease in concentration with in- creasing flow rate, cf. Fig.9. It is apparent, however,

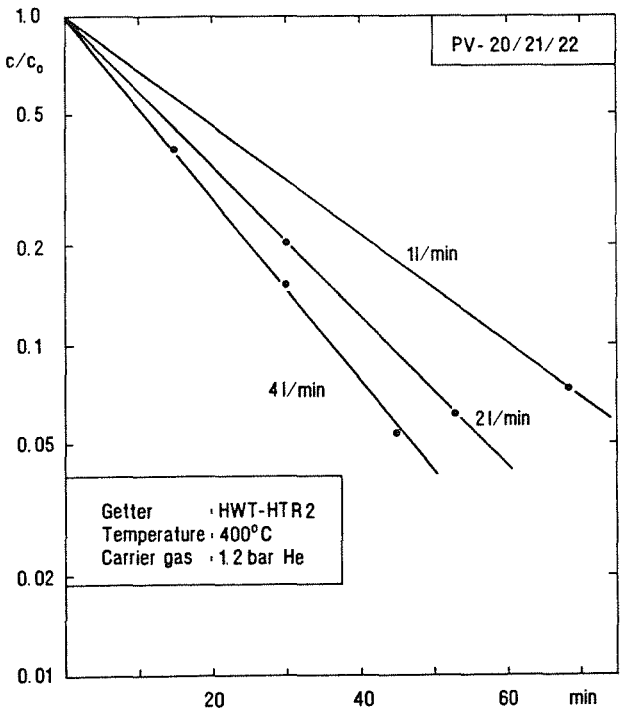

Fig. 9: Removal of CH_4 at different gas flow rates

that there must be an upper limit for the flow rate. Limitations are given, e.g. by the flow resistance of the getter bed and by the compression of the circulation pump; on the other hand, it can be extrapolated from the results shown in Fig. 9 that a flow rate of about 10 l/min would be an optimum value beyond which a further increase in purification velocity is very unlikely. This can be seen from Fig. 10, where the residual concentration of CH_4 is plotted as a function of gas flow rate. Although these results have so far been attained for CH_4 only, it is assumed that they are also valid for other impurities like CO or N_2.

4. Application of two Getter Beds

In the first sorption tests with CO in the presence of H_2, a catalytic influence of the HWT getter on the formation of CH_4 via

$$O + 2\,H_2 = CH_4 + \tfrac{1}{2}\,O_2$$

was observed. As an example, this very undesirable effect is illustrated by the results of test PV-3 at 300°C (see Fig. 11), where the concentration of CH_4 increased while other impurities were already efficiently gettered.

This effect can be largely suppressed by applying two getter beds in series. In such a combination the first getter is operated at 200 - 250°C to reduce the concentrations of CO and H_2; the second getter must have a temperature of at least 400°C if additional CH_4 is to be removed. In Fig. 12, the concentration decrease of three impurity components is shown as measured in test PV-15 with an initial gas volume of 105 l. An additional test (PV-16) was carried out with getter bed temperatures of 250°C and 450°C.

In this case the purification efficiency was considerably higher, because the c_{out}/c_{in} ratios were found to be almost a factor of 3 lower than in test PV-15:

Components	C_{out}/C_{in}		f	
	PV-15	PV-16	PV-15	PV-16
CH_4	0.178	0.064	0.822	0.936
CO	0.066	0.024	0.934	0.976
N_2	0.099	0.033	0.901	0.967

The purification factor f is an indicator of the purification efficiency obtained for a single impurity component:

$$f = \frac{t_{min}}{t_{1/2}}$$

with $t_{1/2}$ = half period of concentration decrease,

t_{min} = minimum value of half period resulting at a 100% impurity removal during each passage of the gas through the purifier arrangement

The minimum value t_{min} can be calculated from the time function for the input concentration

$$c_{in}(t) = c_o \cdot \exp\left\{-\frac{d \cdot t}{p \cdot V}\right\}$$

as

$$t_{min} = \frac{p \cdot V}{d} \cdot \ln 2$$

with

$p \cdot V$ = mass of the gas to be processed (mb·l)

d = gas flow rate (l/min)

t = time (min)

c_0 = initial concentration of the impurity

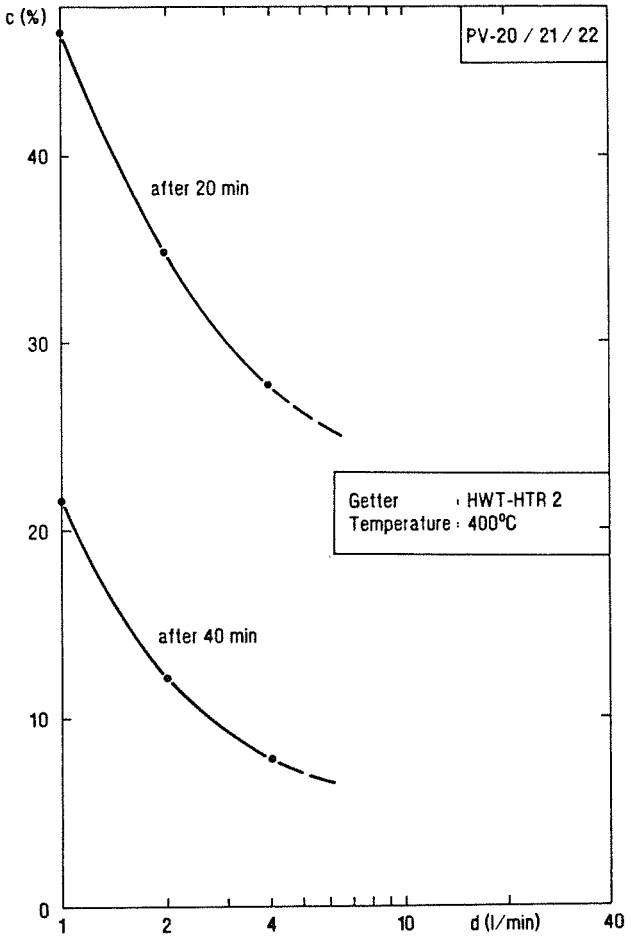

Fig. 10: Residual CH_4 concentration as a function of flow rate

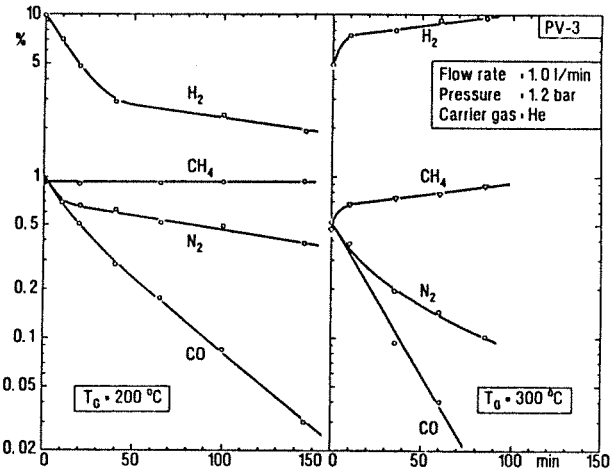

Fig. 11: Simultaneous sorption of various gas components on getter HTR-1

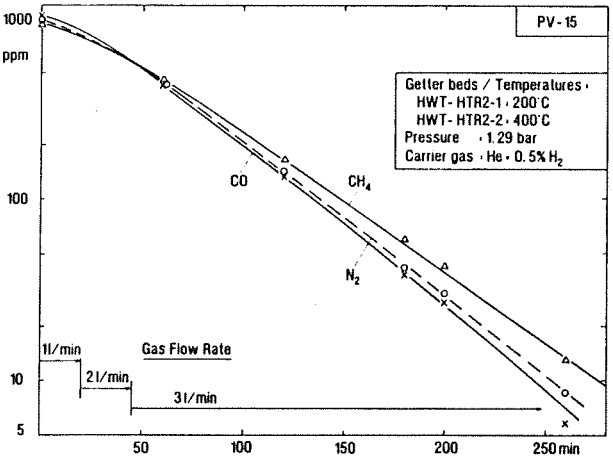

Fig. 12: Simultaneous sorption of impurities by two getters in series

5. Plans for the Near Future

The aim of the next tests is to investigate the sorption of water vapour as a function of getter temperature and flow rate. Concentrations in the range of 1000 - 10 000 ppm humidity can be attained by passing the test gas through a small vessel containing 1 g of $CuSO_4 \cdot 5\ H_2O$. While this hydrate is slightly heated to 50 - 100°C, its water molecules are released with a reprodrucible function of temperature and time. Quantitative measurement of the humidity concentration at the getter input and output will be performed with two sensors of a Panametrix System 5 Hygrometer.

Staff:

H. Albrecht
U. Kuhnes
W. Asel

TEP 3 Tritium Storage

Subtask 3.1

Uranium is the most extensively used getter material for the interim storage and transport of tritium, mainly because of its good thermodynamic and kinetic properties with respect to the absorption/desorption of hydrogen isotopes. Handling of this material, however, is subject to restrictions due to its nuclear nature and its high reactivity with air, resulting in pyrophoricity at room temperature. For the latter reason there is continuing interest in the identification of adequate substitutes.

One promising alternative getter for the storage of tritium is the intermetallic ZrCo, which has been investigated systematically in KfK over the past two years. Recent efforts have concentrated on an investigation of the solubility of H_2 and D_2 in ZrCo alloy at progressively increasing temperatures in the temperature region 200 - 500 °C. Solubilities were measured volumetrically in a conventional apparatus. Pressures were determined with a M.K.S. diaphragm gauge. The data obtained in the region of high hydrogen isotope dilution, i.e. < 3 at. % H or D in ZrCo, were found to obey Sieverts law. According to this law the hydrogen concentration in the solid solution c_H at a particular temperature is proportinal to the square root of the hydrogen isotope pressure p_{H2} (see Fig. 1a and 1b).

$$c_H = K(T)\ (p_{H2})\ 1/2 \qquad (1)$$

were K(T) is Sieverts constant. From the temperature dependance of the Sievert constants enthalpy and entropy values for the solution of H_2 and D_2 in ZrCo were obtained. From the measured hydrogen/deuterium isotope effect

$$K_H/K_D = 1.182 \pm 0.035$$

it is concluded that the lighter hydrogen isotope shows the higher solubility.

Staff:

Devillers
R.-D. Penzhorn
M. Sirch
E. Willin

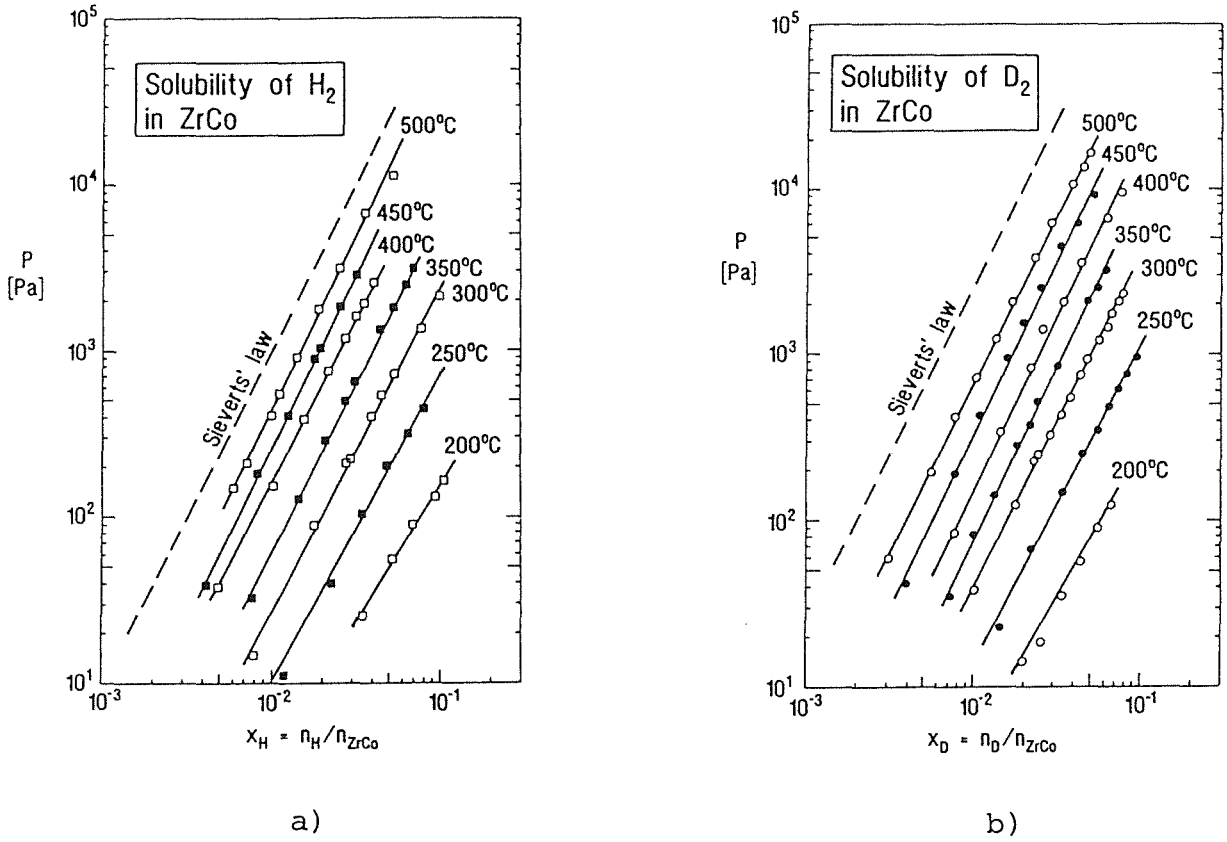

Fig. 1 a) and 1 b): Solubility isotherm in ZrCo of a) hydrogen and b) deuterium

NSN 1 Neutronics Data Base for Shielding

In the framework of this task KfK supports the evaluation and improvement of basic nuclear data, relevant for shielding, and the assessment of the accuracy of shielding calculations being limited by data uncertainties and the methodological treatment of the neutron transport.

Subtask 1.1: Neutron Cross Section Evaluation for Stable Iron Isotopes

A new evaluation of the resonance cross sections of the natural iron isotopes ^{54}Fe, ^{56}Fe, ^{57}Fe and ^{58}Fe is in progress. The following table shows the main characteristics.

These evaluations are completed as far as resonance parameters are concerned. In order to guarantee a good description of the pronounced s-wave resonance minima in the total cross section that are important for shielding applications the Reich-Moore resonance formalism was adopted with carefully adjusted resonance parameters. Since inelastic scattering is energetically forbidden in the range of the evaluation the 1-channel version of the formalism suffices with the exception of ^{57}Fe which, in addition to the elastic channel, has one open inelastic s-wave channel above 14 keV.

The energy dependence of potential scattering is determined by the resonances below and above the range of known resonances and is conventionally calculated statistically from average parameters (strength functions and distant-level parameters). As this is not possible within the ENDF-6 format a new ENDF-6-compatible prescription was derived from resonance theory which allows approximate replacement of all the distant levels by one pair of levels far below and above the range of known resonances.

The covariance information for the resonance parameters remains to be established. Energy scale uncertainties and energy discrepancies between the experimental time-of-flight data sets from different laboratories are quite troublesome for the conventional least-squares approach which admits uncertainties only for cross sections but nor for energies. Therefore the formalism was generalised to two-dimensional uncertainties to facilitate the uncertainty assignments.

Subtask 1.3 and 1.4: Implementation of the Data Base and Modification of Processing Codes

The accuracy of shielding calculations depends on the uncertainties of the nuclear data used in the calculations and on the quality of approximations used for the treatment of neutron transport. At KfK the impact of approximations is being analyzed by using a rigorous method for describing the neutron transport. This method avoids the usual Legendre series expansion of the scattering kernel in the Boltzmann equation through the explicit use of double-differential neutron emission cross-sections. The correct use of these data in shielding calculations is of great importance as the neutron radiation penetrating the bulk shield strongly depends on the angle and energy distributions of the secondary neutrons. By comparing the rigorous S_N-method with the usually applied S_N/P_ℓ-method it is possible to assess the quality of the latter for shielding calculations.

The rigorous S_N-method requires the use of angle-dependent scattering matrices, which cannot be generated by the available nuclear data processing codes. Therefore the processing code NJOY has been modified for this purpose. Additionally it became necessary to develop a special purpose code for treating the energy-angle distributions of neutrons emitted to the continuum, because this data type could not be treated by the current NJOY-version.

The rigorous S_N-method has been implemented in one- and two-dimensional transport codes, called ANTRA1 and ANTRA2. The development of ANTRA2 has been finished recently, including a completely new integration procedure for the scattering integral in the Boltzmann equation. In order to test ANTRA2 a two-dimensional beryllium benchmark experiment performed at FNS/JAERI has been recalculated. Satisfactory agreement with the experiment could be observed for the calculated angle-dependent neutron leakage spectrum. Thus, the rigorous method can be applied in one- and two-dimensional shielding calculations as soon as the double-differential cross-sections of the structural materials (Fe, Cr, Ni) become available on the European Fusion File.

Staff:

F. Fröhner, U. Fischer, A. Schwenk-Ferrero, E. Wiegner

Table 1 - Evaluation of Fe cross sections for EFF-2

Isotope	Abundance (%)	Energy Range (keV)	Number of Levels	Resonance Formalism
^{54}Fe	5.8	0 - 500	164	1-channel Reich-Moore
^{56}Fe	91.7	0 - 862	286	1-channel Reich-Moore
^{57}Fe	2.2	0 - 200	121	2-channel Reich-Moore
^{58}Fe	0.3	0 - 370	93	1-channel Reich-Moore

Remote Handling / Maintenance

Introduction:

Due to the activation of most components of the NET /ITER basic machine, all operations of inspection, maintenance, connection and disconnection, assembly and disassembly will have to be carried out remotely from the very start of the physics phase. Hands-on or semi-remote maintenance will be possible only in limited areas and for some peripheral components.

The maintenance of the in-vessel components has been identified as a key problem. The preferred solution for NET and ITER is the removal of divertor plates and protective tiles through equatorial ports by an articulated boom or an in-vessel vehicle and of blankets by a blanket handling device from top openings. The equipment for in-vessel maintenance will have to operate under extreme conditions of radiation and temperature. The large variety of operations to be carried out requires versatile and replaceable tools attached to different work units with large lifting capabilities. The high availability targeted by NET will require that in-vessel operations have to be carried out with relatively high speed.

Most of the KfK work concentrates on the development of an In-vessel Handling Unit (IVHU) with an articulated boom transporter and different work units (task RHT 1.1). This system is primarily needed for the maintenance or replacement of in-vessel components during short term interventions.

The Experimental Device for In-Torus Handling EDITH is the prototype of this system (task RHT 1.2). It is required to demonstrate that the maintenance of plasma facing components can be carried out with the anticipated reliability and time. It is also needed to optimize the IVHU components and subassemblies and to test different control algorithms.

EDITH will be constructed in full scale, supplemented by full scale mock-ups for divertor plate and protective tiles handling (RHS 3.2). The hardening of sensitive IVHU components for NET/ITER typical temperature and radiation levels are being performed in close cooperation with SCK/CEN Mol (task RHS 2.1 - 3).

The work performed to standardize and qualify basic machine components and to develop remote techniques to assemble and dissassemble these items is described in task RHS 1. The basic machine components to be qualified are:

- Electrical connectors (RHS 1.1)
- Pipe connectors (RHS 1.2)
- Fluid connectors (RHS 1.3)
- Welded connectors (RHS 1.4)
- Cryogenic connectors (HHS 1.6)

The demonstration of the different connection techniques will be performed in a full size mock-up of the NET/ITER connector box (BERT, task RHS 1.5).

In continuation of the NET contract 282/87-10 FU D NET KfK has performed some pre-design studies for a NET Blanket Handling Device (RHI 1). This work is finished.

RHS 1 Qualification of Standard Components

The main objective of this task is to standardize and qualify basic machine components, and to develop remote techniques to assemble and disassemble them. The data sheets resulting from this task for the NET Remote Handling Manual will define the standard components to be used in the NET design. The basic machine components to be qualified are:

- Electrical connectors
- Pipe connectors
- Fluid connectors
- Welded connectors
- Cryogenic connectors

The demonstration of connecting techniques in different test rigs and fullsize mockups is of special importance.

Subtask 1: Electrical Connectors

The objective of this subtask is to select and rationalize a range of electrical connectors suitable for remote handling.

This work follows from the results of the work carried out under NET contracts No. 201-85-1 and 313/88-7.

For general nuclear use, the push - pull type connector was chosen as standard connector, since this connector type conforms quite well with the basic requirements for remote handling and offers nevertheless a broad range of uses. Connectors with interlocking devices on the basis of srews or bayonets require more intricate movements, which are also more difficult to realize by means of a manipulator. Fig. 1 shows the test panel.

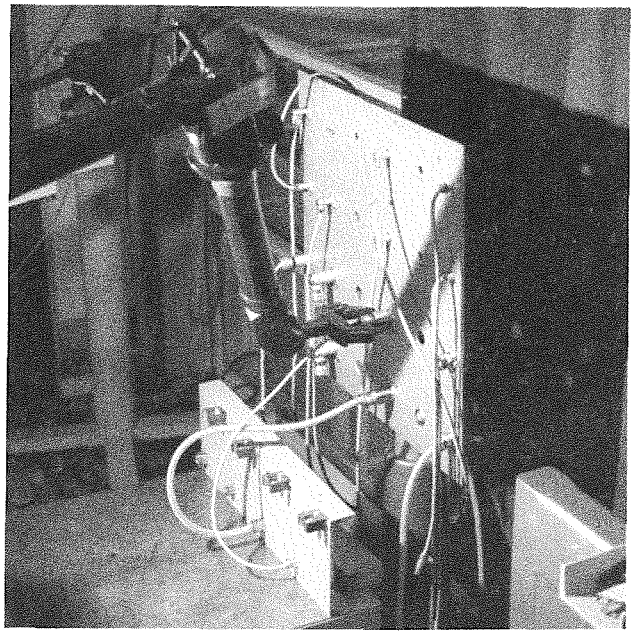

Fig. 1

The specific electrical connector types proposed as standard components for NET were selected after a series of remote operations in a mockup using typical remote handling equipment such as EMSM.

According to the aim of the development program, straight-on and elbow push - pull connectors from two different suppliers, assessed to be the most appropriate for general nuclear use, were selected for remote handling tests.

The two suppliers selected are LEMO SA and Fischer.

The test program has to be understood as a first step in the procedure to qualify remotely handled electrical connectors for application in the NET machine.

The main results gained during testing the connectors can be summarized as follows:

- The determination of the initial parameters and conditions showed that both connector designs are of good quality and well manufactured.
- Elbow connectors should be preferred with respect to plug pick - up and insertion.
- Both connector types can be handled remotely, the elbow connectors easier than the straight - on versions. The tests have also shown that handling of the connectors could be quicker and more reliable realizing some changes in their detailed design.
- A proposal for necessary modifications was made.
- For a safe and reliable handling procedure the manipulator gripper has to be adapted to the connector size.
- As expected, handling properties are influenced to a high degree by the surroundings, especially by the kind of illumination and the camera positioning.
- During the tests, the connectors manufactured by LEMO SA (Switzerland) were showing the most reliable behaviour.
- Changes in the connectors properties were not observed after the test.

The test results were analyzed and compiled in a final report. The report includes video recordings made during the tests, commentaries on the video recordings, pictures taken during testing, and all the previous reports compiled under this task.

The final report was discussed with NET and submitted to NET after some modifications. The follow-on program for

NET-RHEC's for special application was proposed for NET. The test program is under investigation.

Subtask 2: Flange Pipe Connectors

The aim of this task is to select and rationalize a range of flange connectors suitable for remote handling.

These connectors will be used for connecting pipes which may contain water, liquid metal, or vacuum.

In the period under review, the drafted data sheets for the Remote Handling Manual were modified and discussed with NET.

For the remote handling tests with a JET vacuum flange of nom. dia. of 225 mm the test rig was changed for the continuation of the test in a horizontal position.
Fig. 2 shows the test rig with the EMSM disconnecting the JET-Flange.

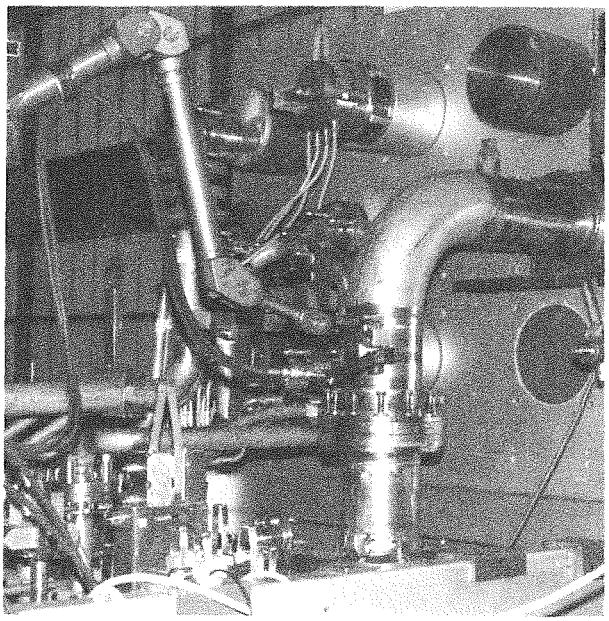

Fig. 2

The test results gained up to now show that some modifications are necessary to improve its remote handling properties. The test results and modifications are given in [2]. The modifications have been generally agreed by JET and NET and will be implemented in the flange for the follow-on tests.

The design of UHV flanges for the Plasma exhaust system has been started. First proposals were provided and discussed with NET and JET. The basic design is similar to the JET UHV-flange design.

The test of the soft iron material as a gasket material for liquid metal pipe connections was continued in FLATEST. The description of the test rig and the first test results are compiled in [3]

The main result is that the corrosion resistance and the handling characteristics of the soft iron gasket were surprisingly good. The tests have been continued with gaskets in different shapes and material combinations.

Subtask 3: Fluid Connectors

This subtask intends to select and rationalize a range of small bore fluid connectors suitable for remote handling.

These connectors will be used for coupling flexible hoses which may contain water or compressed air.

The draft of the Requirement Definition Document (RRD) was provided. [4] The state of the art was investigated.

For general nuclear use, the push - pull connector type was selected as standard component. The preselection of the types of connectors and of suppliers was discussed with NET. [5]

The proposal for a test program was arranged and submitted to NET. [6]

The test rig was designed and manufactured. The types of connectors to be tested were identified. The suppliers Walther Stäubli and Rafix were selected to provide three different types of connectors for the remote handling test. Fig. 3 shows the test rig.

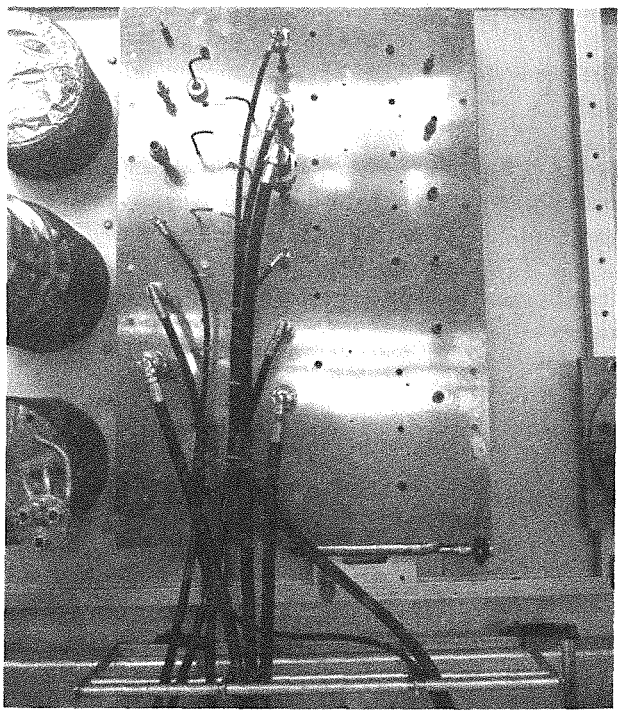

Fig. 3

Subtask 4: Welded Connectors

The main objective of this task is to develop remote techniques and tools to provide welded pipe connections and welded vacuum lip seals for flanges.

In the period under review the modular tools for lip welding and - cutting were commissioned and tested. Fig. 4 shows one of the modular lip welding/cutting tools.

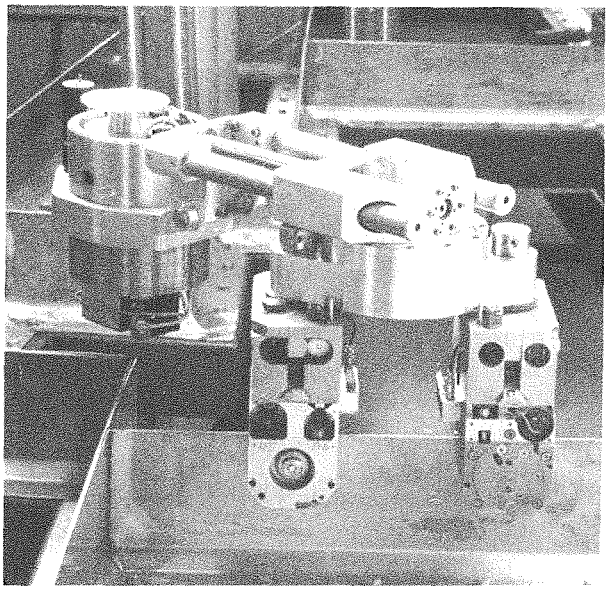

Fig. 4

The welding source and the control system for the welding device were selected and ordered. The installation of the FELIS test rig is in progress.

The status of the work performed for lipwelding is discribed in [7].

In the FEROS test rig, basic tests with already available remotely operated pipe welding and cutting units have been continued.

Investigations on UHV lipwelded seals were started with a survey of locations and of general solutions to show the principle of connecting in general schemes.

The results were compiled in an interim report. [8]

Subtask 5: Demonstration of Connecting Techniques (BERT)

BERT is a full-size mockup of the NET connector box which houses the feed pipes leading to the blanket segments and the lip seals of individual blanket segments. The comparative evaluation of the different blanket conecting strategies is shown in [9].

The BERT test rig is used to test and develop remote handling techniques for pipe connectors and pipe jumpers as well as procedures and equipment for remote cutting and leakproof rejoining of lip seals.

In the period under review the remote exchange of the pipe jumpers connected by flanges was demonstrated.

The operations were carried out with the overhead crane, the turnable hook and the electrical impact wrench attached to the hook.

The layout of the test rig, the installation of supply lines and the remote handling equipment are discribed in [10].

During the test it could be demonstrated that using the overhead crane, it is possible to exchange the pipe jumpers in a reasonable time and with an acceptable reliability.

Details of the procedure as well as details of the pipe jumper design will be given in the interim report under preparation. Fig. 5 shows the actual status of BERT.

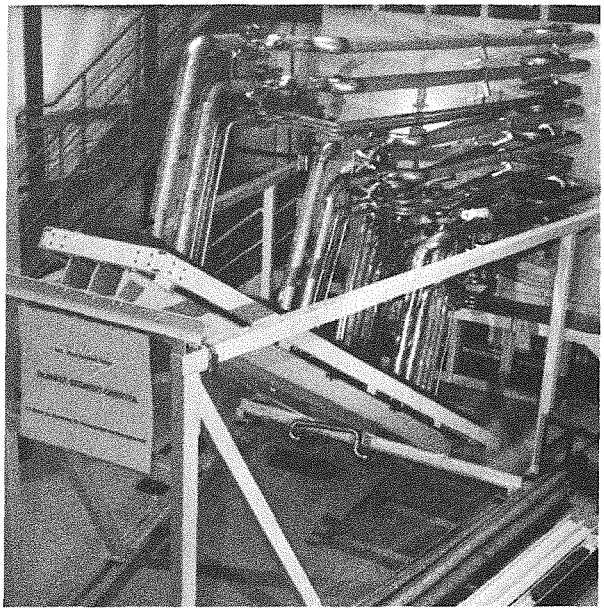

Fig. 5

Subtask 6: Cryogenic Connectors

In the framework of this subtask, development work is carried out on remotely operated cryogenic connections suitable for NET remote handling devices used inside the biological shield.

Several alternative solutions for cryogenic connections were investigated. After extensive discussions with NET one has decided to focus work on the design of three different versions of cryoline connections.

The connectors for cryolines are classified multiple-rigid, multiple-flexible and single-lined according to their arrangement and the number of extension bellows required.

The following assembly drawings show the main characteristics of the versions under investigation.

Fig. 6 shows the regid version, and Fig. 7 the flexible one.

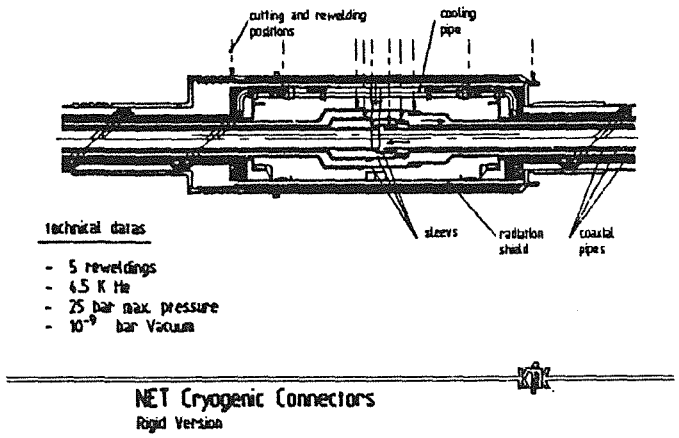

Fig. 6

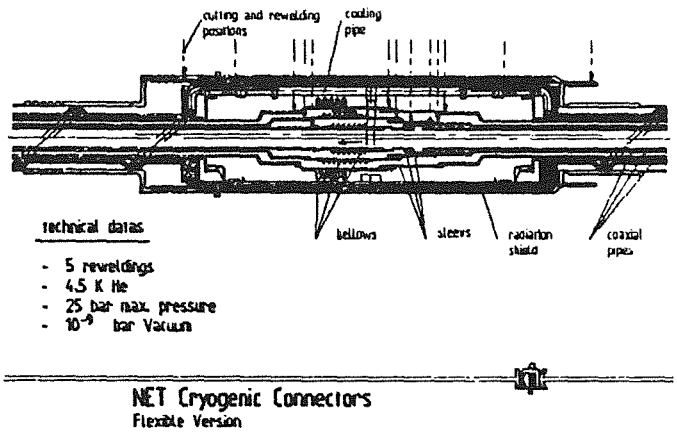

Fig. 7

In the period under review for the multiple-rigid and - flexible connectors, several designs were developed and discussed with NET. The sequences of operations were compiled for and described in tables for each version to such an extent that the remote handling procedure and the necessary tooling could be discussed in detail with the NET-Team. More details are given in [11].

The aim of the discussion was to find a solution meeting the requirements for cryogenic connections as well as for remote handling procedures possible. The design chosen finally is a combination of several previous designs and can be characterized as a compact and modular design for both the rigid and flexible versions which requires a reduced number of different pipe cutting and rewelding tools. Also the number of different remote operations has been reduced significantly during the investigations.

The latest design will be presented to NET mid of July. An interim report is under preparation.

Staff:

R. Gaa	A. Schäf
L. Gumb	M. Selig
U. Kirchenbauer	D. Stern
H. Krause	M. Trettin
R. Müller	R. Ullrich
W. Reeb	

References:

[1] M. Selig, Remotely Handled Electrical Connectors (RHEC's) for General Nuclear Use, Final report NET contract No. 313188-7/FuD/NE.

[2] H. Gutzeit et al., KfK unpublished report of KfK, May 1989.

[3] U. Kirchenbauer, M. Selig, unpublished report of KfK, June 1989.

[4] M. Selig, H. Haas, unpublished report of KfK, Sept. 1989.

[5] M. Selig, H. Haas, unpublished report of KfK, Febr. 1990.

[6] M. Selig, H. Haas, unpublished report of KfK, Febr. 1990.

[7] L. Gumb at al., Vacuum Lip Seals and Tools for NET, Status report for the NET technology programme RHS 1.4, April 1990.

[8] L. Gumb, M. Selig, D. Stern, unpublished report of KfK, March 1990.

[9] U. Kirchenbauer, M. Selig, unpublished report of KfK, June 1989.

[10] U. Kirchenbauer, M. Selig, unpublished report of KfK, July 1989.

[11] M. Selig, L. Gumb, unpublished report of KfK, Jan. 1990.

RHS 2 Material Tests for Remote Maintenance Equipment

Components of the NET In-Vessel Handling Unit (IVHU) are subject to degradation due to irradiation and temperature. They have to be qualified with respect to reliability, accuracy, radiation and temperature as well as to improve their life expectancy as far as possible and in collaboration with the suppliers according to the achieved test results. The material tests include pre-tests, irradiation tests and post-irradiation tests.

Identification of sensitive components, test specifications, acceptance criteria and time schedule are summarized in the KfK report "Material Tests for Components of the In-Vessel Handling Unit" which was sent as draft to NET and discussed in the working group.

Components to be tested prior to their application in operational NET remote handling equipment are motors, resolvers, inclinometers, ultrasonic proximity sensors, power cables, signal transmission lines, cameras, lubricants, position sensors, proximity sensors, fibre optics and multiplexing systems. KfK has taken charge to test these components in collaboration with CEN/SCK MOL, except cameras, fibre optics and some types of proximity sensors.

Subtask 1: Position Sensors for IVHU

With respect to the high environment temperatures and gamma doses KfK has selected four identically made multiturn resolvers which were tested successfully in a heat chamber at 150 °C. A single resolver element was irradiated in the BR2 reactor reaching one Giga-rad (Si) after three weeks and it was shown that its mechanical structure including all coils and their plastic coil holders remained undamaged and accordingly, the electrical integrity was confirmed. However, the insulation of the connecting wires showed severe damages caused by a halogen reaction gas release. From this, the originally used TEFZEL insulation was exchanged by RADOX insulated wires and again, additional temperature and calibration tests were performed.

From all these tests a resolution of 16 bit (multiturn) and an accuracy of 12 bit was achieved and a sufficient temperature compatibility and data reproducibility after temperature variations could be demonstrated.

For the irradiation test in the BR2 reactor with two multiturn resolvers the pneumatic drives and instrumentation components were tested and the irradiation basket will be completed in June 1990 after some minor modifications due to safety aspects to be fulfilled.In parallel, two supplementary irradiation tests with selected plastics were performed with the aim to determine the extent and the implication of molecular fragmentation effects with associated gas releases, namely halogens. Since the mechano-chemical integrity and stability of plastics under high gamma irradiation exposures and temperatures was found documented by furnishers very scarcely in the past, this activity was of high importance with view to all future in-torus sensor applications using RADOX, TEFZEL, VITON, ULTRASON and ULTRAPEK plastics. And as a consequence from this, all VITON seals being part of the pneumatic drives inside the irradiation basket were removed and therefore, the construction of the piston seals had to be modified to ensure an error free operation with a minimum of gas losses without using organic sealing materials. For all other plastic materials, post-irradiation tests and investigations will follow until July 1990.

In May 1990, the resolvers and electronics for the EDITH test device had been ordered. With the objective to investigate the longtime stability and accuracy of radiation hardened resolvers in comparison to standard types, both versions of resolvers will be applied to the joints, therefore. Preparations are under way to perform the necessary calibration work and temperature performance tests after the delivery of all angular encoders with a particulary made test-bank at KfK which will use a 19 Bit reference and will be equipped with an electronically controlled heat chamber for up to 150 °C.

Subtask 3: Drive Components for IVHU

This subtask includes the testing of motors, power cables, signal transmission lines and lubricants.

The selection of electric motors was the result of the comparison of different motor principles and a market analysis. For the comparison DC-brush, DC- and AC-brushless servomotors and stepper motors were considered on the basis of the following criteria:

- Speed range where the torque is almost constant
- Performance (power per size and weight)
- Ratio of peak torque vs. continuous torque
- Overload behaviour
- Compatibility with the environment
- Complexity of motor control
- Availability

The best overall behaviour have AC-brushless servomotors although they require also modifications with respect to temperature and radiation compatibility. Only two suppliers (Maccon and Moog) were able and willing to offer motors adjusted to KfK specification. Test motors were ordered at both companies.

Power and signal transmission cables are to be investigated in a first stage under subtask 1. The first results of these irradiation tests provide the basis for selection, modification and further tests in combination with the motor tests. Lubricants were compared on the basis of experience at CERN and information of suppliers. With respect to the best temperature resistance dry lubricants on the basis of MoS2 will be tested together with the motors.

Some of the technical data of motors which are important for their functionality will be provided by the supplier. They are normally related to ambient temperatures of the environment and have to be completed by measurements up to the NET typical operating conditions. These measurements will be carried out prior to the irradiation tests in a testbed with heating chamber at KfK mid 1990. The results will serve for comparison reasons to identify changes due to irradiation and temperature. The testbed is commissioned and can be tested now.

Irradiation tests will be performed in a test rig at the BR2 at CEN/SCK MOL. The test rig has a He-atmosphere. During the tests the motors will be operated at no-load conditions, at a maximum surface temperature of +250C and at a gamma dose rate of 3 Mega-rad(Si)/hour. The specific components of the test rig for motor testing are designed. The tests are foreseen for November 1990.

After the irradiation test the motors will be tested under the same conditions and in the same testbed at KfK as the pre-tests.

The deviation of important motor parameters between pre- and post-irradiation tests should not exceed 15%.

Staff:

I. Aberle
B. Bartholomay
R. Döbele
B. Haferkamp
W.E. Hörl
D. Klein
K.H. Lang
W. Link
G. Müller
H.A. Rohrbacher
P. Schultheiss
A. Suppan

RHS 3 Mock-up of In-Vessel Components and Test Facilities

Subtask 3.2: Protective Tiles and Divertor Plates Handling Devices

Objective of the task is to design and manufacture a proof of principle remote handling equipment for a rapid tile replacement and the replacement of upper and lower divertor plates. The scope of the work includes designing tools and end-effectors for these tasks which are attachable as work units to the NET articulated boom system (task RHT 1). It will have prototypical features and will be tested in a full scale mock-up with EDITH as basic equipment.

Protective tile handling devices

Investigations for the replacement of protective tiles are based on /1/. The design is in a preliminary stage. First results of the investigation will be available in the second half of 1990.

Divertor plate handling devices (DHD)

The investigations of KfK to design a divertor handling unit are summarized as a first conceptual design in the report "Divertor Handling Unit" and submitted to NET as a draft. The design is based on the ITER configuration and on the requirements described in the documents /2,3,4/. Two options of divertor plate segmentation were investigated, the one with segments which are radially subdivided with respect to the torus (Fig. 1), and another one where the segments are tangentially subdivided (Fig. 2).

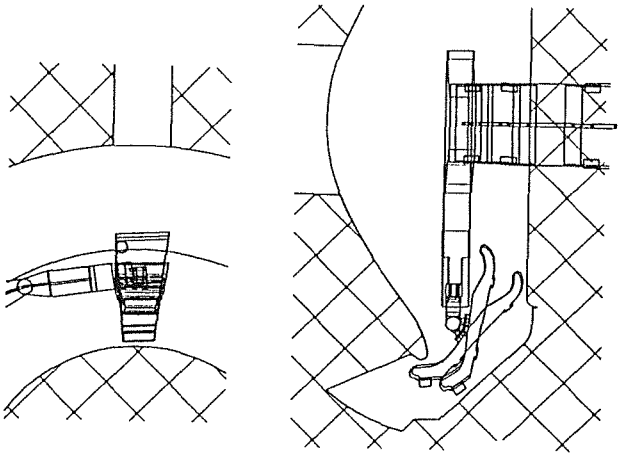

Fig. 1: Replacement of lower divertor plates radially divided

The DHD as a special work unit for the withdrawal and insertion of divertor segments is remotely attachable to the articulated boom transporter (ABT). It is equipped with a gripper to handle the segments. The DHD can be rotated together with the work unit interface by means of a rotation joint which is part of the interface. Combined with the slide

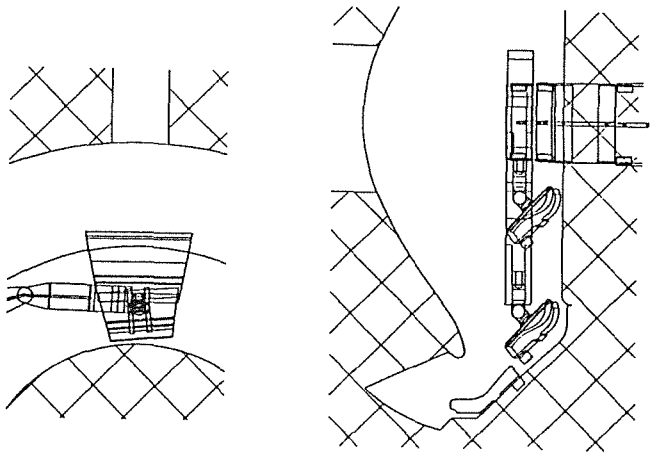

Fig. 2: Replacement of lower divertor plates tangentially divided

and the trolley of the work unit the upper and lower divertor segments are reachable. For the transfer of segments from and into the torus a separate transfer unit is foreseen. It will be inserted through maintenance ports not used at this moment by the ABS. Fig. 3 shows a conceptual design of the DHD. It is composed of the following main components:

The slide is movable at two guiding rods which are fixed at the support frame which again performs the connection between ABT and work unit. The slide is equipped with longitudinal ball bearings and is actuated by redundant planetary roller spindles. They are driven by motors via bevel gearings. The double extension is performed by an additional trolley movable at the slide. Trolley guiding and drives are similar to those of the slide. The upper pitch joint is composed of two Cyclo drives which are actuated via two bevel gear drives. Both Cyclo drives are connected with a common torque arm. Also the rotation joint is based on the use of two Cyclo drives plus spur wheel gears. At the lower pitch joint two Cyclo drives are connected with one common torque arm. All joints are driven by redundantly arranged brushless servomotors.

References:

[1] Reeve, T.: NET 2 - Definition of Requirements for the Design of Prototype Tile Handling Equipment, Doc.Nr.N2/P/023132/1/A, Issue Draft November 1989.

[2] Reeve, T.: Divertor Maintenance Using IVHU - In-Vessel Operation, Doc.Nr. N2/P/0230/2/A, 11.05.1989.

[3] Reeve, T.: Definition of Requirements for the Design of Prototype Divertor Handling Equipment, Doc.Nr.N2/P/023132/2/A, Issue Draft January 1990.

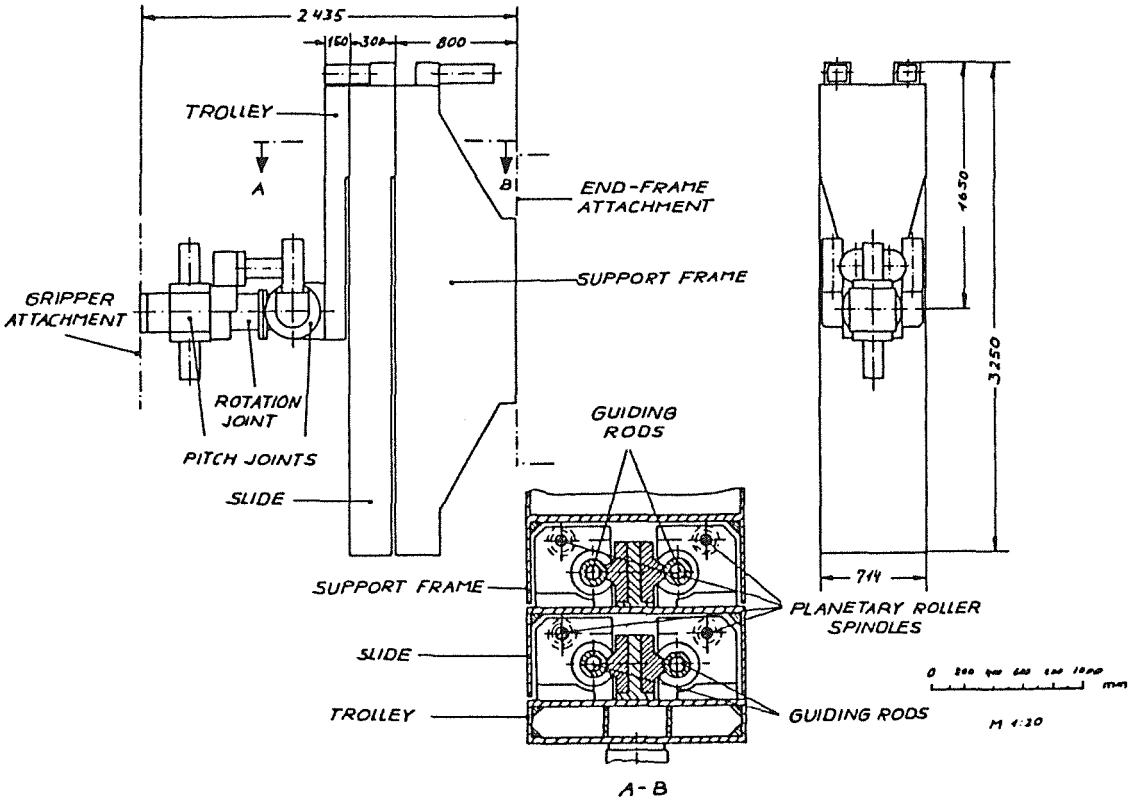

Fig. 3: Divertor handling device

[4] Maisonnier, D.: NET/ITER In-Vessel Transporters - Technical Specification for their Conceptual and Preliminary Design, Doc.Nr. N2/P/3240/1/B, Issue A, 24.10.1989.

Staff:

J. Hübener
W. Link
A. Ludwig
A. Suppan

RHI 1 Blanket Handling Device (BHD)

Subtask 1.1

In continuation of the NET contract 282/87-10FU D NET, NET Blanket Handling Device, KfK has finished the investigation of handling concepts. The results including a proposal for a handling device to withdraw and insert blanket segments are documented in the final report "Blanket Replacement Device - Final Report" from March 1990 which was submitted to NET. At the moment no further activities are ongoing.

References:

Suppan, A., et al., unpublished report of KfK, March 1990.

Staff:

J. Bernert
B. Haferkamp
W. E.Hörl
K. Leinemann
W. Link
E.G. Schlechtendahl
A. Suppan

RHT 1 In-Vessel Handling Unit (IVHU)

The main objective of this task is the design of an In-Vessel Handling Unit (IVHU) for inspection, repair and replacement of NET in-vessel components. Main component of this equipment is a transport system with attachable multi-purpose and special work units. KfK is developing such a system on the basis of an articulated boom. The results of these investigations are summarized in the report "The NET Articulated Boom: Preliminary Investigations and Justification for a Full Scale Prototype". A draft of this report was sent to NET.

Basis of the investigations were the technical specification for NET/ITER in-vessel transporters /1/, the document "Divertor Maintenance Using IVHU" /2/ and the document "Definition of Requirements for the Design of Prototype Divertor Handling" /3/.The articulated boom system (ABS) was preselected as one of two options due to the following reasons:

Practical experience has been gained at JET with a similar boom.

Based on the practical experience, components were improved providing the basis for further consequent development.

This system is independent from the NET device.

Technology used is state of the art.

The articulated boom system and the in-vessel vehicle system as the second option complement each other, i.e. the boom would be used for short term interventions and the vehicle for long-term interventions. It was stated by NET that the development and construction of a prototype of a boom is needed to demonstrate beyond any doubt that the maintenance and replacement of plasma facing components is an operation that can be conducted with the anticipated reliability and time. This prototype is the experimental device for in-torus handling (EDITH) with the following objectives:

Testing and validation of remote handling procedures.

Performance of integral tests of ABS components and subassemblies.

Testing and validation of ABS work units.

Testing of ABS control system features and verification of control systemconcepts.

Testing of the ABS-behaviour at the NET reference conditions but using also the flexibility of the testbed to assess safety margins, to test the dynamic behaviour and verify the dynamic model, to investigate dynamic damping if required, and to test remote maintenance of equipment.

Even though many aspects of the ABS operational behaviour can be predicted from simulation, JET experience or small scale tests, there remains the need for performing tests in full scale mock-ups. Based on the objectives of EDITH and the justification of a full scale mock-up it is usefull to extend the function of the testbed EDITH to the mock-up for the following reasons:

Saving costs and manpower by having only one test device.

Using eventuelly improved and advanced features in the mock-up.

Some components may be used later for the operational NET equipment.

Improvements of EDITH are possible without respect to other functions of the testbed.

The testbed EDITH is integrated in the European Technology Programme and is in accordance with its overall time schedule.

Subtask 1.1: Preliminary Engineering Design of IVHU

The work for the preliminary design of the articulated boom transporter (ABT) was continued.

Mechanics

The overall structure of the ABT is described in the second semi-annual report 1989 /4/. The ABT link system has four yaw joints driven by coaxial drive units, one rotation joint actuated via two Cyclo drives with a common spur wheel gear, and a pitch joint operated by two spur wheel gears which actuate a planetary roller spindle. The latter ones are used to compensate vertical deviations of the boom. The main parameters of the drives are listed in Table 1.

Structural analysis

Taken into account the requirements of high vertical stiffness and low dead weight, an optimization of the link wall thicknesses by a given cross-section (width = 0.6 m, height - stepwise reduced from 2 m for link C1 to 1.73 m for link B4), was carried out. The investigations show that the design with the wall thickness of 8mm for link B3, 6mm for link B2 and 5mm for link L1 represents a reasonable solution.

Although the mean stress level in the links is well below the yield stress, the thin walled structure which is partly under compressive stresses, is prone to buckling. Therefore, detailed buckling analyses have been performed to proof the necessity of reinforcing ribs.

Rough calculations showed that the side walls have the lowest buckling load compared to the other parts of the box.

Parameter	Value
Coaxial drive units for yaw joints	
Maximum angular joint speed	0.15 rad/sec
Number of motors with fail-safe brakes	2
Maximum continuous torque at rated speed	10 kNm
Total transmission ratio	533:1
Total stiffness of the system	2.4 x 10^6 Nm/rad
Efficiency direct/back	>70%/>40%
Drive unit for rotation joint	
Maximum angular joint speed	0.05 rad/sec
Number of motors with fail-safe brakes	2
Maximum continuous torque at rated speed	16 kNm
Total transmission ratio	895:1
Efficiency	80%
Drive unit for pitch joint	
Maximum angular joint speed	0.01 rad/sec
Number of motors with fail-safe brakes	2
Maximum continuous torque at rated speed	110 kNm
Total transmission ratio	4184:1
Efficiency	80%

Table 1: Technical data of drive units

For these side plates calculations have been done using three different methods:

1. application of tables from the standard literature

2. ABAQUS-calculations

3. a simplified procedure developed at KfK.

For perfect plates (all sides simply supported) all three methods agree very well. Due to the stable postbuckling behaviour of plates, moderate safety factors are considered to be sufficient. Further investigations concerning the behaviour of imperfect plates have been done using the methods 2) and 3).

Due to the bending stress distribution the maximum buckling amplitude occurs in the lower part of the plate. The relative deformation is less than 50% of the assumed imperfection (6.25 and 10 mm) and therefore acceptable.

Finally, an analysis of a whole link has been performed using ABAQUS to confirm the buckling behaviour of the plates with its real boundary conditions and to carry an overall check. Also this analysis confirms that the links do not need reinforcing ribs for buckling reasons.

Fig. 1 shows the buckling mode of a side plate, Fig. 2 the corresponding buckling mode for a link under combined bending and torsion.

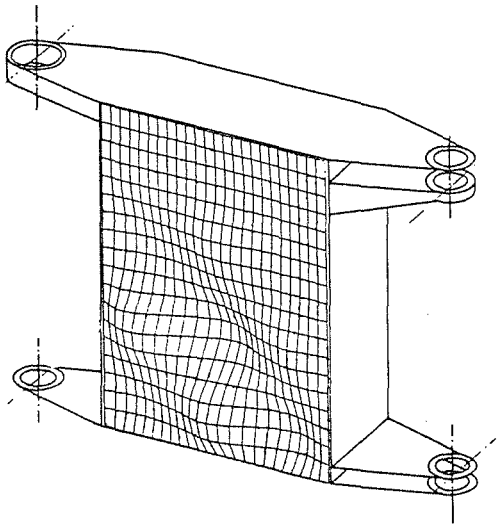

Fig. 1: Buckling mode function for a side plate

Control system

The **RH control system** is a subsystem of the **NET control system**. It is partitioned into RH-AREAS, representing a set of RH equipment grouped around a major device (e.g. in-vessel handling unit, blanket handling unit). Each RH-area has its own **RH- area control system** organised as a hierarchy of computers and controllers dedicated to one RH-

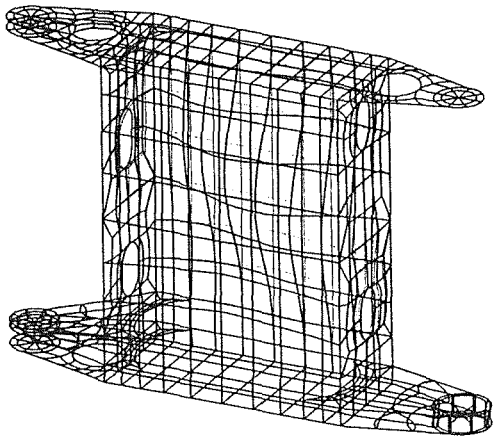

Fig. 2: Buckling mode function for a link under combined bending and torsion

area. To run a RH area control system in the operational phase a **NET remote workstation** (NRWS) is needed.

The proposal for an overall NET remote handling control system concept is documented in /5/. The RH control system is designed according to the man-in-the-loop concept because in contrast to industrial applications in the maintenance area of work a fully automated performance of the work will not be possible. Therefore a mixed-mode control is needed allowing for manual work which might be supported by the control system (computer) and for automatic work which is supervised by the operator. The control system has to enable a close cooperation between man and machine characterized by mutual help and mutual supervision and optimal use of the cognitive and manipulative abilities of the operator.

The control system is designed as a hierarchical control system with three major levels: (1) drive/equipment control, (2) path/motion control, (3) guidance/tasking. To guarantee highest operational flexibility the operator has access to all levels of control. For example if the operator is working with a master-slave manipulator he is using the lowest level of control, the joint angle level. Control of a transporter via a joystick makes use of a higher control level. Control on the task control level means to control the system using commands starting complex preprogrammed motions or using other high level support modules of the control system or the workstation. In general the different hierarchical levels of the control system separate stepwise more task specific functions from more equipment specific ones. The functions of the task control level are implemented on the NRWS, the functions of the RH-area control are implemented as dedicated RH-area control systems.

Work on the conceptual design of the **NRWS** is reported later on. The basic subsystem of the NRWS will be a spatial simulation system: KISMET is the prototype of a spatial simulator developed for the JET-TARM control system and already successfully transferred to various non-fusion applications. KISMET was recently enhanced by a stereo-graphics feature supporting the operator in grasping the depth of a synthetic scene. The KISMET interfaces were completed such that now the following interfaces to related software systems are available: model transfer interface (CAD*I, VDAFS, CATIA, BRAVO3, ROBCAD), motion program transfer interface (IRDATA), online interface to control systems. To facilitate off-line programming and investigations a plot subsystem was implemented for graphical presentation of kinematic data. The camera control via KISMET was added by a speech input subsystem and tested in the CATROB environment. The KISMET commands are documented in /6/.

For the application of KISMET to JET maintenance a model of the ex-vessel working site and the TARM was generated on the CATIA CAD-system and transferred to KISMET. The online link between KISMET and the TARM control system was implemented and successfully tested. Based on the joint position signals KISMET updates the TARM display in realtime. The GBsim simulation system for in-vessel handling was transferred to the IRIS-4D workstation series. The possibilities of integrating the JET camera control into the KISMET environment was investigated and documented.

For the development of geometric/kinematic models of the maintenance equipment and the working site the ROBOT system is available, to check the model consistency a semi-automatic geometry measurement system GMS was developed (see later).

The generation of models, which are suited for real-time simulations, is one of the purposes of the program ROBOT, running in the BRAVO-CAD environment. Version 1.0 has been used again for kinematic design studies, this time for feasability investigations of divertor plate removal paths for ITER using the ABT (Fig. 3).

Besides this, the version 2.0 of ROBOT has been replaced by an enhanced version 2.1. It is furnished with a safer and quicker user interface. Furthermore, it supports the use of libraries and is accomplished by a new simulation module, which will be used for kinematic studies instead of that of version 1.0 in the future. Nevertheless, it is not aimed to compete with real-time simulation systems like KISMET, which will furtheron be provided with geometrical and kinematical models by ROBOT. The features of ROBOT version 2.1 have been described extensively in a user's manual /7/.

ROBOT version 2.1 is currently used to model a simulation scenario for in-vessel handling tasks at ITER, using an ABT. This model package will be updated according to the progress of design, and will be used for simulation studies within ROBOT as well as within KISMET, depending on the objectives and on the complexity of the task under consideration.

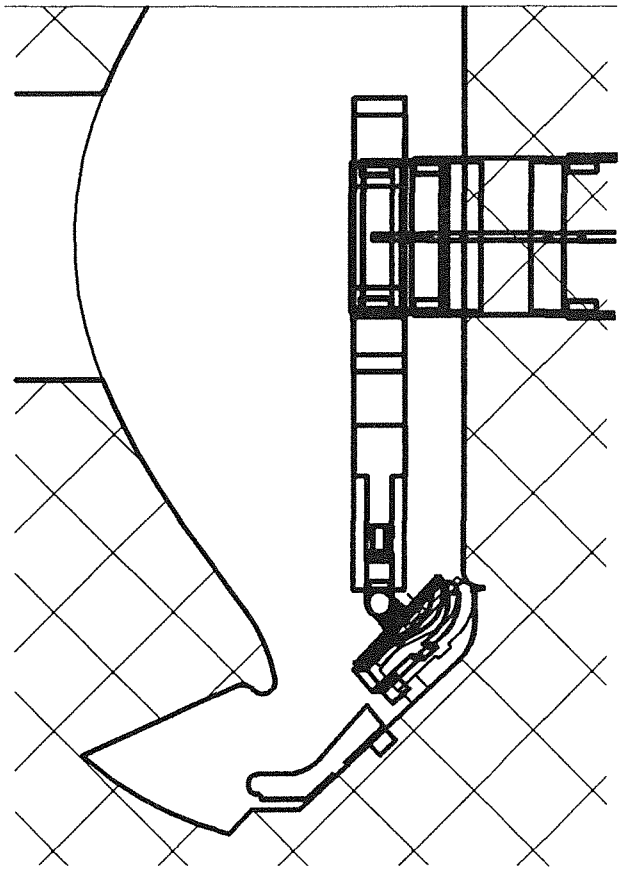

Fig. 3: Divertor plate removal simulation

ABS control system

The ABS control system is the basic subsystem of the ABS-area control system. Other subsystems of the IVHU-area control system are for example the work unit control systems and the camera control system. The ABS control system requirements are documented in /8/. Its main functions are: equipment control (non-motion), motion control, single command execution (manual mode), program execution (automatic mode), on-line teach/repeat, backtracking of paths, operator support functions (e.g. jigs), logging of area control actions. A central feature is the controllability via the NRWS, demanding for a full access to all features of the RH-area control system. There may be implemented a second port to the RH-area control providing the operating interface which represents all the functions the operator directly needs for task execution. This operating interface may be runnable on the NRWS or on the RH-area controller using a network window system allowing the NRWS to access this module and integrate it into the MMI.

Dynamic simulation with AMBOSS

For a complete dynamic simulation of the ABT the AMBOSS (ADAMS-Modelled Boom Simulation System) software environment has been set up. The model concentrates on the ABT actuators with respect to non-linearities.

The current dynamic actuator model shown in Fig. 4 features the following details:

- inertia of the motor, the gears and the link
- gears with transmission ratio
- backlash with damped elasticity at both stops
- gear friction with constant efficiency
- friction of rest:
  The friction torque is increased (by a constant value) when motion stops.
- bearing friction:
  The friction torque depends on the joint load and is treated as static friction.
- deformation of the links:
  One link has two parts which are connected by a linear deformation element (stiffness matrix). The stiffness data are extracted from finite element results.
- control:
  The cascade combination control of the joint actuator comprises servo and PID-position control.
- motor model:
  The present motor model comprises the motor shaft with its inertia and a proportional control circuit.

Achieved results are physically plausible. The implementation of the actuator model into the full ABT model has been started. Validation experiments are proposed for autumn 1990 /9/.

Overall geometry measurement

For the remote maintenance of fusion machines a surveying system will be needed for measuring the geometry of components outside (ex-vessel) as well as inside the vacuum-vessel (in-vessel).

The remote-controlled and CAD-supported surveying system GMS (Geometry Measurement System), developed by KfK for **ex-vessel surveying** is equipped with two digital theodolites, a laser- and a camera-theodolite, completely controlled by a computer /10/. To show the feasibility of the GMS-draft a prototype system, equipped with a single camera-theodolite is built up presently. The software needed for the data transfer CAD <-> GMS and the software for the control of the surveying process is already implemented and successfully tested. During the whole surveying process the operator is guided interactively by the GMS-software and several theodolite parameters (e.g. the speed of the repeating motors) can be changed menu-driven. After an initialization procedure the theodolite is turned automatically into the direction of the nominal point position. For correcting the

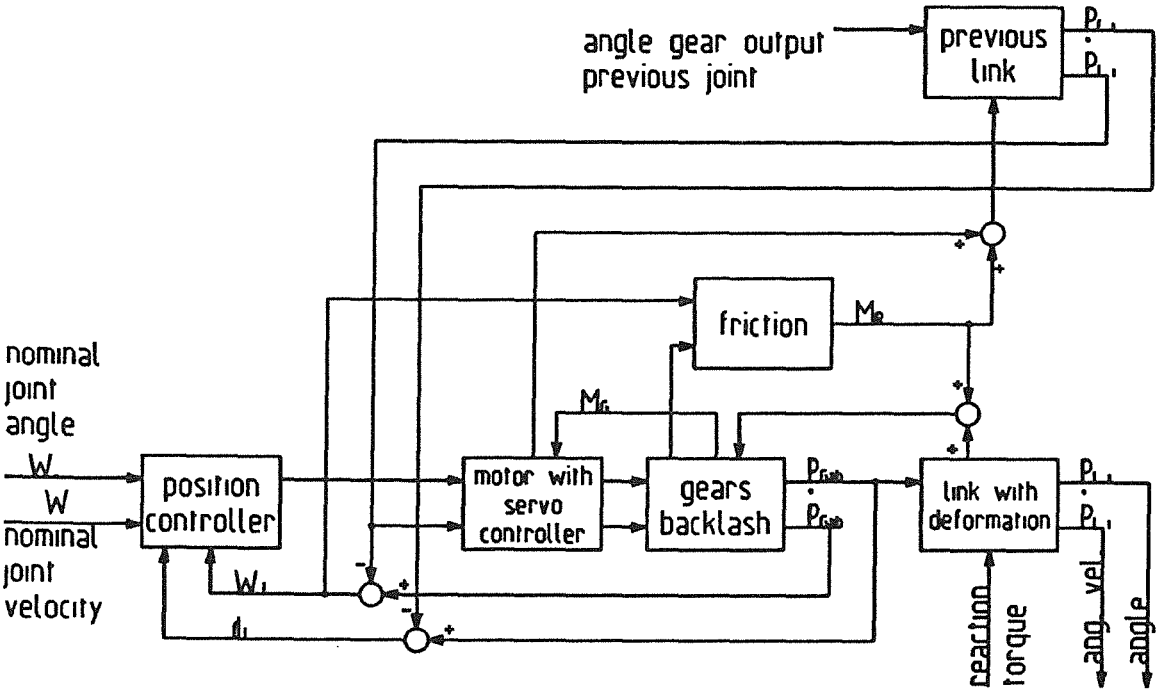

Fig. 4: Dynamic actuator model

theodolite pointings, the operator can use a joystick, the cursor keys or a mouse.

To support the operator a computer graphic can be selectively superimposed the TV-picture. A new enhanced image processing board is installed and the GMS-software has been adapted for this new hardware. The abilities of the graphical support are expanded and the operator can adjust the gain- and offset-values of the digital video image by using a mouse.

To realize the complete remote control, KfK has developed the servo-driven levelling mechanism ALF (Automatic Levelling Facility). ALF is equipped with two inclinometers and the measured inclination is corrected by motor-driven spindles. Based on the experiences with a first prototype, the design of ALF is improved and for temperature compensation special sensors are installed.

The GMS-System is used for surveying the gantry crane system of CATROB and the position of the observation cameras. These experiences can be very helpful for the planned EDITH-surveying. To extend the abilities of the GMS-prototype system, a second digital camera-theodolite with an optional laser adapter shall be still procured this year.

In order not to break the vacuum, periscopes have to be used for the **in-vessel surveying**. Based on the experiences with the ex-vessel surveying a first design concept for a theodolite periscope has been outlined /10/; for building up detailed designs definite informations about the in-vessel surveying processes are needed.

Subtask 1.2: **Design, Manufacture and Testing of an IVHU Full Scale Prototype "EDITH"**

EDITH is the prototypical basic handling equipment for in-vessel components as described in /4/. Differences between EDITH and the NET operational equipment are listed in the following. They are mainly caused by having good accessibility for maintenance and improvement of EDITH and to reduce the costs of EDITH and the mock-up.

The EDITH cantilever arm is shorter than the ABS one and the movable carrier of the ABS is substituted by a fixed support structure.

EDITH will operate at temperatures < 40°C and in a radiation free field.

EDITH is made of ferritic steel which has the same admissible stresses at a temperature < 40°C as the austenitic steel used for the operational equipment at a temperature of +150°C.

The EDITH front link may be manufactured in Al-alloy for the operational equipment.

The remote maintainability of EDITH is limited to one subassembly if there are more than one subassemblies of the same type in order to allow pre-testing.

In a first step of EDITH standard cables and transmission lines are used. Based on the experience of the separate irradiation tests (RHS 2) they will be

substituted later. The same is also valid for other radiation sensitive components.

As mentioned, EDITH will be complemented by a full scale mock-up as it is shown in Fig. 5. The mock-up is based on the

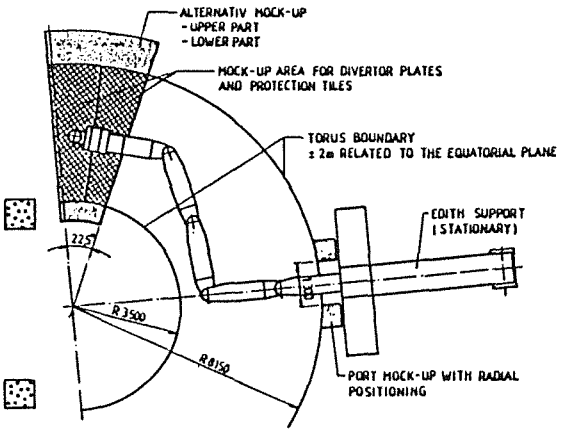

Fig. 5: Scheme of full scale mock-up - plan view

NET torus geometry and simulates two areas of the torus.

One area represents a torus sector of 22.5°. Its center is located perpendicular to the maintenance entry port, thus gaining the maximum loads for the boom. The area is devoted to simulate maintenance operations, e.g. divertor module replacement and tile replacement. In a first step the equatorial plane of the mock-up is at a height of 2m to have relative good access to the boom. In this case the upper half of the torus is simulated (Fig. 6). To simulate also the lower

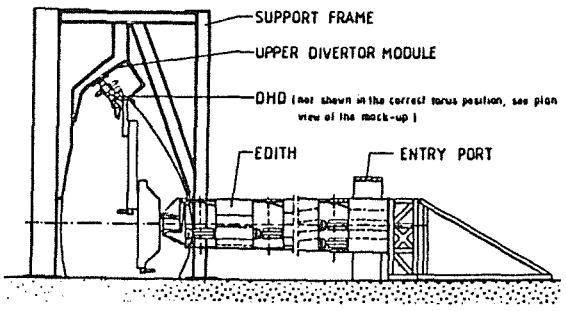

Fig. 6: Scheme of full scale mock-up - upper part

part, in a second step EDITH will be lifted and fixed on an auxiliary support structure (Fig. 7).

The second area of interest is the maintenance port itself to simulate the insertion and withdrawal of the boom. Both areas are connected at a height of 2m around the equatorial plane to simulate the torus boundary.

The mock-up will be completed by the racks for the storage of work units.

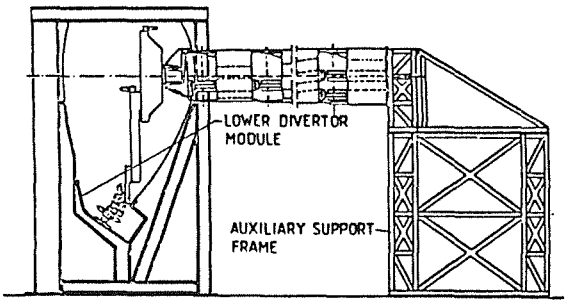

Fig. 7: Scheme of full scale mock-up - lower part

The mechanical part of EDITH and other subassemblies are ordered. For the coaxial drive units an European wide call for tender has been launched. The design of a common interface between boom and the different work units, e.g. manipulator unit, divertor handling unit is ongoing. The testbed will be commissioned at the beginning of 1991. Tests will begin mid 1991. The design of the full scale mock-up is ongoing.

In the process of realizing the **EDITH control system** as a prototype of the ABS control system the JET-TARM control system was investigated for beeing an implementation base. It turns out that the JET-TARM CS functions and components form a subset of the requested ABS functions and components. The TARM high level control system (HLCS) represents the RH-area controller, the TARM low level control system (LLCS) the central equipment controller of the ABS-area. To guarantee a higher flexibility of the LLCS, the hardware was replaced by a MULTIBUS II hardware and the implementation of the software was based on an operating system (iRMX). The implementation language on all levels is C.

The main argument for basing the EDITH control system on the TARM CS was to facilitate the close cooperation with JET especially in the area of MMI (workstation development and enhancements) and advanced control algorithms.

The motion control system has to control EDITH as the central transport unit in the ABS remote handling unit area. It was designed for easy extendability and adaptability allowing to include further enhancements of hard- and software. For example it is possible to add later on subsystems controlling EDITH supporting equipment like camera control units etc. The various subsystems are implementable step by step with the evolving set-up of the complete EDITH system.

Fig. 8 shows how the EDITH control system architecture based on the TARM control system concept is mapped on real hardware. This architecture reveals a hierarchical structure which in turn fits into the concepts of an overall control system architecture for NET remote handling.

The main difference between EDITH and TARM control system is, that the LLCS is now implemented on a

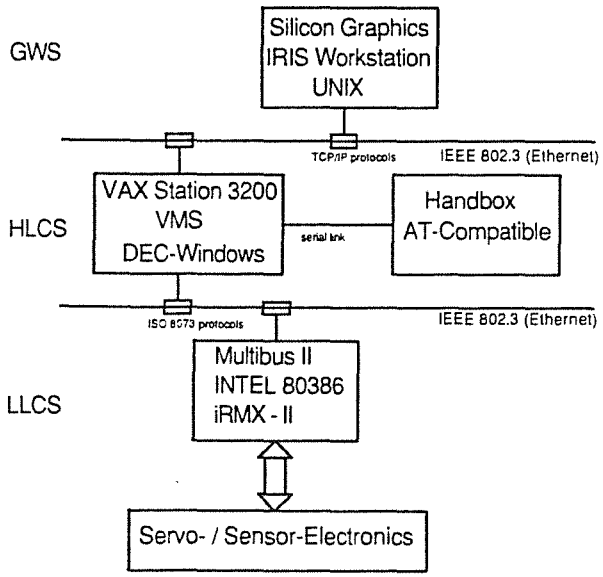

Fig. 8: EDITH motion control system architecture

MULTIBUS II system, running on powerfull CPU-boards (INTEL 80386) with an application software being adapted to the iRMX-II operating system. The reasons for these modifications were the following demands:

- to allow for a step by step development of the final ABS control system, the EDITH control system must be easily expandible with respect to hard- and software. It must be an "Open System", i.e. a system being open to modifications and a high degree of integrability.

- Upgrade to higher performance should easily be possible, as the complexity of the final ABS control system is likely to increase. A demand for higher performance could be coped with either by distribution of functionality or by means of increasing computer power.

Position control is a vital part of the motion control system. The position control has the task to convert as exactly as possible and without delay the desired set point values given for example from the path planning modul into a real motion. The effect of disturbances, e.g. force impacts, have to be compensated.

Although it is intended to use and test in a first implementation stage a single joint control scheme as it was carried out in /11/, one objective of EDITH is testing of advanced control concepts like Inverse Model techniques or adaptive control schemes e.g. /12, 13/, to achieve an excellent dynamic behaviour.

The drive unit control is the lowest level of the control system. It will get the required control signals like revolutions and torques from the position control.

The hard- and software of the EDITH motion control system was specified /14/ and ordered. Delivery date is November 1990.

References:

[1] Maisonnier, D.: NET/ITER In-Vessel Transporters - Technical Specification for their Conceptual and Preliminary Design, Doc.Nr. N2/P/3240/1/B, issue A, 24.10.1989.

[2] Reeve, T.: Divertor Maintenance Using IVHU - In-Vessel Operation, Doc.Nr. N2/P/0230/2/A, 11.05.1989.

[3] Reeve, T.: Definition of Requirements for the Design of Prototype Divertor Handling Equipment, Doc.Nr. N2/P/023132/2/A, issue Draft Jan. 1990.

[4] Kast, G.: Nuclear Fusion Project - Semi-annual Report of the Association KfK/Euratom - April 1989- September 1989, KfK 4677, EUR 11397 EN, November 1989.

[5] Leinemann, K.: Unpublished Report of KfK, November 1988

[6] Kühnapfel, U.: Unpublished Report of KfK, September 1989.

[7] Ludwig, A.: Unpublished Report of KfK, Dec. 1989.

[8] Leinemann, K.: Unpublished Report of KfK, September 1989.

[9] Reim, J.: Unpublished Report of KfK, March 1990.

[10] Köhler, B.: GMS - A High-precision Geometry Measurement System of Large Fusion Reactor Components. IAEA Technical Committe Meeting on Robotics and Remote Maintenance Concepts for Fusion Machines, Karlsruhe, 22.-24.2. 1988.

[11] Süss U.: Unpublished Report of KfK, March 1989.

[12] Weber, W.: Regelung von Manipulator- und Roboterarmen mit reduzierten inversen Modellen. Fortschritt Berichte VDI-Reihe 8, Nr. 183, 1989.

[13] Weber, W., Süss U.: Untersuchung und Realisierung einer adaptiven Gelenkregelung nach dem Referenzmodellkonzept. VDI Berichte Nr. 598, 1986.

[14] Breitwieser H., Frank A., Holler E., Leinemann K., Süss U.: Specification of EDITH motion control system. To be published as KfK report.

Staff:

J. Bernert
B. Dolensky
A. Frank
S. Geiger
B. Haferkamp
E. Holler
J .Hübener
H. Knüppel
B. Köhler
R. Krieg
U. Kühnapfel
K. Leinemann
W. Link
A. Ludwig
G. Müller
W. Pleschounig
S. Raff
J. Reim
E.G. Schlechtendahl
P. Schultheiß
U. Süss
A. Suppan
E. Wehner

Safety and Environment

Introduction:

Within the European Fusion Technology Programme the safety analyses for NET/ITER which are being performed in parallel to the design efforts address mainly three different areas:

Component Related Studies focus on:

- Safety of vacuum vessel and in-vessel components (SEC 1)
- Safety of cryosystems (SEC 2)
- Safety analyses of superconducting magnets (SEC 3)
- Safety of tritium cycle and storage systems (SEC 4)
- Safety of plasma heating and fuelling systems (SEC 5)

Plant Related Studies deal with:

- Radioactivity source terms (SEP 1)
- Environmental impact of tritium and activation products (SEP 2)
- Waste management and decommissioning (SEP 3)

Safety Guidance and Assessment Studies concentrate on:

- Specific safety related recommendations for the design (SEA 1)
- Safety assessments for normal operation and maintenance (SEA 2)
- Reference accident sequences (SEA 3)
- Risk studies (SEA 4)
- Assistance in the preparation of safety reports (SEA 5)

KfK contributes to the following S + E tasks:
SEC 3, SEP 2, SEA 1 (finished), SEA 3, and SEA 5.

The KfK development of safety relevant models and codes for superconducting magnets as well as the performance of validation tests for these codes are described in the magnet task MSA 1.

In the frame of the European Long-Term Safety and Environment Programme KfK performes comparative analyses of some key safety aspects of the D-T and D-^{3}He fuel cycles (LTSE-4). These studies concentrate on accidental hazards to workers and public and hazards, related to waste management.

SEP 2 Environmental Impact of Tritium and Activation Products

Subtasks 2.1 and 2.2

The computer model UFOTRI which dynamically describes the relevant transport processes of tritium in the environment, is now established in a first version. The description of the physical content of the model is available, the report is under publication [1], a summarizing paper has been presented recently [2].

The model was applied in a benchmark exercise for calculating the off-site radiological consequences of an accidental release of tritium in both chemical forms HT or HTO. For the first time, changing weather conditions were selected in this benchmark. Three different weather sequences, all of them from existing meteorological data, were selected as representative to describe a realistic worst case scenario.

The calculations with UFOTRI demonstrate that in the case of a HTO-release the initial meteorological conditions, namely wind speed and atmospheric stratification, are the dominant parameters for the resulting individual peak doses due to inhalation + skin absorption and due to the ingestion pathways. The process of re-emission of HTO with its following transport and dispersion in the atmosphere has a larger influence on the collective doses than on the individual peak doses. However, this process dominates the individual and collective doses resulting from a HT release. In this case the re-emission process increases the inhalation + skin absorption dose by one to two orders of magnitudes.

Additional calculations were performed for a normal operation benchmark. Because a model for calculating doses from effluents under normal operations is under development and will be completed not before 1991, the calculations were carried out using the specific model of the 'AVV Berechnungsgrundlage 1979' [3]. The results lay clearly below those of the other participants, the interpretation needs further discussion. Supplementary calculations with the statistical dispersion model ISOLA [4] were performed to create a site specific weather statistics of Karlsruhe for the year 1982. The use of the results of these statistics (all other parameters remain the same as before) led to an increase of the dose from inhalation + skin absorption by about a factor of 3 in comparison to those values obtained with the benchmark weather statistics.

To evaluate the radiological consequences of accidental releases from fusion reactors, additional activation products have to be considered, which are not yet included in the radionuclide list of the program system UFOMOD [5] and COSYMA [6], respectively. To complete the ingestion pathway, activity concentrations after a single unit deposit of each of the 13 radionuclides V-49, Cr-51, Mn-53, Mn-54, Fe-55, Fe-59, Ni-59, Ni-63, Co-57, Co-58, Co-60, Mn-93 and W-181 on agricultural land have been precalculated by the Gesellschaft fuer Strahlen- und Umweltforschung (GSF) m.b.H., Neuherberg, with the time-dependent radioecological model ECOSYS [7]. To account for the seasonal effects, releases on the 1st of January and the 1st of July have been assumed to be representative of accidents during the winter and the summer vegetation periods. The data will be implemented in the accident consequence codes together with the tritium model to allow for estimating the spectrum of consequences resulting from arbitrary source terms with radionuclide compositions of activation products and tritium.

References:

[1] Raskob, W.: UFOTRI: Program for Assessing the Off-Site Consequences from Accidental Tritium Releases, KfK-report 4605, Kernforschungszentrum Karlsruhe (in preparation).

[2] Raskob, W.: UFOTRI: The Modelling of Tritium Behaviour in the Environemnt in: Proceedings of the 'Seminar on Methods and Codes for Assessing the Off-Site Consequences of Nuclear Accidents', Athen, May 7-11, 1990, (to be published) 1990.

[3] Der Bundesminister des Inneren: Allgemeine Berechnungsgrundlage für die Strahlenexposition bei radioaktiven Ableitungen mit der Abluft oder in Oberflächenwasser (Richtlinie zu § 45 StrlSchV) Bundesgesetzblatt Nr. 21, S 371-435, 1979.

[4] Huebschmann, W. und Raskob, W.: ISOLA V - A FORTRAN 77-Code for the Calculation of the Long-Term Concentration Distribution in the Environment of Nuclear Installations; KfK-report 4606, Kernforschungszentrum Karlsruhe (1990).

[5] Ehrhardt, J., Burkart, K., Hasemann, I., Matzerath, C., Panitz, H.-J. und Steinhauer, C.: The Program System UFOMOD for Assessing the Consequences of Nuclear Accidents; KfK-report 4330, Kernforschungszentrum Karlsruhe (1988).

[6] COSYMA: A New Program Package for Accident Consequence Assessments, A Joint Report by Kernforschungszentrum Karlsruhe (FRG) and National Radiological Protection Board (UK), to be published as EUR-report, 1990.

[7] Matthies, M. et. al.: Simulation des Transfers von Radionukliden in landwirtschaftlichen Nahrungsketten, GSF-Bericht S-882, 1982.

Staff:

J. Ehrhardt,
I. Hasemann
W. Raskob

SEA 3 Reference Accident Sequences

Subtask 3.1

The definition of reference accident sequences has been compoleted in the period reported here. They are compiled in an internal KfK report, January 1990. The sequences defined are:

- RAS-1 Failure in the magnet system.
  Investigated at KfK and ENEA.
- RAS-2 Failure in the tritium system with T release in the containment.
  Investigated at CEA.
- RAS-3 LOCA outside the vacuum vessel.
  Investigated at ECN.
- RAS-4 LOCA/LOFA in the vacuum vessel.
  Investigated at Technicatom and CEA.
- RAS-5 Air ingress into the vacuum vessel.
  Investigated at JRC and CEA.
- RAS-6 Total loss of off-site el. power.
  Investigated at ECN.

This concludes the task SEA 3.1. The associations investigating the RAS's report on their work under SEA 3.2 to SEA 3.8.

Staff:

R. Meyder

Subtask 3.2

To initiate the work for the magnet accidents a requirement definition document for the subtasks SEC 3.1 and SEA 3.2 has been set up and harmonized with ENEA Frascati. According to this KfK investigates the Reference Accident Sequence-1 a (RAS-1 a): Uncontrolled growing normal conducting zone and RAS-1 b: Low Ohm shorts and arcs on a magnet. ENEA will investigate RAS-1 c: Loss of isolation vacuum and RAS-1 d: Loss of cooling for the coils.

The analysis of an uncontrolled growing normal conducting zone, being performed at KfK, requires the development of an appropriate computer code. This is done also at KfK in cooperation with NET. Details on this code development are given under MSA 1.1.

Staff:

R. Meyder

SEA 5 Assistance in Preparation of a Safety Report

Subtask 5.1

As a contribution to the preparation of a preliminary safety report for NET a status report on the safety assessment of the magnet systems has been started in autumn 1989. After discussions of a first draft with the NET Team a second draft of the report on magnet safety has been elaborated as of May 1990.

The report will include a characterization of the magnet systems, the identification of accident sequences, first investigations of accident scenarios, the valuation of possible propagating effects jeopardizing other systems, and finally safety related recommendations for the magnet design.

Up to now, two reference accident sequences with possible major consequences were identified. These are:

- Uncontrolled growing normal conducting zone

- Low Ohm shorts and arcs on a magnet

For both types of accidents further investigations are necessary, both for the TF and the PF coil systems.

The main aim of quench propagation analysis is to prove that subsequent structural failures do not occur; or if structural failure cannot be excluded to show what kind of failures could occur.

Concerning shorts and arcs structural failures cannot be excluded yet. Hence, safety analyses have to strive for a better understanding of the magnet system behaviour under short and arc accidents. Design measures have to be taken to reduce the probability of occurrence of shorts and arcs, and measures to mitigate the consequences have to be foreseen. Especially the case of an arc outside of the magnet in any series current connections has to be excluded by design of the leads; i.e. exclude local overheating, thermal-mechanical excess stresses, and electro-mechanical excess stresses.

Staff:

K.P. Jüngst
W. Kramer
H. Kronhardt
R. Meyder

SEC 3 Safety Analyses for Superconducting Magnets

Subtask 1 Analyses of the Mechanical Behaviour of the PF Coils and of the Central Vault of the TF Coils under Accident Conditions

Under this subtask faults of superconducting magnets are investigated which may lead to undesired displacements or loss of integrity of the coil system. Such a failure of magnet components could probably propagate in damaging e.g. surrounding electrical cables or coolent piping initiating further damage.

The events considered are short currents or erroneous current switching for both toroidal field coils (TF-coils) and poloidal field coils (PF-coils). The investigations performed so far are treating the mechanical integrity of the TF-coils, especially the inner vault, composed by the inboard TF-coil legs.

During normal operation the very high forces produced by the coils directed to the inner vault are symmetrical and uniformly distributed leading to pure compressive loading. But in the case of accidents events have to be studied leading to less favourable asymmetric force distributions which may result in a loss of stability of the coil assembly.

The following cases which are assumed to present worst cases are investigated:

a) discharging of one TF-circuit leading to a symmetrical, but non-uniform loading (producing bending moments in the inner vault)

Assuming an external coil short of one TF-coil leading to asymmetrical loadings:

b1) discharging of the circuit containing the faulty coil

b2) discharging of the unfaulty circuit

b3) discharging of both circuits

c) charging of both circuits, one circuit containing a shorted coil.

For low ohmic shorts case b2) is practically equivalent to case a). Case c), however, is not really relevant since the time scale of charging is very large (time in the order of hours). Thus, such an error will be detected early and dangerous loads can then be prevented.

To determine the load conditions for these cases first transient calculations for the induced electrical currents have to be performed using the code MSCAP [1]. Fig. 1 gives an example for case b1). Then for a selected time where the current values are thought to produce the most unfavourable loads the force distribution is calculated using the code EFFI [2]. Fig. 2 shows the resulting in-plane loads along the coils

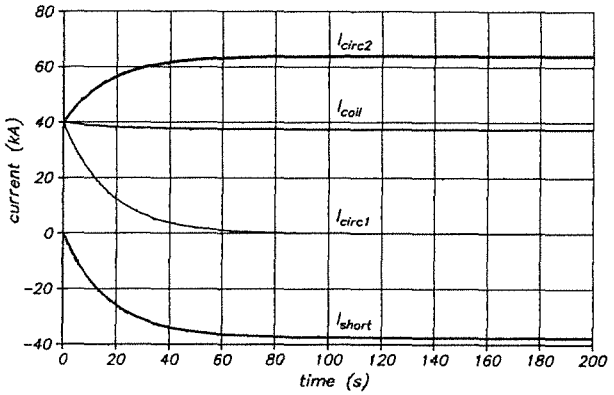

Fig. 1: Discharging of the circuit with a coil short (case b_1)

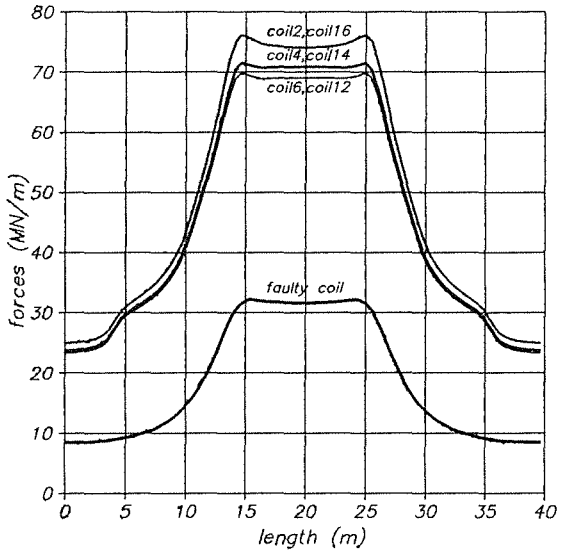

Fig. 2: In-plane loads of the TF-coils (case b_1) along the coil length

beginning at the equator of the outer legs, for instance.

The mechanical analysis then is performed using models with increasing complexity of the details of the structure. With focus on the central vault the identification of critical loading conditions is performed using a fast and simple ring model based on available closed solutions. Fig. 3 e.g. shows the internal forces for case b1). Compared to normal load conditions, where only a compressive force exists, here considerable bending moments and also shear forces occur.

If the most critical cases have been identified a more detailed but also more time consuming analysis will be performed to confirm the results. This has to be done for asymmetrical loadings modelling all 16 coils. Fig. 4 shows the calculated displacements of the coil casings under the in-plane and out-of-plane loading due to case b1 using a combined shell-beam FEM-model (ca. 15000 degrees of freedom, code ABAQUS [3]).

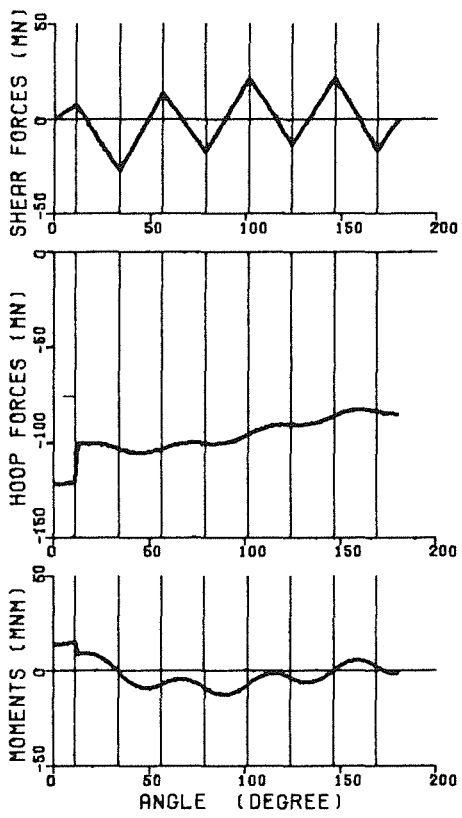

Fig. 3: Central vault, forces along the vault circumference (case b_1)

Concerning the integrity of the vault several conditions must be fulfilled: The yield stress should not be exceeded, at the coil interfaces of the vault the hoop stresses must not be positive and the compressive force at the interface must allow for the shear stress by friction.

So far the tools to perform the described calculations have been prepared and a systematic study is on the way. Later on the influence of faulted PF-coils on the TF-coil case loading will also be investigated.

References:

[1] H.G. Kraus and J.L. Jones, "Hybrid Finite Difference / Finite Element Solution Method Development for Non-Linear Superconducting Magnet and Electrical Circuit Breakdown Transient Analysis", International Journal for Numerical Methods in Engineering, Vol. 23, 1003-1022 (1986).

[2] S.J. Sackett, "EFFI - a Code for Calculating the Electromagnetic Field, Force, and Inductance in Coil Systems of Arbitrary Geometry", UCRL-52402 (1978).

[3] ABAQUS - User Information Manual, Update to version 4.7, Hibbit, Karlsson and Sorensen, Inc.

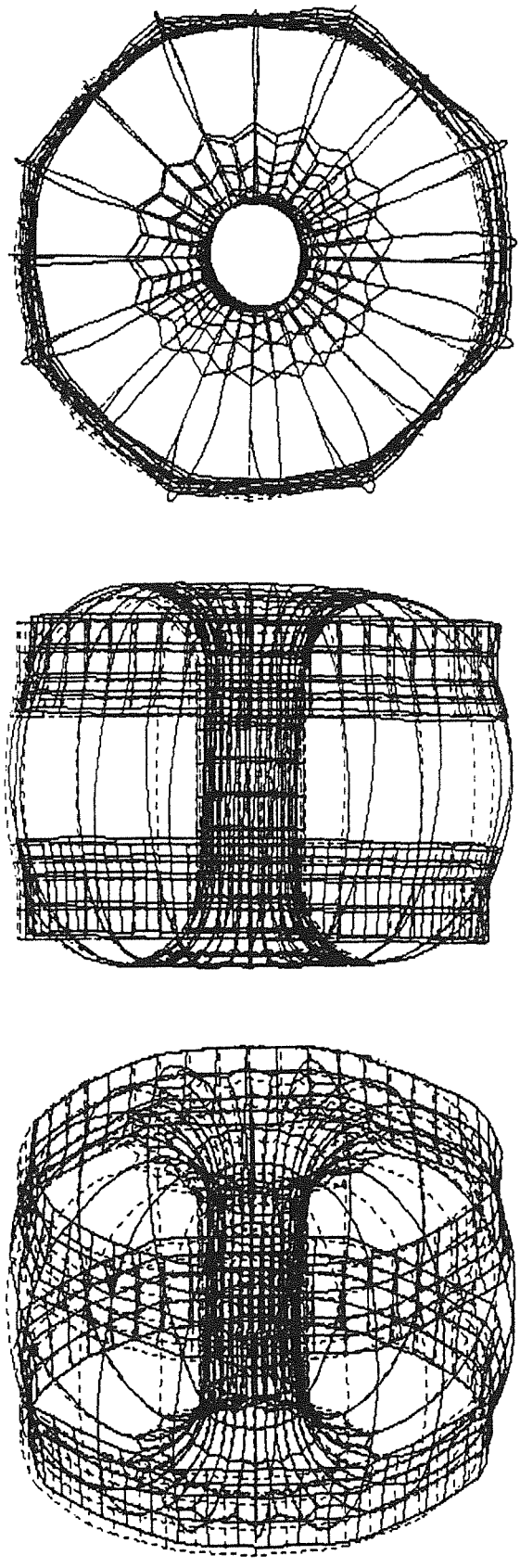

Fig. 4: Displacements (factor 30) of the TF-coil casings for case b_1 calculated with ABAQUS

Staff:

B. Dolensky
R. Krieg
R. Meyder
S. Raff
E. Wehner

LTSE 4 Comparative Analyses of Safety Aspects of the D-T and D-^{3}He Fuel Cycles

Concept of a D-^{3}He Tokamak

Part of the European program on Long Term safety and Environment (LTSE 4) concerning the comparison of D-T and D-^{3}He with regard to reactor safety is covered by KfK. To pursue the comparison a self consistent set of parameters of a D-^{3}He reactor had to be achieved. This turned out to be impossible of course when strictly following the physical and the technical NET/ITER guidelines. Also the results of an earlier study on D-^{3}He by KfK and the University of Madison have been invalidated by experimental results.

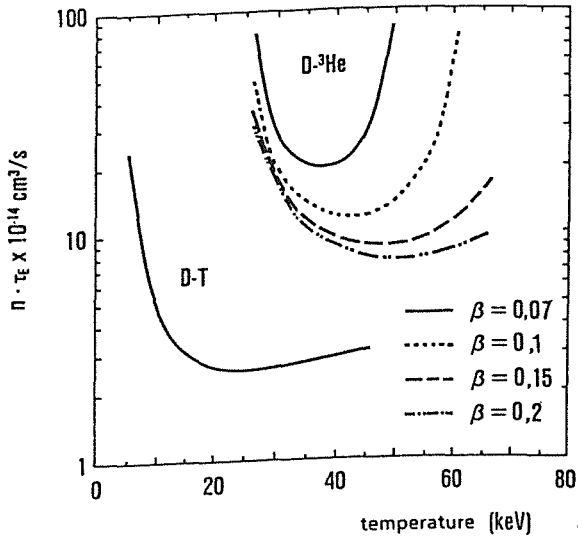

Fig. 1: The relation between n x τ_E and the plasma temperature for the ignition of D-T and D-^{3}He. The additional dependence of the ignition condition for D-^{3}He on several parameters is mentioned in the report.

Nevertheless a self consistent data set was compiled for the LTSE 4 studies. To achieve ignition conditions it was unavoidable to ignore at least partly the current NET/ITER guidelines relying on future development. This procedure seems to be justified since D-^{3}He, if at all will be a fuel of the very far future. Major improvements in the fields of superconductivity, structure materials, plasma physics and especially disruption control would be necessary.

Just to remind Fig.1 shows the ignition conditions for D-T and for D-^{3}He. Different from D-T the relation between the product of plasma density n and energy confinement time τ_E and the ion temperature depends additionally on the Betavalue of the plasma, the minor plasma halfwidth a the magnetic field strength B_0 on axis and on the reflectivity of the first wall for synchrotronradiation. This being due to the strongly increasing production rate and plasma penetration of synchrotronradiation at rising temperatures. (In Fig. 1 the

major plasma radius R_0	9,0 m
minor plasma halfwidth a	4,5 m
magnetic field B_0 on axis	6,13 Tesla
magnetic field B_c at the coil (assuming I/R dependence)	14,6 Tesla

Table 1

R_0	6,07 m
a	2,38 m
B_0	8,4 Tesla
B_c	18,7 Tesla

Table 2

following values were inserted: a=2,5 m B_0=8 Tesla, reflectivity=0,8).

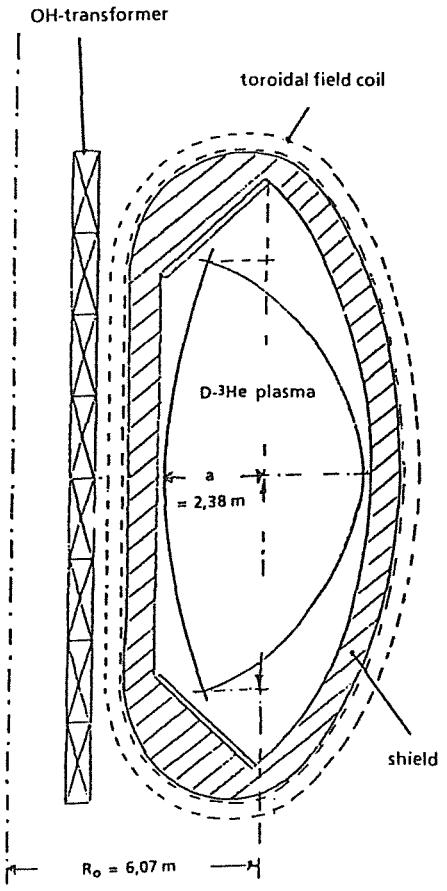

Fig. 2: Cross section of the D-^{3}He reactor concept. The dimensions of the OH-transformer were taken from NET/ITER. The minimum thickness of the shield for the protection of the coils had to be 0,75 m. The distances between the shield and the plasma and between the shield and the coils were taken to be 0,1 m.

	NET/ITER		D-^{3}He	
major plasmaradius R_0	6,0	m	6,07	m
minor plasma halfwidth a	2,15	m	2,38	m
elongation	1,98		2,2	
magnetic field B_0	4,85	T	8,46	T
magnetic field B_c	10,74	T	18,74	T
plasma current	22	MA	71	MA
total reactor power	1,0	GW	2,2	GW
energy confinement time	2,0	s	13,5	s
first wall power density	0,04	MW/m^2	1,9	MW/m^2
divertor power	170	MW	262	MW
2,45 MeV neutron power			24	MW
14,1 MeV neutron power	800	MW	53	MW

Table 3

In a first attempt it was assumed, that the magnetic field strength B_c on the inboard side of the toroidal field coils should not exceed 14 Tesla (this being already above the current guidelines used by KfK in cooperation with the NET team although sometimes accepted for studies). To achieve ignition conditions on the basis of the Rebut-Lallia scaling law for the energy confinement time rather large plasma dimensions were necessary (see Table 1).

Yet it turned out that the distance of the coils at the outboard side was so big that the I/R relation did not hold any more. To achieve 6,13 Tesla on axis B_c had to be 18,4 Tesla.

Thus a more compact version closer to NET/ITER dimensions was preferred of course at much higher values of the magnetic field strength. The results are summarized in Table 2.

Fig. 2 shows the cross section of a D-^{3}He reactor. In Table 3 a few plasma and machine parameters are listed for comparison.

Staff:

R. Klingelhöfer

Test Blanket Development

Introduction:

Within the European Fusion Technology Program blanket development is divided in work for the NET/ITER basic machine and work for the test blankets. In agreement with the NET-Team and after establishing two European working groups KfK has concentrated its efforts on the development of test blankets for NET/ITER. By test blankets we understand blankets for the next step towards a commercial power station, so called DEMO relevant blankets. In the DEMO-reactor, the potential of a fusion machine to produce electricity shall be tested for the first time. Consequently the test blankets have to be designed for DEMO relevance in terms of breeding rate, temperatures and pressure. Structural materials, maintainability, reliability and safety have to satisfy the more stringent requirements of power production in comparison with driver or shielding blankets for the NET/ITER basic machine. The boundary conditions mentioned above cannot be satisfied full scale and at the same time in the test positions available in NET/ITER. Therefore the definition of test objects and the testing program is one of the main objectives of KfK besides the proof of DEMO relevance of the KfK blanket design alternatives.

The European Test Blanket Development Groups mentioned above deal with two development lines, one with solid breeder helium cooled, the other with liquid metal breeder and either liquid metal (selfcooled) or water cooled blankets. Both KfK developed design, the selfcooled lithium-lead blanket and the helium cooled, breeder out of tube, canister blanket are accepted alternatives within the European test blanket development program - see BS-DE and BL-DE tasks. A part of the work defined by the partners - KfK, CEA, ENEA and JRC Ispra - consists of common work, relevant to all blanket designs, whereas the design work itself remains independent for the time being. It is foreseen to reduce the number of blanket alternatives to two in 1994/95, one solid breeder and one liquid metal breeder design, which will than be tested in NET/ITER.

The Solid Breeder Blanket Tasks (BS)

Solid breeder design, already mentioned above (DE-D-1), includes besides the design work proper, also small scale thermomechanical and fabricability tests. The KfK solid breeder material program has concentrated, in agreement with the European partners, on lithium orthosilicate. The program tasks include preparation, characterization, irradiation and postirradiation examination as well as measurement of the physical, chemical and mechanical properties. Of special interest are the in and out of pile tritium release studies, performed at KfK and within the common breeder development program in several European reactors. The KfK breeder program is described in tasks BR-D-1 through D-8. The main non nuclear testing facility to prove the feasibility of KfK's solid breeder design will be the helium loop HEBLO, in which elements as well as canister sections may be tested - see NN-D-1.

The Liquid Metal Blanket Tasks (BL)

Design activities (DE-D-1) concentrate on a solution featuring an inboard / outboard blanket without beryllium as a neutron multiplier. This is so far the only blanket alternative, including solid breeder blankets which allows a sufficiently high tritium breeding rate, not using beryllium.

Of great importance to the development of the selfcooled blanket is the knowhow and the date base of magneto-hydrodynamic behaviour of liquid metal flow aquired in theoretical and experimental studies of task MH-D-1. The test facility MEKKA and the cooperation with Argonne National Laboratory play a central role in MHD development.

In addition to design and MHD activities KfK studies the physico-chemical behaviour, task PC-D-1, especially corrosion of structural materials in the lithium lead eutectic (Pb-17Li) and tritium extraction from Pb-17Li. Task EX-D-1 describes tritium removal and recovery by permeation and cold trapping, task EX-D-2 removal of tritium by solid getters. The sodium-potassium loop WAWIK and the Pb-17Li loop TRITEX are the main testbeds for the experimental studies.

BS DE-D-1 Solid Breeder Test Blanket Design

In the reporting period work continued on a DEMO blanket design of the KfK solid breeder blanket concept and on a NET test object for this blanket. In addition beryllium / steel soldering tests were made and construction of a helium loop for blanket tests is under construction. The latter is described under BS NN-D-1.

The geometrical configuration of DEMO was specified by the Test Blanket Advisory Group and approved by the NET-Team in March / April 1990 so that only a limited time period was available for blanket design work. The new configuration has a better coverage than the earlier NET and DEMO proposal so that 28 canisters could be placed on the outboard side (see Fig. 1). Moreover the space behind the divertors could be used for blankets.

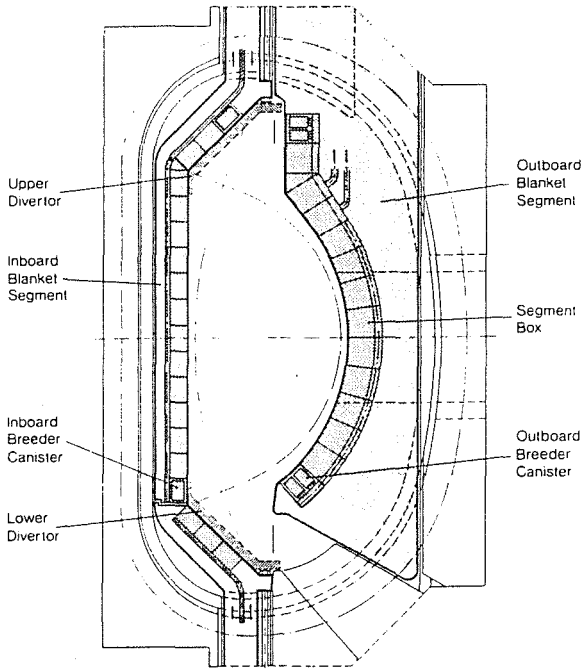

Fig. 1: DEMO-reactor with solid breeder canister blanket

With this configuration a tritium breeding ratio of TBR = 1.15 was obtained in a realistic 3D Monte-Carlo calculation which included all effects such as ports, saddle loops, space between blankets, pumping ducts etc.

The calculation of electro-magnetic forces from plasma disruptions was extended to the case of vertical plasma movement [1]. The characteristics of this movement were specified by the NET-Team: In about 40 ms the plasma axis is shifted vertically by 1.50 m thereafter the current quench occurs linearly within 20 ms. The torque-forces and bending moments exceed those of the current quench case without plasma displacement by nearly an order of magnitude and lead to stresses which are far beyond the ASME design rules.

For the NET test object first the box had to be designed which fits to the horizontal ports, contains a water cooled first wall, and can be connected on the back side to a transport cask. To prevent contact with the room atmosphere the connection is made by a double door air lock system. Some design iterations were necessary to take into account all constrains from the ITER design which was taken as reference for the horizontal ports. A schematic drawing with the main dimensions is shown in Fig. 2.

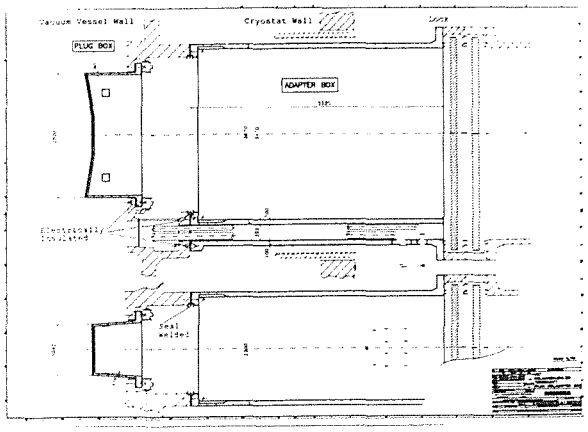

Fig. 2: Box for the insertion of test objects into horizontal ports of ITER

The box consists of two components a plug box and an adapter box. Both are flanged on the vacuum vessel by electrically insulated air tight bolts which have to be opened by a remote handling system from inside the box. The supply lines for the test object and first wall cooling are connected at the upper surface of the adapter box by NET standarized remote handling equipment.

Fig. 3 shows the test plug of the KfK canister blanket design which is mounted on rails together with the necessary shield.

To cope with the electro-magnetic forces from disruptions side wheels are also foreseen on the top part of the carriage.

Design work for the periphery of the ITER (NET) test plug was continued. The circuits consist of the helium coolant system with purification unit, the purge system with tritium extraction, and ancillary systems. As an example Fig. 4 shows a flow sheet of the purge gas system. The one bar pressure helium purge flow loaded with tritium and hydrogen is transported in double walled tubes to the tight caisson where heat removal, tritium extraction and gas purification systems are located.

In a He/H_2O heat exchanger the purge flow is cooled down to room temperature and in adsorbers the water component is separated. After heating the purge flow again tritium and hydrogen gas is separated from the flow by silver-palladium permeation filters. The tritium hydrogen mixture is stored in uranium beds. The helium flow then is purified from nitrogen and other gases in a low temperature (100K) adsorber system. Thereafter the purge gas is heated up again in a recuperative

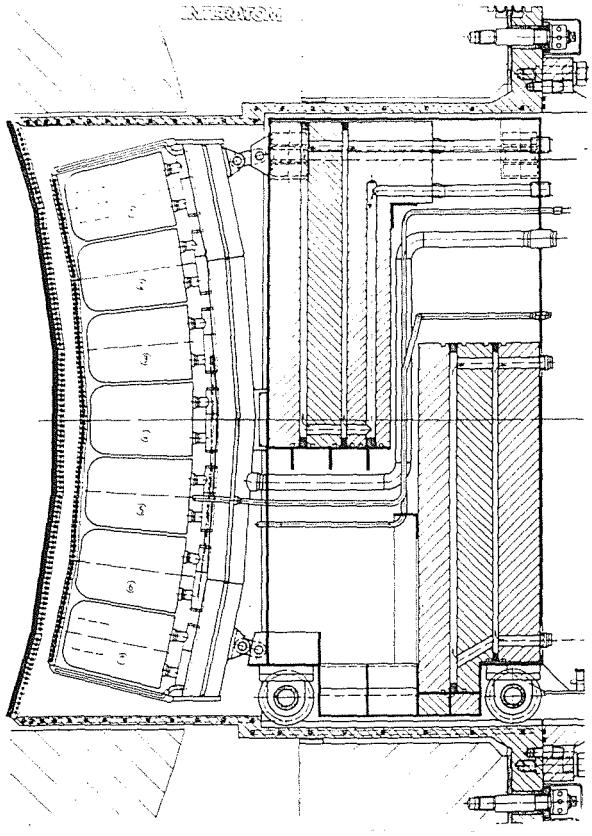

Fig. 3: ITER test module of the KfK solid breeder canister blanket design

heat exchanger and is brought to its design pressure of one bar.

In case that the two fully independent main coolant systems fail the purge system can act as an emergency coolant system for decay heat removal. In this mode of operation only the main coolers and the blowers are used the rest of the system is bypassed.

Beryllium / Steel-Soldering Test

The KfK blanket concept ist characterized inter alia by heat removal through coolant tubes which are soldered within beryllium plates. Soldering has to ensure good thermal contact and sufficient stability of the component up to temperatures of close to 500°C. Due to lack of experience with beryllium / stainless steel solders and the high importance of this manufacturing step to the blanket concept manufacturing tests were performed in cooperation with W.C. Heraeus, Hanau.

In a first series of wetting tests a wide spectrum of silver solders have been tested. Besides to austenite 316L, the tests related to martensitic MANET. After completion of these pilot tests the only candidates left for further investigations have been the ternary AGCuSn-solders with 5% and 10% tin content. With the two selected solders tests were performed in which the coolant tubes made of steel 316L were soldered to two beryllium segments which had been provided with semi-circular grooves. The sequence of the soldering cycle has been

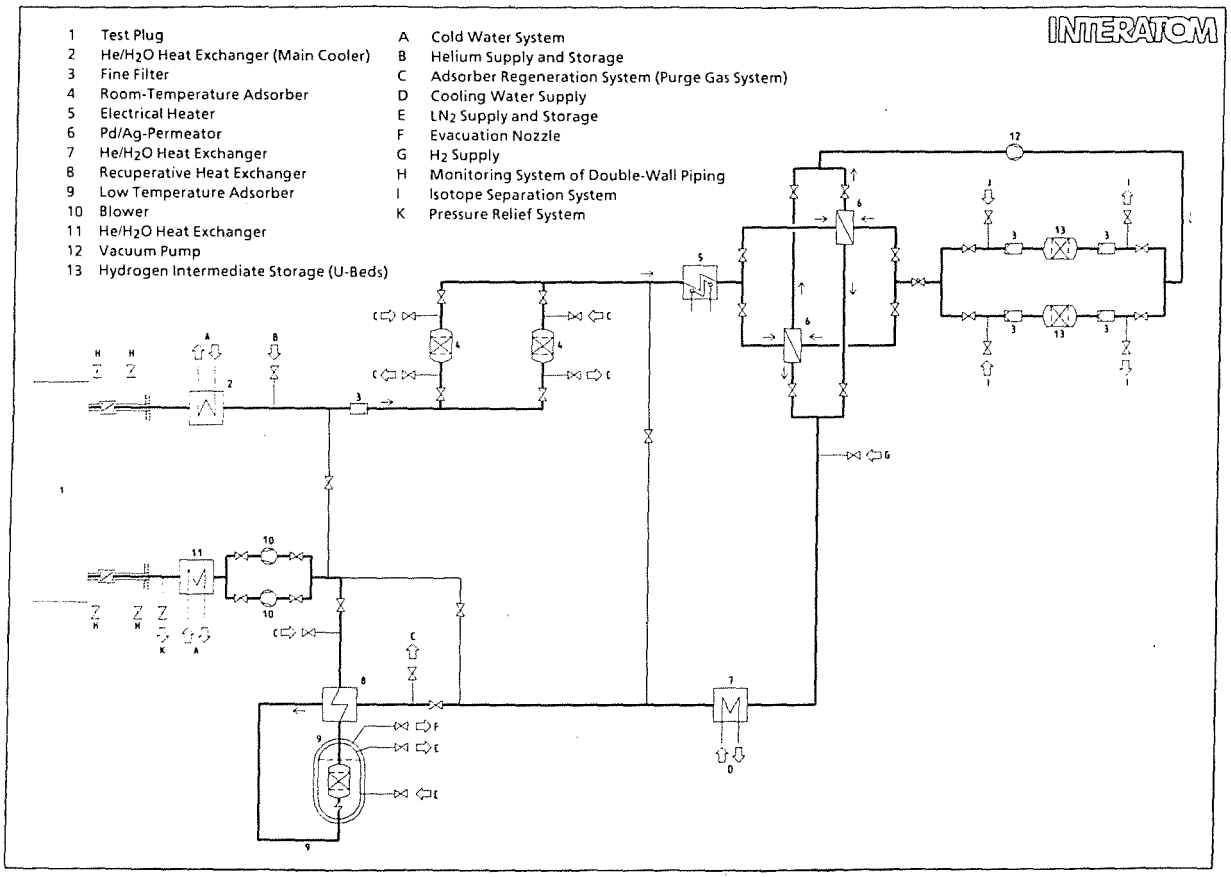

Fig. 4: Purge gas system for NET test plug with canister blanket

adapted to the size of the beryllium elements contained in the DEMO blanket.

The soldering tests have evidenced that reliable Be/Be and Be/steel solders can be achieved with the Ag60Cu30Sn10 solder at 700°C soldering temperature. Values of about 200 N/ mm^2 were measured for the shear strength of the steel / beryllium compound at room temperature. Considering the relatively long duration of soldering, this corresponds to the values of Be/Be-soldering known from the literature. The soldered specimens were examined at 500°C, too. At that temperature level the shear strength was still at least 70 N/mm^2.

Reference:

[1] L. Boccaccini "Berechnung der elektromagnetischen Kräfte im Blanket eines Tokamakreaktors beim Plasmastromabbruch und Bestimmung der dadurch hervorgerufenen mechanischen Spannungen" KfK 4757 (1990).

Staff:

L. Boccaccini
E. Bojarsky
M. Dalle Donne
U. Fischer
M. Küchle
P. Norajitra
G. Reimann
H. Reiser

BS BR-D-1 Preparation of Ceramic Breeder Materials

Staff:

E. Günther
U. Hain
J. Heger
H. Wedemeyer

The preparation of lithium containing monosilicates, especially Li_4SiO_4, and metazirconates, Li_2ZrO_3, are under development to be used as breeder materials within the European Fusion Program. The development was concentrated on the optimization of sintered specimen of Li_4SiO_4 concerning the grain-size distribution as discussion arises on a possible influence of grain-sizes on the tritium release behavior at lower temperatures (350-400 °C).

The sintered lithium orthosilicate breeder material, used for different irradiation experiments and material property tests, was so far not specified with respect to the grain-size distribution. Due to strong grain growth during the sintering process, the grain-sizes were measured to be in the range of 50 to 100 µm. Detailed studies of the sintering process showed that the grain growth depends on a variety of parameters, such as heating rate, sintering temperatur, ... The main results are: 1. at temperatures of up to 950 °C there is no grain growth but the densification is small (~80% th.d.), 2. at 950 to 1025 °C there is only a slight grain growth but densification increases significantly, 3. at 1025 to 1030 °C there is a maximum in densification (>90% th.d.) combined with small grain growth (2-10 µm) depending on sintering time, 4. at temperatures above 1030 °C there is a strong increase in grain growth combined with decreasing densification. In summary, it is possible to fabricate grain-size controlled lithium orthosilicate breeder materials.

Lithium metazirconate powder and pebbles (~80% th.d.) were fabricated for the irradiation experiments TRIDEX-5 and ALICE-3. Batches of pure lithium orthosilicate powder and pebbles were prepared for thermophysical property measurements.

References:

D. Vollath, H. Wedemeyer, H. Zimmermann, H. Werle:
Doped Lithium Orthosilicates, Preparation and Properties, 4th Intern. Conf. on Fusion Reactor Materials (ICFRM-4), Dec. 1989, Kyoto, Japan.

D. Vollath, H. Wedemeyer:
Process for the Preparation of Lithium Metazirconate, 4th Intern. Conf. on Fusion Reactor Materials (ICFRM-4), Dec. 1989, Kyoto, Japan.

H. Wedemeyer, H.-J. Ritzhaupt-Kleissl:
Lithiumkeramik für Fusionsreaktoren: Herstellung und Charakterisierung. Jahrestagung Kerntechnik '90, Nürnberg 1990, S. 577-580.

BS BR-D-2 Characterization of Ceramic Breeder Materials

The characterization work of ceramic breeder materials was continued. One of the main activities were the characterizing analyses of the lithium silicate and lithium zirconate discs, prepared by KfK/IMF III for the SIBELIUS irradiation experiment.

The following analyses were carried out: geometric measurement, X-ray diffractometry, mercury intrusion porosimetry, helium pycnometry and structure analysis by ceramography.

The results of the geometric measurements - weight, length, diameter and density - showed, that the reproducibility of the samples was quite good, the standard deviations for diameter and density lie - with one exception - well below 1%. The X-ray diffractographs for the silicate specimens showed mainly orthosilicate with traces (about 5%) of metasilicate. Also, the zirconate samples consisted mainly of Li_2ZrO_3, with small amounts of ZrO_2, preferentially at the surface. The mercury intrusion density was 2.16 g/cm^3 (90.4% th.d.) for the silicate specimen, with an open porosity of 4.5% and pore channel diameters generally smaller than 100 nm. The density of the Li_2ZrO_3 was determined to be 3.65 g/cm^3 (88.0% th.d.). The amount of open porosity was also 4.5%, but, in contrast to the silicate, about one third of the open porosity has channel diameters larger than 100 nm.

By interpretation of the He-pycnometry results, the values for the closed porosities can be calculated:

$Li_4SiO_4 : \rho_{cl} = 2.4\ \%$

$Li_2ZrO_3 : \rho_{cl} = 4.8\ \%$.

Ceramographic analyses showed that the structure of the silicates seems to be more regular than that of the zirconates.

References:

K.R. Kummerer, H.-J. Ritzhaupt-Kleissl:
Comparative Irradiation of Different Lithium Ceramics, 4th International Conference on Fusion Reactor Materials (ICFRM-4), Dec. 1989, Kyoto, Japan.

Staff:

R. Hanselmann
W. Laub
Chr. Odemer
H.-J. Ritzhaupt-Kleissl

BS BR-D-3 Irradiation Testing and Post Irradiation Examination

1. Irradiation Testing

In the previous semi-annual reports the two breeder ceramic irradiation campaigns DELICE 03, performed in the OSIRIS reactor, Saylay, and ELIMA 2, performed at HFR, Petten, as an international comparison experiment called COMPLIMENT (Comparison of Lithium Materials Damage Effects by Fast Neutrons and 6Li (n, α) T-Reactions) have been repeatedly described. In the ELIMA experiment at HFR the thermal neutrons had been largely shielded by a cadmium screen; therefore, the rate of damage due to (n, α) reactions is higher by a factor of five in the DELICE 03 experiment.

Meanwhile, both irradiation campaigns have been completed and the post-irradiation examinations for which a dedicated fusion ceramic laboratory had been erected in the KfK hot cells have yielded first results.

The following Fig. 1 shows in a direct comparison the configuration of the breeder ceramic columns in the two irradiation experiments as well as the axial plots of the neutron fluxes in the OSIRIS reactor and in HFR.

After evaluation of the results of dosimeter measurements and determination of the final neutron fluxes it will be possible to determine the dose and rate of damage, respectively, of the individual specimen pins from the plan showing the specimen positions.

For irradiation experiments concerning tritium release see task BS BR-D-4.

Staff:

H.E. Häfner
K. Heckert
K. Philipp

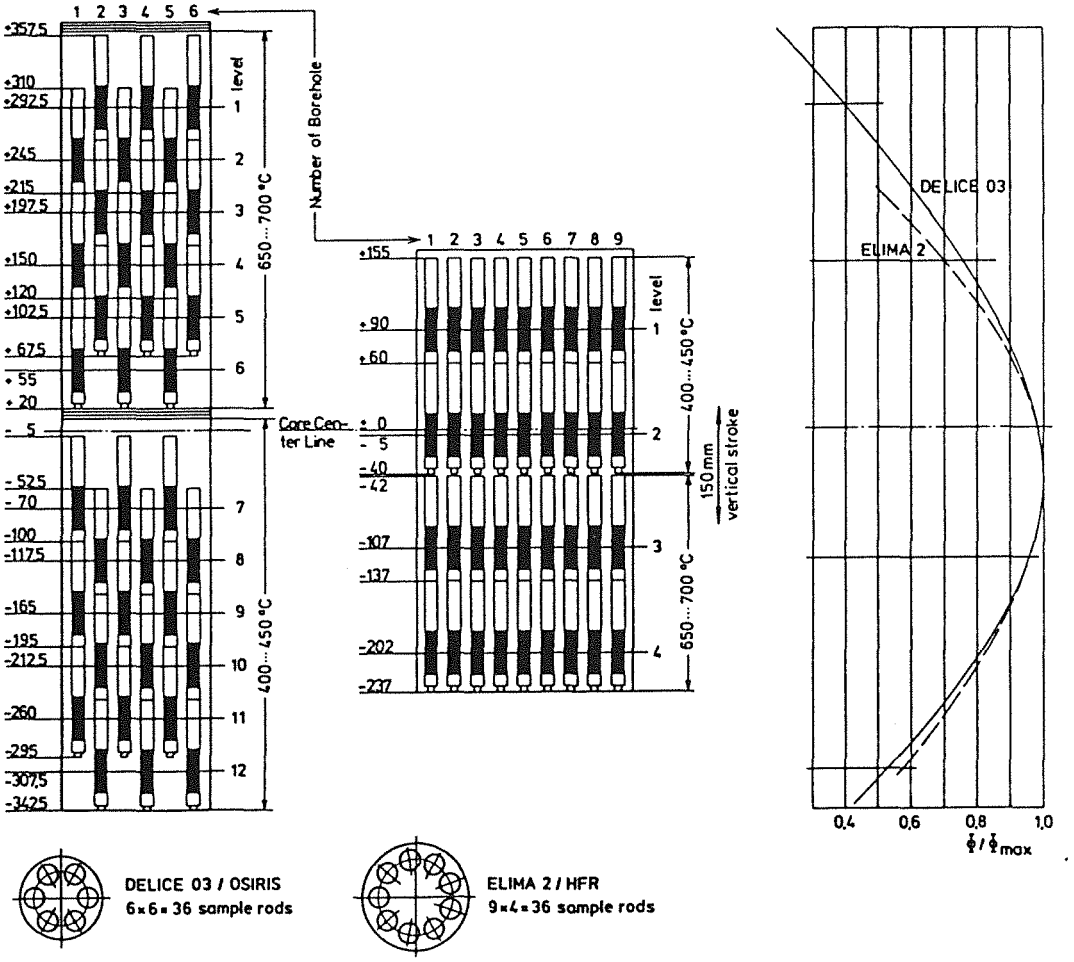

Fig. 1: Arrangement of the samples in the comparative irradiation experiment COMPLIMENT

2. Post Irradiation Examination

The solid breeder concept requires ceramic compounds with high lithium content, good tritium extraction characteristic at moderate temperatures, mechanical integrity, minor swelling and chemical compatibility to the containment. Measurement and comparison of the properties of various breeding ceramics irradiated in closed capsules at different temperatures and neutron fluences are carried out in the Fusion Ceramics Laboratory (FKL) . For the European COMPLIMENT experiment (Comparison of Lithium Materials Damage Effects by Fast Neutrons and ^{6} Li(n,α)T Reactions): Li_2O, $LiAlO_2$, Li_2ZrO_3, Li_2SiO_3, Li_4SiO_4 samples were irradiated at (670-720) K and (920-970) K at the reactors HFR-Petten and OSIRIS-Saclay, respectively. After irradiation the sample rods were transfered to the FKL at KfK. Post irradiation examination (PIE) and distribution of selected samples to the European partners of the fusion program are now in progress (Fig. 2).

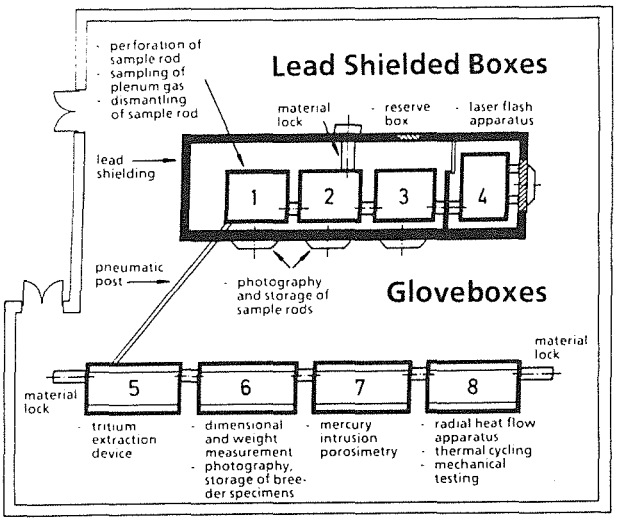

Fig. 2: Scheme of the new fusion ceramics laboratory (FKL)

The FKL laboratory was designed and built by the division HVT-HZ (Hauptabteilung Versuchstechnik-Heiße Zellen). It consists of 4 lead shielded boxes (Fig. 3) and 4 gloveboxes (Fig. 4). The lead shielding (thickness 20 cm) reduces the radiation intensity from the neutron activated sample containers. Manipulators are used in the lead shielded boxes for handling of the sample capsules. Tritium containing breeding ceramic samples are handled in the gloveboxes. An inert and dry atmosphere (N_2) is needed within the boxes to protect the ceramics from oxydation and water vapor. Oxygen and humidity content of the nitrogen gas is reduced by a closed gas processing loop to 5 vol. ppm (Fig. 5). Humidity is collected by a molecular sieve. Oxygen from leackage into the boxes is extracted by a heated copper bed. Tritium gas is removed by oxidation by means of a copper oxide bed. The resultant tritiated water vapor is collected by a molecular sieve located downstream the copper bed.

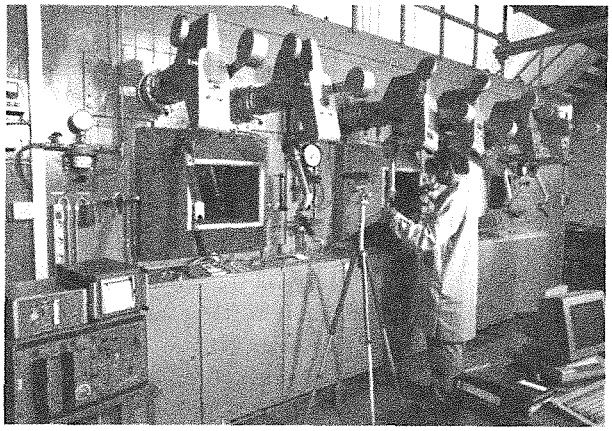

Fig. 3: Lead shielded boxes

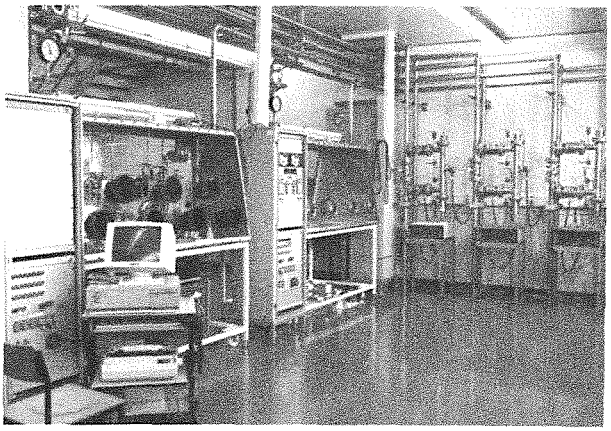

Fig. 4: Two of the four gloveboxes (no. 7 and no. 8)

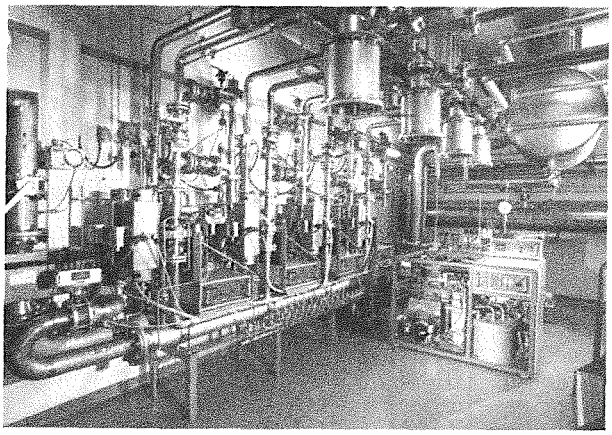

Fig. 5: Gas regeneration device for the inert atmosphere of the boxes

Several operation modes of the box ventilation like closed circuit and once through operation are possible. A three step pressure gradient is maintained from the laboratory outside to the interior of the boxes at all operation modes. The

tritium activity of the atmosphere within the laboratory and the boxes is continuously recorded.

Irradiated sample capsules are stored in the lead shielded box no. 1, visually inspected and photographed. The capsules are perforated in an evacuated vessel located in box no. 1 and a part of the expanding plenum gas is sampled in a gasometer. Dismantling of the sample rods is performed under inert atmosphere of the cell. The samples are photographed and packed in new capsules for storage and transportation. Capsules containing breeding ceramics are controlled with a γ-detector before transferring via pneumatic post into the unshielded glovebox no. 5. Weight and geometric dimensions of the samples are measured in glovebox no. 6.

Tritium extraction characteristics are investigated at different temperatures according to a special program (box no. 5). The released tritium activity is detected by an ionization chamber. Purge gases with various percentages of H_2 or H_2O are used to optimize the tritium extraction characteristic. The reference purge gas consists of helium with 0.1 vol.% H_2. For determination of the tritium activity of the plenum gas the gasometer is connected to the ionization chamber and purged with the reference gas.

Irradiation induced swelling and open porosity changes of the samples are measured by mercury intrusion porosimetry (box no. 7). Swelling decreases the density which is determined from the volume of mercury displaced by the sample and the previously measured weight of the sample. The abundance and size distribution of the open pores are calculated from the volume of mercury penetrating the open pores as a function of the pressure applied. This technique is also used for unirradiated reference samples.

Changes of the thermal diffusivity of window and breeding ceramic pellets due to irradiation is measured by the laser flash apparatus located in box no. 4. A laser flash is absorbed on the front side of a black colored pellet and the time-dependent increase in the emission of infra-red light on the opposite side of the pellet is recorded. The thermal conductivity of beds of sintered and molten lithium orthosilicate (Li_4SiO_4) pebbles (mean diameter of the pebbles 0.5 mm) will be measured by the radial heat flow method in glovebox no. 8. Thermal cycling followed by mechanical testing is applied to breeding ceramics to study thermo-mechanical properties.

Selected samples are transfered to the shielded metallographic unit located in the same building for further characterization. Photographs of cut - and fractured surfaces are taken by a scanning electron microscope. The elemental composition of selected regions of the samples is determined by analysis of the characteristic X-rays. The abundance and size distribution of grains and closed pores are explored by image analysis. Crystallographic phases and irradiation induced swelling are studied by X-ray diffractometry. Neutron activated impurities in the samples are checked by analysis of the γ-spectrum taken with a germanium detector.

Staff:

L. Dörr
Th. Eberle
R. Hanselmann
D. Knebel
V. Prech
D. Schild
P. Weimar
H. Ziegler
G. Lehrmann
K. Schneider
H.E. Häfner
H. Werle
W. Nägele

BS BR-D-4 Tritium Release

In assessing the performance of ceramic breeders, tritium release is an important aspect. KfK concentrates on lithium silicates, espcially orthosilicate, and metazirconate. Purged inpile tests and out-of-pile annealing experiments are performed.

The joint CEA/KfK inpile test LILA/LISA3 was finished October 1989 after three reactor cycles (46 FPD). Metazirconate samples of CEA, Mol and KfK and pure and Al-doped orthosilicate of KfK were tested. The main results are:

1) The kinetics of the pure and the doped orthosilicate pellets detoriated steadily with time by about a factor ten from beginning to end of irradiation. This very disturbing behaviour was not oberserved for any of the other hitherto inpile tested KfK sample.

2) At 400°C and for He + 0.1 vol% H_2 purge gas
   - the doped orthosilikate is less than a factor two faster than the pure orthosilicate
   - the KfK metazirconate is a factor three faster than the KfK orthosilicate but, probably because of the larger grains, nearly a factor ten slower than the metazirconate pellets of Saclay and Mol.

3) For all samples the kinetics does not change if the neutron flux is varied by a factor two, indicating first order controlled tritium release

4) For all samples the kinetics is drastically improved by adding H_2 or H_20 to the purge gas.

The first joint European medium-term inpile test EXOTIC-5 performed at the HFR Petten was finished February 1990 after six reactor cycles (136 FPD). Important results for the KfK sample (orthosilicate sinter granulate 0.5 mm ∅, type WB2, 81%TD)are:

1) No irradiation induced changes of the tritium release kinetics were observed

2) At 400°C and for He+0.1vol%H2 purge gas, the residence time (43h) is about a factor three larger than that of the preliminary reference Schott 86 spheres (15h)

PIE tritium release measurements of the (closed capsule) irradiations DELICE 1 (metasilicate 65 and 85% TD) and DELICE 2 (meta- and orthosilicate, 65 and 90% TD) have been finsihed, those of the joint European fast/thermal neutrons irradiation COMPLIMENT have been started.

References:

W. Breitung, H. Werle
"Experimental Evidence for Tritium Release Controlling Processes in Lithium Silictes"
Fourth Int. Conf. Fusion Reactor Materials (ICFRM-4), Kyoto, December 1989

Staff:

W. Breitung
T. Eberle
J. Lebkücher
M. Möschke
H. Werle

BS BR-D-5 Physical and Mechanical Properties

Thermophysical properties of HIP-Li_4SiO_4 produced of spherical powder solidified from a Li_4SiO_4 melt were compared with those of pressureless sintered material. The specific heat agreed within the error range of measurement. The thermal expansion coefficient of HIP-Li_4SiO_4 up to 608 °C was $(2.89 \pm 0.09) \times 10^{-5}$ K^{-1} compared to 2.09×10^{-5} K^{-1} for the pressureless sintered samples. In the range of transition (608 - 720 °C) the thermal expansion coefficient equals zero, while for the high temperature phase it is $(3.29 \pm 0.1) \times 10^{-5}$ K^{-1}.

The investigations of the mechanical properties of nonirradiated ceramic breeder materials have been continued with measuring the ultimate compressive strength of Li_4SiO_4, Li_2SiO_3 and $LiAlO_2$ at temperatures up to 700 °C. Results are shown in Table 1.

Table 1: Ultimate compressive strength of ceramic breeder materials at room temperature and 700 °C.

Material	Density % TD	Grain size µm	Compressive strength, MPa	
			RT	700 °C
Li_4SiO_4				
XI	78	15	220	43
X	90	100	105	69
Li_2SiO_3				
VIII	93	10	455	380
VII	83	6	350	225
VI	83	8	385	18
$LiAlO_2$				
LP[1]	88	< 1	550	550
MP[2]	73	< 1	375	375

[1] Low Porosity

[2] Medium Porosity

Young's modulus, ultimate compressive strength, and thermal shock resistance of Li_4SiO_4 doped with Al and Mg have been determined and compared with nondoped material. The results are shown in Table 2. Whereas the Young's modulus was only slightly changed by doping, a distinct reduction in strength can be noticed. The thermal shock resistance characterized by the critical temperature difference in heating up tests (in a Sn metal melt) was improved by Mg doping and was made worse by Al.

Table 2: Mechanical properties of lithium orthosilicate.

	Li_4SiO_4	$Li_{3.7}Al_{0.1}SiO_4$	$Li_{3.8}Mg_{0.1}SiO_4$
Young's modulus, GPa	80 ± 5	88 ± 1	75 ± 1
Poisson ratio	0.25	0.25	0.25
Ultimate compressive strength, MPa[1]	250 ± 10	55 ± 8	83 ± 9
Critical temperature difference, K	475	360	500

[1] related to 20 µm grain size, and about 10 % porosity.

Staff:

M. Blumhofer
G. Haase
B. Schulz
H. Zimmermann

BS BR-D-6 Compatibility

To investigate the chemical interactions of Li_4SiO_4 and Li_2SiO_3 with stainless steel (AISI 316) at defined H_2O partial pressures, reaction experiments have been performed at 600, 700 and 800 °C in a flowing gas atmosphere with a constant H_2O partial pressure of 10 Pa (100 vpm) and 100 Pa (1000 vpm). The gas flow was about 25 l Ar/h. For comparison also Li_2O/AISI 316 compatibility experiments were carried out.

The results obtained at 700 and 800 °C for a partial pressure of 100 Pa are shown in Fig.1. The figure depicts the different reaction behaviour of Li_4SiO_4 and Li_2SiO_3 compared to Li_2O with stainless steel (ss). It is important to note that Li_2O shows a better compatibility behaviour than Li_4SiO_4 and Li_2SiO_3, also at a H_2O partial pressure of 10 Pa. This behaviour of Li_2O is in contradiction to results obtained by compatibility experiments with closed capsule systems where Li_2O caused always the strongest attack of stainless steel. In these capsule experiments a defined quantity of water was added to the Li-compounds to simulate a certain reaction potential, and it was demonstrated that the extent of interaction depends on the initial water concentration. But the reaction potential was high at the beginning and decreased with time whereas in the gas flow experiments a constant H_2O partial pressure has been maintained. As a result, the reaction products are different for the Li_2O/ss system but not for the Li_4SiO_4/ss and Li_2SiO_3/ss system. This may be one of the reasons for the different reaction behaviour of Li_2O with stainless steel in the systems described. Further gas flow experiments will be performed at 600 and 900 °C to clarify in detail the different reaction behavior of Li_2O. Concerning the compatibility behaviour of the Li-silicates, Li_4SiO_4 attacks stronger than Li_2SiO_3, similar to the capsule reaction experiments.

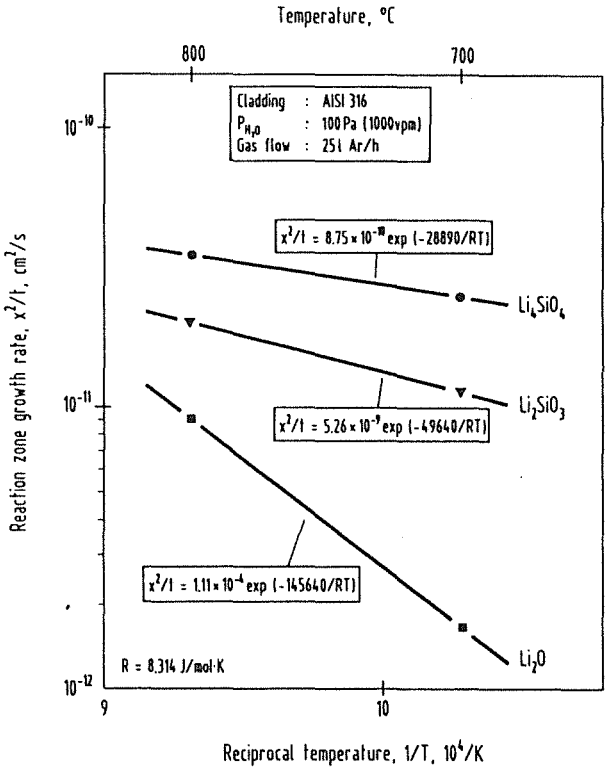

Fig. 1: Comparison of the reaction zone growth rates of various breeding materials with stainless steel for 100 Pa H_2O pressure.

Staff:

J. Burbach
P. Hofmann
H. Metzger

BS BR-D-7 Constitution, Interaction with Water Vapour

The experimental investigation of the Li_2O-ZrO_2 phase relations was continued and completed. Solidus and liquidus temperatures were measured in the system by thermal analysis methods and pyrometrical measurements. Determination of the lattice constants of the phases in two-phase fields showed that for the intermediate compounds there are no extended ranges of homogeneity. On the basis of the experimental results obtained so far, a phase diagram of the Li_2O-ZrO_2 system is proposed (Fig. 1).

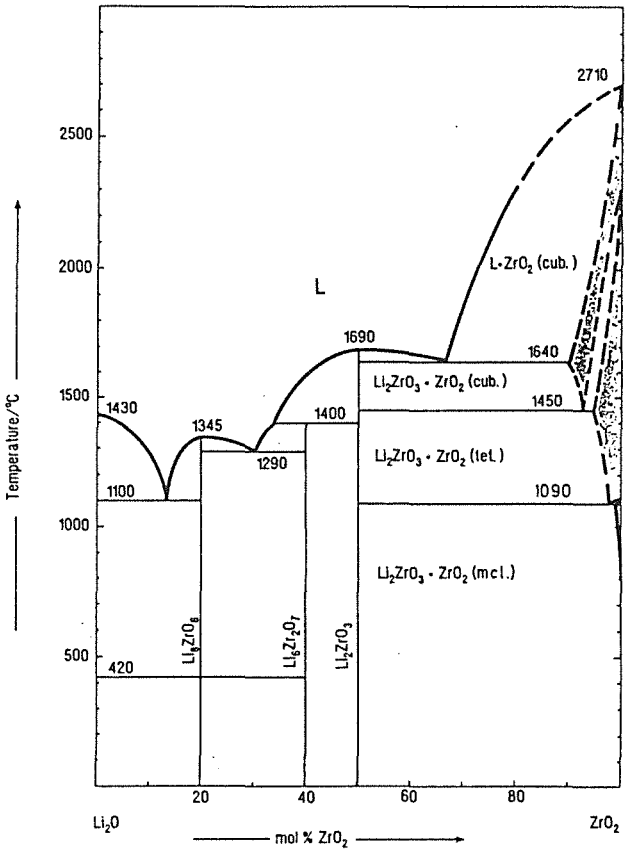

Fig. 1: Phase diagram of the Li_2O-ZrO_2 system.

The investigations of the interaction of Li_4SiO_4 with water vapour were continued with pure as well as with doped (2.2 wt.-% SiO_2) material. The aim of the tests was to contribute to an explanation of the complex water release mechanism by associating distinct release steps to different bonding mechanisms. This was achieved by comparing theoretical activation energies with experimental values gained from thermal gravimetry runs. The comparison resulted in the determination of three temperature ranges. In the low temperature range (80 - 300 °C), release of physically adsorbed water is observed to occur in several partially overlapping peaks, depending on the origin of the samples. The measured activation energy (39 - 43 kJ/mole) agrees well with the heat of vaporization of water (40 kJ/mole).

In the temperature range between 300 and 500 °C the desorption of water bound by hydrogen bridges is superimposed to the desorption of physically adsorbed water. The desorption of chemisorbed water fixed by OH bondings starts above 500 °C. In the range between 600 and 720 °C, dehydroxylation of OH groups bound coordinatively to Li occurs. The measured activation energy is 115 - 145 kJ/mole, corresponding to the activation energy of the dissociation of the Li-OH bonding in Li_2O (124 kJ/mole). In addition to the breaking of the Li-OH bondings, water is formed by recombination of adjacent OH groups and water molecules are released into the gas phase. The formation of water is favoured by the presence of hydrogen (100 ppm) in the purge gas.

Doped Li_4SiO_4 and pure Li_2ZrO_3 show similar release behaviour compared to pure Li_4SiO_4 with the exception that the release reaction at ~ 650 °C is hardly perceptible.

Staff:

Ch. Adelhelm
D. Linder
V. Schauer
G. Schlickeiser
A. Skokan
H. Strömann

BS BR-D-8 Mass Spectrometric Free Evaporation Measurements on Lithiumorthosilicate Surfaces

In previous studies Knudsen effusion equilibrium data of ceramic tritium breeders have been obtained and used to determine the maximum possible sublimation rates of vapor species emitted from ceramic breeder materials. From these data the overall evaporation process can be formulated and upper temperature limits with respect to vaporization losses can be defined. In an actual blanket, the maximum possible evaporation rates may, however, not always be attained. The minimum sublimation rates are given by the Langmuir free evaporation rates. To get more insight into the details of the sublimation of ceramic breeders, a free evaporation study with mass spectrometric analysis of the vapor effusing from the surface of lithium orthosilicate has been initiated. The information obtained can also be of relevance to the understanding of the thermal desorption step during release of tritium from ceramic breeder surfaces.

For the Langmuir effusion rate studies an existing Finnigan MAT mass spectrometer was modified. In particular, the electron bombardment heating system was replaced by high frequency heating. This modification has the following advantages: i) in the temperature range of the measurements no heat shields are required and particle reflection is minimized, ii) the metallic sample support body is heated to a uniform temperature, iii) the background pressure is substantially reduced, and iV) measurements are not influenced by the parasitic ionization of lithium as observed with electron bombardment heating.

The source employed in this study consists of a flat surface of a polycrystalline solidified melt of lithium orthosilicate. This type of surface simulates melt of litium orthosilicate pebbles. The lithium orthosilicate was supplied by Schott as spherical particles of 300 - 500 µm diameter. By X-ray analysis of the Li_4SiO_4 no Li_2SiO_3 was detected as phase impurity (detection limit 5 mol %).

The partial pressures of the free evaporating gas species, p_i, were calculated from the measured ion currents, I_i, according to eqn. (1)

$$p_i = K = \frac{I_i \cdot T}{\sigma_i \cdot x_i \cdot Y_i} \qquad (1)$$

where T is the temperature, σ_i the ion cross section, x_i the atom fraction of the measured isotope and γ_i the gain of the elecron multiplier.

The partial pressures of Li, O, O_2, Li_2O, and LiO are observed above lithium orthosilicate within the temperatrue range 1281 - 1550 K. A change in the slopes of the vapor pressure curves occurs at about 1501 K instead at 1528 K, the melting point of pure Li_4SiO_4. This melting point depression is thought to be caused by the presence of some Li_2SiO_3, the thermal decomposition product of the Li_4SiO_4. Because of the incongruent nature of the sublimation of Li_4SiO_4 it is not possible to completely avoid the formation of a second condensed phase.

From a comparison between averaged data of several Langmuir evaporation runs and Knudsen effusion results it is apparent that

- the lithium pressures in free evaporation are lower by about a factor of ten than those of the equilibrium pressures
- the pressures of atomic oxygen in free evaporation are much higher than those calculated from the O_2 pressures measured in Knudsen effusion experiments
- the O_2 pressures measured in free evaporation are considerably lower than those required from oxygen mass balance considerations.

It is customary to relate the pressures obtained in Langmuir evaporation studies (p_L) to those from Knudsen effusion measurements (p_K) by the equatio

$$\alpha = p_L / p_K \qquad (2)$$

where α is the evaporation coefficient. From the Langmuir and Knudsen evaporation studies presently in progress evaporation coefficients α of lithium in the temperature range of the measurements will be determined.

Staff:

S. Huber
H.R. Ihle
R.-D. Penzhorn
P. Schuster

BS NN-D-1 Helium Blanket Test Loop

The Helium Blanket Test Loop (HEBLO) is being built in the IMF for thermomechanical tests on gas cooled blanket components. It was designed such that a shortened blanket canister with a maximum of eight cooled beryllium plates can be subjected to thermal cycling with 200 ° amplitude at a maximum temperature of 460 °C. On the other hand, a blanket canister of the NET test blanket can be operated isothermally. The operation pressure of the loop is 80 bar.

Meanwhile, the helium circulation compressor is under fabrication. The design of all components of the loop system has been terminated. The orders have been placed for the 115 kW cooler and the intermediate heat exchanger used to set the helium temperature level from 50 °C to 260 °C at the inlet of the temperature cycle test facility. The bidding documents for the measurement and control system have been completed.

Staff:

E. Bojarsky
M. Dalle Donne
H. Deckers
H. Lehning
H. Reiser

BL DE-D-1 Liquid Metal Test Blanket Design

Blanket Segments

The temperature and stress analysis of the first version of a self-cooled Pb-17Li blanket concept for a DEMO-reactor has been completed. This version is characterized by a 300 mm thick zone of beryllium as neutron multiplier leading to tritium self-sufficiency without breeding blankets at the inboard region of the torus. For this blanket version both coolant inlet and outlet tubes are connected to the top side of the segments. This arrangement of the coolant supply lines is possible only at the outboard blanket segments. For the inboard segments it would result in an excessive high magneto-hydro-dynamic (MHD) pressure drop due to the higher magnetic field strength and the more limited space at this region compared to the outboard region.

Feasible self-cooled blanket concepts at the inboard region require a tokamak design allowing for either coolant supply lines at top and bottom side of the blanket segment or inboard segments splitted into an upper and a lower half with seperate supply lines for each half.

The three possibilities of attaching coolant supply lines to an inboard segment are shown schematically in Fig. 1. In a very rough approximation, the MHD pressure drop can be calculated using the equation

$$\Delta p = K \cdot B^2 \cdot v \cdot L .$$

with: K constant, B magnetic field strength, v liquid metal velocity, perpendicular to B, L duct length

The velocity v is determined by the volumetric flow rate $\dot{V}$, the thickness t and the width w of the blanket segment.

Table 1 shows the MHD pressure drop of the inboard blanket segment for the three options.

	Option A	Option B	Option C
v	$\dot{V}/0.5 \cdot t \cdot w$	$\dot{V}/t \cdot w$	$0.5\ \dot{V}/0.5 \cdot t \cdot w$
L	2 H	H	H
$\Delta p/(K \cdot B^2)$	$4 \cdot \dot{V} \cdot H/t \cdot w$	$\dot{V} \cdot H/t \cdot w$	$\dot{V} \cdot H/(t \cdot w)$

Table 1: MHD pressure drop for the three inboard blanket options

In principle, the pressure drop is equal for option B and C but higher for option A by a factor of four.

Fortunately, the new specification of the DEMO-reactor as provided by the Test Blanket Advisory Group (TAG) allows for a inboard blanket design accordingly to option C. Therefore, this option has been selected as reference concept for the self-cooled Pb-17Li blanket. Scoping calculations have shown that the tritium breeding ratio and the cooling conditions are comparable to the version using a beryllium multiplier as investigated previously. The new design as shown in Fig. 2) therefore offers the unique possibility to avoid the need for beryllium inside the blanket at all.

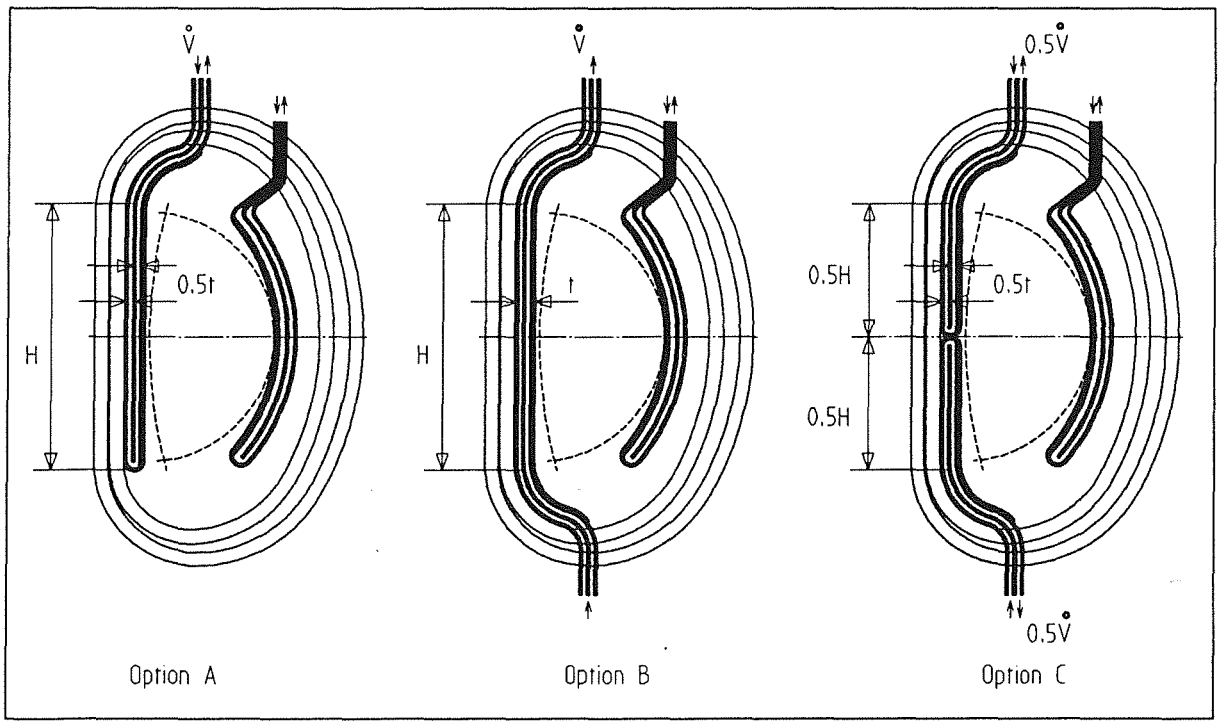

Fig. 1: Arrangement of coolant supply tubes to the inboard segment

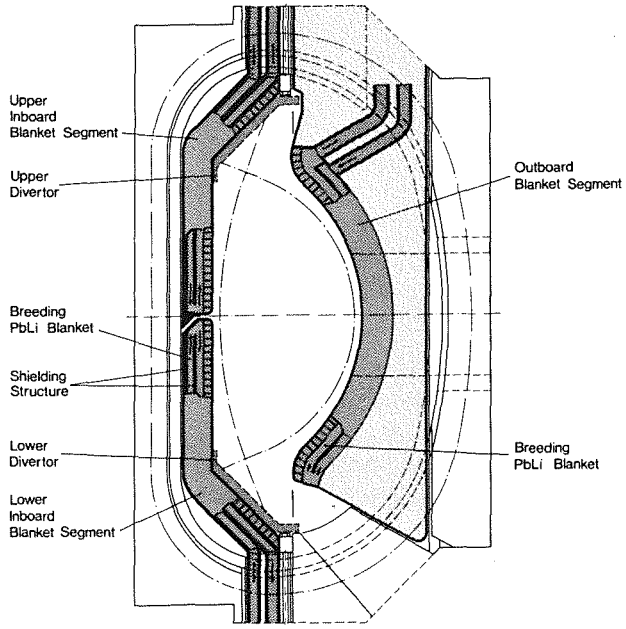

Fig. 2: Self-cooled Pb-17Li blanket in a DEMO reactor

Staff:

K. Arheidt
E. Bojarsky
V. Casal
H. Deckers
U. Fischer
C. Günther
H. John
S. Malang
R. Möller
P.Norajitra
H. Reiser

BL PC-D-1 Corrosion of Structural Materials in Flowing Pb-17Li

Staff:

Ch. Adelhelm
H.U. Borgstedt
G. Frees
D. Linder
Z. Peric
G. Streib

The steady state corrosion rates which were measured in tests at 500 and 550°C in the PICOLO loop in flowing Pb-17Li eutectic (v = 0.3 m/s) were related to calculated values. The calculation was based on hydraulic parameters of the test section in PICOLO. The constants of the corrosion equations for the two test temperatures

$$\Delta R\,[\mu m] = k \cdot t\,[h]$$

(in which ΔR is the loss of material, t the time and k the constant)

are compared in the Table. If we consider that the calculation was performed with the use of the uncertain values of the solubility of steel elements in Pb-17Li, the agreement of measured and calculated values was satisfactory.

The development of self-healing insulating layers on the structural material of the blanket walls was started with the aluminizing of some specimens of MANET steel. The insulating phase, α-alumina, should be formed by oxidation of the Al rich surface. Thermodynamic considerations and measurements of oxygen potentials in molten Pb-17Li indicated that alumina should be reduced by liquid lithium, while the reduction might not occur at the oxygen potentials in the eutectic alloy.

One electrochemical oxygen meter immersed in Pb-17Li was prepared for a coulometric titration of the oxygen content, which will be performed at the University Clausthal.

Reference:

[1] H.U. Borgstedt and H.D. Röhrig, Recent Results on Corrosion Behaviour of MANET Structural Steel in Flowing Pb-17Li Eutectic, 4th Internat. Conf. on Fusion Reactor Materials, Kyoto, Japan, 4-8 Dec. 1989, accepted for publication in J. Nucl. Mater. 176 (1990).

Temperature of Test [°C]	Corrosion constant as measured [$\mu m \cdot h^{-1}$]	Corrosion constant as calculated [$\mu m \cdot h^{-1}$]
500	$-1.47 \cdot 10^{-2}$	$-4.2 \cdot 10^{-2}$
550	$-1.04 \cdot 10^{-1}$	$-1.64 \cdot 10^{-1}$

BL PC-D-2 Impurities and Clean-up of Molten Pb-17Li

As in any liquid metal system also in a molten Pb-17Li blanket, impurities may cause safety and operational problems. Different impurities are of different concern for the operation of the blanket. Corrosion of the structural material will result in mass transfer processes with deposition of corrosion product particles. This may block narrow flow channels. Transport of carbon or other interstitial elements may change the properties of the metallic surfaces. Radioactive impurities may cause maintenance problems, besides radiation exposure of the operators.

The aim of this work is to characterize the different kinds of impurities in a molten Pb-17Li system, to study their behavior, and to find methods for the removal from the liquid metal.

1. Behaviour of Po-210 in Molten Pb-17Li

A large number of radioactive impurities will be formed if the molten eutectic mixture Pb-17Li* is irradiated in a fusion reactor blanket. One of them is Po-210, formed by activation of bismuth impurity:

$$\text{Bi-209}\,(n,\gamma)\,\text{Bi-210}\,(\beta^-)\,\text{Po-210}$$

However even if Bi free LM is used, Po-210 will be formed after an extended operation time of the reactor because of the formation of bismuth from lead:

$$\text{Pb-208}\,(n,\gamma)\,\text{Pb-209}\,(\beta^-)\,\text{Bi-209}$$

Po-210 is of special concern. It is a radio-toxic alpha emitting nuclide with a half live of 138 days. The element has a high vapor pressure, and even some of its chemical compounds are highly volatile. Maintenance problems will occure in the LM as well as in all parts of the covergas system, especially if tritium is to be extracted into a gas phase.

Experiments to investigate the behavior of Po-210 in the LM have started. The polonium was deposited on silver foils, which were then dissolved in the LM. Stirred samples of 60 to 70 grams Pb-17Li were oxidized at different temperatures by air for 20 minutes. Then the metal and the formed oxides were analyzed.

It was found that Po-210 was enriched in the oxides. The enrichment factors depend on the temperature (Fig. 1).

Because it was not possible to obtain completely oxide-free metal samples, the factors may be even higher. However the influence of the Li-concentration in the LM must be investigated. During the oxidation Li migrates into the oxides and the concentration in the metal goes down. At a temperature of 520°C the final Li-concentration in the metal was only 0.42%.

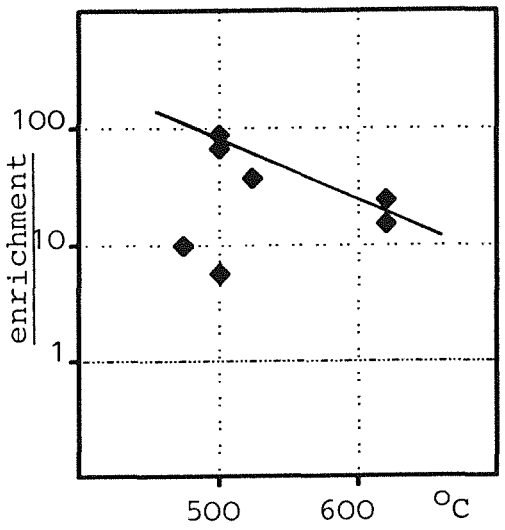

Fig. 1: Enrichment factors for Po-210 in oxides, formed during 20 minutes oxidizing stirred Pb-17Li samples by air. (Bq/g oxide)/(Bq/g metal)

The experiments will continue with an improved technique. It will be investigated if Po-210 can be extracted from the LM by a smaller amount of oxides. Also evaporation rates of Po-210 from the LM into an Ar or He Atmosphere, and plateout on metallic surfaces will be studied.

Staff:

S. Bender
H. Feuerstein
H. Gräbner
J. Oschinski

2. Pb-17Li Loop TRITEX

The facility TRITEX [1] will be used for the experiments. It is a ferritic stainless steel loop (1.4922). About 80 kg of molten Pb-17Li are pumped around by an electro magnetic pump. Fig. 2 shows a flow sheet.

TRITEX has a number of features which can be used for the investigation. A cold trap is operated in a bypass to the main flow. Here impurities may be deposited like in other liquid metal systems. The cold trap can be replaced for investigations in the laboratory. A magnetic trap is in the main circuit, planned to protect narrow gaps in the EMP and in the flow meters from blocking. This trap too can be removed for analysis. In addition a mechanical filter is in the main flow (Mo-wire mesh). Finally there are liquid metal-covergas interfaces in experimental volumes.

One of these is equipped with an observation window. One other is inside of an argon filled glove box. At low flow rates it can be opened to check the surface for floating impurities.

*) The liquid metal abbreviation LM will be used in this test for the molten eutectic mixture Pb-17 Li.

Staff:

H. Feuerstein
H. Gräbner
S. Horn
G. Kieser
J. Oschinski

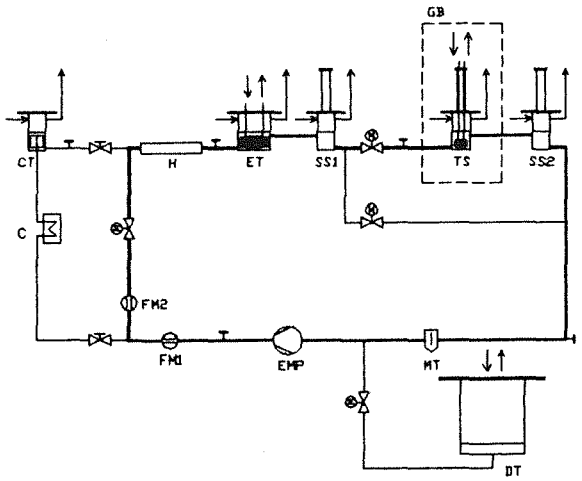

Fig. 2: Flow sheet of the loop TRITEX.

EMP	=	electro magnetic pump
FM	=	flow meters
H	=	heater
ET	=	expansion volume
SS 1, 2	=	sampling sections
TS	=	test section
MT	=	magnetic trap
C	=	cooler
CT	=	cold trap
DT	=	drain tank
GB	=	glove box

Last not least radioactive tracers can be used in TRITEX, because the facility is located in a radiation controlled laboratory.

So far TRITEX has operated for about 1000 hours under different conditions. After this time no deposits were found in the cold trap or in the magnetic trap, only some oxides were floating on surfaces of Pb-17Li.

Besides the facility TRITEX small austenitic thermal convection loops [2] are operated in the laboratory. Because of the higher corrosion rate of this steel, in the liquid metal particles of different shapes were found in a diffusion type cold trap and at the covergas interface. Even if the operation conditions were frequently changed in this loops, the particles will be investigated to learn more about the behavior of corrosion products in austenitic Pb-17Li systems.

References:

[1] H. Feuerstein et.al., J. of Nucl. Mater. 155-157 (1988), p. 520.

[2] H. Feuerstein et.al., Fus. Engin. Des., to be published in 1990, also paper 61, ICFRM-4, Kyoto 1989.

BL EX-D-1 Tritium Extraction by Permeation and Cold Trapping

The selected tritium removal technique for the self-cooled Pb-17Li blanket with an intermediate NaK loop consists of tritium permeation into the NaK and precipitation as tritide in a cold trap. For tritium recovery, the cold trap is heated up and the tritium is pumped off.

The test facility WAWIK was built for the investigation of hydrogen (protium) removal and recovery. In a first test series, a cold trap was loaded with hydrogen for about 10 days, transferred to the glovebox, demounted and the hydride precipitations on the wire mesh packing were analyzed both visually and by electron microscopy. Typical crystal sizes on the wires are about 0.1 mm. The packings were transferred to an oven for hydrogen recovery. The release rates are very similar to those for hydride crystals generated in a thermal convection loop (compare [1]). In the meantime, a second cold trap was loaded; analyses are presently performed.

The transient build-up of tritium inventory in the Pb-17Li and NaK loops was calculated for a test plug to be used in NET [1]. Fig. 1 shows the tritium flow sheet and the results. Steady-state conditions are reached after several days if the cold trap is operating from the beginning. This time period can be shortened to less than one day if the cold trap starts operation after about 18 hrs. The total tritium inventory (including cold traps) is about two grams. Steady-state inventories for a DEMO reactor were assessed to 314 or 464 g depending if one or two recovery cycles per day are assumed [2].

An engineering assessment [3] was made for the use of a vanadium getter for tritium removal from Pb-17Li (see BL EXD-2) for a DEMO reactor [3]. For presently assumed tritium permeation barriers to the steam generator, this process results in very large getter bed dimensions. However, a combination of gettering and cold trapping would result in very small processing components and a moderate tritium inventory. For very high tritium barriers gettering alone could be an attractive process.

References:

[1] J. Reimann: Tritium Inventory and Recovery for a Self-cooled Pb-17Li Blanket; to be published in Fusion Engineering & Design.

[2] S. Malang, H. Deckers, U. Fischer, H. John, R. Meyder, P. Norajitra, J. Reimann, H. Reiser, and K. Rust: Self-cooled Blanket Concepts Using Pb-17Li as Liquid Breeder and Coolant; to be published in Fusion Engineering & Design.

[3] J. Reimann, H. Feuerstein: Gettering and/or Cold Trapping for Tritium Recovery from Self-cooled Pb-17Li Blanket; to be presented at the 16th Symp. Fus. Techn., London, Sept. 1990.

Staff:

L. Bühler
R. Kirchner
D. Rackel
J. Reimann

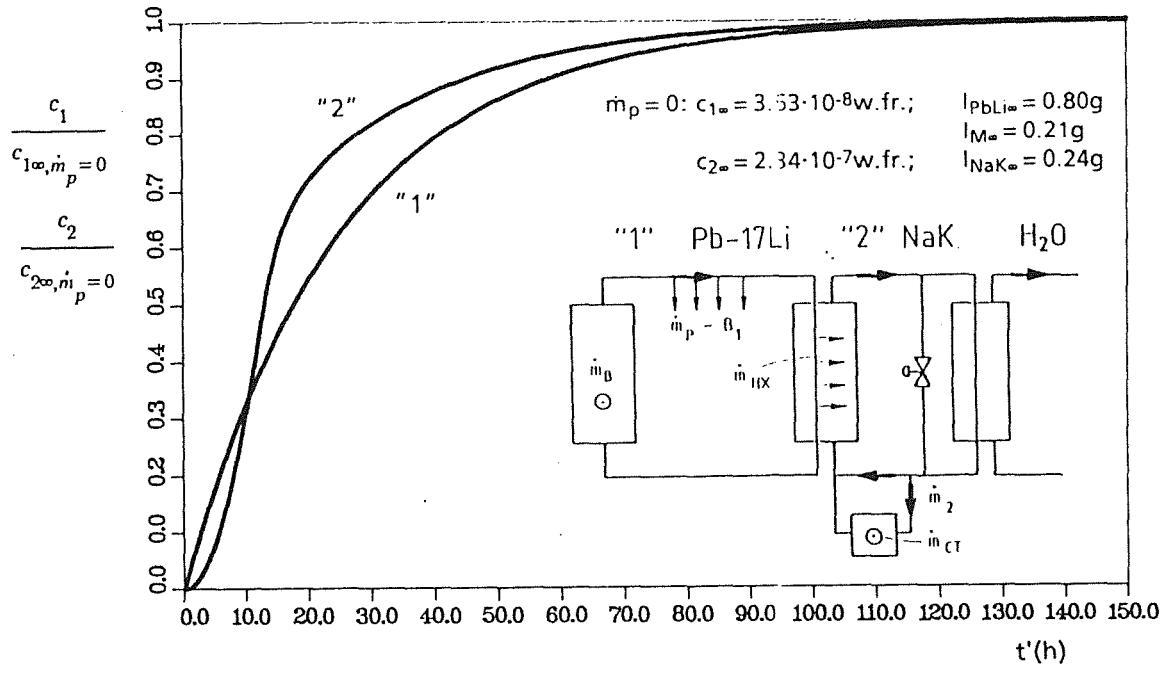

Fig. 1: Tritium concentrations and inventories (permeation through the piping $\dot{m}p = 0$).

BL EX-D-2 Tritium Extraction from Molten Pb-17Li with Solid Getters

Several methods were proposed for the extraction of tritium from a molten Pb-17Li blanket. This work is concerned with the use of solid getters.

Inparallel to the facility TRITEX [1] small thermal convection were used to study the behaviour with molten Pb-17Li. Deuterium was used instead of tritium. The loops and some of the results were described in [2] and [3].

Deuterium was dissolved in the Pb-17Li from sample gas streams in one of two expansion volumes. Different kinds of getter metal samples were submerged into the liquid metal in a second expansion volume. 0.1 mm thick foils of Ti, β-metal and V were used, with surface areas between 1 and 100 cm^2. All materials were obtained from Goodfellow company. Before use, the foils were vacuum annealed at 10^{-5} mbar for several hours up to 700 °C.

Results

Even at low temperatures, all investigated getter metals are able to extract deuterium from molten Pb-17Li. Because vanadium is very stable in the molten eutectic [4], most of the tests were done with this metal.

The rate of deuterium uptake is proportional to the concentration of D-atoms in the liquid metal, corresponding to the square root of the equilibrium partial pressure. The rate shows only a weak temperature dependence, as seen in Fig. 1. It is constant for a long time, and up to loadings of the vanadium of several at %. Within the error margings the rate of deuterium-uptake by vanadium is the same as the rate of degassing to an argon covergas. It is assumed that the rate controlling step is the diffusion of deuterium atoms through a liquid metal boundary layer at the interface.

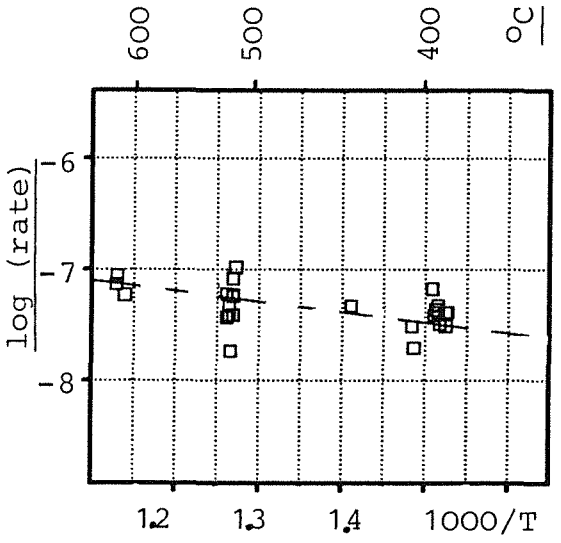

Fig. 1: Rate of deuterium uptake from molten Pb-17Li by vanadium foils. Dashed line is the degassing rate into a gas phase (1) (2). The rate is given in ($mol/s \cdot m^2 \cdot mbar^{1/2}$).

The recovery of the deuterium from the vanadium can be done at moderate temperatures. There is no need to remove the Pb-17Li for this process.

For an engineering assessment see BL EX-D-1.

The experiments will continue. In a modified thermal convection loop trace amounts of tritium will be used. With the facility TRITEX (1), the influence of the liquid metal flow rate will be investigated.

References:

[1] H. Feuerstein et. al., J. of Nucl. Mater. 155-157 (1988), p. 520.

[2] H. Feuerstein et. al., Fus. Engin. Des., to be published in 1990.

[3] H. Feuerstein et.al., paper 61, ICFRM-4, Kyoto 1989.

[4] H. Gräbner et.al., J. of Nucl. Mater. 155-157 (1988), p. 702.

Staff:

H. Feuerstein
H. Gräbner
S. Horn
J. Beyer
J. Oschinski
G. Kieser (DTI)

BL SA-D-1 Functional Analysis of a Liquid Metal Self-cooled Blanket

The functional analysis of the self cooled Pb-17Li blanket will follow the line proposed by CEA and ENEA for the safety assessment of NET, performed for the Overall Plant Accident Scenarios Working Group.

In a first step the functions of the blanket system are identified. There are about 40 different functions. These functions are then attributed to the following subsystems:

- Pb-17Li system
- NaK intermediate system
- NaK auxiliary system
- interface containment system
- blanket control and driving system

On the level of the subsystems for the blanket system the interaction between functions and subsystems and sub-systems and systems is described by matrices. The next step is a failure mode and effect analysis. I.e. it is assumed that a function is lost and it has to be judged whether this loss will have a safety related consequence or not. If yes the matrices help to identify safety related initiating events (functional fault tree) and to determine the probability of the occurance of a function failure.

In the next step functional event trees are built up to identify the consequences of a specific loss of function in more detail than in the failure mode and effect analysis. The product of failure probability and consequences gives the risk of a function failure. This risk can be mitigated by introduction of safety features reducing the concequences of a failure.

Staff:

R.Meyder

BL CO-D-1 Flow Channel Inserts

In a blanket with liquid metal cooling an electric potential is induced when the liquid metal is flowing perpendicular to the magnetic field. This potential has short-circuits both in fluid sections not being in motion perpendicular to the magnetic field and in the structures of the channel housings. The converted electric power has to be produced by additional pumping power of the fluid. The first short-circuits are predominantly summarized as three-dimensional effects (caused by bendings, variation of cross-section of flow channels). The second short-circuits are wall effects. They can be avoided completely by electric insulation of the wetted surfaces. Uninsulated steel structures in a blanket of a fusion reactor would create unacceptable pressure losses.
To reduce the second class of electrical short-circuits so-called flow channel inserts (FCI) are developed (Fig. 1). They consist

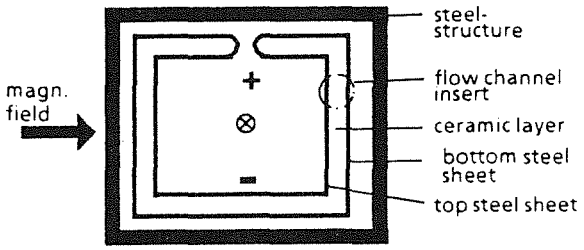

Fig. 1: Schematic view of a flow channel insert

of two thin steel sheets with a ceramic layer between them. At the edges the sheets are welded together, to protect the ceramic layer from a chemical attack of the liquid metal. The FCI are preformed and are loosely fitted into the flow channels. A longitudinal slot enables pressure equalization between the gap to the channel structure and the cross-section inside the flow channel. This slot does not enable an electric short-circuit through the channel housing. The development of fabrication methods is performed together with MBB.

The methods selected are:

- shaping of the two steel sheets.
- Plasma-spraying of the inner steel sheet with a metal bonding (Cu, CuTi, Ni, FeCr).
- plasma-spraying of the sprayed surface with a ceramic insulation layer (Al_2O_3 ($+TiO_2$), $MgAl_2O_4$).
- plasma-spraying of the outer steel sheet with metal (Cu, CuTi, Ni, FeCr).
- Diffusion welding of the two coated steel sheets in a pneumatic isostatic hot press process.
- Welding of the two steel sheets at the edges.

The diffusion welding process was developed by MBB. A pressure of $30 \div 40$ bar is applied at temperatures up to 1000 °C. With this process good tensile strength of the laminated element was achieved only when $Al_2O_3 + TiO_2$ was used as insulation material ($10 \div 25$ MPa). With the other insulation materials only poor bonding was achieved. But $Al_2O_3 + TiO_2$ was found to be electrically conducting in many cases. The carrier gas for plasma-spraying ($Ar + H_2$) reduces the TiO_2 in the Al_2O_3-TiO_2-mixture. To achieve good insulation the following modification of fabrication methods has been investigated.

- replacement of $Al_2O_3 + TiO_2$ by pure Al_2O_3 or by $MgAl_2O_4$ and diffusion-welding with high pressures of 1200 / 2000 bar and 900 °C.
- choice of a metal for diffusion welding with high bonding energy to ceramic (FeCr, CuTi), diffusion welding with high pressure).
- plasma spraying of $Al_2O_3 + TiO_2$ with an inert carrier gas ($Ar + N_2$).

With these modifications numerous diffusion welding experiments were carried out. The metallurgical review and first measurements of electrical insulation show good results. But the ultimate assessment and the choice of the adequate parameters for best bonding and insulation has to be done.

Staff:

V. Casal
M. Gegenheimer

BL CO-D-2 Liquid Metal Components and Testing

The development of the ancillary loops and its components for heat and tritium extraction for the blanket test moduls in ITER as well as for the breeding blankets in a DEMO reactor has been continued in cooperation with Interatom / Bensberg.

The following critical points have been investigated:

1. Thermal behavior of the ITER-loops.
   Due to the cyclic operation mode of ITER (for instance 200 s offburn time after 1000 s burn time) the components in the cooling circuits, especially in the Pb-17Li-loop are exposed to sudden temperature changes. Using the ABAQUS-program, stress calculations have been carried out for the most critical points of the heat exchanger. The results show that the combined loads caused by cyclic temperature gradients and the inner pressure are not exceeding the allowed stress limit.

2. Conceptual design study of a DEMO heat exchanger.
   An integral three fluid heat exchanger (steam generator) for the transfer of heat from Pb-17Li to water and of tritium from Pb-17Li to NaK is proposed for the DEMO ancillary loops. Several versions have been studied to select this important component.

   Concerning a minimal NaK inventory, the potential of a water-NaK reaction, and with respect to maintenance problems, the straight pipe double-walled heat exchanger with water-steam in the inner pipe seems to be the most favourable type for the DEMO loops followed by the helical double-walled heat exchanger.

3. Optimisation of the DEMO-steam cycle.
   The steam cycle has the function to convert thermal to electrical power. Considering the thermal efficiency of the conversion, the sensitivity of the heat exchanger pipe bundle against temperature differences over the cross section and the possibility to compensate the interruption of the steam production in the offburn time of the plasma, a steam circuit with saturated steam at a pressure of 7 MPa and a temperature of 286 °C at the turbine inlet has been selected.

4. Pipe concept for Pb-17Li ducts (ITER and DEMO).
   It has been investigated if the required large diameter piping system is feasible at all for Pb-17Li having a density of nearly 10 000 kg/m3. Calculations have shown, that the pipes with diameters of 0.15 m (ITER) and 0.5 m (DEMO) have to be supported at maximum distances of 3.4 m and 6 m, respectively, to withstand the high statical loads and dynamical forces caused especially by earthquakes.

5. Investigation of the afterheat removal by natural convection.
   Calculations showed that in the case of an unintended stop of the Pb-17Li pump the development of a natural convection flow is efficient enough to prevent overheating of the blanket walls if the center of the heat exchanger is located at least 5 m above the center of the blanket segment

Staff:

H. John
S. Malang

Long Term Program for Materials Development

Introduction:

KfK's activities in materials development for nuclear fusion have mainly been devoted to the qualification, characterization and irradiation testing of a martensitic steel which principally exhibits better heat load bearing properties and higher neutron irradiation resistance, and has the potential of reduced activation levels by appropriate modifications.

For NET with its much reduced wall temperature a martensitic steel is no longer feasible mainly due to irradiation embrittlement effects in this temperature regime. The former MAT programme dealing with pre- and post-irradiation properties of the martensitic MANET steel is being pursued as a prerequisite of Blanket development capable of supporting the conditions of a Demonstration Reactor, but formally it has been attributed to the EC-Long Term Programme. Characterization of the MANET 1 heat has been completed with a parameter study on the influence of heat treatment on creep rupture. A second heat, MANET 2, with a slightly modified composition in some minor alloying constituents is being fabricated. While waiting for the new material the methodology of impact testing has been studied, and instrumented testing machines for different specimen sizes have been installed (MAT 1.6).

Since cyclic operation is well within the DEMO scenario thermal fatigue remains to be an important issue. The approach made in the MAT-program is cyclic electrical heating of hollow specimens which are fixed at their ends at a reference temperature for zero strain. Several test stands have been set up and thermal fatigue tests have been performed which show, as for austenitic steel 316 L, a decreased number of cycles to failure as compared to isothermal mechanical fatigue. The array of data on LCF has been further increased, and a significant influence both of temperature and of strain amplitude on structural changes and fracture behaviour could be determined. Further work is devoted to higher strain rates and tests with different hold times (MAT 1.9).

The activities in the irradiation embrittlement field have been continued with the implementation of the instrumented impact testing method with subsize notch specimens in the Hot Cells and a verification of former test results with an uninstrumented impact pendulum device. First tests with MANET-samples from the SIENA irradiation programme have indicated that ductile-brittle transition temperature shift remains to be an important issue for martensitic-ferritic steels (MAT 1.11).

The Dual Beam testing program with MANET specimens has been continued with a systematic variation of He-deposition and damage production and post-irradiation LCF tests. The temperature was 450°C in both cases. No significant decrease of fatigue life by damage could be observed, and only a moderate influence of the He-content. The LCF tests were followed by comprehensive microstructural examinations. Attention was drawn to a possible influence of test atmospheres on LCF data. It could however be demonstrated that this does not hold for strain-controlled experimental procedures. Preparations for in-beam LCF testing are ongoing (MAT 9.2).

Within the Low Activation Materials (LAM) programme the fundamental work of a proper determination of element activation in a fusion environment has been pursued. Main emphasis has been laid on the inclusion of secondary nuclear reactions which take place by energetic charged particles stemming from high energy neutrons. In some cases minor alloying elements or even tramp impurities may thus cause higher long-term activation levels than previously anticipated. On the other hand it can be corroborated that an LA-optimized ferritic steel can offer significantly lower dose rates in the long term, compared to the presently used nuclear grade steels (LAM 2.1).

Experimental heats of LA martensitic steels have been characterized with regard to heat treatment, tensile and creep rupture properties and impact strength. The optimum values of MANET have not yet been achieved. Some interesting effects have been observed which have elucidated the influence of certain constituents on alloy properties (LAM 3).

LAM 2.1 LAM Element Activation

Calculations of Neutron-Induced Activation in Fusion Reactor Materials

Work on improvements of processing codes and nuclear data libraries for activity calculations in structural materials was continued. A deficiency of hitherto performed calculations was the neglection of so-called "sequential (x,n) reactions" which can produce important contributions to the total induced radioactivity. Therefore, appropriate estimates of neutron and charged particle induced activation, related surface γ-dose rates, decay heats, biological hazards, etc. must include all kinematically allowed reactions and reaction chains. For this purpose a suitable modification of existing computer codes and of currently available nuclear data libraries was necessary (for more details see last Semi-annual Report).

In the reporting period the inventory-code version FISPACT/KfK and the new KfK-library KFKXN have been further improved. Additional modifications of the inventory code now allow to follow any sequence of mixed (n,x) and (x,n) reaction chains. Moreover, a large fraction of existing experimental double differential ($d^2\sigma/dE_n \cdot dE_x$) and of differential ($d\sigma/dE_x$) cross sections for stable nuclides in the mass range $23 \leq A \leq 60$ have been added to the initial KFKXN library. Even when restricting to data needs for activation estimates of Fe-, V- and Cr-basis alloys, there is still a large number of lacking cross sections which must come from suitable nuclear model calculations. Work for this task is in progress; at present, a few semi-empirical models are tested which can provide lacking cross sections with sufficient accuracy at low calculational effort.

With the existing means of programming and library capabilities more advanced activation calculations for some important Fe-basis alloys have been performed. A typical result is shown in Fig. 1 which illustrates the predicted surface γ-dose rates as a function of cooling time. The results refer to irradiations in the first wall assuming a spectrum typical for the Culham DEMO (solid breeder) reactor, a 5 MW m^{-2} first wall loading, and 2.5 years irradiation time. In the calculations the most important sequential (x,n) reactions as well as all alloying and non-avoidable tramp-impurity elements have been included. It can be seen that the LA-optimized materials CeTa-C858 (KfK), LA12Ta (UK), and OPTSTAB2 (UK) give largely reduced long-time dose rates compared to the non-LA adjusted materials MANET2 (KfK) and 316L (USA): Beyond ~ 100 years after irradiation the reduction in dose rates for LA materials is ~ 2-4 orders of magnitude. Distinguishing between martensites (MANET2, CeTa-C858, LA12Ta), and austenites (OPTSTAB2 and 316L) another remarkable feature can be observed: While the considerable reduction in dose rates at long cooling times for the austenitic LA steel OPTSTAB2 is only gained at the expense of increased values at short times (< 1 year), this does not apply for the two LA martensites (CeTa-C858 and LA12Ta).

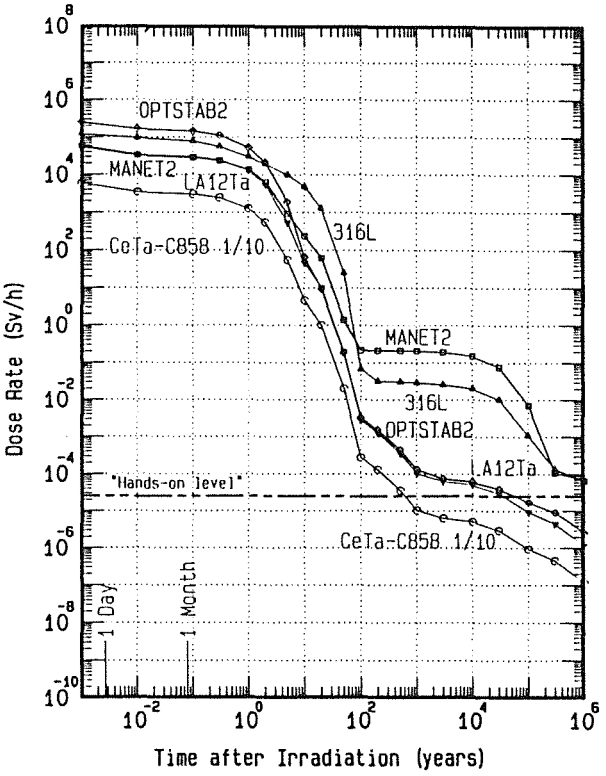

Fig. 1: Calculated surface γ-dose rates versus time after irradiation for some important fusion materials. For materials specifications and irradiation conditions see text.

In addition to work on completing codes and libraries, preparations for experimental benchmark data testing have been made. Using a special sensitivity option of the FISPACT code, provides information on the most important reactions governing the total-induced activities. Such results lead to a suitable selection of data to be tested in a presently prepared experimental program at the Karlsruhe Isochronous Cyclotron (KIZ). In connection with experimental activities on LA materials, the IMF II has also participated in current international discussions about high-intensity high-energy neutron sources for fusion materials testing and for fusion-relevant cross section measurements.

References:

[1] S. Cierjacks: Low-activation Materials Development and Related Nuclear Data Needs, Invited Paper, IAEA Advisory Group Meeting on the Status and Requirements of Nuclear Data for Radiation Damage and Related Safety Aspects, Vienna, September 19-22, 1989.

[2] S. Cierjacks, Y. Hino: The Role of Sequential (x,n) Reactions on Element Activation of Fusion Materials and Related Nuclear Data Needs; OECD/NEA Publication on a NEANDC Specialists Meeting on Neutron Activation Cross Sections for Fission and Fusion Energy, Argonne, Sept. 1989, p. 19, (1990).

[3] S. Cierjacks, Y. Hino: The Influence of Sequential (x,n) Reactions on Total Element Activities; J. Nucl. Mater. 170, 134-139 (1990).

[4] S. Cierjacks: High-Intensity 14-MeV Cut-off Neutron Production by the $^{1}H(t,n)^{3}He$ Source Reaction, J. of Fusion Energy, Vol. 8, Nos. 3/4, p. 193-200 (1990).

[5] S. Cierjacks, Y. Hino: Sequential (x,n) Reactions; an Important Reaction Mechanism for Element Activation in Fusion Reactor Materials, 4th Int. Conf. on Fusion Reactor Materials, Kyoto, Japan, December 4-8, 1989.

Staff:

S. Cierjacks
Y. Hino

LAM 3 Development of Low Activation Ferritic-Martensitic Steels

In two martensitic 10% chromium steels the alloying elements W, Ta, Ce and Hf, resp., were substituted for Nb, Mo and Ni. Both the tensile and the creep rupture properties lie with the frame of the previously investigated batches of steel 1.4914. Compared with steel MANET 1, the creep rupture strength of the low activating steel is less, whereas the elongation at fracture is higher. The notch impact strength of the cerium alloyed steel is relatively high.

It has been demonstrated in instrumented notched bar impact bending tests that the embrittling effect of delta ferrite stems from a carbide seam in the interface δ-ferrite/matrix. If this particular carbide precipitation is avoided by fast quenching and low annealing tempering temperatures, delta ferrite alone does not produce negative effects. It has been observed in creep rupture tests that delta ferrite contents up to 5% have no negative effects.

There have been observations of anomalies in creep curves of martensitic 9 - 14 % Cr steel under long-term loading [1]. Examples are shown in Fig. 1 (heats 3, 4, 5, 6, 8, 9). To avoid such unfavorable properties in low activation alloys to be developed, a careful investigation of the reason for the observed anomalies has been carried out. It could be shown [1], as illustrated in Fig. 2, that unfavorable high Al:N-ratios cause the anomalies in this class of alloys. It has also been suggested [1] that nitrogen not bound as Al N may form carbonitrides which seem to be more stable as to dissolution or coarsening) than the corresponding carbides and, therefore, can prevent the onset of the creep anomaly described above.

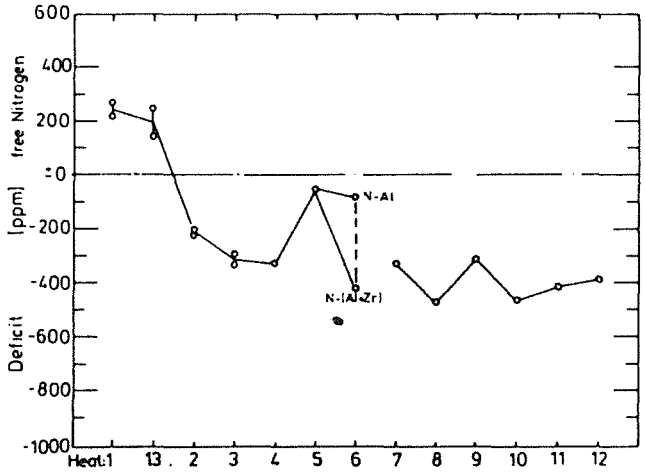

Fig. 2: Surplus or deficit of nitrogen after stochiometric formation of AlN at the heats 1-13

Staff:

K. Anderko
E. Materna-Morris
L. Schäfer
M. Schirra

Reference:

[1] M. Schirra, K. Anderko, Steel Research 61 (1990) 242.

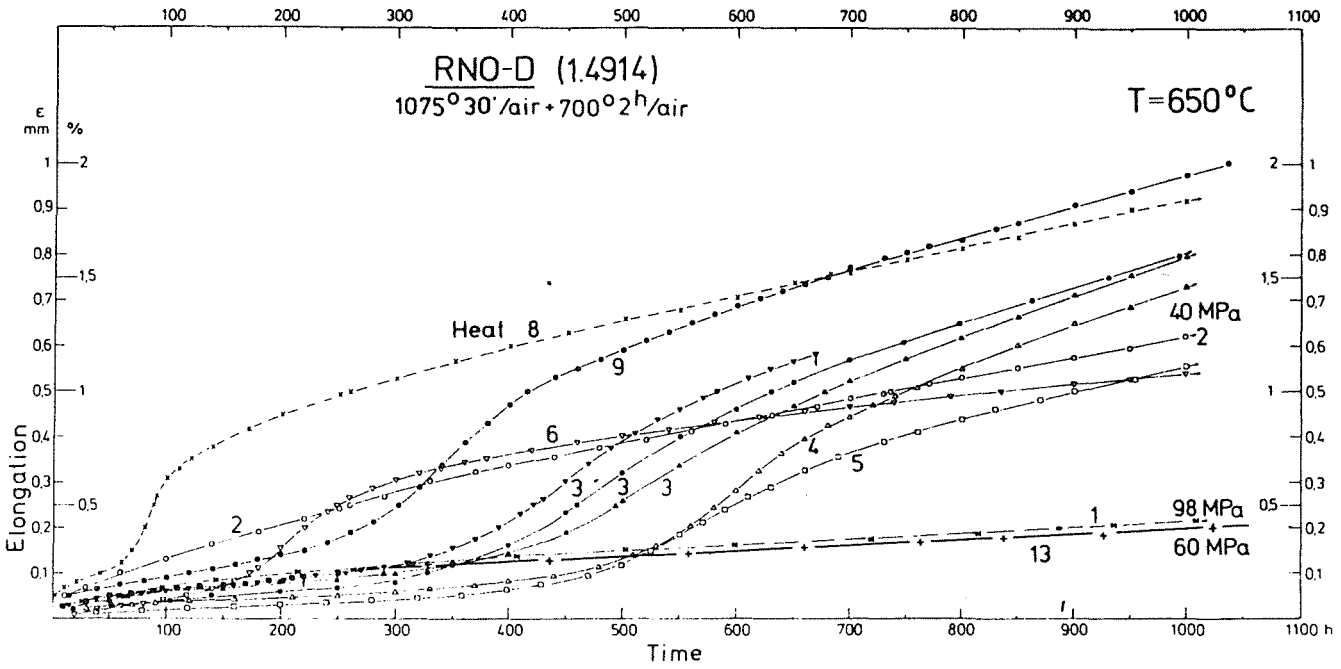

Fig. 1: Creep strain/time curves with and without creep anomalies

MAT 1.6 Characterization and Optimization of MANET 1 and 2 Steels

Within the framework of activities aimed at characterizing and optimizing the martensitic steel MANET 1 as a structural material, creep rupture tests were performed with continuous strain measurement in three conditions of heat treatment and at four testing temperatures (500 to 650°C) as shown in Fig. 1. At the test temperature 500°C the 10^4 h-

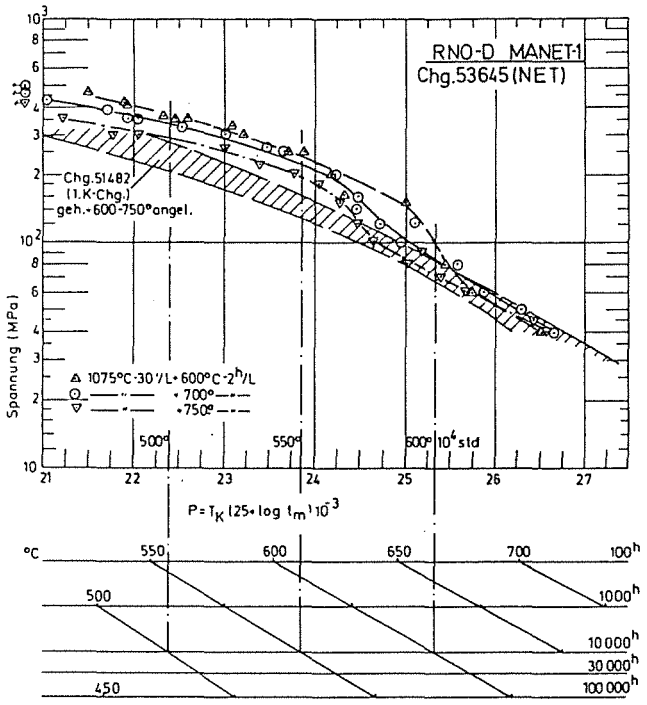

Fig. 1: Larson-Miller parameter plot of rupture life of MANET 1

creep rupture strength varies between 290 and 360 MPa, depending on the state of heat treatment, whereas the elongation at fracture is 20%. Fracture is of the transcrystalline type.

The impact strength, which is measured in notched bar impact bending tests, is of high importance for the applicability of ferritic steels in fusion systems. The conventional method of testing provides useful material data required by the user. However, if the material behaviour is to be understood and the material improved specifically, additional data have to be derived from instrumented notched bar impact bending tests. During the period of reporting a large 150/300 Joule pendulum type impact testing machine for ISO-V standard specimens (10 x 10 x 55 mm) and a small 15/50 Joule pendulum type impact testing machine for medium sized (5 x 5 x 55 mm) and very small sized (3 x 4 x 27 mm) specimens were equipped with modern data acquisition and processing systems as well as with a software corresponding to the state of the art. By this, optimum conditions have been created both as regards the characterization and optimization of the martensitic chromium steel MANET 2 as structural material and for the envisaged basic investigations into the influence exerted by the specimen size. Five heats of MANET 2 have been melted and plates, sheets and rods are being fabricated. The material will be available at KfK Karlsruhe in August 1990 for tests and distribution to the European Associations.

Staff:

B. Dafferner
L. Schäfer
M. Schirra
C. Wassilew

MAT 1.9 Pre- and Post-Irradiation Fatigue Properties of 1.4914 Martensitic Steel (MANET)

Thermal cycling of large components is a serious problem for the designer. The structure considered in the present case is the first wall of a fusion reactor. Its surface, in the actual design concept, will be subjected to radiation heating from the plasma facing side which may lead to severe thermal stresses. Due to the discontinuous operational mode, thermal cycling will generate oscillating temperature gradients. These, depending on the loading conditions, will cause elastic or elasto-plastic reversed deformation, giving rise to thermal fatigue which at present is considered as the most detrimental lifetime phenomenon for the structure considered. The investigations of MAT 1.9 are devoted to this problem.

The studies to be reported within MAT 1.9 are:

- The influence of temperature upon isothermal low-cycle fatigue behaviour of MANET 1 (S-GRIM and H-GRIM specimens).
- Cyclic stress behaviour of MANET 1 (S-GRIM specimens) at RT and 650°C.
- Thermal fatigue of AISI 316 L with a ΔT between 350 and 550°C and comparison with isothermal fatigue data.
- First thermal fatigue results of MANET 1 with a ΔT of 500°C.

1. Isothermal fatigue of MANET 1

Tests on H-GRIM and S-GRIM specimens have been performed at room temperature and 650°C with total strain ranges from 0.3 to 1.5%. Herewith all continuous cycling tests with a strain rate of $\dot{\varepsilon}=3\cdot10^{-3}$/s on tube as well as on solid GRIM specimens are completed and a detailed report is in preparation. Furthermore first results with $\dot{\varepsilon}=3\cdot10^{-4}$ and $3\cdot10^{-5}$/s are available.

For H-GRIM specimens the number of cycles to fracture N_f vs. total strain range $\Delta\varepsilon_t$ at room temperature and 650°C are shown in Fig. 1. The data points are mean values from at least two tests. Concerning H-GRIM specimens it was found that their total strain range is limited to ≤0.6% at 650°C. If larger $\Delta\varepsilon_t$-values are used, specimens begin to bulge which results in a change of stress conditions. At room temperature, tests up to a total strain range of 1% are possible. Fig. 1 shows that the difference of N_f-values between room temperature and 650°C is larger in comparison with the results of S-GRIM specimens for the same temperatures. On S-GRIM specimens (Fig. 2) it is obvious that for both temperatures the number of cycles to fracture is not as much different as on H-GRIM specimens especially for small and large amplitudes. Moreover it was found that for $\Delta\varepsilon_t<0.5\%$ at room temperature the fracture of the specimens occurs no longer within the gauge length but outside of the ridges in the thread.

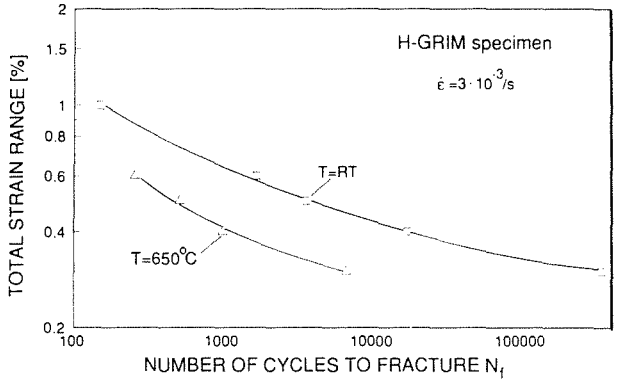

Fig. 1: Total strain range vs. number of cycles to fracture for H-GRIM specimens of MANET 1.

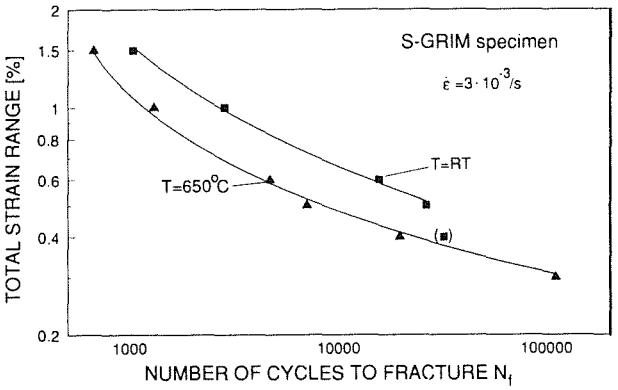

Fig. 2: Total strain range vs. number of cycles to fracture for S-GRIM specimens of MANET 1.

An indication for this behaviour gives the maximum tensile stress σ_{max} as function of cycles (Fig. 3). For $\Delta\dot{\varepsilon}_t=0.4\%$ σ_{max} remains nearly unchanged up to 40'000 cycles. At the end of the test a large increase of stress suddenly occurs. This could be the reason that specimens break outside the gauge length. At 650°C for $\Delta\dot{\varepsilon}_t=1.0\%$ a continuously cyclic softening can be observed whereas for a strain range of 0.4% σ_{max}-values remain nearly constant up to 10^3 cycles before a decrease of stress occurs. At room temperature cyclic softening of stress is less pronounced as at 650°C.

The main results of continuous cycling tests with a strain rate of $3\cdot10^{-3}$/s are:

- Small differences of N_f-values at room temperature and 650°C for S-GRIM specimens.

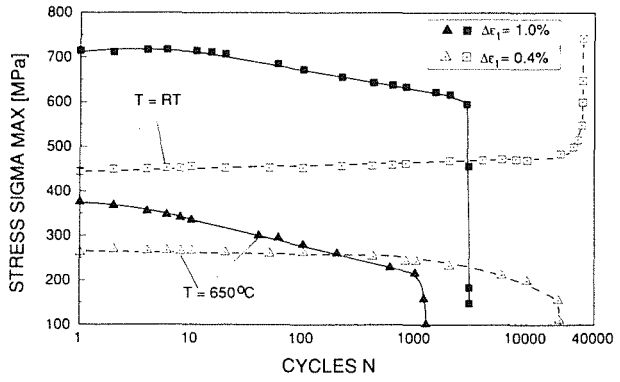

Fig. 3: Maximum tensile stress σ_{max} vs. number of cycles N for MANET 1 (S-GRIM specimens).

- Depending upon temperature and strain range, either cycling softening or hardening occurs.
- A strong increase of stress at the end of test for low temperatures and small Δ_t-values.

2. Thermal fatigue

2.1 Thermal fatigue of AISI 316 L

The experiments with a ΔT between 350 and 550°C, without hold times, are completed and compared to isothermal LCF-data in a similar temperature range. Due to the fact that the thermal fatigue testing device is not able to control the total mechanical strain amplitude $\Delta\dot{\varepsilon}_{t,m}$, both the stress range $\Delta\sigma$ and $\Delta\varepsilon_{t,m}$ change with the number of cycles, hence only the measured values during the stabilized hysteresis loop are shown. Total mechanical strain amplitudes between 0.4% and 1.4% are evaluated. From this data set the total mechanical strain amplitude $\Delta\dot{\varepsilon}_{t,m}$ is plotted versus the number of cycles to failure N_f in Fig. 4 and compared with data sets from literature of different kinds [1]:

- Thermomechanical fatigue data on AISI 304.
- Biaxial thermal fatigue data on W.Nr. 1.4436.
- Isothermal strain controlled low cycle fatigue data in a temperature range RT and 430°C and
- Isothermal strain controlled low cycle fatigue data in a temperature range 527°C to 600°C.

In the low temperature range (RT and 430°C), the isothermal low cycle fatigue data fit very well with the biaxial thermal fatigue data, cycled in a similar temperature range. So one can conclude that there is only a negligible influence from the

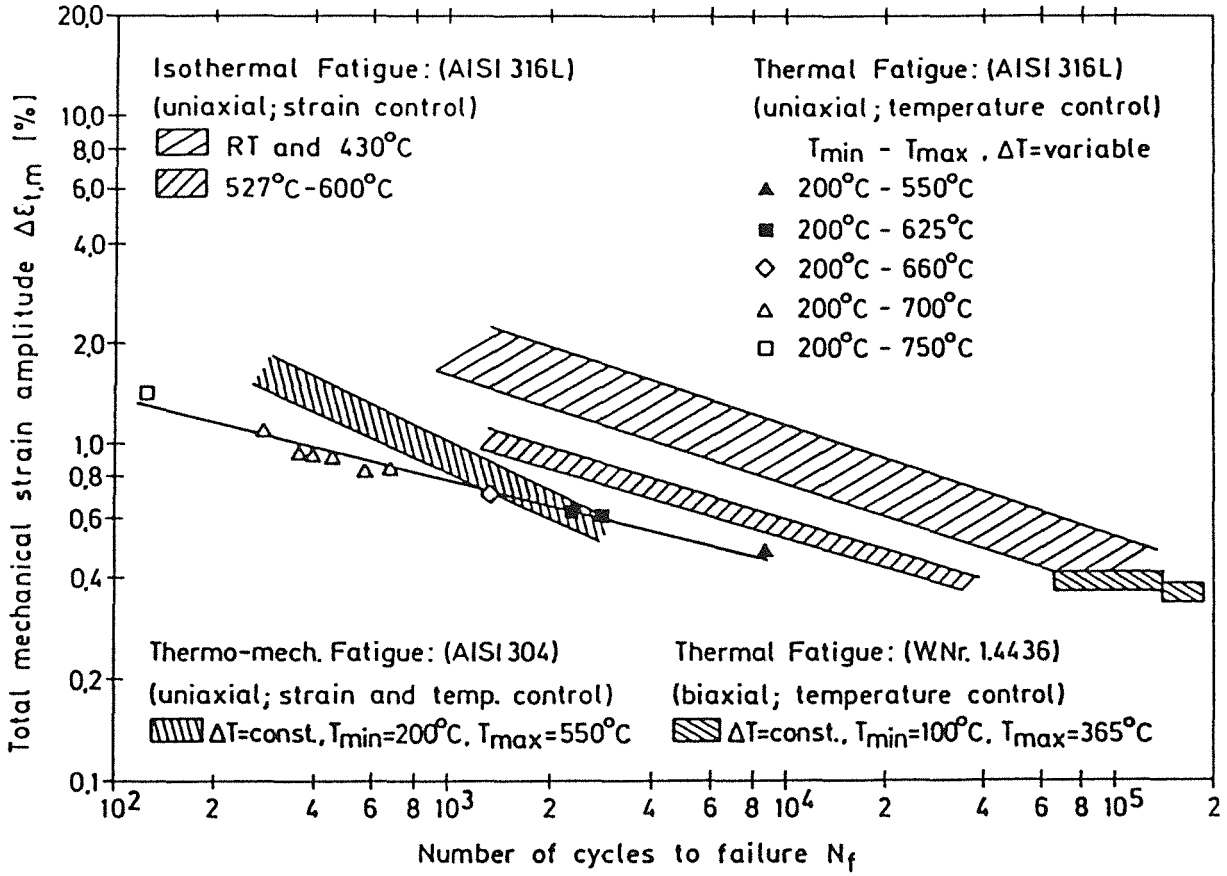

Fig. 4: Comparison of own thermal fatigue data of biaxial, thermomechanical and isothermal strain controlled fatigue data in an $\Delta\dot{\varepsilon}_{t,m}$ versus N_f-diagram

biaxial stress condition and the cyclic thermal loading in this temperature range.

For the comparison in the higher temperature range (527°C to 600°C), only uniaxial data are available. The number of cycles to failure of thermally cycled samples have been found to be about a factor of three shorter than of those strain cycled under isothermal conditions. That holds even if the maximum temperature of the thermal fatigue test coincide with the temperature of the isothermal strain controlled test.

In good agreement is the result that thermomechanical fatigue, where ΔT is kept constant and the variation in total strain amplitude is generated by changing the mechanical strain, reveals higher N_f-values than thermal fatigue. The higher the additional mechanical strain, the better is the approach to the isothermal strain controlled low cycle fatigue data.

From this comparison it follows that thermal fatigue lives are found to be considerably shorter than isothermal fatigue lives at temperatures equal to the mean temperatures of thermal cycling and even shorter than at the maximum temperatures of thermal cycling.

2.2 Thermal Fatigue of MANET 1

Preliminary calibration experiments for the test matrix in the temperature range of a fixed $T_{min} = 200°C$ and a variable T_{max} between 500 and 700°C had been completed on MANET 1.

First results at $\Delta T = 500°C$ show - with more scatter than it was usually obtained on AISI 316 L - at similar total strain amplitudes a considerably reduced number of cycles to failure compared to isothermal LCF-data at 450°C on S-GRIM specimens.

The cyclic stress in tension σ_{max} after a few cycles decreases until failure occurs. The amount of σ_{max} is the double of σ_{min} during the whole test, although it was started at a mean temperature with zero stress.

The total mechanical strain $\Delta\dot{\varepsilon}_{t,m}$ increases continuously, without reaching a stable range of saturation, as it is known from austenitic steels.

Reference:

[1] C. Petersen and G. Rubiolo, Proceedings of ICFRM-4, Kyoto, Japan, Dec. 4.-8. 1989, to be publ. in J. Nucl. Mat.

Staff:

W. Baumgärtner
M. Boček
C. Petersen
D. Rodrian
W. Scheibe
R. Schmitt
H. Schneider
W. Schweiger

MAT 1.11 Post-Irradiation Fracture Toughness of MANET Steel

The efforts during the last two years have been concentrated on developing an instrumented impact testing system, which is capable of performing experiments on irradiated KLST V-notch impact specimens. The KLST V-notch sample is a sub size bend specimen with a geometry of 3x4x27mm and a notch length of 1mm. The experiments can be carried out at test temperatures in the range of -150 and 550°C. Reliability tests of hardware and software components of the system carried out during the last months have shown an excellent behaviour and accuracy.

In following a brief survey, which is based on a literature study the about methods, principles, and the increased gain on internal materials specific variables of instrumented impact experiment as well as the aims of the proposed investigations of the SIENA project are given. Historically, the Charpy V-notch impact test has been one of the most popular dynamic fracture tests. The energy absorbed in breaking the specimen is calculated from the maximum amplitudes of the pendulum hammer before and after impact. This test method, which is inexpensive and easy to perform, has been widely used as a screening test for evaluating toughness changes caused by variations in chemical composition, microstructure, and in our specific case by irradiation embrittlement.The Charpy test is further used to identify a temperature for a given steel above which low energy fracture does not occur. Although the understanding of dynamic fracture phenomena has rapidly increased in the past 15 years. It is still difficult to analyze dynamic fracture tests. Over the last few years new, more quantitative, dynamic fracture tests have been developed. Two different analytical methods, a continuum and a microstatistical method, have been pursued concurrently in the 1980's. Much of the progress in developing dynamic fracture test methods was driven by the requirements to ensure nuclear reactor integrity.

The usefulness, the ease of application of the Charpy V-notch test, and the progress in the recording technique and the microcomputer systems encouraged the development of the instrumented V-notch test. However the resulting load versus time curves show characteristic oscillations and thereby make all attempts to obtain accurate material - specific intrinsic quantities difficult. Nevertheless it yields additional qualita-tive information on load, respectively energy, partitioning to determine the specific load values for general yield, initiation of unstable fracture, crack arrest and the fracture mode transition from ductile to brittle.Thus, the instrumented Charpy V-notch test does not provide a toughness parameter, such as the critical stress intensity value, K_{Ic}, that is used to calculate critical stresses respectively flaw sizes for a structural component. The main differences between Charpy V-notch and the fracture mechanics test are listed below:

1. The triaxiality

Charpy tests are carried out commonly on 10 mm thick specimens, whilst K_{Ic} tests are performed on material of sufficient thickness to ensure plane strain conditions. The degree of triaxiality obtained in a K_{Ic} test is therefore constant, while the triaxiality in the Charpy specimen is a function of temperature. At the lower shelf range of the Charpy transition curve, plane strain conditions are possible.

2. The notch root radius

The Charpy specimen has a machined V notch which has a root radius of 0.25mm, respectively, 0.1mm for the DIN-KLST (sub size). The K_{Ic} specimen has a fatigue crack. The differences in the root radius will probably modify the transition temperature measured by the two tests.

3. The strain rate

The standard K_{Ic} test is carried out under slow loading, the Charpy test under impact loading.

4. Fracture initiation/propagation toughness

The value of K_{Ic} is a measure of the amplitude of the singular stress distribution ahead of the crack tip at the point of crack initiation. The conditions required to drive the propagating crack completely through the specimens are not measured. The energy measured in the uninstrumented Charpy test is the sum of the energy required to initiate fracture and to propagate the crack through the specimen. Also, the energy required to propagate the crack becomes a greater portion of the total energy as the upper shelf of the transition curve is approached. Nevertheless in the instrumented Charpy V-notch test energy and load can be broken down into the partial values for initiation and propagation.

In view of the factors listed above successful correlations between standard Charpy and K_{Ic} tests are more likely in the lower shelf of the transition curve, where differences between the two tests are minimized, especially with regard to triaxiality and energy for fracture initiation.

The limited success of correlation between the Charpy V-notch energy obtained from standard uninstrumented tests and K_{Ic} led to the next step in the dynamic bend test evolution, namely the provision of a fatigue crack at the root of the V-notch. The intention was to transform the Charpy V-notch specimens into a dynamic fracture mechanics test specimen. For materials in which fracture occurs before general yield, the critical stress intensity I_{Id} (fracture toughness under impact conditions) is calculated from the maximum load F_m sustained by the specimen as shown in Fig. 1, the crack length a, and the specimen width W and thickness B according to the linear elastic fracture mechanics.

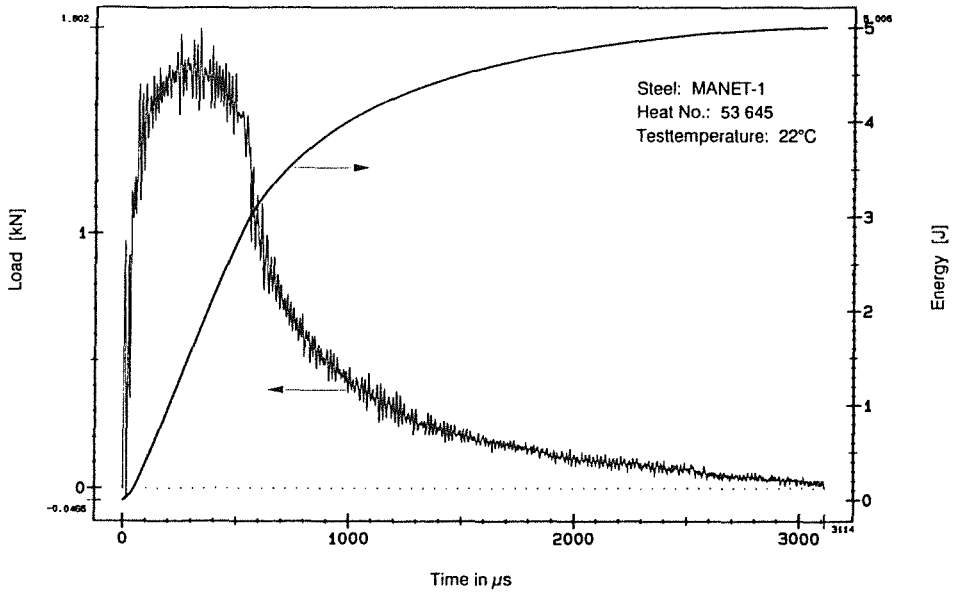

Fig. 1: Load/energy vs. time of MANET-1 steel tested at 22°C

$$K_{Id} = \frac{4F_m}{BW^{1/2}} f\left(\frac{a}{w}\right)$$

Fig. 1 represents the load/energy versus the time of an unirradiated KLST V-notch specimen of the the 12% Cr Steel MANET-1 tested at a temperature in the lower shelf range of the Charpy transition curve.

For materials exhibiting general yielding, an energy based value of the J-integral can be calculated as a measure of the fracture toughness and one can determine the point on the load versus time record at which the fatigue crack becomes unstable. The ductile fracture toughness J_{Ic} is determined from the true specimen energy E_m as shown in Fig. 2 and the remaining ligament depth (b = W - a) using the expression

$$J_{Ic} = \frac{2E_m}{Bb}$$

Fig. 2 represents the load/energy versus the time of an unirradiated KLST V-notch specimen of the 12% Cr Steel MANET-1 tested at a temperature in the upper shelf range of the Charpy transition curve.

Nevertheless, these equations are applicable only for load rates amenable to a quasi-static treatment.

In order to carry out a quasi-static analysis the inertial load oscillations must die out, which requires a load time longer than three times the oscillation period τ.

The need for a dynamic analysis to evaluate a three-point bend impact test at high loading rates was clearly shown by Loss et al. [1], who affixed strain gauges on (larger than Charpy) specimens near to the crack tip to avoid many of the spurious wave effects recorded by hammer gauges, and by Kalthoff and his colleagues [2], who measured crack tip stress intensities directly using caustics.

Thus, through a series of modifications, the dynamic bend test has evolved from the largely qualitative, but useful, Charpy V-notch test to a quantitative fracture mechanics test that is still relatively inexpensive, easy to perform and reliable.

Taking into account that the provision of a fatigue crack at the root of the V-notch is unsuitable for irradiated specimens, stan-dard sub-size (KLST) are used to determine the K_{Id} value. Considering further that irradiated specimens are in general embrittled, plane strain conditions are ensured at the lower shelf range of the Charpy transition curve.

To learn handling the system by using manipulators a series of impact tests with unirradiated original MANET-1 KLST V-notch specimens of the SIENA project has been successfully performed in the Hot Cells. Experiments on irradiated SIENA as well as ISIS KLST V-notch specimens have been started.

References:

[1] F.J. Loss, Ed.: "Structural Integrity of Water Reactor Pressure Boundary Components," Progress Report Ending Feb. 1976, NRL Report 8006, Naval Research Laboratory,Washington, DC, August 1976.

[2] J.F. Kalthoff et al.: "Measurements of Dynamic Stress Intensity Factors in Impacted Bend Specimens," Committee on Safety of Nuclear Installations Specialist Meeting on Instrumented Precracked Charpy Testing, EPRI NP-2102-LD, Electric Power Research Institute, Palo Alto, CA, Nov. 1981.

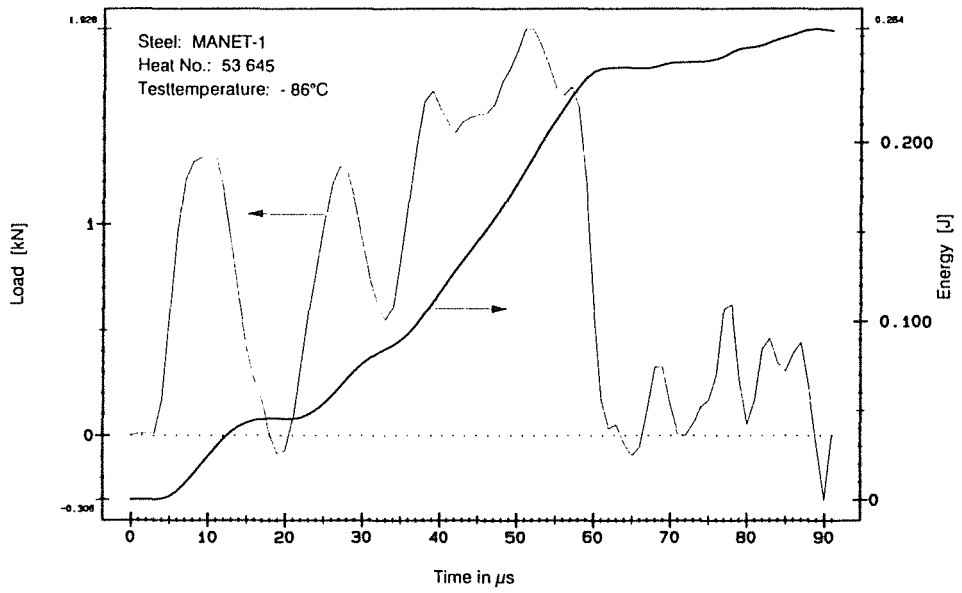

Fig. 2: Load/energy vs. time of MANET-1 steel tested at 86°C

Staff:

B. Dafferner
A. Kräutter
O. Romer
C. Wassilew

MAT 9.2 Investigation of Fatigue under Dual-Beam-Irradiations

The Dual Beam Facility of KfK, where alpha-particles (104 MeV) and protons (15-40) MeV are focussed onto a target, was developed as a research tool for materials within the European Fusion Technology Programme. This Dual Beam Technique allows the simulation of fusion neutrons by the systematic variation of hydrogen, helium and damage production in thick metal and ceramic specimens as well as the simulation of Tokamak relevant thermal and mechanical loadings in proposed first wall materials.

1. Development of in-beam-fatigue experiments

Fully instrumented in-beam low cycle fatigue tests on macroscopic specimens as they are envisaged here are of special complexity because they combine simultaneously the irradiation technology with the push-pull fatigue testing. While the former is completely tested and already under operation, several developments for fatigue tests like the vacuum irradiation chamber, the strain transducer feeding electronics, the heating and cooling devices or the remotely controlled data acquisition and process management are now in the construction or testing phase. Altogether, the preparations for in-beam low cycle fatigue experiments are well under way.

2. Influence of test environment on fatigue life of MANET

Because push-pull type, stress-controlled experiments on the martensitic steel DIN 1.4914 (MANET 1), which were done elsewhere, have shown that even at room temperature the lifetime of specimens tested in vacuum is about an order of magnitude higher than those tested in air, the test environment is presently under discussion. Within the framework of the development of in-beam fatigue experiments strain controlled push-pull low cycle fatigue experiments (real strain $\Delta\varepsilon_t = 1\%$, 0.10 Hz) on hollow specimens with a constant square cross section along a gauge length of 13 mm were performed at room temperature in air and vacuum ($<10^{-2}$ Pa), respectively. The development of the axial stress amplitude in Fig. 1 with the resulting average numbers of cycles to failure $N_f(\text{air}) = 2814 \pm 6.0\%$ and $N_f(\text{vacuum}) = 3191 \pm 9.3\%$ leeds to the conclusion, that at least at room temperature the test environment does not significantly influence fatigue life. This result also indicates that reliable fatigue life data on materials which show cyclic softening like this class of steels should be done with a well defined strain controlled set-up. A more systematic investigation of this topic is planned in MAT 1.9.

3. Postirradiation low cycle fatigue experiments and microstructural examinations

To emphasize the effect of different He-dose/damage ratios on the low cycle fatigue behaviour, LCF specimens (hollow GRIM geometry) made of the martensitic steel MANET 1 were irradiated at 450°C with a fusion typical He-dose/damage ratio of about 10 appm He/dpa and a much higher one of 170 appm He/dpa in vacuum (5×10^{-3}Pa) at a typical defect rate of 2×10^{-6} dpa/s. The irradiation temperature was controlled by the flow rate of the helium gas inside the tubular specimens. After irradiation, the specimens were transferred to the Hot Cells and low cycle fatigue tested in air at test temperatures equal to the irradiation temperature. The results of the strain controlled LCF-experiments are given in Fig. 2. The stress amplitude of the four irradiated specimens follows closely the scatterband of ten unirradiated controls at 450°C as predicted from earlier investigations into the influence of irradiation temperature. Obviously the additional strengthening induced by an increase of the helium content from 12 appm to 200 appm is only small at a fixed damage level.

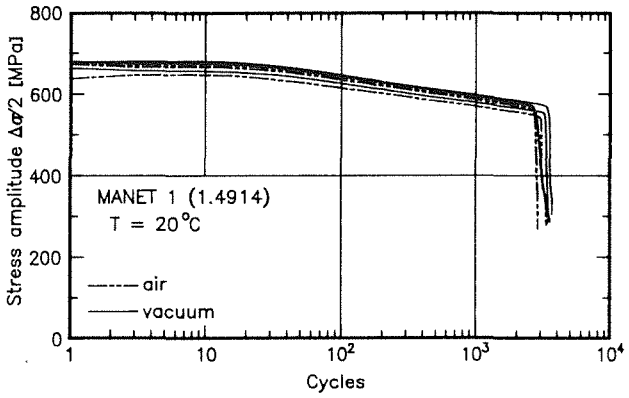

Fig. 1: Influence of test environment on fatigue life in strain controlled low-cycle fatigue experiments. $\Delta\varepsilon_t = 1\%$, frequency = 0.1 Hz.

Consequently, only a small decrease in fatigue life is observed in the specimens containing 65 appm and 200 appm He, respectively, while N_f of the two specimens with only 12 appm is in the scatterband of the unirradiated ones. It is, therefore, likely that at least at lower damage levels the small loss of fatigue life is related to the helium content rather than to the He-dose/damage ratio.

After the mechanical testing the broken specimens with their different irradiation conditions (300-600°C, 200 appm He, 1.2 dpa, cf. previous semi-annual report KfK 4677; 450°C, 12-200 appm He, 0.4-1.2 dpa) were examined by means of scanning (SEM) and transmission electron microscopy (TEM). SEM-fractography reveals crack initiation at the inner surface (Fig. 3, bottom) of the hollow specimen at large precipitates and grinding grooves. The cracks propagate perpendicular to the applied stress leaving typical fatigue striations behind. The analysis of all fracture surfaces could not establish significant differences between irradiated and unirradiated specimens, even at He-contents of 200 appm. The rupture mode between 300 and 600°C remains always ductile and transcrystalline.

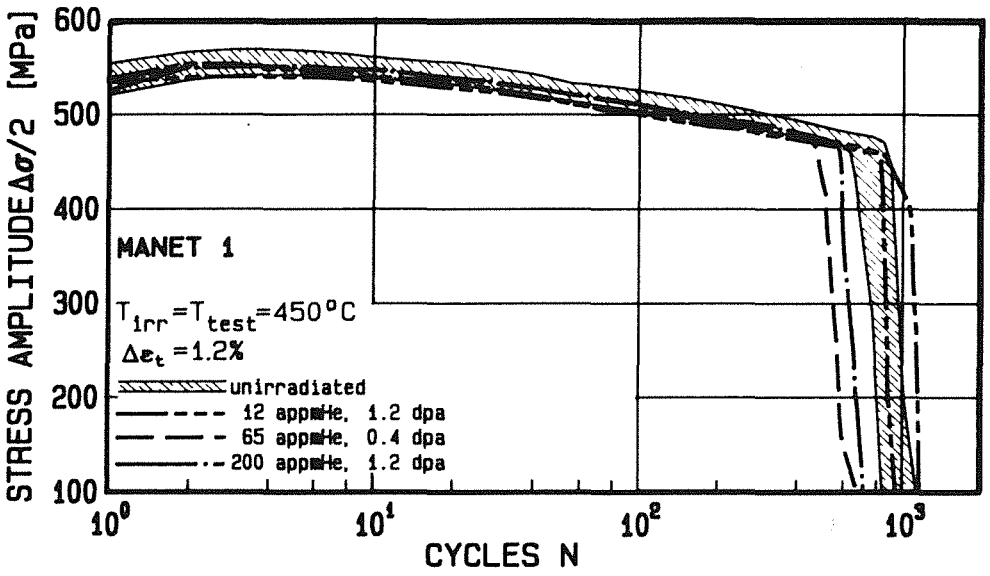

Fig. 2: Evolution of the stress amplitude at 450°C for 10 unirradiated specimens and specimens post-irradiated at He-dose/damage ratios of about 10 and 170 appm He/dpa, respectively.

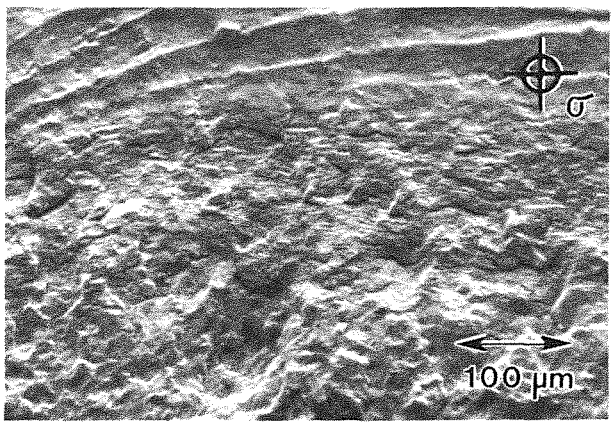

Fig. 3: SEM fractograph of an irradiated (200 appm He, 1.2 dpa) and fatigue tested specimen at $T_{irr} = 300°C$, stress direction is indicated.

The TEM-micrographs (Fig. 4) show the original microstructure (a) and the microstructure after irradiation and fatigue testing (b,c). The tempered martensitic lath-structure (a) with its high dislocation density changes during the fatigue test into a microstructure with distinct equiaxed subcells (b) and dislocation-free areas inside these cells. Neither the subcell formation nor the considerable reduction of dislocation density is affected by the presence of 200 appm He. The speculation that the cyclic motion of the dislocations during fatigue testing could sweep small helium clusters and bubbles to the lath and subgrain boundaries, where they could accumulate and have an adverse effect on lifetime, was not confirmed. After helium implantation and fatigue testing at all temperatures investigated, bubbles were found not only at the deep sinks like lath boundaries or surfaces of precipitates but also in the matrix.

Fig. 4 c shows that even at 600°C a considerable part of He-bubbles in irradiated and fatigued specimens is observed in the matrix.

References:

[1] R. Lindau and A. Möslang
Contribution to 4th Int. Conf. on Fusion Materials, Dec. 1989 (Kyoto); to be publ. in J. Nucl. Mat.

[2] R. Lindau and A. Möslang
Jahrestagung Kerntechnik '90, May 15-17, 1990 (Nürnberg), p. 601, ISSN 0720-9207.

Staff:

S. Baumgärtner
G. Bürkle
R. Lindau
A. Möslang
D. Preininger
G. Przykutta

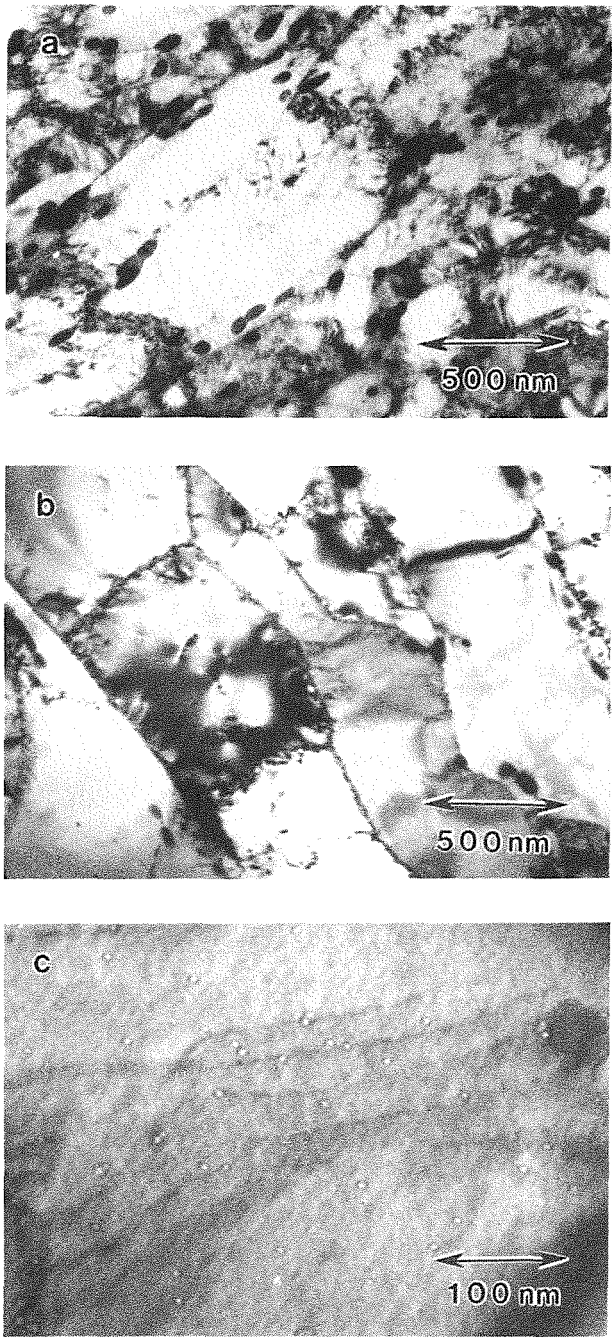

Fig. 4: TEM micrographs of MANET 1
a) unirradiated, not cycled;
b) cell structure at 520°C, and
c) He-bubble distribution at 600°C in irradiated (200 appm He, 1.2 dpa) and continuously cycled ($\Delta\varepsilon_t = 1.2\%$) specimens

Development of ECRH Power Sources

Introduction:

The task aims at developing mm-wave power to supply current plasma experiments and NET/ITER with electron cyclotron wave (ECW) systems. Stage I of the present KfK gyrotron development programme was the development of a gyrotron prototype at 140 GHz with a power output of at least 100 kW and a pulse length of at least 100 ms. This stage I has been achieved successfully at the end of 1989. The frequency of 140 GHz appears to be well suited for most applications, whereas higher power (~ 1 MW) and extended pulse length, (quasi cw-) operation, will be required in future. The plasma experiments of IPP Garching ASDEX-Upgrade and Wendelstein VII AS present an intermediate goal for the development in terms of pulse length and power requirements. ECRH development is therefore subject of cooperation of IPP Garching (plasma experiments), University of Stuttgart (microwave transmission) and KfK (power generation and microwave diagnostics). Gyrotron design and prototype testing is the specific task of KfK, whereas fabrication of subsystems and complete gyrotron tubes is done by industry. A particular aspect of transmitting very high power is the window which seals the UHV-tube from the transmission line. In a similar manner the plasma has to be separated from the transmission line by a window which is subjected to neutron damage effects. Materials studies are referred to under PPM 4.

Gyrotron prototype

After extended developments by operation of TE_{03} modular gyrotron devices[1], a prototype tube with single TE_{03}-mode cavity, nonlinear uptaper and FC75 cooled double disc alumina output window with a fine-adjustable disc distance was manufactured and assembled by industry and has been tested at KfK. The main difference of the prototype gyrotron to the modular gyrotron is that the whole tube was brazed to form one unit, and the cylindrical copper resonator was electropolished to get a better surface quality, and hence reduced rf losses.

A peak output power level of 300 kW in the TE_{03}-mode at 12 A beam current was measured with short pulses (0.5 ms) after parameter optimization. The overall efficiency had a maximum value of 33 % around 8 A beam current.

The output power and efficiency versus beam current are shown in Fig. 1 and Fig. 2, respectively. For comparison, results for different modular gyrotrons are also shown.

The short pulse operation of the prototype gyrotron was followed by single pulse operation with up to 100 ms duration. An output power of 120 kW with longer pulse duration (100 ms) was obtained reproducibly in the TE_{03}-design mode at 140.2 GHz.

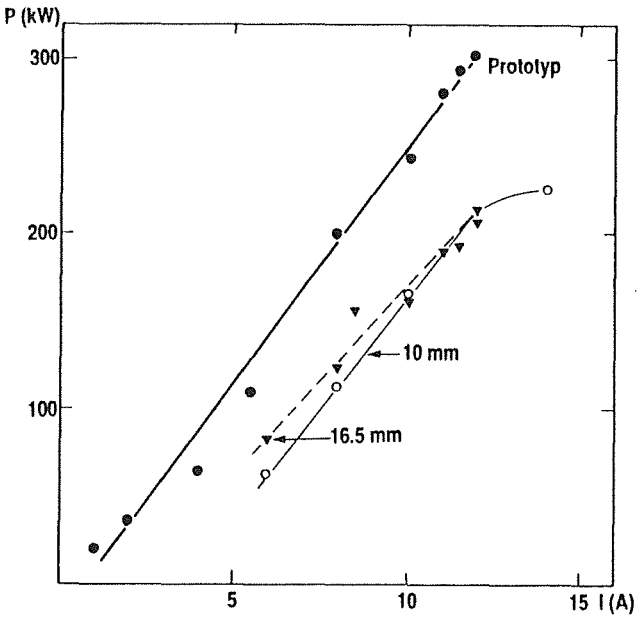

Fig. 1: Output power as function of beam current in the TE_{03} design mode at 140.2 GHz for different gyrotron resonators

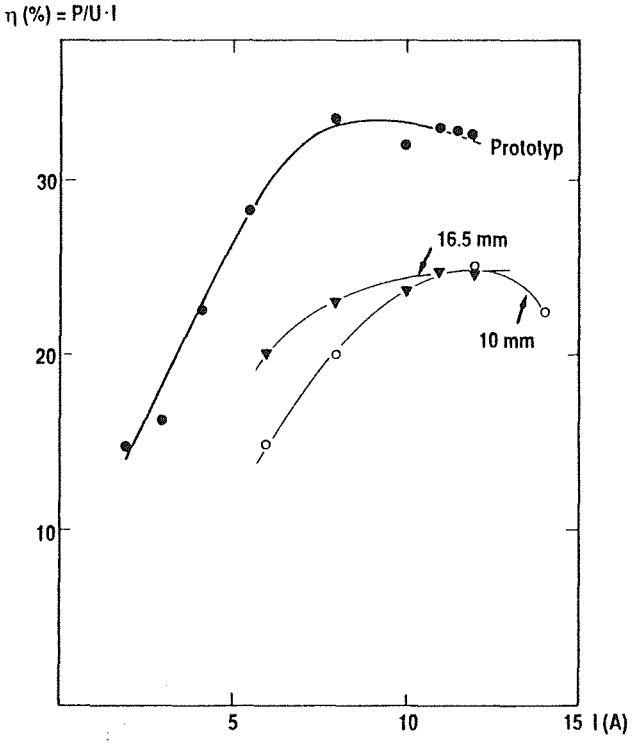

Fig. 2: Efficiency as function of beam current in the TE03 design mode at 140.2 GHz

This prototype gyrotron was delivered to IPP Garching for the use in the planned high plasma density experimental programme of the Advanced Modular Stellarator W VII-AS.

High power gyrotrons

Needs for high power have been identified for all large plasma physics and engineering devices (e.g. W VII AS, ASDEX-UPGRADE, FTU, JET, W VII-X, NET, etc). The specification aims as an ECW system with a frequency around 140 GHz and a unit power of the order of 1 MW/CW. To get technological results which are relevant for CW operation at high power an intermediate step is required. This is considered to be a cylindrical cavity gyrotron capable of 0.5 MW, 1 s at 140 GHz.

The power limit in the TE_{03}-mode gyrotron was studied in more detail. The temperature rise of the water-cooled resonator wall was observed for long pulse operation (100 ms) with the help of thermocouplers placed into boreholes of the resonator wall (3 mm from the inner surface). Significant heat pulses were obtained and correlated with the pulse length. During and after the long pulse operation a restriction of the original oscillating region of the TE_{03}-mode in the beam voltage/modulation voltage diagram and an irreversible frequency increase by a small amount ($2 \cdot 10^{-3}$) was observed. This "aging" of the cavity appears to be mainly due to the ohmic skin losses in the resonator walls, where modifications of the shape and additional losses caused by growing surface roughness lead to essential deterioration of output power and efficiency, and to the stresses in the ceramic output window discs.

With the prototype gyrotron the 120 kW/100 ms operation was repeated several times over longer periods and no further deterioration occured.

This experimental experience identifies the difficulties in the development of high power high frequency CW gyrotrons. The TE_{03}-mode as the interaction mode is not extrapolative to 1 MW/CW operation because it causes untolerable wall losses. Only whispering gallery mode (WGM) and volume mode (VM) gyrotrons[2] are now considered to have the potential to meet the 1 MW/CW goal in the mm-wave source development for future multi-megawatt ECW systems. The VM cylindrical cavity gyrotron oscillator appears to be the primary candidate.

In addition, frequency tuning capability and electron beam recovery aspects (separation of mm-waves and e-beam) as well as the need of insulation gaps in the tube make an internal conversion of the rotating asymmetric VM into a linearly polarized Gaussion free-space mode, combined with a lateral output coupling scheme[3] mandatory.

VM gyrotron

Therefore, as a next step, KfK intends to build a $TE_{10,4}$-mode modular (VM) gyrotron with an output power of 0.5 MW, a pulse length up to 200 ms and a frequency of 140 GHz.

The TE_{03}-mode cavity has to be replaced by a VM resonator and a quasi-optical output mode transducer has to be implemented into the tube. A $TE_{10,4}$-mode cavity and the electron beam gun for such a gyrotron have been designed. The electron beam gun has been ordered from industry. A new compression zone and the nescessary output taper have also been designed and will be fabricated. The existing superconducting magnetic field system will be used for the first modular VM gyrotron.

References:

[1] G. Gantenbein, G. Hochschild, W. Baumgärtner, E. Borie, H. Budig, G. Dammertz, O. Dumbrajs, P. Grundel, T. Geist, A. Hornung, M. Kuntze, R. Lehm, Z. Liao, A. Möbius, N. Münch, H.-U. Nickel, H. Oppermann, B. Piosczyk, G. Redemann, R. Vincon, H. Wenzelburger; Experimental results with a TE_{031}mode gyrotron at 140 GHz. 14th Int. Conf. on mm Waves and I R, Würzburg, Oct. 1989.

[2] E. Borie, O. Dumbrajs, R.K. Gupta, A. Möbius, B. Piosczyk, H. Wenzelburger; A high power gyrotron operating in a WGM for KfK, 14th Int. Conf. on mm Waves and I R, Würzburg, Oct. 1989.

[3] A. Möbius, M. Thumm; Operating of a helically cut quasi-optical antenna with hybrid modes, 14th Int. Conf. on mm Waves and I R, Würzburg, Oct. 1989.

Staff:

W. Baumgärtner
E. Borie
H. Budig
G. Dammertz
O. Dumbrajs (TU Hamburg-Harburg)
U. Feißt
G. Gantenbein
T. Geist (UNI Karlsruhe)
P. Grundel
G. Hochschild
A. Hornung (UNI Karlsruhe)
M. Kuntze
R. Lehm
A. Möbius
N. Münch
H.U. Nickel
H. Oppermann
B. Piosczyk
G. Redemann
R. Vincon

Studies for NET and ITER

Introduction:

By granting study contracts to KfK, NET draws upon special expertise available in the laboratory. In contrast to the technology tasks which extend over a longer period of time and consist in most cases of experimental work, study contracts are agreed on short notice and are of limited duration. On the average, five manyears per year of KfK manpower are spent for this kind of arrangements. Subjects scatter widely according to the need arising from the design activity for NET/ITER.

NET Remote Workstation

The remote handling equipment at NET like the in-vessel handling unit (IVHU), the bridge mounted transporter and others will be controlled from the Remote Handling Control Room via the NET Remote Handling Workstations (NRWS). These workstations represent the operator's interface to the equipment control systems and the remote handling site. But interfacing is not the only purpose: the NRWS shall help the operator in performing his maintenance tasks. The NRWS represents the top-level (task level) component of the hierarchical remote handling control system shown in Fig. 1.

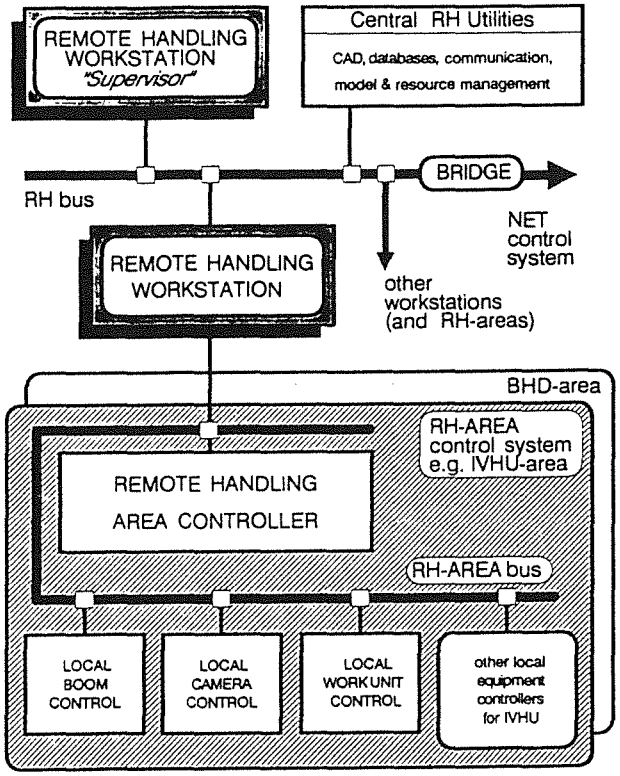

Fig. 1: Hierarchical NET remote handling control system: The NRWS provides the man-machine interface and general operation support software tools.

Based on a state-of-the-art report concerning the JET remote workstation as well as workstations used in similar applications (e.g. space, off-shore, reprocessing) a workstation providing an advanced tele-operator support tailored to NET/ITER needs was worked out [1]. The goal of the NET study was to define the functionality of a remote handling workstation and its hardware and software architecture.

The remote handling workstation has to fulfill two basic functions: (1) to provide the man-machine interface (MMI), that means the interface to the control system of the maintenance equipment and to the working environment (telepresence) and (2) to provide high level (task level) supporting functions (software tools) during the maintenance work and in the preparation phase.

The basic control of the equipment (e.g. the movement of the IVHU) is concentrated in equipment specific operating modules (software) integratable into the NRWS via dedicated software interfaces and accessible by the operator using the NRWS input and output devices. The functional modules for general operator support are (Fig. 2): (1) Planning, programming, (2) Integrated viewing (3) Monitoring, (4) Training, (5) Guidance, (6) Communication, dialog, (7) Configuration, (8) Logging, (9) Commissioning, testing. The NRWS provides an "intelligent handbook" guiding the operator through planned procedures illustrated by animated graphical working sequences. For unplanned situations decision aids are available in form of offline simulators. Monitoring of the maintenance work is done with respect to spatial, functional, and procedural information.

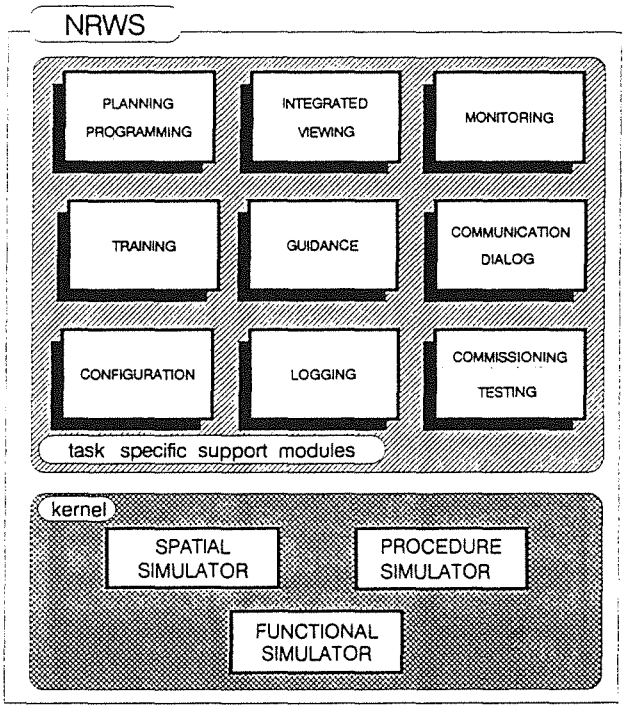

Fig. 2: Functional modules of NRWS: The task specific operator support modules are based on three simulators.

Concerning the man-machine interface, an important module of the remote handling workstation besides the standard components of man-machine interfacing is a module for graphical scene presentation supplementing viewing by TV. The technique of integrated viewing is well known from JET BOOM and TARM control using the GBsim and KISMET software.

A possible screen layout for guiding the operator through preplanned maintenance procedures is shown in Fig. 3. The procedures are represented by a special graph, the advancement of the work is represented by the flow of tokens in this graph. The operator gets detailed information about the actual state or selected elements of the procedure.

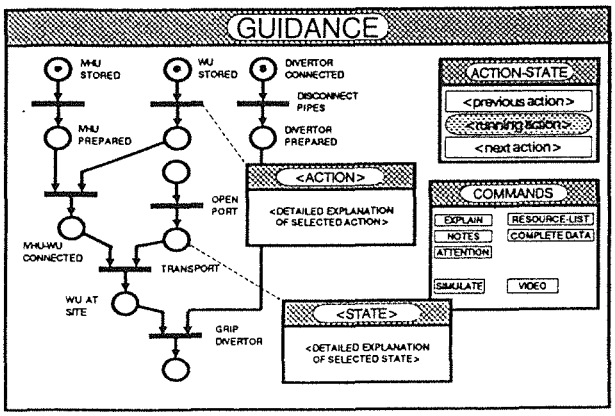

Fig. 3: Guidance window of NRWS:
The operator is guided through preplanned maintenance produceres represented by a special network with marked actual annotations.

These task specific modules are based on three types of models of the maintenance equipment, the working environment, and the maintenance tasks: (1) a spatial (geometric/kinematic) model, (2) a model representing the maintenance procedures, and a (3) functional model of the equipment. These models are the database of the three related simulation modules which form the kernel of the whole support system.

A central point of the architectural design was to guarantee a high flexibility with respect to hardware and software. Therefore the remote handling workstation is designed as an open system based on widely accepted standards allowing the stepwise integration of the various modules starting with the basic MMI and the spatial simulation as standard components.

The compatibility with the NET overall control system is guaranteed by using the same hardware and software standards important for integration and maintenance.

References:

[1] Leinemann, K.: Unpublished report of KfK, May 1990.

Staff:

K. Leinemann

Doses due to Tritium Releases by NET - Data Base and Relevant Parameters on Biological Tritium Behaviour

The assessment of the radiological impact of tritium releases is an essential part of the safety considerations which go in parallel with the development of fusion reactor technology. In the current stage of development it is necessary to predict the impact of probable tritium releases for licencing purposes. Mathematical models and computer codes are effective tools for this task.

This study reviews the current knowledge on the tritium behaviour in biological systems after a tritium release to the atmosphere considering different chemical forms of tritium that can be released by a fusion reactor (HT, HTO and tritiated organics). It deals with tritium uptake by plants, standing at the beginning of several food chains, the tritium turnover in animals, the different pathways by which tritium can reach man and finally its behaviour in man, representing the end consumer. In the last chapter of the study, a choice of existing computer codes for dose estimations due to chronic or accidental tritium releases has been compared with respect to tritium uptake by plants and the ingestion pathway.

Computer codes developed at different institutions to estimate the dose due to tritium from the ingestion pathway differed in the results for a given tritium release by about one order of magnitude. So it became necessary to compare the methodes and assumptions of the models. The submodels for the ingestion pathway of following computer codes were regarded:

- ISOLA IV, from KfK (FRG)
- TRITMOD, from SRL (USA)
- TRIDOS, from SRD/UKAEA (UK)
- OHTDC, from CFFTP (Canada)
- COMA, from NRPB (UK)
- FOTRI, from KfK (FRG)
- TRILOCOMO, from Studsvik (Sweden).

The computer codes ISOLA IV, TRITMOD an TRIDOS are able to predict the behaviour of tritium for chronic release situations. UFOTRI and TRILOCOMO can only be used for accidental releases and OHTDC and COMA can calculate both release situations.

For routine releases, rather simple models are used, as the so called "specific activity model", in which equilibrium conditions in the atmosphere-soil-plant system are assumed. Generally, this is a reasonable approach but relatively insensitive to changing activity concentrations and varying meteorological conditions. Furthermore, in case of HT emissions the reemission of HTO from the soil cannot be considered adequately.

Since equilibrium conditions cannot be anticipated for accidental releases, more sophisticated models are required for this purpose. They should be able to model the time dependent behaviour of tritium in the environment and its dependences from different environmental parameters in order to achieve an acceptable level of accuracy.

In the case of an HT release, all models calculate HT deposition to soil, conversion to HTO and subsequent uptake by plants. TRITMOD is the only model that considers additionally HT deposition to vegetation and conversion to HTO and OBT.

HTO uptake by plants from the atmosphere can be modelled assuming a fixed specific actifivity ratio between the tritium concentrations in air humidity and TFWT (tissue free water tritium) of plants or by calculating the specific activity ratio from atmospheric and plant parameters (e.g. resistance model). Fixed specific activity ratios are assumed in ISOLA IV (1,0), TRIDOS (?) and COMA (0,5). TRITMOD, OHTDC and UFOTRI calculate the specific activity ratio according the model proposed by BELOT et al. (1979) and take the uptake of HTO from soil also into account. In TRILOCOMO a more specific model is used, considering additionally the leaf temperatur in dependence of the radiant heat load. The formation of OBT from HTO in vegetation water is only considered in TRITMOD, COMA and UFOTRI.

The submodels describing the tritium behaviour in animals are based on the balance of tritium inputs and outputs using transfer coefficients to calculate the tritium transport between the different compartments. All models use dairy and beef cattle as reference animal. TRIDOS and COMA additionally consider tritium in sheep, which are typical for agriculture in the UK.

Tritium intake by inhalation and skin absorption by animals is considered in all models, with the exeption of skin absorption by sheep in COMA. The ingestion of tritium with drinking water by animals is neglected in TRIDOS and COMA because it is assumed to be uncontaminated. OHTDC assumes for drinking water the same concentration as the water in the topsoil compartment.

Only TRITMOD, COMA and UFOTRI consider the ingestion of OBT by animals. In COMA it is assumed that OBT from plant material is only transfered to the water compartment of the animal. TRITMOD and UFOTRI also consider the transfer of plant OBT to animal's OBT (meat) and the transfer of plant and animal's OBT to milk.

For the distribution of human diet average food habits for different countries, ages and sexes are assumed. In TRITMOD the human diet is divided in food rich in protein and fat and food rich in carbohydrate. Seasonal effects in the distribution of tritiated compounds in the human diet in dependence of the time of release are considered in TRIDOS.

The ingestion of tritium with drinking water by man is handled differently. OHTDC assumes that drinking water for man has the same tritium concentration as water in the deepest soil compartment considered. UFOTRI and COMA neglect the uptake of tritium by drinking water for accidental releases. The other models consider tritium uptake by

drinking water but the way to estimate the tritium concentration is not described in the literature.

When the intake of tritium by the different pathways is estimated, the committed effective dose equivalent is calculated using the dose conversion factor for tritium in Sievert per Becquerel intake. This factor bases in all models on the data of water balance in the Reference Man according ICRP 23 (1975) and includes the quality factor, the biological half-life and the mass of affected tissue. All models use the quality factor of 1 and an average biological half-life of tritium in the body of 10 days. The dose conversion factors vary only slightly in the different models from 1,6 E-11 to 2,0 E-11 Sv/Bq for adults (whole body).

Only in TRITMOD the specific activity of the organic fraction in man is calculated additionally considering the uptake of food rich in protein and fat and food rich in carbohydrates. However, it is not clear in which way this concept will affect the resulting dose. The other models do not consider the increase of dose due to ingestion of OBT and incorporation of tritium into organic substances of man.

In the opinion of the authors, the submodels for tritium uptake by plants, animals and man in TRITMOD seem to be most realistic for the purpose to estimate doses due to chronic tritium releases, because modelling is combined with measurement studies at the Savannah River site over a long period of time. The model includes a number of parameters which are not considered in most other models, e.g. the transport of OBT from vegetation to animals and man.

Among the codes for accidental release situations, UFOTRI considers the most parameters relevant for the ingestion pathway. The code includes different stomatal resistances for day and night conditions and during rain, als well as OBT formation in plants and transfer of OBT to animal's food products.

Comparing the results from the literature study and the practical application in the models, there are possibilities to refine the models in the following items.

Plant models

1. Consideration of different plant species:

For modelling the tritium uptake by plants mean values for different species are assumed, for instance for stomatal resistances of leaves during day or night conditions and for the leaf area index, respectively. However, it is known that the uptake rates of atmospheric HTO are different for various plant species under the same environmental conditions. Since only leaves are considered, this would only be valid for grass and green vegetable, not for fruits and grains.

2. Consideration of tritium translocation:

The transport of tritium from the leaves to other edible parts of different agricultural used plants is not considered in any model. This could be important for tritium releases occuring in the time before harvesting.

3. Consideration of diurnal variations in stomatal resistances:

Stomatal resistances, which directly affect HTO uptake from the atmosphere and also transpiration, can vary during the light period depending on the leaf water potential. These resistances will increase rapidly when the leaf water potential drops below a threshold value when plants are under water stress. The estimation of this effect would require informations of soil parameters.

For improvement of plant modelling, the knowledge on diurnal variations of stomatal resistances and photosynthetic intensity in dependence on photosynthetically active radiation, air temperature and humidity should be included. Observations of plant species, leaf area index and soil parameters should also be considered. Since many parameters are site specific they should be included in the model as variable input parameter.

Animal models

All models contain the tritium cycling in dairy and beef cattle which is well studied. Depending on the consumption habits of man other representative animals are included, for instance sheeps for UK. Models could be refined by including the tritium uptake by other sources of meat like pig, fish and poultry. The fraction of OBT in meat and milk should be estimated, because it is essential for realistic dose estimations.

Human models

All models compared use the ICRP model based on human date for the ICRP Reference Man (ICRP 23, 1975) to calculate a dose conversion factor. But they neglect the increase of dose due to ingestion of OBT and tritium incorporation into human OBT. For dose estimations considering the ingestion pathway of tritium additionally to inhalation and skin absorption, it is necessary to take OBT into account, for instance by modified dose conversion factors for different kinds of food or by available models. The enhancement of the quality factor for tritium from 1 to 2, which was proposed by the Joint Task Group of the ICRP and the ICRU in 1986, should also be taken into consideration.

Staff:

S. Diabaté
S. Strack

Fatigue Characterization of Jacket Materials at 4 K

Introduction:

The objectives of this task are to characterize the fatigue-life and fatigue crack growth behaviour of superconducting jacket materials at cryogenic temperatures.

The investigations concerning the fatigue life of the materials A410 (~ 316 LN) and Incoloy 908 were finished. The results show the high performance of the Incoloy 908 as compared to A410. This can be attributed to the high yield strength of the material Incoloy 908.

For the FCGR (Fatigue crack growth rate) investigations the measurement techniques were established. The compliance method and the direct crack advance monitoring via travelling microscope were used both to ensure the ultimate safety of the readings in the cryogenic regime. An RR-test with the bulk material carried out between EMPA, Dübendorf and KfK showed marginal differences of the results at ambient temperature. The cryogenic tests conducted at KfK show clearly that between 30-7 K there is no temperature influence on the FCGR. For A410 base material FCGR-data were established for load ratios of R = 0.1, 0.4, and 0.7, respectively.

Fatigue life results

Figures 1 and 2 show the performance of the A410 and Incoloy 908. The estimated lines for R = 0.1 and R = 0.7 can be assumed to be linear (in the semilogarithmic scale) up to 10^6 cycles. In the cryogenic regime there exists still little knowledge beyond this cycle number. The findings confirm the safe limit to be below the yield strength. For uncracked members the design philosophy "safe life" can be applied for stresses below 1000 MPa, in case of A410 and below 1200 MPa in case of Incoloy 908, respectively. However, if a material bears flaws at the very start few cycles are necessary to fracture the specimen, as was the case with a specimen in Fig. 1.

The R ratio 0.1 is a more severe condition than the 0.7. The weld metal has a significantly lower (~ 10 %) performance as compared to the base metal. This is true for both materials. In addition, the fractured surfaces of the already broken specimens indicate according to the SEM observations that the crack initiation is the main controlling parameter for the materials performance.

Presumably ~ 90 % of the total cycles are consumed for the crack initiation and only the small remaining percentage is responsible for the fracture.

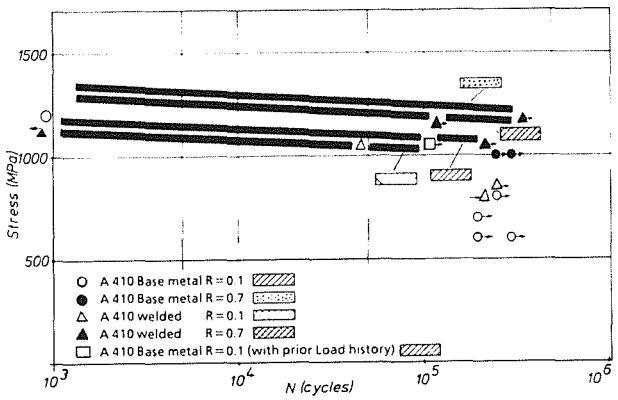

Fig. 1: Fatigue life results of the Böhler material (~ 316 LN) A410 in bulk and in as welded condition. Both materials are aged at 700 °C for 50 hours.

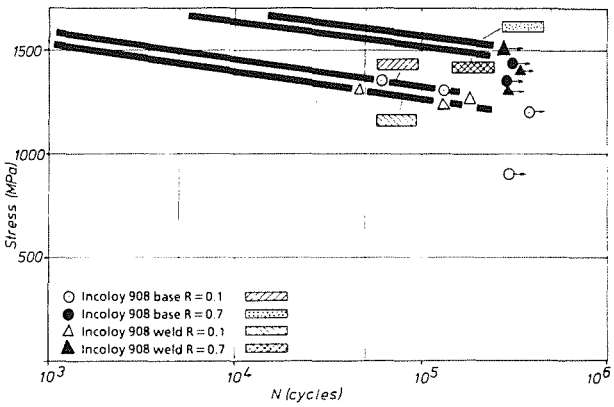

Fig. 2: Fatigue life results of the Incoloy 908 material in bulk and in as welded condition. All materials are aged at 700 °C for 50 hours.

FCGR Investigations at ambient temperature

295 K measurements were carried out with the material A410 in as received and aged conditions at KfK and at EMPA, Dübendorf. Two specimens were machined at KfK according to the KfK standard dimension (a/W = 0.34, where a crack length and W the width of specimen are). One specimen was aged before machining, whereas the other one was in the as received condition. These specimens were sent to EMPA for the purpose of the comparative FCGR investigations at R = 0.1. KfK received two specimens (aged and as received) from EMPA. The specimens had the same dimensions with the only difference of the a/W ratio, which was 0.26 in case of EMPA. These bulk material measurements were carried out in T-L (Transverse-Longitudinal) orientation. Each Laboratory tested 5 specimens in total, two specimens being the exchanged ones and the three remaining from the same heat, but machined and tested at the same site. These investigations were necessary for the following reasons.

- To compare the results for being sure of the accuracy of these measurements.

- To adjust the machine parameters before the start of the FCGR tests.

- To set up the measurement technique necessary to the subsequent cryogenic investigations.

For the FCGR measurements the most important issue is the exact recording of the crack position during the crack propagation. To achieve this the compliance method was used as described previously. Fig. 3 shows the results of the compliance readings of several different tests carried out with 316 LN type weldments.

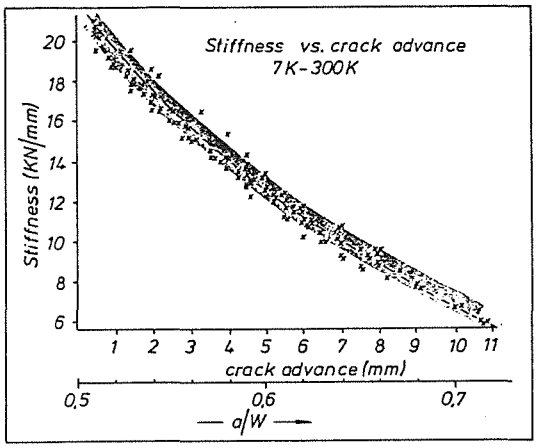

Fig. 3: Load vs. displacement results of the FCGR specimens. The diagram shows the calculated stiffness of the specimens according to the results (load vs. displacement) dependent on the crack tip position a/W. The points are the findings of 11 different specimens. The crack propagation was in the 316 LN type weldment. No temperature influence could be determined.

The scatter of the individual readings give hence a relatively high degree of error. Therefore in the preliminary phase of this task the compliance method was discarded. However, during the current room temperature measurements of the bulk material we could determine, that this was not the case. The specimens this time were mirror polished both sides and the fine grid of 0.5 mm spacing was placed on the surface by mechanical means. Using two fiberscopes the average of the crack position could be determined very accurately. The crack propagates during the cyclic loading with almost a random law considering the left and the right side of the specimen, respectively.

Fig. 4 shows the relative difference between left side and right side in mm. vs. the crack advance.

The variation from specimen to specimen can be explained by material inhomogeneities and the specimen tolerances in the pin holes. Some seconds of angle differences (i.e. specimen

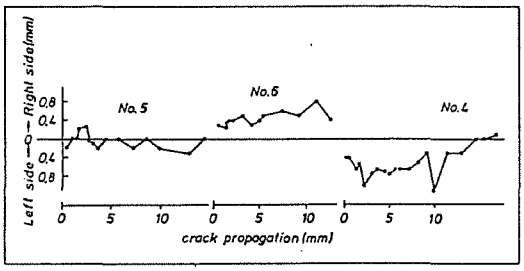

Fig. 4: The crack front parallelity under the influence of crack propagation for the material A410. Monitoring of the crack position was carried out with two fiberscopes (x 7.5) on both mirror polished sides of the specimens. The readings give the relative difference between left and right side of the monitored surface.

surface must bei 90 ° to the pin holes), which violates the exact unidirectionality of the specimen in the machine may influence the parallelity of the crack propagation front. Monitoring of the specimens both sides and taking the arithmetic mean of the crack advance thus averages the scatter of the compliance readings. Fig. 5 shows the compliance readings of the 5 individual specimens.

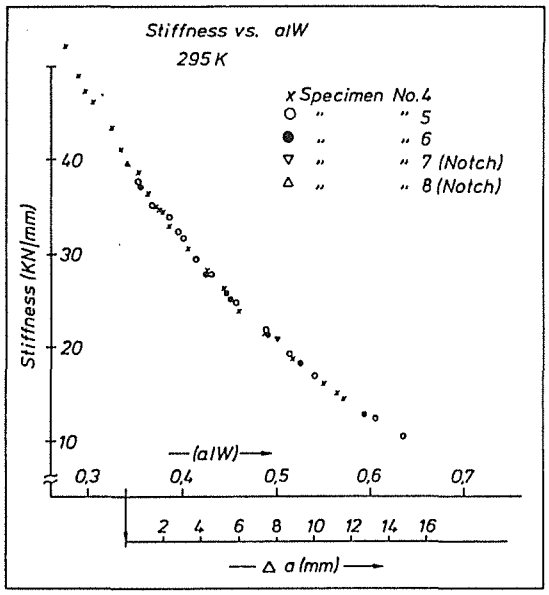

Fig. 5: Stiffness vs. crack position a/W of 5 different specimens of the material A410 at 295 K. Crack positions were determined by two fiberscopes. The positions are evaluated by taking the mean of both sides.

The values are within a narrow scatterband, which gives an accurate compliance line (stiffness vs. crack advance). The inaccuracy may be below ± 0.1 mm crack position. This line was thus taken to follow the crack propagation in the cryogenic regime.

The FCGR results of the five specimens (two received from EMPA and the other three machined at KfK) are given in the Figures 6. Figure 6 shows the FCGR behaviour at 295 K with

the material A410 in aged and in as received condition. All points determined from different specimens are merged in these two diagrams.

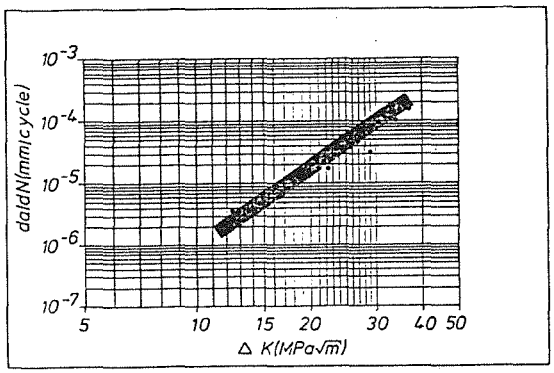

Fig. 6: 295 K FCGR (da/dN vs. range of stress intensity factor) results of the material A410 in aged condition. The points are determined from two different specimens. S6 sent by EMPA and S5 machined at KfK.

No significant difference could be determined between the aged and as received condition at 295 K. The results from EMPA also fall within the determined band and there is no difference between the aged and as received condition. Between EMPA findings and KfK results there is little difference. The difference becomes significant at high ΔK regime (> 20 Mpa√m). However, both laboratories agree that there is no major difference in the test results.

FCGR results in the cryogenic regime

The FCGR investigations in the cryogenic regime were carried out both with the compliance method and the direct monitoring by fiberscope. The role of the fiberscope was to determine the crack initiation and the control of crack advance. This was necessary because of limited test duration. The cool down plot of a specimen and the temperature variation are shown in Fig. 7. The temperature could be attained to be constant within ± 0.4 K. However, there could be clearly determined, that the temperature does not influence the FCGR in the cryogenic regime. Between 30 K and 6,5 K no difference in FCGR could be observed. This is true for the bulk metal as well as for the weldments.

Therefore the majority of the tests was carried out between 15 K and 25 K. The readings were checked during the test from time to time by decreasing the temperature to 7 K. After obtaining some points at 7 K the temperature was again increased to 25 K. The reason for this type of test was the economics with the liquid helium consumption. At 7 K the consumption is ~ 10 Liters/h, whereas at 25 K this value drops to ~ 3 Liters/h.

Figure 8 shows the findings for the bulk material A410 and its TIG-weldment. The FCGR at 25 K and R = 0.1 is higher compared to the 295 K FCGR. This means that in the cryogenic regime the crack propagates faster. This has been

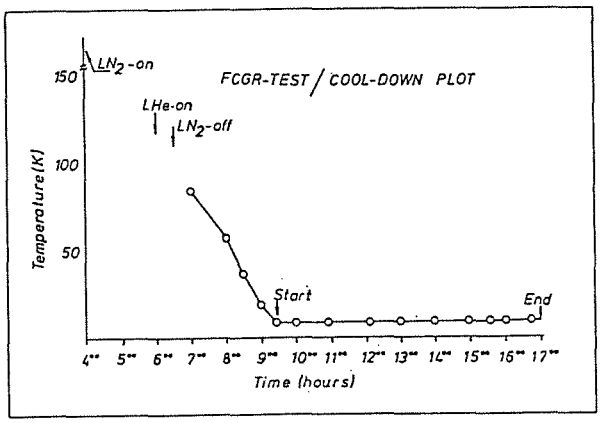

Fig. 7: Typical cool down plot of the machine. Temperature variation after the start is within ± 0.4 K.

also determined for 304 LN material (295 K → 77 K) by Lawrence Berkeley Lab. The R ratio 0.4 seems to be more severe than the 0.7 in the low ΔK regime (< 10 MPa √m). The curve with R = 0.7 shows the decreased FCGR performance at high ΔK regime (> 10 MPa √m) as compared to the R = 0.4 load ratio case. Comparing these diagrams with the recently determined 316 LN weld metal FCGR shows that the weld metal has enhanced properties as compared to the bulk metal at 295 K. The weldment was produced in this case by the multipass TIG process. The flash butt welded jacket material specimens will be tested within the next months. However, we expect that the results will be comparable. The cryogenic performance of the weldment is significantly higher than in the 295 K case. To clarify these findings and to set up a theory, work is now under progress. In addition, it seems that all these results are well explainable.

Staff:

A. Nyilas
H. Raber

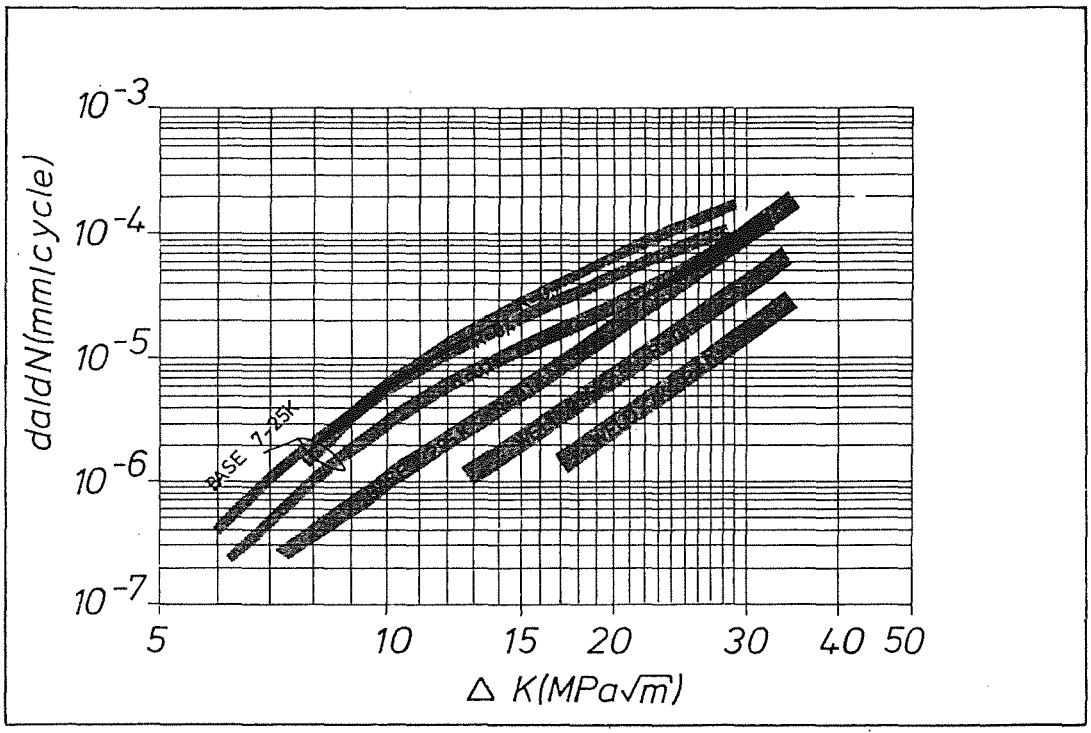

Fig. 8: Cryogenic FCGR (da/dN vs. range of stress intensity factor) results of the bulk material A410. No temperature influence between 25 K and 7 K. The results were gained from 5 different specimens. The crack propagation in the weld metal was in the welding direction.

Doses due to Activation Product Releases by NET Plasma Facing Components - Review and Procurement of Data Base

The program systems UFOMOD and COSYMA are being used for NET to calculate acute and long term doses to individuals and the general public for accidental releases of activation products. Some of these activation products, which might be relevant for dose assessments, are not included in the list of radionuclides considered in both accident consequence codes. To extend their applicability, a contract has been given to the Gesellschaft für Strahlen- und Umweltforschung (GSF) mbH, Neuherberg, to calculate with the time-dependent radioecological model ECOSYS activity concentrations in foodstuffs as basic input for the ingestion modules of both codes.

This work was completed in the first quarter of 1990. As input for the model ECOSYS, foodchain transfer factors have been determined from a critical review of the literature for the radionuclides Cr-51, V-49, Mn-53/54/56, Fe-55/59, Ni-59/63, Co-57/58/60, Mo-93 and W-181. With these data, time-dependent activity concentrations and time-integrated acitivity concentrations were calculated in milk, beef, pork, wheat, potatoes, leafy-, fruit-, and root vegetables for a deposition of 1 Bq/m^2 on 1st of January and 1st of July assuming an interception of 100% during the growing period of the plants considered. The activity concentrations are given at the time points 1 d, 7 d, 30 d, 100 d, 200 d, 1 a, 2 a, 3 a, 5 a, 10 a, 20 a, 50 a and 70 a after deposition.

The data calculated within the contract are now being implemented in the accident consequence code systems UFOMOD and COSYMA together with the corresponding dose-conversion factors. Work will be completed with preliminary dose calculations for activation product releases.

Staff:

J. Ehrhardt
C. Steinhauer

Vacuum Pumping Support

Vacuum flow calculations were carried out for the NET/ITER-reference design of one exhaust duct part system, consisting of two parallel ducts, one common header and three connected cryopumps (two pumps running) as shown in Figure 1. The results give confidence, that adequate exhaust performance can be expected during burn time with a helium pumping speed of 100 m3/s for each pump, duct diameters of approxiametely 2 m and a diameter of the pump entrance nozzles of 1.5 m.

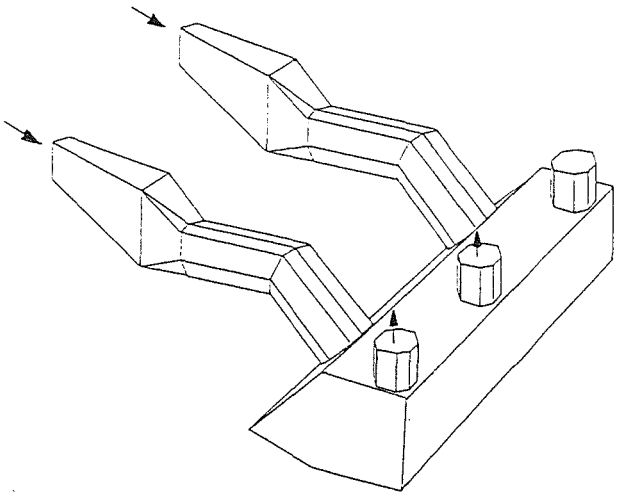

Fig. 1: NET/ITER exhaust duct part system (not scaled)

The Monte Carlo program used for the calculation of the transmission probability assumes random molecular flow conditions at the entrance of the divertor channel. This is not true during burn time, of course. To overcome these difficulties, the real particle flow schemes in the vicinity of the divertor plates will be investigated in more detail at NET/ITER and the results of these calculations will be combined with the duct calculations mentioned before. As contribution hereto, the transmission probability of some fictive duct systems with modified entrance geometries was determined.

The program used to calculate the overall vacuum flow performance was improved. Specific versions for cryopumps and for turbomolecular pumps are available now with improved input/output capabilities.

The general "Vacuum Design Code" of Process Applications, Inc., Oak Ridge, USA, was studied in some detail. As a first trial utilisation, the performance figures of the NORMETEX 1300/600 pump combination, as measured within the fusion technology program at KfK, were introduced into the data base of this code and first test calculations were carried out.

Staff:

R.A. Müller

Test of Stress Induced Degradation of Subcomponents of the NET OH Conductor

In this contract the effect of both axial tensile and transverse compressive stress/strain on the critical current of the basic strand and different cable in conduit (CIC) conductors from ABB and LMI will be investigated. Up today only the samples of ABB have been delivered, and the most important tests of these samples were carried out successfully in our FBI test facility. These extended tests include measurements of the critical current, I_c, versus magnetic field, B, I_c as a function of axial strain. ε_a, at B = 12.5 T, and the stress-strain curves at 4.2 K.

The main results of all samples are summarized in Table 1, and a typical Ic vs. ε_a characteristic for a CIC subcable (sample A 29 S 2 L, braided cable with 29 strands of 0.93 mm Ø in a SS 316 conduit, 9 mm Ø) is shown in Fig. 1: The drastic dependence of I_c vs. ε_a (loaded curve) is affected by the prestress of the steel conduit onto the Nb_3S_n filaments. This results in an I_c degradation of I_{co}/I_{cm} = 0.41 at 12.5 T, where I_{co} represents the critical current at ε_a = 0 and I_{cm} the maximum of Ic at $\varepsilon_a = \varepsilon_m$. An irreversible axial strain, ε_{irr}, occurs at that strain, where the I_c curve under unloaded condition declines stronger than the loaded one, i.e. between point 3 and 4. Also shown in Fig. 1 is the cycling behaviour at different strain levels of this sample. 100 cycles between 0.29 and 0.69 % and again between 0.54 and 1.01 % had no effect on the I_c vs ε_a curve.

The tests of the transverse stress effects on I_c for the ABB conductors, and the measurements of the LMI samples are in preparation.

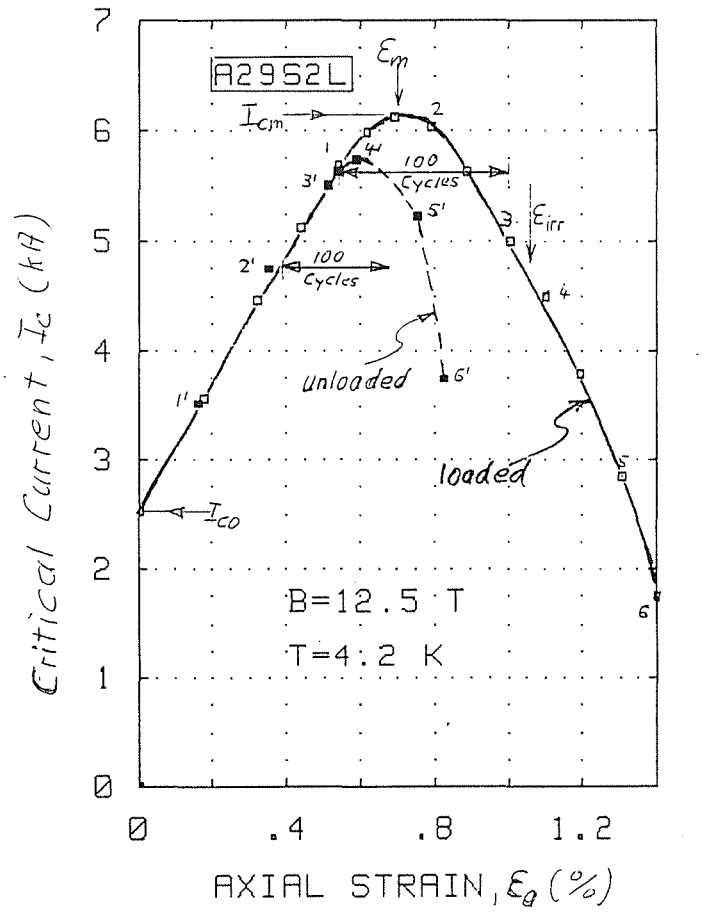

Fig. 1: Behaviour of the critical current for the ABB conductor under static and cyclic strain

Staff:

W. Specking

Table 1: Main results

Sample No.	I_{co} (A)	B (T)	I_{co}/I_{cm}	ε_m (%)	ε_{irr} (%)	Sample Characterization
A1 U 2 L A1 U 4 L A1 U 6 L A 1 U 7 L	204 197 203 199	13 " " "	0.92 0.91 0.88 0.87	0.20 0.20 0.20 0.24	0.44 - 0.63 0.46 - 0.65 0.57 - 0.71 0.55 - 0.75	Basic strand, 0.96 mm ø, MJR Nb3 Sn, delivered by TWCA
A 27 S 1 L A 27 S 2 L	3.250 3.217	12.5 "	0.54 0.53	0.70 0.72	1.04 - 1.15 1.00 - 1.20	Subcable 27 strands in conduit SS 316, 9 mm ø, delivered by ABB
A 29 S 1 L A 29 S 2 L	2.708 2.533	" "	0.45 0.41	0.68 0.71	1.05 - 1.21 1.00 - 1.10	Subcable 29 strands, conduit SS 316, 9 mm ø, ABB
A 81 S 1 L	10.430	"	- *	- *	- *	Subcable 81 strands, conduit 14.3 mm ø, ABB
A 87 S 1 L	8.800	"	~ 0.5 **	~ 0.6 **	-	Subcable 81 strands, conduit 14.3 mm ø, ABB

* I_c vs ε_a test not possible due to current limit of 10 kA of power supply

** Extrapolated, due to kind of test facility

Laser Beam Welding Technology Optimization for Long Longitudinal Welds of the NET Conductors

The application of laser beam welding technology was successfully demonstrated for the conductor of the Polo model coil. The gained experience is being under evaluation. For the welding parameter optimization of thick longitudinal welds like needed for NET conductors a contract for a collaboration with the Institut für Lasertechnik is being in preparation. (See also task MOC 1.)

Staff:

S. Förster
A. Nyilas
U. Jeske
A. Ulbricht

Appendix I: Allocation of Tasks

Task No.	Title	KfK Departments
Plasma Facing Components		
PSM 3	Pre- and Post-Irradiation Low Cycle Fatigue of Reference 316 L Steel and Welds	IMF IV
PSM 8	Coatings and Surface Effects on 316 L	IMF I, IMF IV
PPM 1	Material Characterization and Neutron Irradiation Effects in Graphites, CFCs and Ceramic Composites	IMF I
PPM 4	Material Characterization and Irradiation Effects in Ceramic Insulators	IMF I, IMF IV
PDT 1	Thermomechanical Tests of First Wall Mock-ups	IMF IV, IRB
PDT 2	Tests of Divertor Samples and Mock-ups	IRE
Magnets		
MTC 1	Industrial Manufacturing of a few km of React-and-Wind Nb_3Sn Conductors and of TF Model Coils	ITP
MIC 1	Manufacturing and Testing of Short Length Full-Size A 15 W/R Conductor (Inner Coil)	ITP
MOC 1	Manufacturing and Testing of Short Length Full -Size NbTi Conductor (Outer Coil)	ITP
MOC 2	Design and Manufacture of one Outer Coil (NbTi) and Installation in TORE SUPRA	ITP
MTF 2	Upgrade of the TOSKA Facility for Model Coils Testing	ITP, HIT
MSA 1	Safety Relevant Models and Experiments for NET Magnets	ITP
Tritium (Fuel Cycle)		
TPV 1	Development of Solid Particle Separators for Plasma Exhaust	HIT
TPV 2	Optimization of the Cryogenic Vacuum Pumping of Helium	HIT
TEP 1	Cryosorption on Molecular Sieves or Alternative Cryosorbents	IRCH
TEP 2	Plasma Exhaust Processing Alternative Options	IRCH
TEP 3	Tritium Storage	IRCH
TCP 3	Detritiation of Containment and Confinement Atmospheres	IRCH
Nuclear Engineering / Basic Blanket		
NSN 1	Neutronics Data Base for Shielding	INR

Remote Handling / Maintenance

RHS 1	Qualification of Standard Components	HIT
RHS 2	Material Tests for Remote Maintenance Equipment	HIT, IRE
RHS 3	Mock-up of In-Vessel Components and Test Facilities	HIT
RHI 1	Blanket Handling Device (BHD)	HIT, IRE
RHT 1	In-Vessel Handling Unit (IVHU)	HIT, IRE, IDT
RHT 2	Upgrading of Existing Force Reflecting Servomanipulators	HIT

Safety and Environment

SEC 3	Safety Analyses of Superconducting Magnets	IRE
SEP 1	Radioactivity Source Terms	IRE
SEP 2	Environmental Impact of Tritium and Activation Products	INR
SEA 1	Specific Safety Related Recommendations for the Design	IRE
SEA 3	Reference Accident Sequences	IRE
SEA 5	Assistance in Preparation of a Safety Report	IRE
LTSE 4	Comparative Analyses of Safety Aspects on the D-T and D-^{3}He Fuel Cycles	IMT

Blankets

BS - Solid Breeder Test Blankets

BS DE-D-1	Solid Breeder Test Blanket Design	IMF III, INR
BS BR-D-1	Preparation of Ceramic Breeder Materials	IMF III
BS BR-D-2	Characterization	IMF III
BS BR-D-3	Irradiation Testing	IMF III
BS BR-D-4	Tritium Release	INR
BS BR-D-5	Physical and Mechanical Properties	IMF I
BS BR-D-6	Compatibility	IMF I
BS BR-D-7	Constitution, Interaction with Water Vapour	IMF I
BS BR-D-8	Thermomechanical Characterization	IRCH
BS NN-D-1	Helium Blanket Test Loop	IMF III, INR

BL - Liquid Metal Test Blankets

BL DE-D-1	Liquid Metal Test Blanket Design	IMF III, INR, IRB
BL PC-D-1	Corrosion of Structural Materials in Flowing Pb-17Li	IMF I, IMF III
BL PC-D-2	Impurities and Clean-up of Molten Pb-17Li	HIT
BL EX-D-1	Tritium Extraction by Permeation and Cold Trapping	IRB
BL EX-D-2	Tritium Extraction from Molten Pb-17Li with Solid Getters	HIT
BL MH-D-1	Liquid Metal MHD	IRB
BL MH-D-2	Code Development, Alternative Design Options	IRB
BL SA-D-1	Functional Analysis of a Liquid Metal Self-cooled Blanket	IRE
BL SA-D-2	Electromagnetic Forces	IRE
BL CO-D-1	Flow Channel Inserts	IRB
BL CO-D-2	Liquid Metal Components and Testing	IRB

Long Term Program for Materials Development

LAM 2.1	LAM Element Activation	IMF II
LAM 3	Development of Low Activation Ferritic-Martensitic Steels	IMF II
LAM 5	Development of Non-Ferrous Low Activation Alloys	IMF II
MAT 1.6	Characterization and Qualification of 1.4914 NET Heats MANET 1 and 2	IMF II
MAT 1.9	Pre- and Post-Irradiation Fatigue Properties of 1.4914 Martensitic Steel (MANET)	IMF II
MAT 1.11	Post-Irradiation Fracture Thoughness of MANET Steel	IMF II
MAT 2.2	In-Pile-Creep-Fatigue Testing of MANET	IMF II, IMF III
MAT 9.2	Investigation of Fatigue under Dual-Beam Irradiations	IMF II

Development of ECRH Power Sources — ITP, IDT

Appendix II: Table of NET Contracts

Theme	Contract No.	Working Period
Electrical Connectors for Remote Handling	313/88-7 FU-D/NET	09/88 - 05/89
Study of a Plasma Exhaust Purification System for NET Based on Catalytic Reduction of Impurities: Phase 2 - Engineering Study	322/88-8/FU-D/NET	10/88 - 10/89
NET Remote Workstation	332/88-11 FU-D/NET	12/88 - 11/89
Doses due to Tritium Releases by NET-Data Base and Relevant Parameters	364/89-2/FU-D/NET	3/89 - 8/89
Fatigue Characterization of Jacket Materials at 4 K	372/89-4/FU-D/NET	5/89 - 6/90
Doses due to Activation Product Releases by NET Plasma Facing Components - Review and Procurement of Data Base	377/89-5/FU-D/NET	6/89 - 12/89
Test of Stress Induced Degradation of Subcomponents of the NET OH	392/89-8/FU-D/NET	10/89 - 10/90
Vacuum Pumping Support	394/89-8/FU-D/NET	9/89 - 12/90
Laser Beam Welding Technology Optimization for Long Longitudinal Welds of the NET Conductors	408/90-1/FU-D/NET	2/90 - 11/90

Appendix III: KfK Departments Contributing to the Fusion Project

Kernforschungszentrum Karlsruhe GmbH Telephone (07247) 82-1
Postfach 3640 Telex 17 724 716
D-7500 Karlsruhe 1 Telefax/Telecopies (0) 07247/825070
Federal Republic of Germany

KfK Department	KfK Institut/Abteilung	Director	Ext.
Institute for Data Processing in Technology	Institut für Datenverarbeitung in der Technik (IDT)	Prof. Dr. H. Trauboth	5700
Institute for Materials and Solid State Research	Institut für Material- und Festkörperforschung (IMF)	I. Prof. Dr.K.-H. Zum Gahr II. Dr. K. Anderko III. Prof. Dr.K. Kummerer IV. Prof. Dr. D. Munz	3897 2902 2518 4815
Institute for Neutron Physics and Reaktor Engineering	Institut für Neutronenphysik und Reaktortechnik (INR)	Prof. Dr. G. Keßler	2440
Institute for Reactor Components	Institut für Reaktorbau-elemente (IRB)	Prof. Dr.U. Müller	3450
Institute for Radiochemistry	Institut für Radiochemie (IRCH)	Prof. Dr. H.J. Ache	3200
Institute for Reactor Development	Institut für Reaktor-entwicklung (IRE)	Prof. Dr. D. Smidt	2550
Central Engineering Department	Hauptabteilung Ingenieur-technik (HIT)	Dr. H. Rininsland	3000
Institute for Technical Physics	Institut für Technische Physik (ITP)	Prof. Dr. P. Komarek	3500
Institute for Meteorology and Climate Research	Institut für Meteorologie und Klimaforschung	Prof. Dr. F. Fiedler	2093
Project Division Plant	Projektbereich Anlagen (PBA)	Dr. Engelhardt	2057
Central Experimental Engineering Department	Hauptabteilung Versuchstechnik (HVT)	Dr. Schubert	3114
- Hot Cells	- Heiße Zellen	DI. Enderlein	3650
- Tritum Laboratory Karlsruhe	- Tritiumlabor Karlsruhe	DP. Jourdan	2514
Central Safety Department	Hauptabteilung Sicherheit	DP W. Kölzer	2660

Appendix IV: Fusion Project Management Staff

Project Manager	Dr. J. E. Vetter	ext. 5460
Secretariat:	Fr. I. Sickinger Fr. I. Pleli	ext. 5461 ext. 5466
Project Administration, Documentation	BW G. Kast	ext. 5462
Studies, NET Contacts	Dr. J.E. Vetter	ext. 5460
Blanket Development and Test Facilities	DI H. Sebening	ext. 5464
Superconducting Magnets Gyrotron Development	Dr. J.E. Vetter	ext. 5460
Tritium Technology Structural Materials	Dr. H.D. Röhrig	ext. 5463
Safety and Environmental Impact, Remote Handling	DI A. Fiege	ext. 5465

Address: Kernforschungszentrum Karlsruhe GmbH
Nuclear Fusion Project Management

Post Office Box 3640, D-7500 Karlsruhe / Germany

Telephone No: 07247-82- Extensions ....

Telefax No: 07247 - 82 - 5467

Telex No: 17 724 716